AN EXPERIMENTAL STUDY ON
OFF-DESIGN PERFORMANCE AND NOISE IN SMALL PUMPS

A THESIS SUBMITTED TO
THE GRADUATE SCHOOL OF NATURAL AND APPLIED SCIENCES
OF
MIDDLE EAST TECHNICAL UNIVERSITY

BY

FATMA CEYHUN ŞAHİN

IN PARTIAL FULFILLMENT OF THE REQUIREMENTS
FOR
THE DEGREE OF MASTER OF SCIENCE
IN
MECHANICAL ENGINEERING

JUNE 2007

Approval of the Graduate School of Natural and Applied Sciences

_____

Prof. Dr. Canan ÖZGEN

Director

I certify that this thesis satisfies all the requirements as a thesis for the degree of Master of Sciences.

_____

Prof. Dr. S. Kemal İDER

Head of Department

This to certify that we have read this thesis and that in our opinion it is fully adequate, in scope and quality, as a thesis for the degree of Master of Sciences.

_____

Prof. Dr. O. Cahit ERALP

Supervisor

Examining Committee Members

Prof. Dr. Kahraman ALBAYRAK(Chairman)(METU,ME) _____

Prof. Dr. O. Cahit ERALP(METU,ME)   _____

Prof. Dr. Mehmet ÇALIŞKAN (METU,ME)   _____

Prof. Dr. S. Engin KILIÇ(METU,ME)   _____

Dr. Songül BAYRAKTAR(ARÇELİK A.Ş.)   _____

I hereby declare that all information in this document has been obtained and presented in accordance with academic rules and ethic conduct. I also declare that, as required by these rules and conduct, I have fully cited and referenced all material and results that are not original to this work.

Name, Last Name: Fatma Ceyhun ŞAHİN

Signature:

ABSTRACT

AN EXPERIMENTAL STUDY ON
OFF-DESIGN PERFORMANCE AND NOISE IN SMALL PUMPS

Şahin, Fatma Ceyhun

M.Sc., Department of Mechanical Engineering

Supervisor: Prof. Dr. O. Cahit Eralp

June 2007, 162 pages

This thesis study is focused on experimentally investigating pump noise at design and off-design operations and its relations with pressure fluctuations. Small size pumps are placed in a semi-anechoic chamber and operated at various system conditions and various rotational pump speeds. Pump operational data, noise data and time dependent pressure data are recorded. Fast Fourier Transform spectra of noise and pressure data are compared. Coherence spectrum between sound pressure level and hydraulic pressures are obtained. Data processing, Fast Fourier Transform and cross correlation are conducted with specific software Soundbook SAMURAI. The experiments have indicated that system characteristics or pump size do not have any influence on the noise of pump. On the other hand, pump characteristics are found to be distinguishable by means of peak frequencies on the sound spectra which are proportional to blade passing frequency. Results of cross correlations also show that, pump outlet pressure is a more significant source of noise than pump inlet pressure.

Key words: Centrifugal pump, Sound spectrum, Noise, Pressure fluctuation.

ÖZ

UFAK BOY POMPALARDA TASARIM DIŞI PERFORMANS VE GÜRÜLTÜ ÜZERİNE DENEYSEL BİR ÇALIŞMA

Şahin, Fatma Ceyhun

Yüksek Lisans, Makina Mühendisliği Bölümü

Tez Yöneticisi:　　　Prof. Dr. O. Cahit Eralp

Haziran 2007, 162 sayfa

Bu tez çalışması pompaların tasarım şartlarında ve tasarım dışı şartlarda çalışma gürültüleri ve bunların basınç ile ilişkilerinin deneysel olarak araştırılması üzerine yapılmıştır. Küçük boyda pompalar yarı yankısız bir odaya yerleştirilmiş, değişik sistem koşullarında ve değişik dönme hızlarında çalıştırılmıştır. Pompa çalışma verileri, ses verileri ve zamana bağlı basınç verileri kaydedilmiştir. Gürültü ve basınca ait FFT spektrumları karşılaştırılmıştır. Ses basınç düzeyleri ve hidrolik basınç arasındaki eşevrelilik spektrumu çıkarılmıştır. Veri işleme, FFT analizi ve çapraz korelasyon Soundbook SAMURAI yazılımı ile gerçekleştirilmiştir. Deneyler göstermiştir ki sistem karakteristiği veya pompa boyutu pompanın gürültüsü üzerinde etkili değildir. Diğer yandan pompa karakteristiği ses spektrumlarında kanat geçme frekansı ile orantılı frekanslardaki sıçramalarla fark edilmektedir. Aynı zamanda çapraz korelasyon sonuçları göstermiştir ki pompa çıkış basıncı pompa giriş basıncından daha önemli bir gürültü kaynağıdır.

Anahtar Kelimeler: Santrifuj pompa, Ses spektrumu, Gürültü, Basınç değişimi.

To My Family

ACKNOWLEDGMENT

TABLE OF CONTENTS

LIST OF TABLES

LIST OF FIGURES

NOMENCLATURE

ψ	Pressure coefficient
φ	Flow coefficient
Q	Volumetric flow rate (m^3/s)
f	Frequency (Hz)
bpf	Blade passing frequency (Hz)
fft	Fast Fourier Transform
D	Diameter (m)
St	Strouhal number
N,n	Pump speed (rpm)
H	Pump head (mH$_2$O)
NPSH	Net Pressure Suction Head
L$_p$	Sound pressure level (dB)
L$_W$	Sound power level (dB)
Q$_\theta$	Directivity Factor
R	Room Constant
p	Pressure (Pa)
ρ	Density (kg/m^3)
S	Surface area (m^2)
δ	Deviation
α	Absorption coefficient
V	Voltage (mV)
V	Linear velocity (m/s)

CHAPTER 1

INTRODUCTION

In this study, small utility pumps which are commonly centrifugal are the focus of interest. Operational noise of small size pumps are to be investigated.

Noise is a result of frequent disturbance in elastic media. This disturbance may be in stagnant air or flowing fluid. Vibration is the main source of noise. Besides the vibration of a machine, the delivered water in the casing of pump in an appliance may also cause noise. A pump is definitely a source of noise with its rotating impeller. Noise is dominated by tones at the *blade passing frequency (bpf)*, which is defined as the frequency of blades passing a stationary point, and higher harmonics. In a centrifugal pump, this is a consequence of the strong interaction between the periodic flow discharging radially from the impeller or cut off leading to the exit duct. A spatially distorted inlet flow field interacting with the rotor may also generate similar tones. In addition to these, broadband noise is generated by trailing edge/flow interaction, turbulent boundary layers and fluctuating separated flow on the impeller blades and housing [1].

For a pump, the operating point resulting with the highest efficiency is called the *design point*. Any other operating condition is related with *off-design* performance. Referring to the flow rate at design point, Q_d, for high specific speed pumps, operating at $Q/Q_d < 1.0$ is more critical and for low specific speed pumps, operating at $Q/Q_d > 1.0$ is more critical [2]. $Q<Q_d$ operations are called *part-load* operations.

Minimum disturbance is satisfied at the design point of a machine, in addition to maximum efficiency. Hence, the possible most silent operation condition is the

design point of a machine with minimum vibration generation. However, blade passing frequency is unavoidable. Off-design operations are distinguishable with enhanced generated noise other than blade passing frequency.

The aim of this thesis study is experimentally observing the acoustic signature of noise at design and off-design conditions for small size pumps as used in house appliances. Experiments in scope of this study are conducted on noise, produced by small size centrifugal pump of a dishwasher.

Previous studies are summarized in Chapter 2. Most of them were focussed on the generation of the blade passage frequency tones. Only few of them have investigated the broadband noise sources, which are identified to be a result of off-design performance.

The dominating phenomena interrelated with off-design can be classified as;
- Cavitation
- Recirculation
- Surging
- Prerotation
- Separation
- Rotating stall

Theoretical background information of these phenomena is presented in Chapter 3.

For pumps, disturbance in a wide band frequency occurs in case of cavitation. Inlet or outlet pressures can also be a source of flow induced noise although pressure levels are marginally stable.

The experiments are conducted in a semi-anechoic test room. Experimental work has been performed in two main phases. In the first group of experiments, characteristics of the centrifugal pump of a dishwasher machine, used in the experiments, are

evaluated. These and the calibration experiments for the semi-anechoic test room are described in Chapter 4.

Chapter 5 describes the set-up and the experimental procedure for the noise experiments in detail.

The experimental results are reported in Chapter 6 and discussed in Chapter 7.

CHAPTER 2

LITERATURE SURVEY

In the literature, there are experiments with estimated results concerning vibrational or acoustical relations between turbomachine performances. Results are usually reported on graphs of frequency spectra. Information concerning amplitudes of levels is rare.

Air Force and Navy-USA studies provide tables about sound pressure levels. Tables 2.1 and 2.2 show estimated sound pressure levels generated by a pump, at a distance of 1 m from its surface, as a function of pump power, from these studies [3].

Mongeau et al. [4] have investigated the phenomenon of rotating stall in a centrifugal pump with air. The pump impeller was operated without diffuser and casing. Measurements of acoustic noise radiated in the pump surroundings were made in parallel with fluid dynamic measurements in order to establish correlations [4]. Choi et al. conducted an experimental investigation of noise generation by large-scale flow-field instabilities in a pump rotor, referring to the study by Mongeau et al.

In both of the studies, Worthington Model D-1011 water pump impeller was operated with air. The impeller had seven backward swept blades and its performance characteristics were determined from the static pressure difference (Δp) between the impeller inlet and the discharge, at various flow rates. The non-dimensional static pressure rise through the impeller ($\psi = \Delta p / \rho V_{tip}^{2}$), plotted versus flow coefficient ($\varphi = Q / \pi b D V_{tip}$) constitutes the non-dimensional operating curve for the impeller. The impeller was originally designed to have a maximum efficiency at

4

$\varphi = 0.062$. Extensive flow measurements were performed over a range of flow rates at $\varphi = 0.06$ (low flow rate), $\varphi = 0.09$ (medium) and $\varphi = 0.12$ (high flow rate) [1].

The frequency of the sound pressure radiated by the pump was scaled by using either the ratio of the acoustic wavelength and the impeller diameter or the ratio of the frequency over the blade passing frequency (bpf). The non-dimensional Strouhal number is introduced and defined as the ratio of frequency to bpf [4];

$$St = (fD/Vtip)(\pi/n)(f/bpf) \qquad\qquad (2.1)$$

Figure 2.1 illustrates the experimental set-up used by Choi et al., where the blade passing frequency was in the range from 280 Hz to 420 Hz. In the experiments, the unsteady discharge flow field was measured with both single and crossed hot-wire probes. To measure the unsteady static pressure on impeller blades, pressure transducers manufactured by the PCB Corporation (model 103A11) were used. The impeller blade surface pressure is measured by a sensor attached to the opposite side of an impeller blade through a 2.5 mm diameter pinhole [1].

Table 2.1. Overall pump sound pressure levels at 1 m from the pump. (From Army, Air Force and Navy, USA 1983a.) [3]

Speed Range (rpm)	Drive motor nameplate power	
	Under 75 kW (dB)	Above 75 kW (dB)
3000-3600	72+10log kW	86+3log kW
1600-1800	75+10log kW	89+3log kW
1000-1500	70+10log kW	84+3log kW
450-900	68+10log kW	82+3log kW

Table 2.2. Frequency adjustments for pump sound power levels. Subtract these values from the overall sound pressure level to obtain octave band sound pressure levels. (From Army, Air Force and Navy, USA 1983a.) [3]

Octave band centre frequency (Hz)	Value to be subtracted from overall sound pressure level (dB)
31.5	13
63	12
125	11
250	9
500	9
1000	6
2000	9
4000	13
8000	19
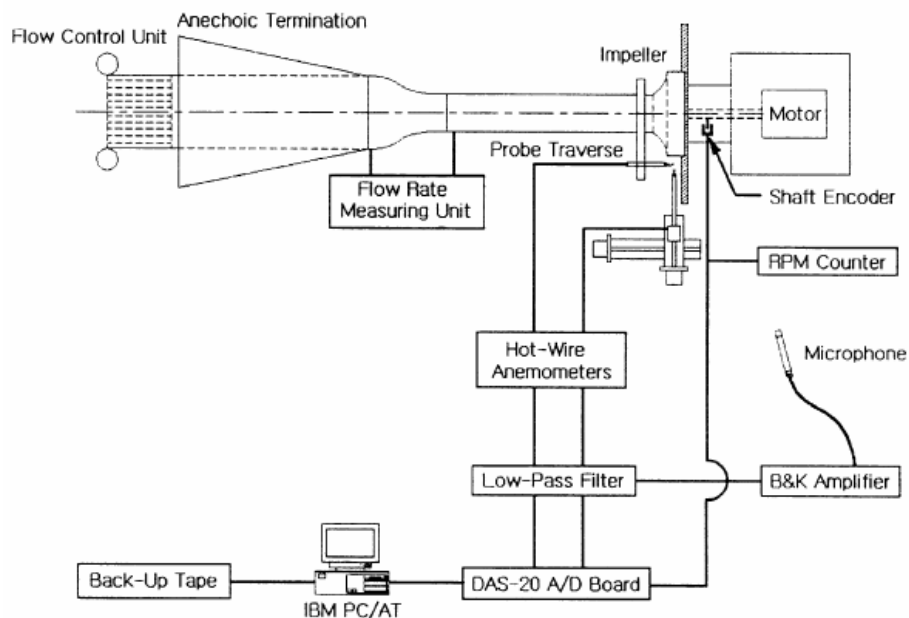
Figure 2.1. Test set-up and data acquisition system [1].

The spatial distribution of the stall pattern has a strong influence on the sound radiation efficiency. The modal components of the flow fluctuations that are a multiple of the number of impeller blades generate most of the radiated noise [4]. Comparison of noise and the surface pressure spectrum is shown in Figure 2.2. One can see by observing the surface pressure spectrum that the peaks at m = 7 and 14 generate more acoustic noise than the modes with higher amplitudes (m = 8, 9…, 13) [1]. This phenomenon was first observed by Mongeau et al. Radial back plate was installed to the seven-bladed pump impeller in order to keep the discharge velocity in radial direction. Then, the fundamental frequency of the radiated noise appears to be 74% of the bpf, corresponding to the frequency of the m = 7 harmonic of the fluctuations. Similarly, the m = 14, m = 21, m = 28, … modes act like the second, third, forth, … harmonics in the noise spectra. The reason for this is that the flow oscillations are in phase throughout the impeller for these modes. Other modal components will not radiate as much because flow oscillations have circumferential phase variations from blade to blade, and acoustic self-cancellations occur in near field [4].
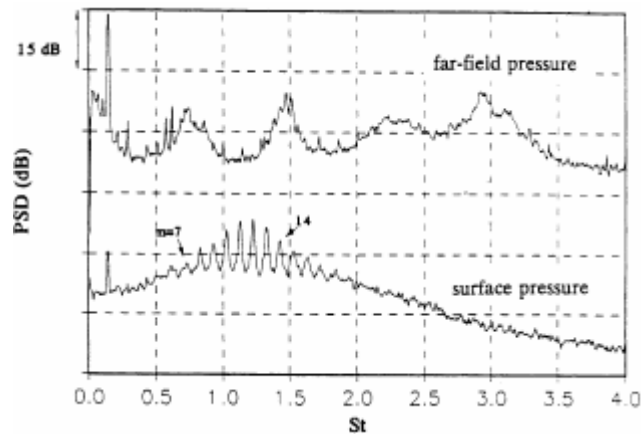
Figure 2.2. Farfield noise and surface pressure spectrum [1].

All the modes in the pressure spectrum will generate noise from each blade, but those with mode numbers equal to the number of impeller blades (m = 7, 4, 21 …) generate noise that is synchronized. Acoustic waves from different blades interfere with each other and result in relatively less noise propagating to the far field at the frequency. It is also expected that the sound pressure level of the spectrum peaks measured at the far field are influenced by the acoustic cancellation due to the non-compact distribution of the sources on seven different impeller blades. The coherence between the noise and the surface pressure, shown in Figure 2.3, demonstrates the high correlation level at the frequencies corresponding to m = 7 and 14. The peak at St $\approx$ 0.14, i.e., shaft rate, in the noise and coherence spectra is generated from the slip-ring unit mounted on the motor shaft. The high coherence level at m = 7 and 14 indicates that the peaks in the noise spectrum are generated from the unsteady pressure fluctuation on the impeller blades [1].
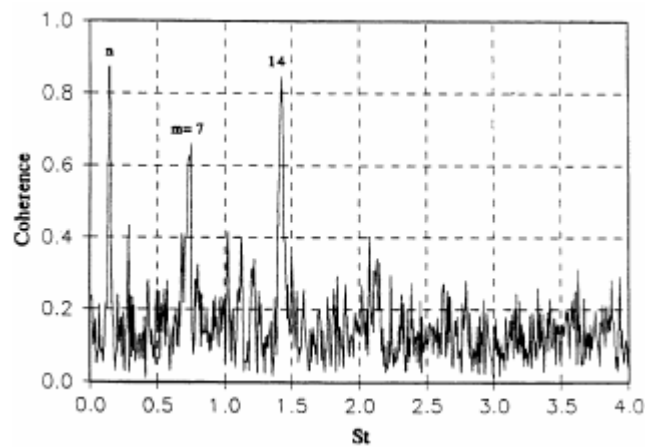
Figure 2.3. Coherence of farfield noise and surface pressure spectrum [1].

Choi et al. [1] have reached to the following conclusions:

(1) The jet-wake flow pattern found in the impeller blade passages induces a strong vorticity field near the trailing edge of each blade. This vortex is unstable and it influences the flow discharging from the adjacent passage, and destabilizes the jet-wake flow in the passage.

(2) The unstable passage flow causes a periodic pressure fluctuation on the blade surfaces. This unsteady flow is found to be coherent from blade to blade and forms a rotating instability pattern around the impeller discharge. This instability pattern has a rich harmonic content and a well-defined precessing speed.

(3) The rotating discharge instability in the impeller discharge is very similar in its behaviour to the phenomenon known as rotating stall found in centrifugal impellers and diffusers. However, the origin of each of these flows and some of their characters are found to be quite different.

(4) The surface pressure spectrum measured at the trailing edge of each blade revealed a cluster of peaks, which were identified with integer mode numbers. The modes synchronized with the number of impeller blades (mode 7, 14, 21, …) were shown to generate noise more efficiently than the other modes. Consequently, the radiated noise spectra were shown to be dominated by harmonically related broad humps [1].

Mongeau et al. [4] called acoustic phenomena related to the impeller rotational speed, for example the blade passage frequency, a Strouhal effect. An acoustic phenomena occurring at a fixed frequency, independent of the rotational speed was called Helmholtz effect.

$$He = \frac{fD}{a} = St \cdot Ma \cdot \frac{n}{\pi} \qquad\qquad (2.2)$$

Pure tones at bpf and its harmonics were observed when impeller was operated with a volute casing. Results at $\varphi=0.06$ for ten different rotational speeds are in figure

Figure 2.4. Source spectral distribution function measured in the inlet duct vs. St number. Volute-type discharge configuration, $\varphi = 0.06$ [4].

This low-frequency acoustic signature is typical of centrifugal fans and centrifugal water pumps in which the interaction of spatially rotating non-uniform mean flow at the impeller discharge with the stationary cut off or with diffuser stator vanes, generating noise [4].

When impeller without casing was examined sharp humps were present in the acoustic signature. Results for $\varphi = 0.09$ and $\varphi = 0.03$ are given in Figure 2.5 and 2.6.
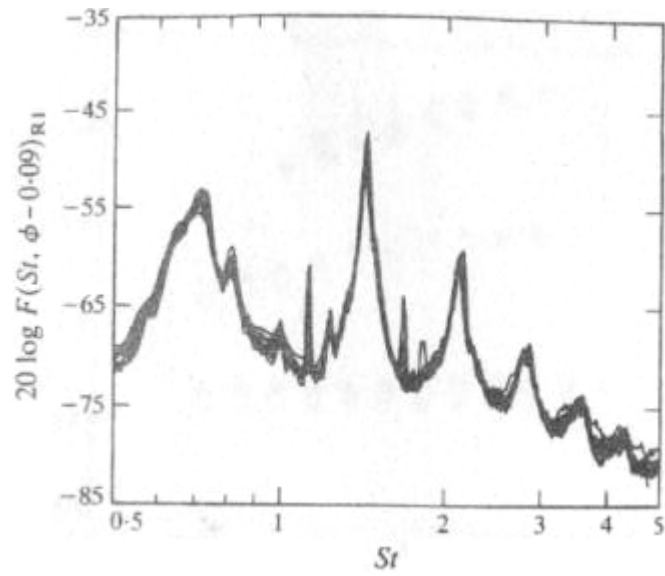
Figure 2.5. Source spectral distribution function measured in the inlet duct vs. St number. Rounded impeller configuration, $\varphi = 0.09$ [4].
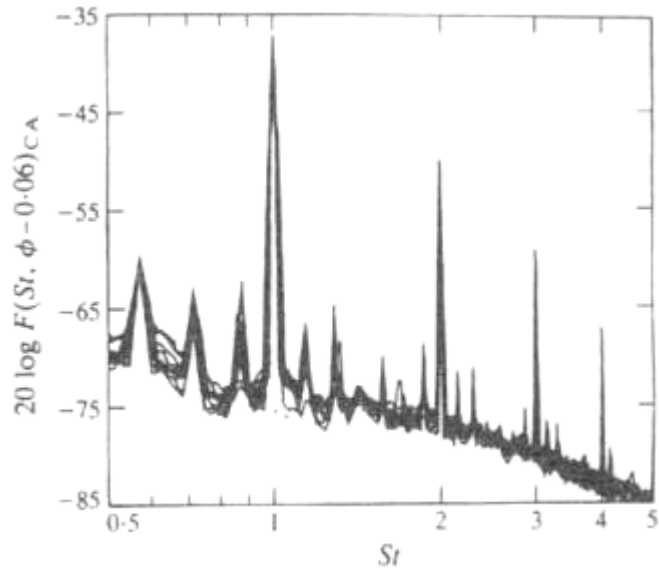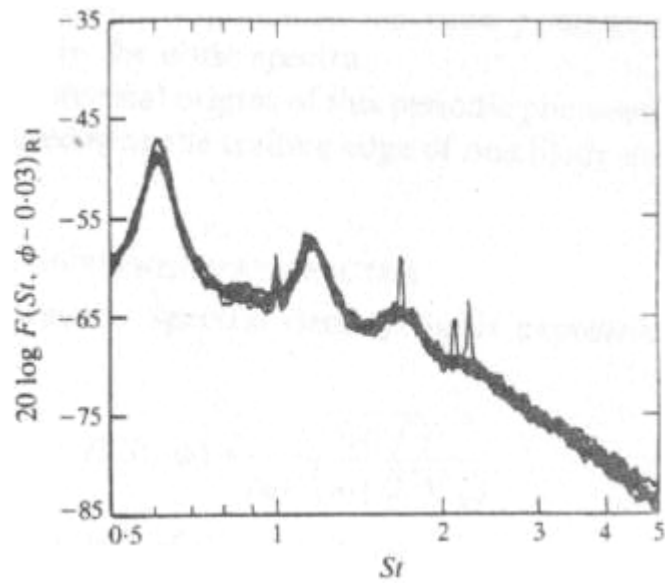

Figure 2.6. Source spectral distribution function measured in the inlet duct vs. St number. Rounded impeller configuration, $\varphi = 0.03$ [4].

The most remarkable feature of these peaks was that they occur at frequencies other than the bpf and its harmonics. There were virtually no more peaks at the bpf and its harmonics. This was an indicator of fundamental change in the sound generation process. Comparing these figures, important changes in the relative magnitude of each peak can be observed. The tonal character of the source is most pronounced at $\phi = 0.09$ where the peaks are sharper and higher in magnitude relative to the underlying broadband component of spectra. The hump become broader as the flow rate is increased or decreased from this operating point [4].

It was concluded that when a blade passage was partially obstructed, or when blades were not alike or not evenly spaced, the modes that are not multiples of the number of blades radiate noise [4].

Maaloum et al. [5] tested the rotor of a fan, equipped with the same diameter of the rotor hub and with a contour duct having an internal diameter equal to the external diameter of the fan, for various flow rates at a constant rotational speed. Measurements of the unsteady aerodynamic pressure were collected at 20 mm from the trailing edge of the machine, or acoustic pressure in far field at 4 m from the fan in accordance with the standard ISO 5136. The pressure fluctuations near the trailing edge explain the aerodynamic instability produced by the machine. The blades passing frequency and their various harmonics are well highlighted.

The level of the acoustic pressure varies strongly according to the flow rate, presenting a minimum near the nominal point. A boundary layers separation occurs at low flow rate because of an important effect at the leading edge of blades. The unsteady forces become influential, resulting in an emergence of the discrete frequencies noise. The spectral analysis in the Figure 2.7 shows that the level of the acoustic pressure is strongly attenuated when the inlet flow is homogenized.
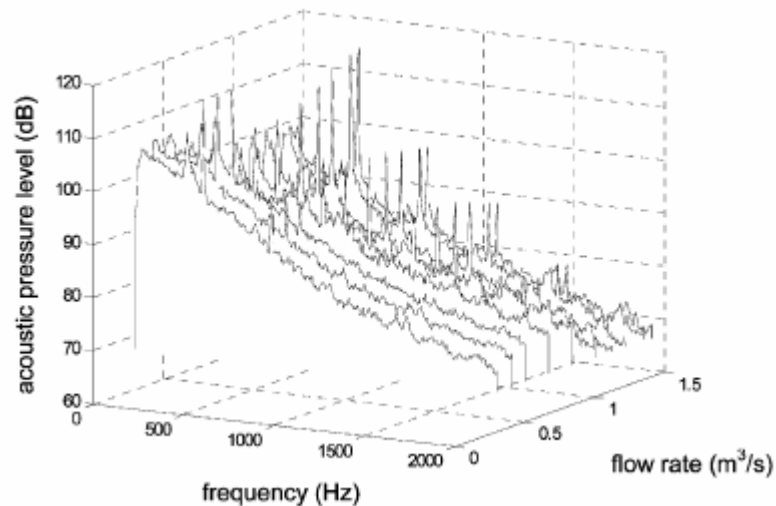
Figure 2.7. Acoustic pressure level vs. the flow rate. N = 2850 rpm, measure in near field by Maaloum et al. [5]

This experimental work showed that the presence of the duct contour and lack thereof have a great influence on the acoustic signature of the studied fan. The discrete frequencies noise and the broadband noise were affected by this flow organization at the aspiration as well as the strong influence of the distortions upstream on the acoustic specifications of the machine [5].

By Breugelmans and Şen [6], time-dependent static pressure measurements on the suction pipe wall and on the volute diffusing part front shroud wall were performed with fast response piezoelectric pressure transducers. Time-dependent yaw angle measurements in the suction pipe were measured near the outer radius of the inlet suction pipe, using vane-potentiometer systems at 180º apart test stations, for the complete pump characteristics. Resulting plots show that the flow is perfectly axial and steady at nominal flow rate, Q_N. As the flow rate is decreased, slight fluctuations start to be observed. Large fluctuations are observed in a small flow region which is referred to as prerotation. Further throttling makes the inlet flow tangential at measuring stations and the angular fluctuations are strongly diminished. The flow

13

tends towards a solid body rotation in the suction pipe. The tangential velocity and pressure perturbations are maximum in the small range where the *transition from axial to tangential flow* at the outer radius takes place. The spectral analysis of the angular fluctuations is performed for the flow rates Q = 0.717, 0.700, 0.680, 0.647, 0.447 and $1.00Q_N$. The blade passing and its harmonics are the dominant frequencies at the nominal flow rate. The energetic content of the fluctuating components shifts from blade passing to sub impeller rotational frequency during the transition, whereafter the low frequency content diminishes again. The sub impeller frequency is similar to a rotating stall cell phenomenon in compressors. At the occurrence of prerotation, the power spectra for the inlet flow angle change drastically. The low frequency contribution is increased by three orders of magnitude and the dominant frequencies are 27 Hz and 44 Hz with the harmonics at $Q = 0.717Q_N$. The content at the low frequency range is further increased by two orders of magnitude at $Q = 0.700Q_N$ and harmonics have disappeared. The large flow fluctuations have only a low frequency content. The largest angular deviations were observed at $Q = 0.680Q_N$. Further throttling decreases the contribution of the low frequencies in the power spectra and a slight shift towards higher frequencies is observed at $Q = 0.44Q_N$. Towards the shut-off, a continuous reverse flow seems to be established near the outer part over 360º of the circumference of the suction pipe and also the low frequencies contribution will further diminish [6].

Ali [7] used a closed circuit type set up with a transparent suction pipe immediately before the pump, in order to visualise the suction flow pattern. NPSH tests were performed at four constant flowrates. Pump characteristic was determined with head and power output at three different speeds vs. flowrates. Recirculation inception point test conditions were inlet velocity vs. flowrate. In this test the flow velocity, in direction opposite to the main flow, near the impeller was measured using a pitot tube. At partial flow rates, with reduced NPSH, suction pressure signal and vibration signal are recorded. The pump was in surge at approximately $0.8Q_d$ and approximate suction pressure was 42.46 kPa. The frequency of this cavitation related surge was found to be approximately 0.1 Hz [7].

Neise et al. [8] preferred to place microphones on a rotatable plate and measure the sound pressure circumferentially at a specified radial distance. In a study on Rotating Blade Flow Instability in Axial Turbomachines, with Kameier, meeting the requirements of DIN 24 163 for measurement of the aerodynamic fan performance was considered. Outlet duct of the tested fan was anechoically terminated in order to avoid axial standing waves in the duct, resulting from the sound reflections [8]. It was in accordance with the standardized in-duct method DIN EN 25 136, ISO 5136. A 1/2 in microphone equipped with a turbulence screen was mounted in a rotatable duct section. The pressure fluctuations on the interior casing wall were monitored by using 1/8 in microphones (Brüel & Kjaer type 4138) which were mounted flush with the inner wall. To measure the unsteady blade pressures, four miniature pressure sensors were mounted in small grooves of the impeller blades. Experimental set-up is shown in Figure 2.8 [9].
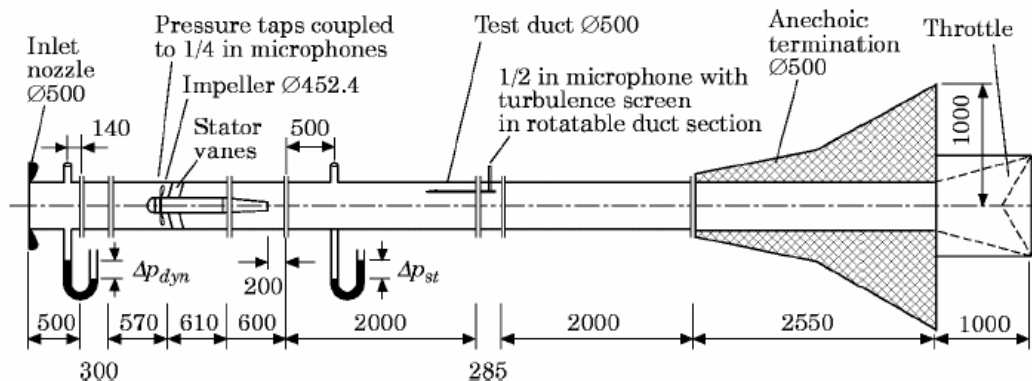

Figure 2.8. Experimental set up by Kameier and Neise (dimensions in mm) [9].

In a study by Holste and Neise [10], dominant aerodynamic noise sources of a propfan model were examined to achieve conclusions about the noise generation mechanisms. It was emphasized that:

- One can establish an experimental technique for assessing the tonal noise characteristics of aircraft engines which does not require ideal acoustic environmental conditions, i.e., free field conditions.
- One can predict the sound pressure radiated into the far field based on the acoustic pressure modes measured in the acoustic near field [10].

Near field pressure fluctuations (in the exit plane) of the propfan model CRISP (Counter Rotating Integrated Shrouded Propfan) were measured with conventional 1/4 inch microphones. The measurements were performed in the open test section of the German-Dutch Wind Tunnel.

For the unsteady pressure measurements, two microphone rakes, each carrying three 1/4 inch microphones with nose cones at the radial positions, placed on a rotatable cylinder at 180º angular distance were mounted directly on the hub behind the exit plane. Six microphones were moved in the circumferential direction and with this arrangement, the pressure fluctuation were measured at 120 equally spaced angular positions ($\Delta\varphi = 3º$).

Three two-channel FFT analyzers (HP-3562A) were used to measure the spectra of the six microphone signals. The analyzers were triggered by a one-pulse-per-revolution signal to obtain the averaged complex pressure spectra.

In this way all non-rotational signal components, such as the turbulent pressure fluctuation of the jet flow, were suppressed. To eliminate leakage effects due to variations of the impeller speed, the sampling frequencies of the FFT analyzers were synchronized with the rotor speed [10].

Bayraktar [11] performed experiments on noise of a centrifugal fan in order to verify numerical results and investigate effect of geometrical modifications on the fan noise character.

In her work, experiments were conducted in the Anechoic Room of Arçelik A.Ş. Research and Development Centre, on a reflective surface and Semi-Anechoic Room of Arçelik A.Ş. Dishwasher Plant. Sound pressure measurements were conducted with five microphones around the fan surfaces. Microphones were placed 0.5 m away from reference fan surfaces. The fan was hanged such that the reference point was 0.8 m above the reflective ground. A-weighted sound pressure level spectra are plotted in 1/3 octave band.

Bayraktar [11] concluded that, the acoustical characteristics of the fan can be numerically simulated if the fan blades are regularly distributed. On the other hand, if the fan had unevenly distributed blades, it was recommended to perform laboratory experiments for the analysis of the radiated noise.

Neise and Arnold [8] have reported that very good agreement is observed between in-duct sound power levels and free-field sound power levels in the frequency region of higher order sound propagation with the revision of the in-duct method ISO/DIS 5136:1999. Two other basic acoustic test methods based on sound pressure measurement are the reverberation room methods ISO 3743-1/2 and the free-field method over a reflecting plane ISO 3744. These methods are used for the determination of sound power radiated into free space. The two reverberation room methods are applicable to small-to-medium size fans only because of the size restriction in the standards. The free-field method ISO 3744 covers the one-third octave band frequency range from 50 to 10 000 Hz and is applicable to all types of noise. A detailed comparison of freefield method, reverberation room method, and in-duct method as applied to fans was given by Neise [12].

ISO 3743-1/2 are applicable only for octave bands between 125 Hz and 8000 Hz, while ISO 3744 and ISO 5136 cover the range 50-10000 Hz for one-third octave bands. Up to 315 Hz, the in-duct method yields the best accuracy. It becomes slightly less accurate than the freefield method for frequencies up to 4000 Hz [8]. One can deduce from Table 2.3 that accuracy of free filed method is significantly low for

frequencies 50-80 Hz. Between the centre frequencies 400 Hz and 5000 Hz, the method is really accurate.

Acoustic anechoic chambers are used in free-field method. These test rooms have surfaces that absorb more than 99% of incident sound energy over the frequency range of interest, thereby approximating a free field. Room surfaces are covered with sound-absorbing wedges. Anechoic chambers are used in precision-grade measurements [13]. Semi-anechoic room includes one perfectly reflecting surface which is usually the floor. Absorption coefficient for that single surface must not exceed 0.06. Semi-anechoic room is defined as the room in which a free field over a reflecting plane is obtained. It is a fact that an isolated surface, perfectly reflecting for sound applications, is a symmetry plane.

Table 2.3. Estimated standard deviations of reproducibility of sound power levels according to various ISO-Standards [8].

f (Hz)	ISO 3743-1	ISO 3743-2	ISO 3744	ISO 5136
50			5·0	3·5
63	—	—	5·0	3·0
80			5·0	2·5
100			3·0	2·5
125	3·0	5·0	3·0	2·0
163			3·0	2·0
200			2·0	2·0
250	2·0	3·0	2·0	2·0
315			2·0	2·0
400			1·5	2·0
500	1·5	2·0	1·5	2·0
630			1·5	2·0
.	.	.	.	.
.	.	.	.	.
3150			1·5	2·0
4000	1·5	2·0	1·5	2·0
5000			1·5	2·5
6300			2·5	3·0
8000	2·5	3·0	2·5	3·5
10 000			2·5	4·0

CHAPTER 3

THEORY OF PART LOAD PERFORMANCE PHENOMENA IN PUMPS AND NOISE

In this study, part loaded performance phenomena are investigated for off-design operating conditions. Basic principles of acoustics have guided the interpretation of the experimental work. A few number of reasonable assumptions based on these acoustic principles have facilitated the comparison of measured sound data.

3.1. Part Loaded Performance Phenomena in Pumps

One can summarize the off-design phenomena interrelated with part loaded performance as follows;

- Cavitation
- Recirculation
- Surging
- Prerotation
- Separation
- Rotating stall

3.1.1. Cavitation

Cavitation is defined as the local vaporization of the liquid due to the dynamic conditions. Local vaporization may occur when the local pressure reduces to the

vapour pressure of the liquid at the local temperature. Therefore, cavitation occurs where the fluid velocity is high and the general local pressure level is low [14]. It is possible to approach the velocities necessary to produce cavitation at the discharge if only the concept of discharge recirculation is introduced [15].

Net positive suction head (NPSH) is a parameter used to track the occurrence of cavitation. Available NPSH is the difference between minimum head in the system and vaporization pressure of the fluid per unit weight. In a pump, the fluid has the minimum energy just before entering the pump i.e. at the suction side. In a turbine, fluid looses energy when exiting from the turbine. Required NPSH is the minimum value to avoid cavitation. Critical i.e. required NPSH is low at design point meaning that the best operating point is $Q/Q_d = 1.0$, not only from the highest efficiency point of view but also from cavitation point of view. For $Q/Q_d > 1$, NPSH values decreases and finally classical cavitation occurs. For $Q/Q_d < 1$, NPSH increases but the critical NPSH also increases accordingly. Consequently it brings the pump to the *part load cavitation condition* [2].

3.1.2. Recirculation

At partial flow rates, the pressure field is distorted and at point of *recirculation*, pressure gradient reverses and a localised reversal of the flow takes place. Earliest experimental studies reveal that recirculation starts to develop at a flow rate significantly lower than the design flow and after it has appeared, its intensity starts to increase with any further reduction in the flow rate, reaching a maximum at shut-off [16]. Recirculation can occur at the discharge or the suction side of the impeller or at both sides. Other than these, a third recirculation phenomenon is the flow of fluid from the impeller discharge back to the suction side through the wear ring clearances. Above design flow rate, such as in part-loaded operation, suction recirculation should start due to the favourable effect of increased difference between

the fluid and the blade relative angles. However, this increases the flow velocity and consequently prevents the liquid returning to the suction side [15].

3.1.3. Surging

Phenomenon of sudden drop in delivery pressure is called *surging*. Pumps with unstable characteristic surge when they are part loaded. The origin of the pressure variation lies in the fact that, at certain times, the pressure in the discharge line is higher than the pump head and a tendency to reverse flow appears. When the pumps capacity is reduced by throttling the discharge, additional resistance in the throttling valve requires higher heads, until the capacity Q_b, shown in the Figure 3.1 is reached. At the instant the capacity is reduced below Q_b, the pump head will be lower than the pressure in the system and there will be a tendency for the flow to reverse with the operating point moving from point B to shut-off, A. But as soon as the flow is reduced the pressure in the system begins to drop and the pump will again begin to discharge into the system until the pressure is built up to the maximum head at capacity which is at capacity Q_b. Since the demand from the system is only for a $Q < Q_b$, there will again be a tendency reverse the flow and the cycle will be repeated [17].

A form of instability usually referred to as *inlet surging* or *cavity surge* exists within the recirculation range. This surge mode is associated with low flow and reduced NPSH values, which results in a large spinning cavity growing and collapsing in the suction pipe. This, in turn, causes a surge with a very high amplitude and low frequency pressure pulsations [2].
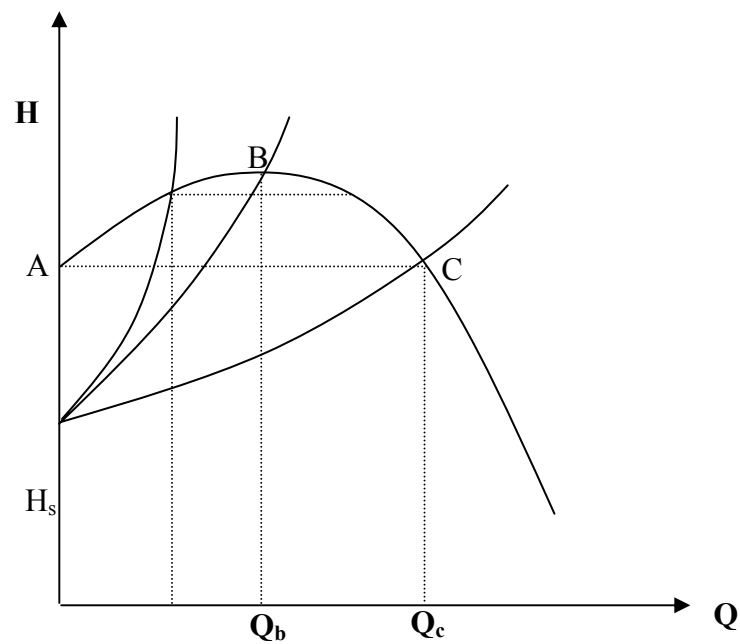
Figure 3.1. Unstable pump characteristics [17].

3.1.4. Prerotation

One of the low NPSH problems is *prerotation*. A negative angle of incidence, caused by partial flow rate, is the main reason of prerotation. In the presence of prerotation the pressure distribution in the suction pipe assumes a parabolic shape, as shown in Figure 3.2 [18]. The result of this parabolic shape is explained such that; the reduction of flow rate causes the flow suddenly become three dimensional. That flow has negative axial velocity component at the outer part of the pipe (reverse flow) and flow is forward in the inner part of the pipe.
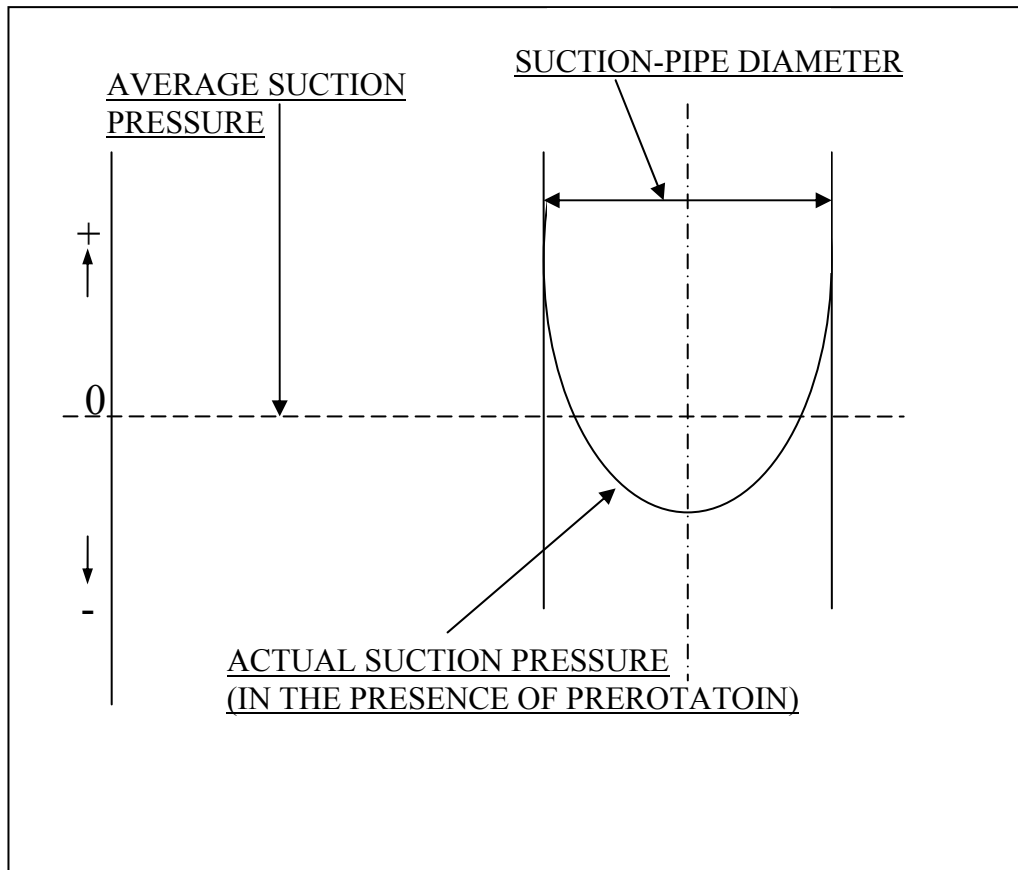
Figure 3.2. Pressure distribution at the suction pipe causing prerotation [18].

The considered flow has an overall swirling character where the tangential component has its maximum value near the wall and decreases regularly towards the rotation axis. The swirling flow has the same direction of rotation as the impeller, hence named as "Prerotation" [6]. In high specific speed impellers, the low-pressure zone created by prerotation contacts a large portion of the blades inlets [18]. After prerotation, low pressure zone fills with vapour and flow cross-section is reduced. Consequently velocity increases and so angle of incidence. As soon as the cavity collapses because of eliminated prerotation, the total cross-sectional area of the suction pipe becomes available for the liquid flow. This, in turn, reduces the velocity of incoming liquid and the incidence angle. Consequently, prerotation develops again, starting the cycle [18].

23

Observations by Yedidiah [16] showed that further lowering NPSH stopped prerotation and on the trailing faces of blades large cavities are converted into large vapour-filled cavities. This can be observed in the Figure 3.3. As a result, the pump began operating quietly again, although it developed a lower total head.
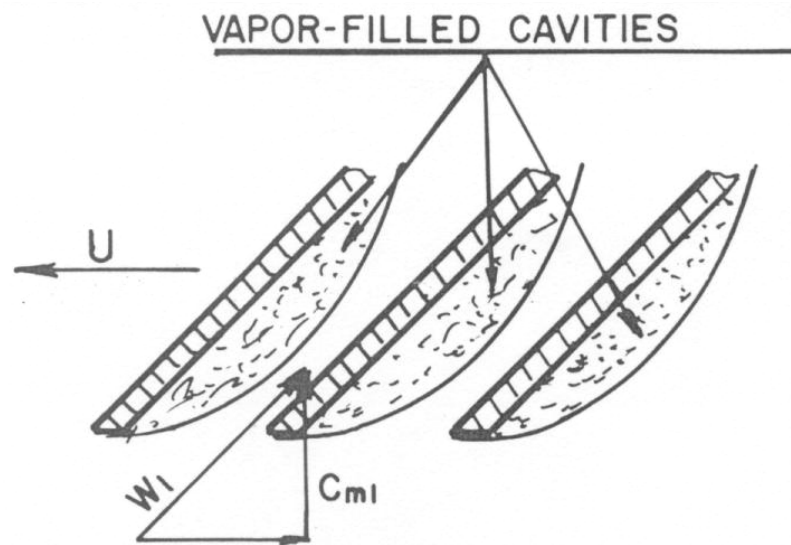

Figure 3.3. Vapour-filled cavities blocking blade passage [18].

3.1.5. Separation

Separation is a result of adverse pressure gradient. Fluid can flow in the direction of negative pressure gradient. If this gradient increases and it is equal to zero at some location, flow can also continue with inertial forces even in the positive pressure gradient direction. After a while, inertial forces cannot recover this adverse pressure gradient and the fluid cannot follow the contour of blades. After separation, pressure remains constant on the blade surface.

3.1.6. Rotating stall

High incidence, which may be a result of reduced flow rate, causes the blade row to *stall* eventually, which is followed by *local separation* [15]. It was indicated that mixed flow and axial impellers do not have good off-design performance and for these pumps, at high specific speeds, stalling and consecutive phenomena are more likely initiated at part-load operations [2].

A non-uniformity in the flow may cause a breakdown in one channel, say B in the Figure 3.4, causes fluid to be deflected in such a way that channel C receives fluid at
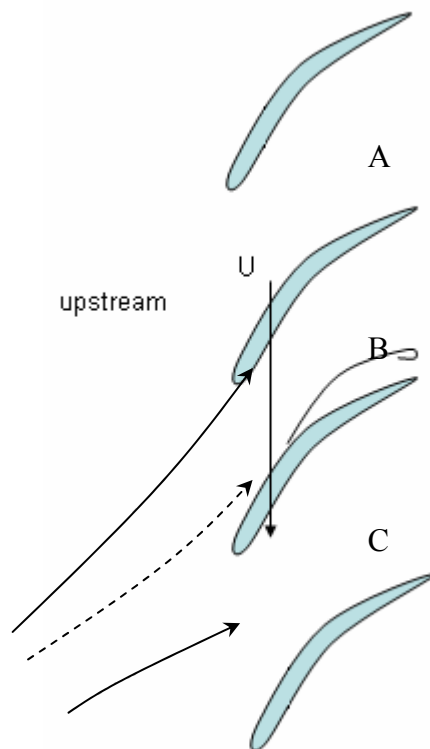
Figure 3.4. Rotating stall [19].

a reduced angle of incidence while the other channel, A, receives at an increased incidence and consequently *stalls*. That flow is recovered by reduction of incidence to channel B. Thus the stall passes from channel to channel [19]. This phenomenon is called *rotating stall* since its rotation is in opposite to the direction of impeller rotation.

3.2. Noise

Unwanted sounds are classified as noise. Sound of a pump carries no intelligible information and if the pump is operated in a house appliance, sound will interfere with human comfort. Therefore, one should try to depress sound as much as possible. Sound of the pump investigated in this study is the noise generated by impellers and flowing fluid.

3.2.1. Definitions on Sound

Small amplitude pressure perturbation in an elastic media is called *sound* if fluctuation frequencies are in-between audible range. Sound is known to be a wave phenomenon and 20 Hz – 20 kHz is the audio range [3].

Instantaneous sound pressure level is the value of the fluctuating pressure superimposed on the atmospheric static pressure due to the presence of a sound wave. *Sound pressure levels* (L_p) are expressed in deci-Bells (dB) as a meaningful value for time-mean-square of the instantaneous sound pressures:

$$L_p = 10 \cdot \log(\frac{p_{rms}^2}{p_{ref}^2}) \quad dB \qquad (3.1)$$

where p_{ref} = 20 μPa.

L_p depends on distance from the sound source, acoustical characteristic of the environment, directional characteristics of the source with respect to listening position [3].

Sound power is the rate at which airborne sound energy is radiated by a source. It is defined for a source and it is constant at any location. *Sound power level* (L_W) is used to express sound power. A relation between sound power level and sound pressure level counting location and environment is:

$$L_p(f) = L_W + 10 \cdot \log(\frac{Q_\theta(f)}{4 \cdot \pi \cdot r^2} + \frac{4}{R(f)}) \quad dB \qquad (3.2)$$

For an omnidirecitonal source;

$Q_\theta = 1$ In air (suspended)

$Q_\theta = 2$ On a surface

$Q_\theta = 4$ Intersection of two surfaces

$Q_\theta = 8$ Intersection of three surfaces

Q_θ is a function of frequency but not distance.

$R(f)$ is the room constant expressed in m^2 units [3]:

$$R(f) = \frac{S \cdot \overline{\alpha}}{1 - \overline{\alpha}} \qquad (3.3)$$

$$\overline{\alpha} = \frac{\Sigma(\alpha \cdot S)}{\Sigma S} \qquad (3.4)$$

In free field R(f) → ∞. Free field is supposed to be *anechoic*. Anechoic literally means without echoes. Anechoic refers to the absence of audio reflections. The closest thing to this situation in nature is the great outdoors, but even here there are

reflections from the ground, various objects, etc. It is almost impossible to create a truly anechoic environment, as there is no such thing as a perfect sound absorber. At high frequencies, it is possible to create near-anechoic conditions, but the lower the frequency, the harder this is because the absorption is wavelength dependent [20].

Above definitions are adequate for steady and continuous noise. However, usually noise may be continuous but not steady. Time-varying sound is usually described statistically in terms of *equivalent sound pressure level* (L_{eq}) for a given period:

$$L_{eq} = 10\log\frac{1}{T}\int_0^T 10^{L(t)/10}\,dt \qquad\qquad (3.5)$$

Exceedence level is defined to express sound pressure level which is exceeded for a percent of time. L_x, generally expressed in dB(A), is the sound pressure level exceeded for *x%* of the time. L_1 will give a measure very close to the maximum sound pressure level and L_{99} will give a measure very close to the minimum sound pressure level [3].

3.2.2. Noise generation

Blade passing frequency (bpf) is an expected noise generator during turbomachine operation.

Minimum noise level can be obtained when a turbomachine is operating at design point and the above listed off-design conditions are interrelated with noise generation.

The presence of flow induced phenomena such as cavitation and recirculation is indisputable when individual peaks, which represent blade passing frequency or rotational speed with their harmonics, are masked out by the growth in the wide band

frequency range [15]. Vibration threshold increases in a wide and high frequency band, usually between 500 Hz and 2000 Hz, because of bubbles [21]. It was cited that the peak noise corresponds to the point where erosion damage is most severe. The noise level drops as cavitation increases possibly due to absorption of sound by large cavities. For low frequencies (0-3 kHz) mechanical noise is likely to interfere with measurements [7].

Surge is its own a frequently repeating cycle and fluctuations in head and capacity are also accompanied by power and speed oscillations [17].

The special landmark of prerotation source of noise is a sound like heavy hammer blows which occurs at a relatively low frequency. Yet this noise may stop because of further decreasing NPSH and pump head also declines [18].

Rotating stall may lead to aerodynamically induced vibrations resulting in fatigue failures [19].

In the literature, it is also stated that some impellers become noisy when they are cut down. The reason is that inlet to outlet diameter ratio exceeds half and consequently the suction recirculation capacity suddenly increases to the discharge recirculation capacity [15]. Diameter ratio holds special interest for axial pumps since it must exceed 0.5.

CHAPTER 4

EQUIPMENT AND CALIBRATION

Small scaled centrifugal pumps which are used to circulate water into dishwashing machines were tested in the scope of this study.

The maximum value of size independent type number i.e. *specific speed* for a centrifugal pump is 1.0. Operating with specific speed less than unity, a centrifugal pump can give high head rises to the fluid with low volumetric flow rates. A simplified diagram for a centrifugal pump is shown in the Figure 4.1.
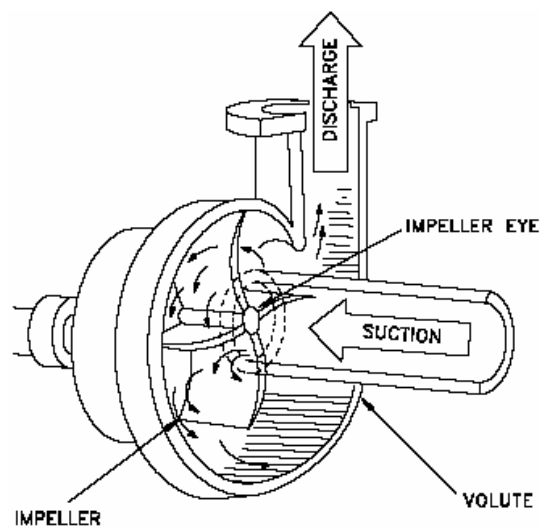

Figure 4.1. A simplified diagram of a typical centrifugal pump [22].

Experimental studies in the scope of this thesis were conducted with two pump casings provided by ARÇELİK. Pump casings differ from each other with their sizes and they are assembled with impeller and the same electric motor. First pump casing is the smaller one that will be mentioned as *small pump* and the larger pump casing will be mentioned as *large pump*. General specifications of pumps such as design point and type number at different operating speeds are given in Table 4.1. Impellers have seven backward blades

Table 4.1. General specifications of investigated pumps

Small Pump				**Large Pump**			
Rotational speed (rpm)	Q_d **(l/s)**	H_d **(m)**	**Type number** $\dfrac{\omega Q^{1/2}}{(gH)^{3/4}}$	**Rotational speed (rpm)**	Q_d **(l/s)**	H_d **(m)**	**Type number** $\dfrac{\omega Q^{1/2}}{(gH)^{3/4}}$
2175	0.64	2.01	0.62	2175	0.94	2.11	0.72
2375	0.61	2.57	0.55	2375	1.18	2.4	0.80
2570	0.74	2.87	0.60	2570	1.24	2.85	0.78
2770	0.72	3.63	0.53	2770	1.24	3.5	0.72
2965	0.8	4	0.56	2965	1.38	4	0.74
3160	0.64	5.58	0.42	3175	1.46	4.6	0.73
3365	0.96	5	0.59	3375	1.52	5	0.74

A frequency converter was used to regulate pump speed and obtain seven different speeds from 2200 rpm up to 3400 rpm.

Pumps were placed in a *semi-anechoic test room* available in the Fluid Mechanics Laboratory of Middle East Technical University Mechanical Engineering

Department. *Anechoic* or *semi-anechoic test rooms* are constructed to simulate free field. Anechoic test rooms are composed of six sound absorber surfaces and semi-anechoic test rooms have one sound reflector five sound absorber surfaces. Reflector surface which is obviously a symmetry surface is usually the floor.

Properties of the semi-anechoic test room used in the experiments are:

- Dimensions: 3 x 4 x 2.4 m
- Ceramic coating on the floor
- Rock Wool, Glass Wool, Styrofoam on the walls and ceiling coatings
- Approximately 20 cm wall thickness
- Tulle curtain (to prevent dust)

An air conditioner is placed on the ceiling. This A/C is allowed to run unless acoustical data are collected.

The pumps were put on a tripod with metallic legs and wooden seat in the test room. In order to minimize the reflective effect of this tripod, legs were coated with rock wool and a foam plate was placed between the wooden seat and the pump. Sound absorption coefficients of rock wool and foam, which were used to cover tripod, were compared in an Acoustic Impedance Tube available in Acoustics Laboratory of METU Mechanical Engineering Department.

Soundbook Acoustic Measuring System from SINUS Messtechnik GmbH was used to collect and store sound pressure data.

Prior to correlation experiments, the test room was calibrated according to ISO 3745. The characteristics of pumps are measured. The pump characteristic curves for seven different rotational speeds are given in Appendix B.

4.1. Calibration of Test Room

The test room is first calibrated for the point of semi-anechoic test room criterion in order to verify the extent of deviations of the test room from ideal semi-free field condition. This work was performed in accordance to the International Standards ISO 3745, which is one of the ISO 3740 series [23]. The methods defined in the standards are specified on two surfaces, enveloping noise source in the test room. These surfaces are sketched in the Figure 4.2. Equation is applied for both surfaces and *area-weighted level difference* was defined:

$$L_{W1} - L_{W2} = L_{p1} - L_{p2} - 10 \cdot \log(\frac{\dfrac{Q_{\theta 1}}{4 \cdot \pi \cdot r_1^2} + \dfrac{4}{R_1}}{\dfrac{Q_{\theta 2}}{4 \cdot \pi \cdot r_2^2} + \dfrac{4}{R_2}}) \qquad (4.1)$$

Since semi-anechoic room is assumed to be an approximation to free filed R(f) → ∞. Q_{θ} is a function of frequency but not distance. Consequently equation (4.1) turns out to be:

$$\delta = L_{p1} - L_{p2} - 10 \cdot \log \frac{S_2}{S_1} \quad dB \qquad (4.2)$$

To comply to International Standards ISO 3745, measurements of sound pressure level should give such a result that area-weighted level difference is equal to or less than 0.5 dB. If $|\delta| \leq 0.5 \ dB$ is satisfied, the test room and measurement surface, S_1, are considered to be appropriate.

Hemispherical surfaces are defined to collect the data. Ratio of test areas, S_2/S_1, is not allowed to be less than 2. The microphone locations on the second surface shall correspond to those on the first surface. For this purpose, ropes, determining the path for two microphones, are tightened from the centre of floor to the top corners of the room.
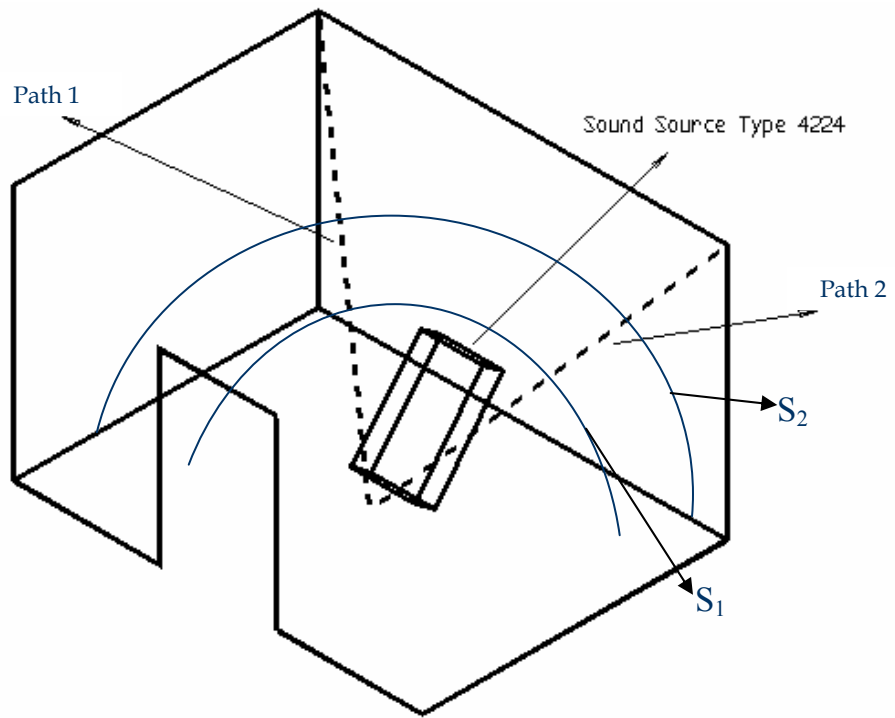
Figure 4.2. A sketch for the calibration of the test room.

Average sound pressure levels, emitted by Brüel & Kjær Sound Source Type 4224, for both surfaces were measured using Brüel & Kjær microphone Type 4166 and HP 35665A Dual Channel Dynamic Signal Analyser. Sound Level Calibrator Type 4230 was before collecting data. The area-weighted level difference was calculated and sound pressure levels were plotted for 1/3 octave band frequencies in Figure 4.3. The general trend of both spectra is similar. However, minor differences in quantative values are observable.

Almost none of the area-weighted level difference has satisfied the necessary condition, $|\delta| \leq 0.5 \, dB$, because of some experimental restrictions such as:

- Sound source is not exactly omni-directional.
- Sound Source Type 4224 is not exactly at centre.
- The second path is closer to the sound source and reactive effects are dominant.

Real sound power levels are given in the sound source specifications. With the help of equation (3.2), $L_W - L_p$ values were calculated. In free field R(f) becomes $\rightarrow \infty$. Directivity depends on the frequency. Then equation (4.1) leads to;

$$\frac{L_{W2} - L_{p2}}{L_{W1} - L_{p1}} = 10 \log\left(\frac{S_2}{S_1}\right) \qquad (4.3)$$

Theoretically, S_2/S_1 is constant for all centre frequencies. Figure 4.4 shows the resultant graphic for area ratios. In the experiments this ratio was not constant. However, it was almost constant between the centre frequencies 315 Hz and 800 Hz, where the deviations were relatively small for path 1, blue curve in Figure 4.4. In the experiments conducted on the second rope, the deviations were slightly greater. But still the area ratios have oscillated around 3. The latter was probably a result of reactive effects.
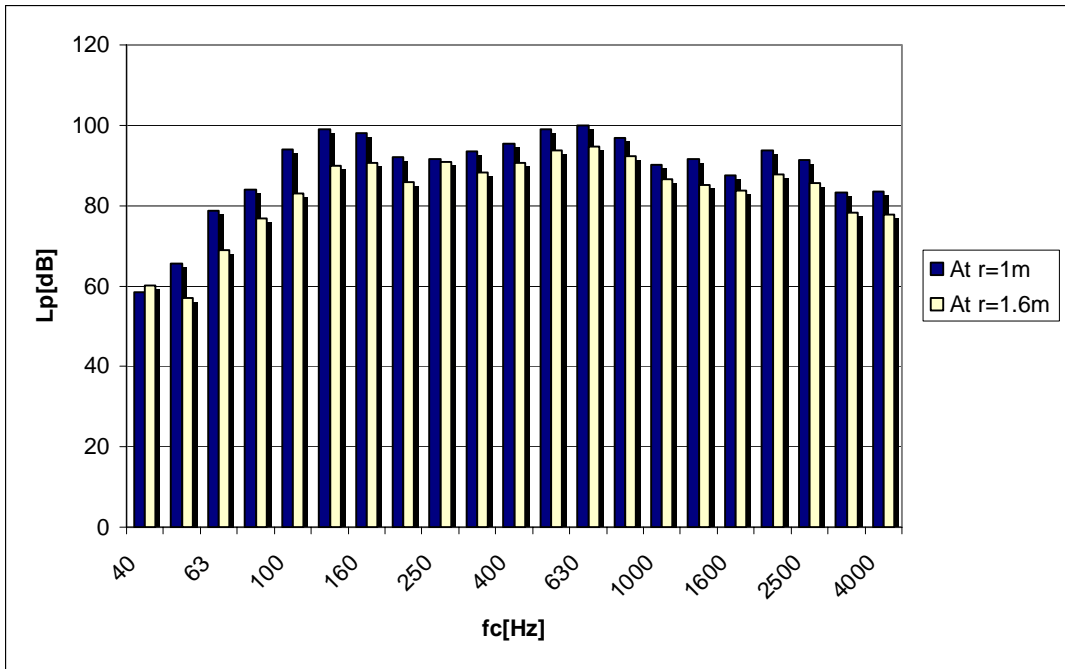
(a) Path 1
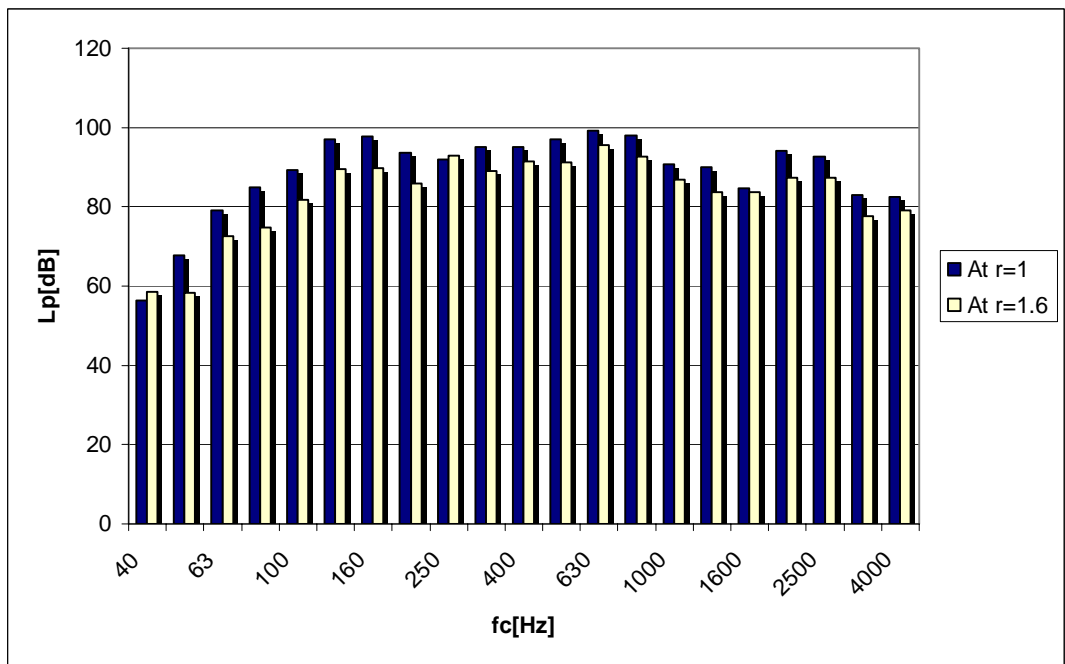
(b) Path 2

Figure 4.3. Sound Pressure Levels for Semi-Anechoic Test Room Calibration on Path 1(a) and Path 2 (b).

36
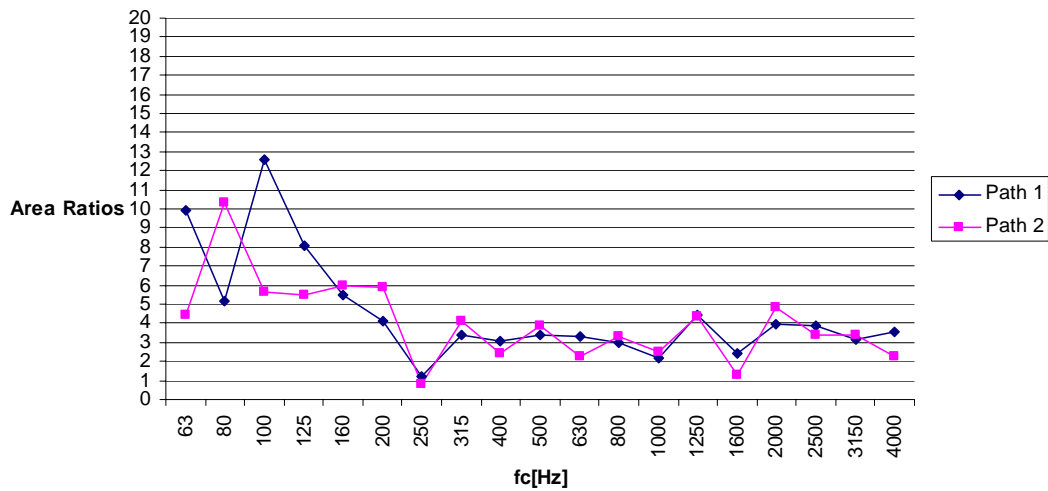
Figure 4.4. Acceptable centre frequencies of the test room that simulate free-field.

The semi-anechoic test room available in the Fluid Mechanics Laboratory gives very accurate results for free field simulating measurements between centre frequencies 315 Hz and 1000 Hz. The results are still good between 200 Hz and 1600 Hz and, can be considered acceptable between centre frequencies 160 Hz and 4000 Hz. Raw data and sample calculation are given in the Appendix A.

4.2. Sound Absorption Coefficient Comparison

Absorptive materials used in the construction of the test room and also covering the tripod in the test room have been tested. Absorption coefficients of foam and rockwool are compared to each other. Experiment set consists of a rigid plastic tube with internal diameter 69 mm and length 1.2 m, sample holder made of dense tuff, amplifier unit, dual beam 20 MHz oscilloscope and a microphone tracing in the tube. Circular specimens were placed at the end of the tube with the sample holder.

Sample holder is a very rigid and reflective material. It was chosen on purpose not to transmit but to reflect energy which was not absorbed by the specimen. Procedure of this experiment necessitates considering sound energy data at the antinodes and nodes. For a perfectly reflecting surface, nodes are available. However, specimens were absorptive and because of phase difference no zero amplitude was available, instead numerically minimum amplitude was observed. Another assumption is that specimen surface was assumed to be antinode. Absorption coefficient is frequency dependent. Minimum and maximum amplitude values were recorded for three different frequencies for each specimen. Absorption coefficient was calculated starting from the ratio of reflected energy to the total energy:

$$r = \frac{E_r}{E_t} = \left(\frac{V_1 - V_2}{V_1 + V_2} \right)^2 \qquad\qquad (4.4)$$

$$\alpha = 1 - r \qquad\qquad (4.5)$$

Where V_1 and V_2 denote the maximum and the minimum amplitude, respectively, for a specified frequency. Results are summarized in Appendix A.

4.3. Pump Characteristics Tests

Speeds of ARÇELİK dishwasher pump are; 2175 rpm, 2375 rpm, 2570 rpm, 2770 rpm, 2965 rpm, 3160 rpm, 3365 rpm. Characteristics of the pumps for these seven different speeds are determined using the facilities of the product development laboratory of ARÇELİK. The same reservoir has served for suction and discharge and is large enough to prevent elevation difference. Discharge was to the atmosphere and geometric head was not to exceed 20 cm. Inlet and outlet pressures were measured with pressure transducers connected to the points nearest to the casing. Besides the frictional losses, the only minor head loss is due to the gate valve at the end of discharge line. Flow rate was controlled with this valve. Discharge water was

collected for 10 seconds and weighed, in order to determine the volumetric flow rate. For the large pump, this procedure was applied for 5 seconds because of high flow rates. Pump speed was controlled with a frequency converter. Electrical power was supplied by a variant fixed to 230 V. A wattmeter was connected between the variant and frequency converter to provide just a curve but not real numerical values for efficiency of the pumps.

Starting from the fully open position, data is recorded according to 50 mbar increments of outlet pressure. At least three values are recorded for each data and results are checked for *Chauvenet's Criterion*. For very small flow rates, more frequent data are preferred. However, the pumps are unstable and especially for the large pump, surge phenomenon is probable and sudden efficiency drops are unavoidable in the graphs. In Appendix B pump performance characteristic graphs and efficiency curves are given.

CHAPTER 5

EXPERIMENTS

In this study, near field sound pressure level of the small size centrifugal pump is the focus of interest. Pressure fluctuations in the pump inlet and outlet are also examined.

In the Semi-Anechoic Test room, there should not be any sound source but only the pump. Hence, the pump with driving motor is placed in the centre of the room and water tanks are placed out of the semi-anechoic test room to prevent water flow noise interfering with pump noise. Pump noise experiments are conducted with a sound data acquisition system, Soundbook SAMURAI. Microphones of type GRAS 26CA-61988 and GRAS 26CA-61989 are connected to 8 channel Soundbook to record fft spectra of pump noise. Technical specifications for microphone preamplifiers are given in Appendix F.

In order to investigate frequency of pressure fluctuations, pressure transducers of FGP XPM5 2900 and FGP XPM5 2899 are connected to Soundbook and fft spectra for water pressure fluctuations are reported. Technical specifications for pressure transducers are given in Appendix F.

5.1. Experimental Set-Up

The experiments are conducted with two different set-ups in order to find out whether system characteristics will affect the noise data of the pump. The first set-up is designed with a low geometric head and the second one has a high negative

40

geometric head. Elevation of the pump and microphone positions are also different for two set-ups. It was aimed to improve sound level measurement technique for the second set-up.

Some detailed photographs of experimental equipment and set-ups are given in Appendix C.

5.1.1. Set Up 1

The small pump sucks the water from a reservoir with a cross-sectional area of 5 m^2. That provides constant water level. Geometric head is about 40 cm. Discharge is to the atmosphere. Major losses are dominant in the system and elbows with the discharge gate valve cause minor head losses. Sketch of the Set-up 1 is shown in Figure 5.1, comprising the reservoirs, semi-anechoic room, pump and pipe connections. The pump is placed on a tripod in the middle of the room at an elevation of 60 cm. Rigid steel pipe system is used on the floor to avoid any interference with the reflective property of the floor. On the other hand, rubber hose is used for all connections other than those on the reflective floor in order to avoid reflections. Outlet pressure is measured with pressure transmitter and inlet pressure is measured with a U-tube mercury manometer. A wattmeter is connected between frequency converter and the motor in order to record true values of electrical power consumed by the pump. Microphones are placed 1 m away from the pump. All the measuring equipment assembly is placed in the semi-anechoic test room. Figure 5.2 shows the picture of the pump and the measuring equipment in the Semi-Anechoic Test Room. Four microphone positions are illustrated in the Figure 5.3.
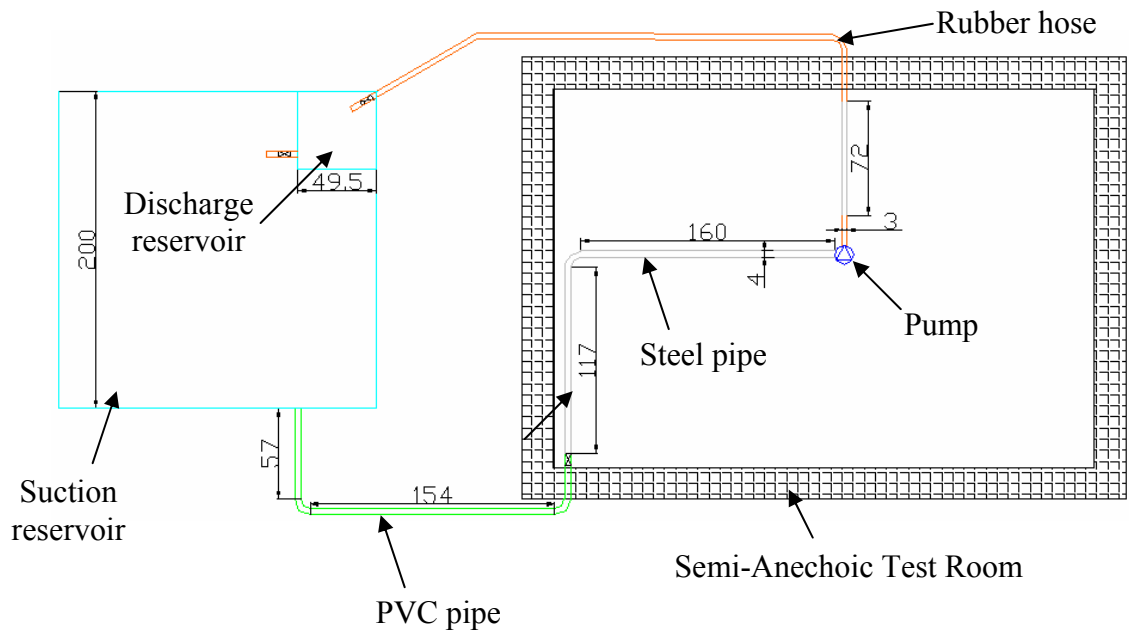
(a) Top view.
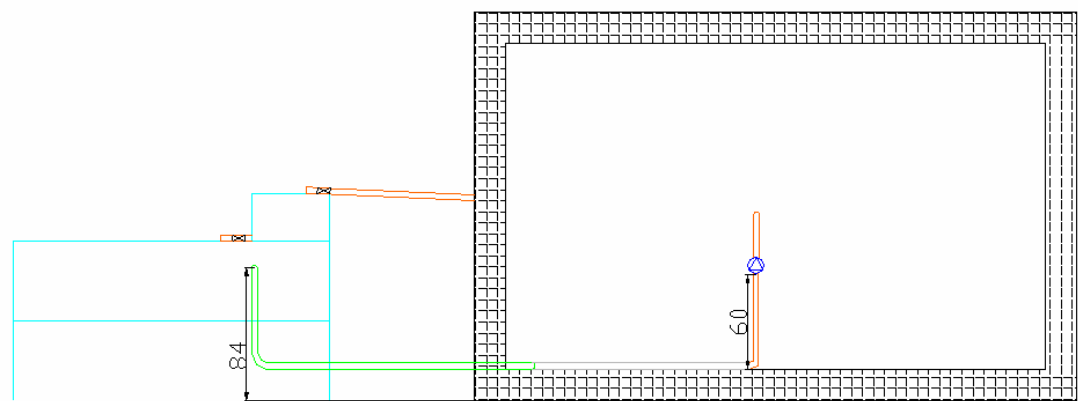
(b) Front view.

**Figure 5.1.** Schematic view of Set-Up 1
(Dimensions are given in cm)
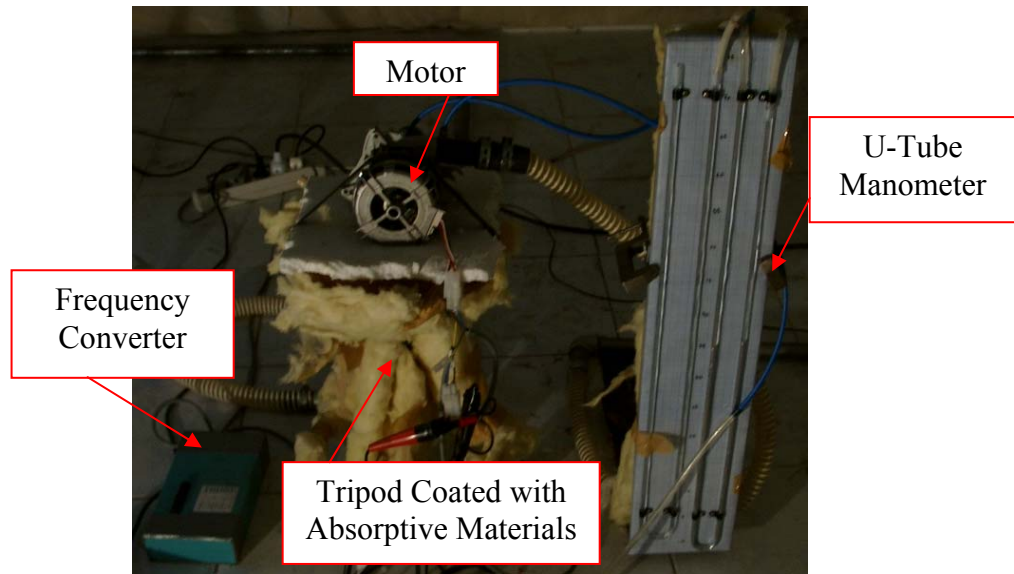
(a) Right side photograph.
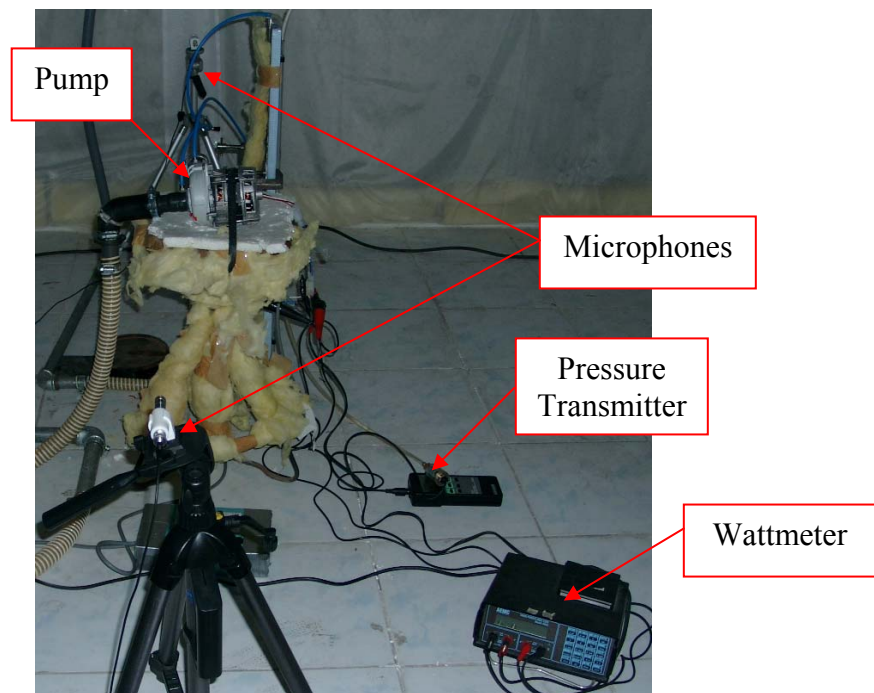
(b) Front side photograph.

Figure 5.2. Pictures for the small pump and experimental equipment
in the Test Room.
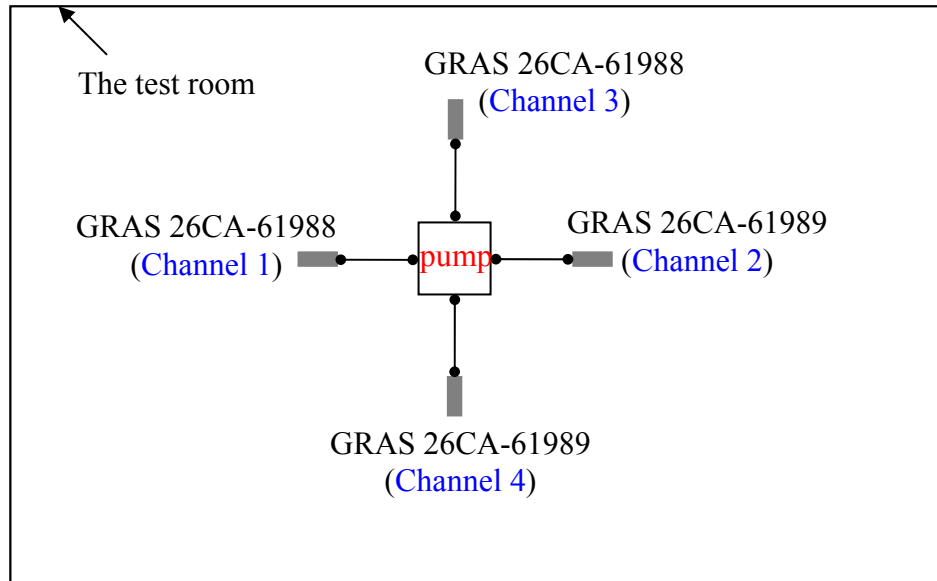
Figure 5.3. Microphone positions for Experimental Set-up 1

5.1.2. Set Up 2

In order to avoid cavitation, suction reservoir is elevated and the pump is operated in a system with negative geometric head. Suction reservoir has a cross-sectional area of 0.42 m^2. A second pump is used to feed back suction tank to provide constant water level. Suction and discharge tanks are kept out of the semi anechoic test room. Schematic view of the Set-up 2 is given in Figure 5.4. Inlet and outlet pressures are measured with pressure transmitter. Electrical power consumed by the pump is measured with wattmeter. The pump is placed in the middle of the room at an elevation of 1.1 m. Microphones are placed 1 m away from the pump on the diagonal of the test room. Picture of pump and microphones is shown in Figure 5.5. All the measuring equipment are placed in the semi-anechoic test room. Four microphone positions are illustrated in the Figure 5.6.
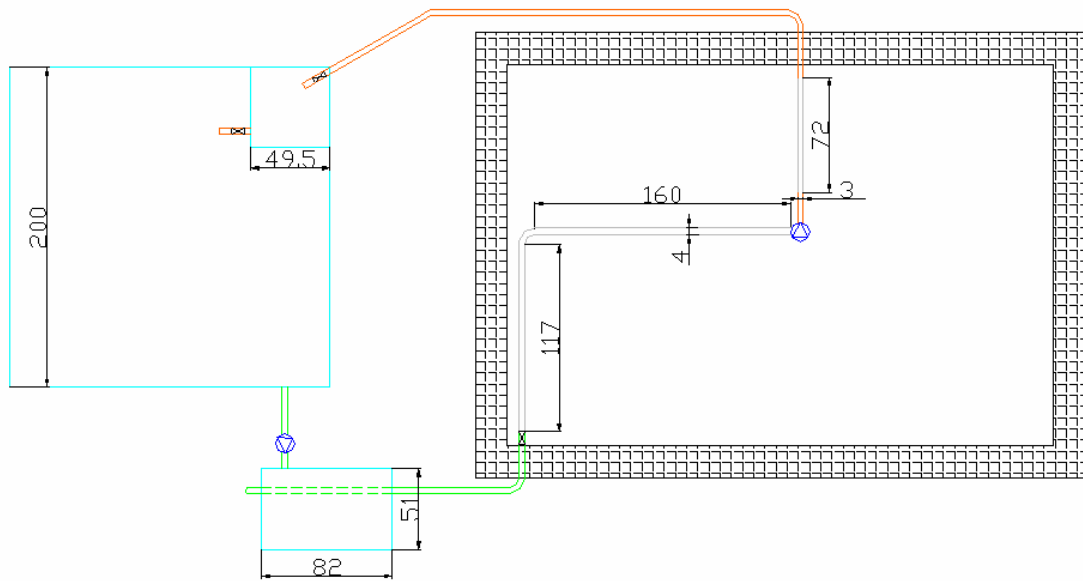
(a) Top view.
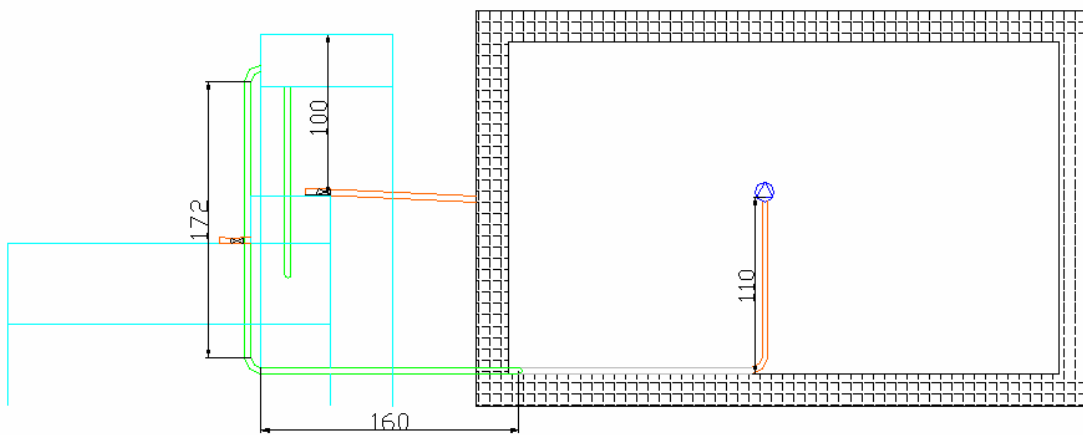
(b) Front view.

Figure 5.4. Schematic view of Set-up 2
(Legends as in Figure 5.3(a))
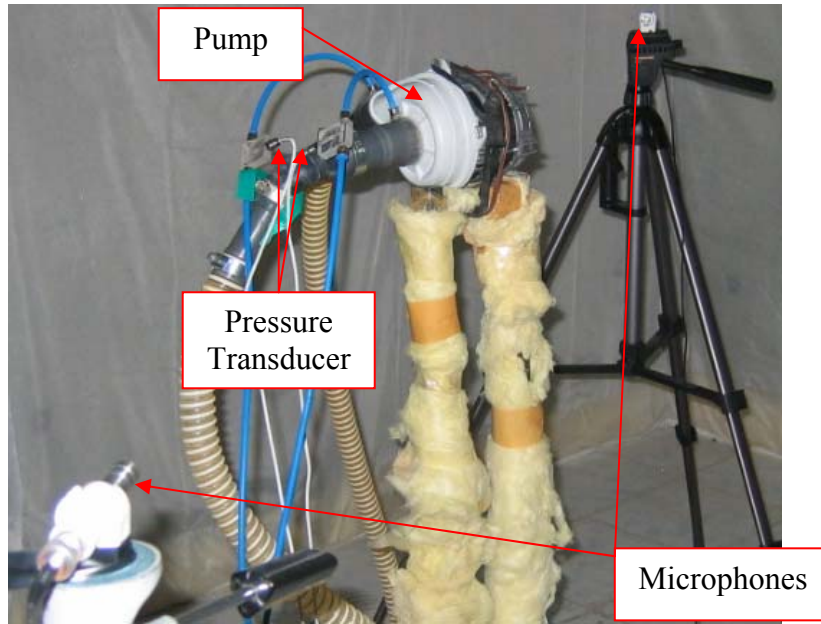
Figure 5.5. Photograph of the large pump and microphones in Set-up 2.
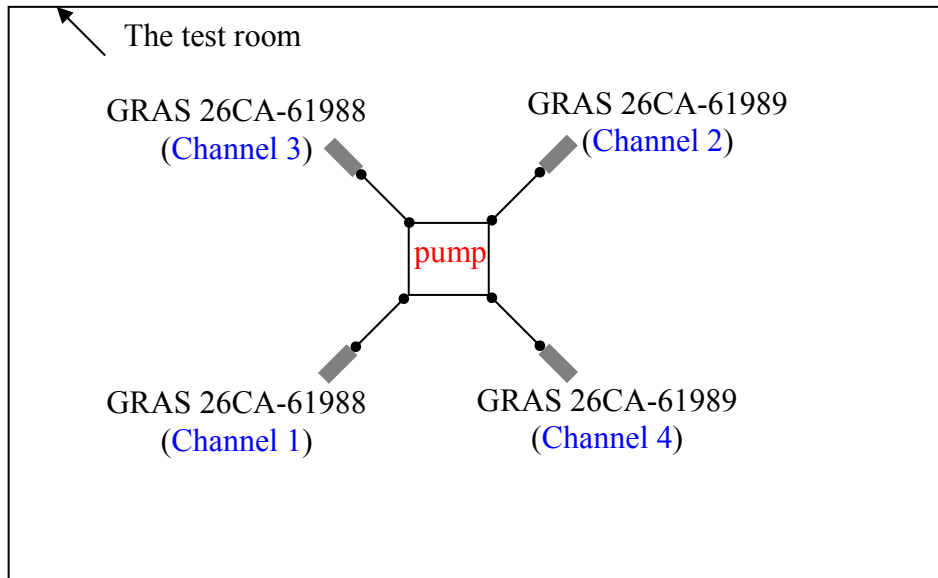
Figure 5.6. Microphone positions for Experimental Set-up 2

5.2. Experimental Procedure

Three sets of experiments are conducted to collect sufficient data for comparison of pump noise in different systems and with different characteristics.

① Small pump noise measurement,

② Small pump noise and time dependent inlet-outlet pressure measurement,

③ Large pump noise and time dependent inlet-outlet pressure measurement.

Besides, solo motor noise is also detected. Background spectra are recorded for each experiment. Pumps were not operating but water noise out of the test room was provided and background noise was measured. Time dependent pressure data were also recorded during background measurements.

5.2.1. Sound of the Small Pump

Sound of the small pump is determined with a series of experiments on Set Up 1. Only the pump noise is recorded besides the pump characteristic data. Similar to the pump characteristic experiments, flow rate is adjusted with the gate valve at the end of discharge line according to outlet pressure and four measurements are recorded for each flow rate. A scale is placed on the wall of discharge tank to measure volumetric flow rate.

Pump noise measurements are conducted for the above mentioned seven different pump speeds at various flow rates.

5.2.2. Sound and Pressure Variation of the Small Pump

Pump noise measurements are repeated on Set-up 2. Time dependent inlet and outlet pressure data are also recorded synchronous. FGP XPM5 2900 and FGP XPM5 2899 pressure transducers are used at the inlet and outlet of the pump respectively.

Similar to the previous experiments, flow rate is adjusted with the gate valve at the end of discharge line according to outlet pressure. The same discharge tank with the scale is used in the second experimental set-up.

The aim of repeating experiments is obtaining oscillations of pressure values in order to compare them with sound pressure values.

5.2.3. Sound and Pressure Variation of the Large Pump

Large pump is connected to Experimental Set-up 2. Pump noise is measured and time dependent inlet and outlet pressure data are recorded synchronous. FGP XPM5 2900 and FGP XPM5 2899 pressure transducers are connected to the inlet and outlet of the large pump respectively.

Flow rate is adjusted with the gate valve at the end of discharge line according to outlet pressure. The discharge tank with the scale is used. In this third set of experiments, only three system characteristics are examined. The first one is the shut off condition. The second one is with the fully open discharge valve. Finally the third one is conducted such that the outlet pressure is adjusted to the average of that of the two previous measurements.

CHAPTER 6

EXPERIMENTAL RESULTS

Off-design performances of centrifugal pumps are investigated with a special interest on noise. Two pumps which differ in size are operated in two different set-ups which have different geometric heads. Small pump is operated in both set-ups in order to investigate effect of system characteristics on the noise of pump. Inlet and outlet pressure fluctuations are also recorded in Set-up 2 for both pumps, in order to correlate sound data with hydraulic pressure.

Fast Fourier Transform and Cross Analysis are conducted with software SAMURAI. Hanning window is applied for fft and linear repeat is used for averaging in cross analysis. Peak frequencies at the sound and pressure spectra are normalized with reference to bpf and they are compared for all experiment sets.

Solo motor noise is considerably low. Sound level spectra are plotted in narrow band and 1/3 octave band in the Appendix E. Peaks at 50 Hz and 100 Hz are caused by electric noise. Peaks at 630 Hz and 1000 Hz are the effect of ball bearings and peaks at the vicinity of 2200 Hz is the result of stator blades on the electric motor. Sound level of stator blade peak is usually not masked on pump noise spectra. Peaks on motor noise spectra, having low sound level, are not sharp on pump noise spectra.

Background sound level is high for low frequencies. Sound level drops and stabilizes by approaching to bpf and it has no effect on peak frequencies. Spectra for background sound pressure level and pressure variation are plotted in the Appendix E. There are peaks on the background pressure spectra at 1670 Hz and at its harmonics. These peaks sometimes mask hydraulic pressure peaks.

49

6.1. Sound of the Small Pump

The average sound pressure levels of four microphones are calculated and plotted in cascades, in Figures 6.1-6.7. Peak at bpf is observed for seven pump speeds. 2 bpf, 3.5 bpf and harmonics of 3.5 bpf are distinguishable for most of the pump operation conditions. These dominating peak frequencies are listed according to pump rotational speed in Table 6.1. Table 6.2 summarizes the peak frequencies other than harmonics of 3.5 bpf.

Table 6.1. Dominant peak frequencies observed on the sound spectra for seven rotational speeds of small pump.

Rotational Speed (rpm)	bpf	2 bpf	3.5 bpf	7 bpf	10.5 bpf
2175	✓	✓	✓	✓	
2375	✓	✓	✓	✓	
2570	✓	✓	✓	✓	✓
2770	✓	✓		✓	✓
2965	✓			✓	
3160	✓				
3365	✓		✓	✓	

The sound pressure levels are obtained at different operating points. Hence, shut off, 0.23 l/s, 0.34l/s, 0.46 l/s are obtained at 2175 rpm. This is shown in cascade form in Figure 6.1. The bpf for seven blade pump rotating with a speed of 2175 rpm is 254 Hz. In Figure 6.1, second harmonic of bpf is at 500 Hz especially marked when the valve is fully closed. When the valve was fully open the flow rate became 0.5 l/s. At the design point, pump delivers 0.6 l/s of water so that 0.5 l/s is close to design point with an efficiency of 60%.

Table 6.2. Secondary peak frequencies on the sound spectra
for seven rotational speeds of small pump.

Rotational Speed (rpm)	Non-Dimensional Peak Frequencies (f/bpf)						
2175					5.3		
2375				4.3			8
2570				4.3	5		
2770		2.7	3.56				
2965	1.73	2.6	3.6	4.33		6	
3160	1.76	2.71	3.39	4.2	5.15	5.82	6.64
3365			3.7	4	5.47		

When the pump was operating at 2375 rpm, the noise data was collected at five different operating points. These are, shut off, 0.3 l/s, 0.45 l/s, 0.5 l/s and fully open valve condition. Fully open valve resulted with 0.52 l/s. Sound spectra are for that rotational speed is given in Figure 6.2 in cascade form. When the pump is operating at 2375 rpm, bpf is 277 Hz. There are high amplitudes at 5.2 (1450 Hz) bpf and 6.14 bpf (1700 Hz) especially when the pump efficiency is higher than 55%.

Shut off condition, 0.19 l/s, 0.4 l/s, 0.5 l/s, 0.57 l/s, 0.59 l/s, 0.63 l/s were examined when the pump rotational speed was 2570 rpm. Noise spectra cascade for that pump speed is depicted in Figure 6.3.

When the pump speed was 2770 rpm, the pump was operated at eight different operating points one of which was shut off condition. Flow rates 0.18 l/s, 0.36 l/s, 0.51 l/s, 0.58 l/s, 0.63 l/s, 0.65 l/s and 0.67 l/s were tested. Noise spectra in cascade form for 2770 rpm is shown in Figure 6.4. For that pump speed bpf is 323 Hz and it is observed for shut off condition and for the flow rate 0.18 l/s. Because of wide band frequencies between 2.6 bpf (875 Hz) and 3.56 bpf (1150 Hz), 3.5 bpf (1130 Hz) is masked.
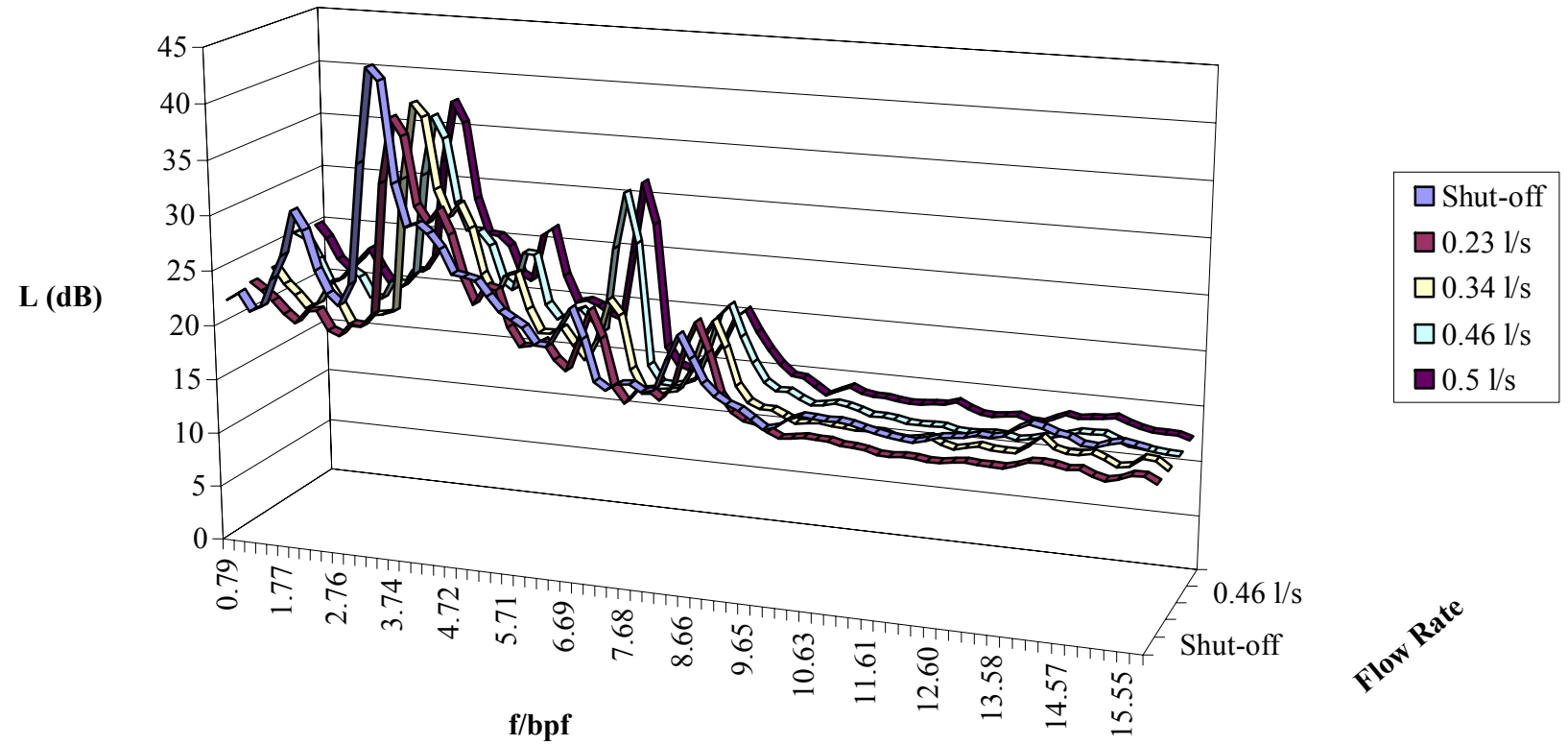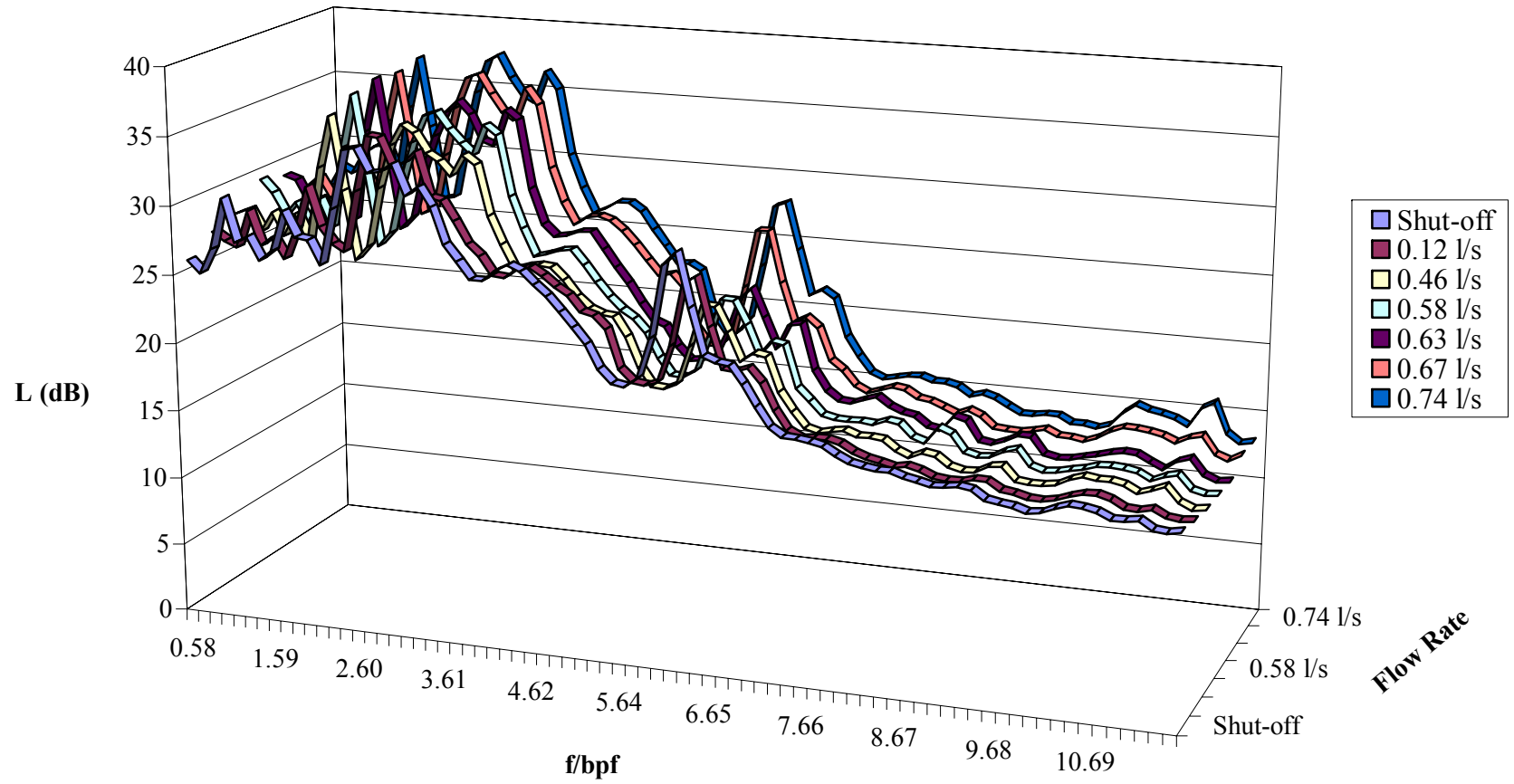
Figure 6.1. Small pump noise fft spectra for 2175 rpm.
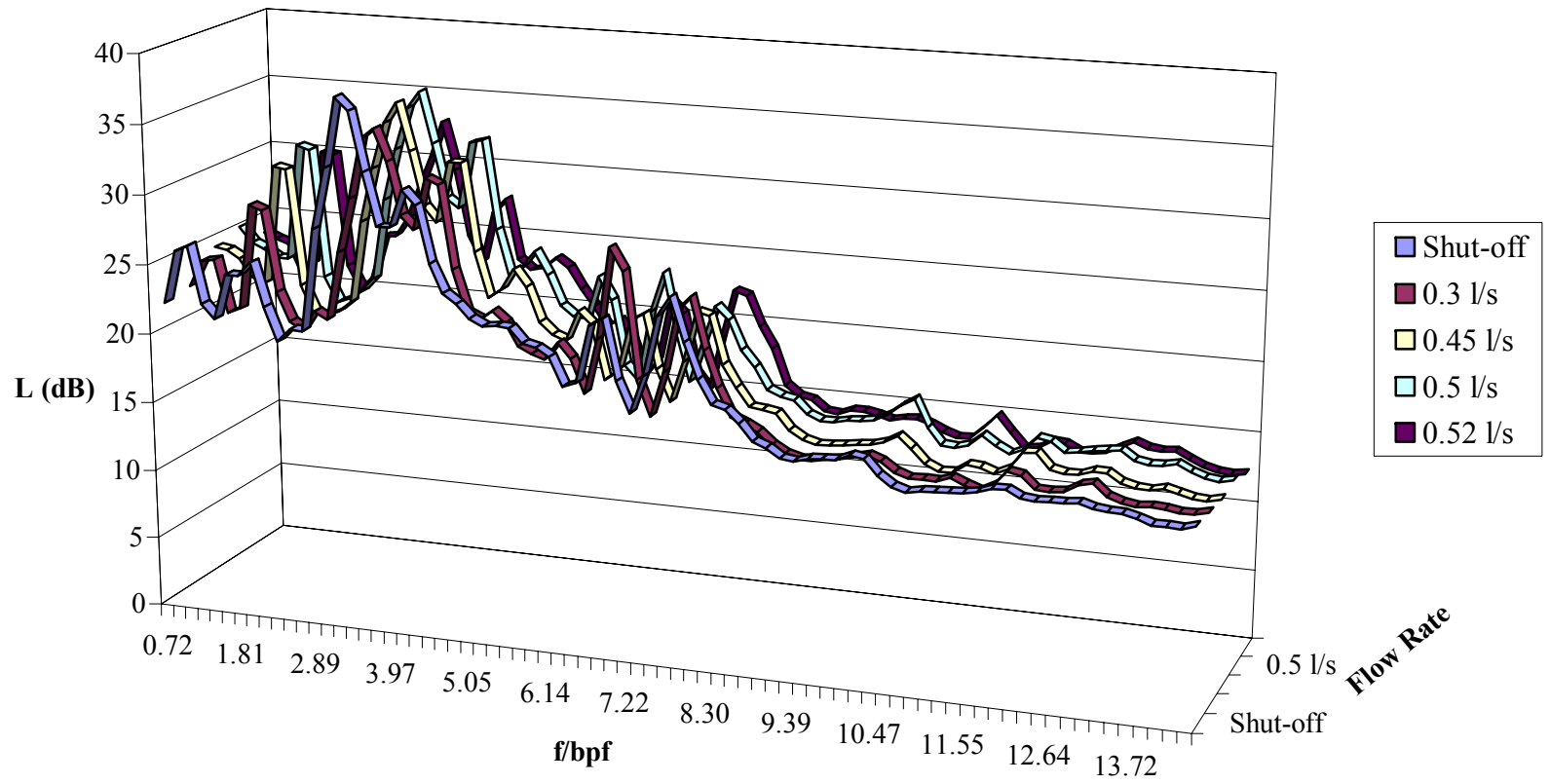
Figure 6.2. Small pump noise fft spectra for 2375 rpm.
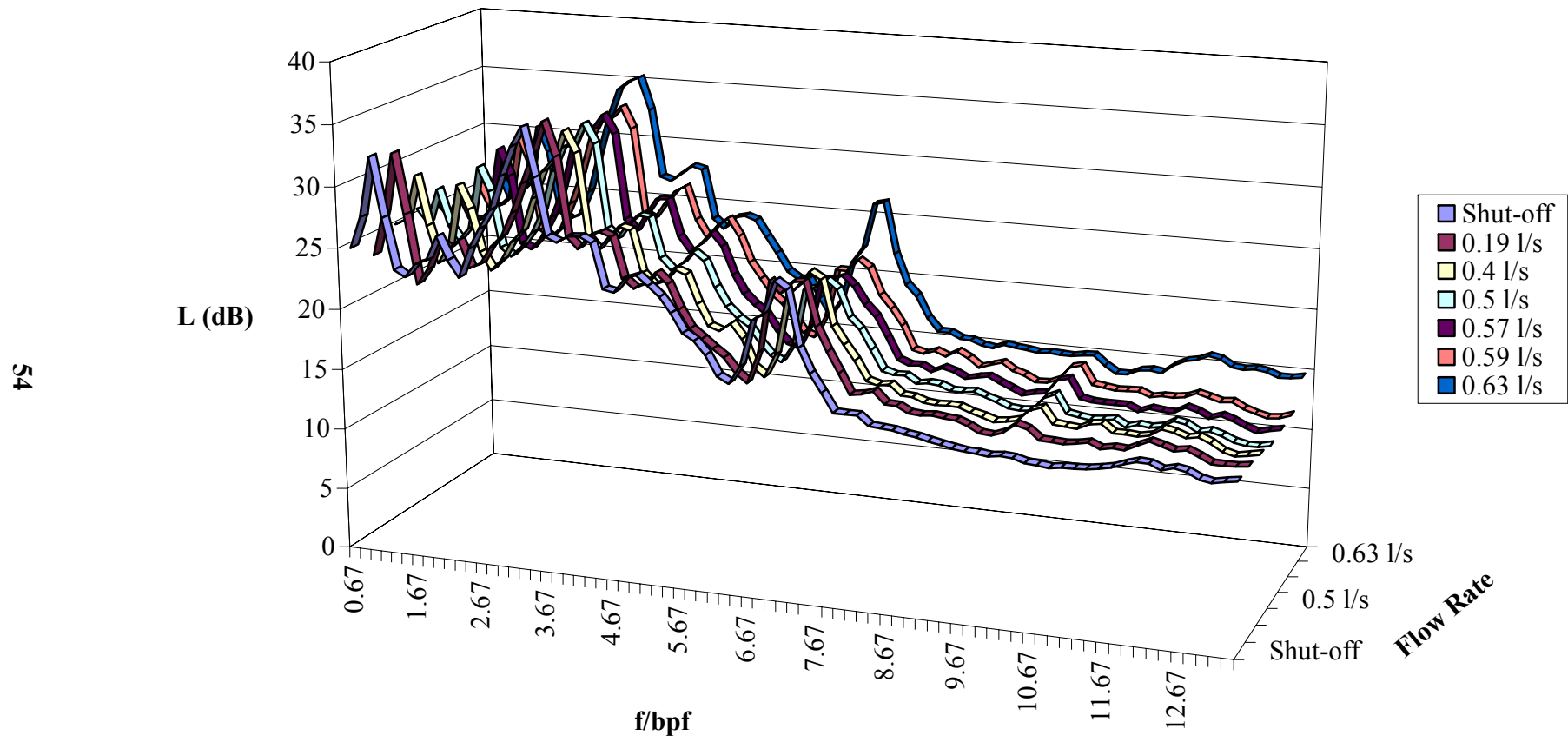
Figure 6.3. Small pump noise fft spectra for 2570 rpm.
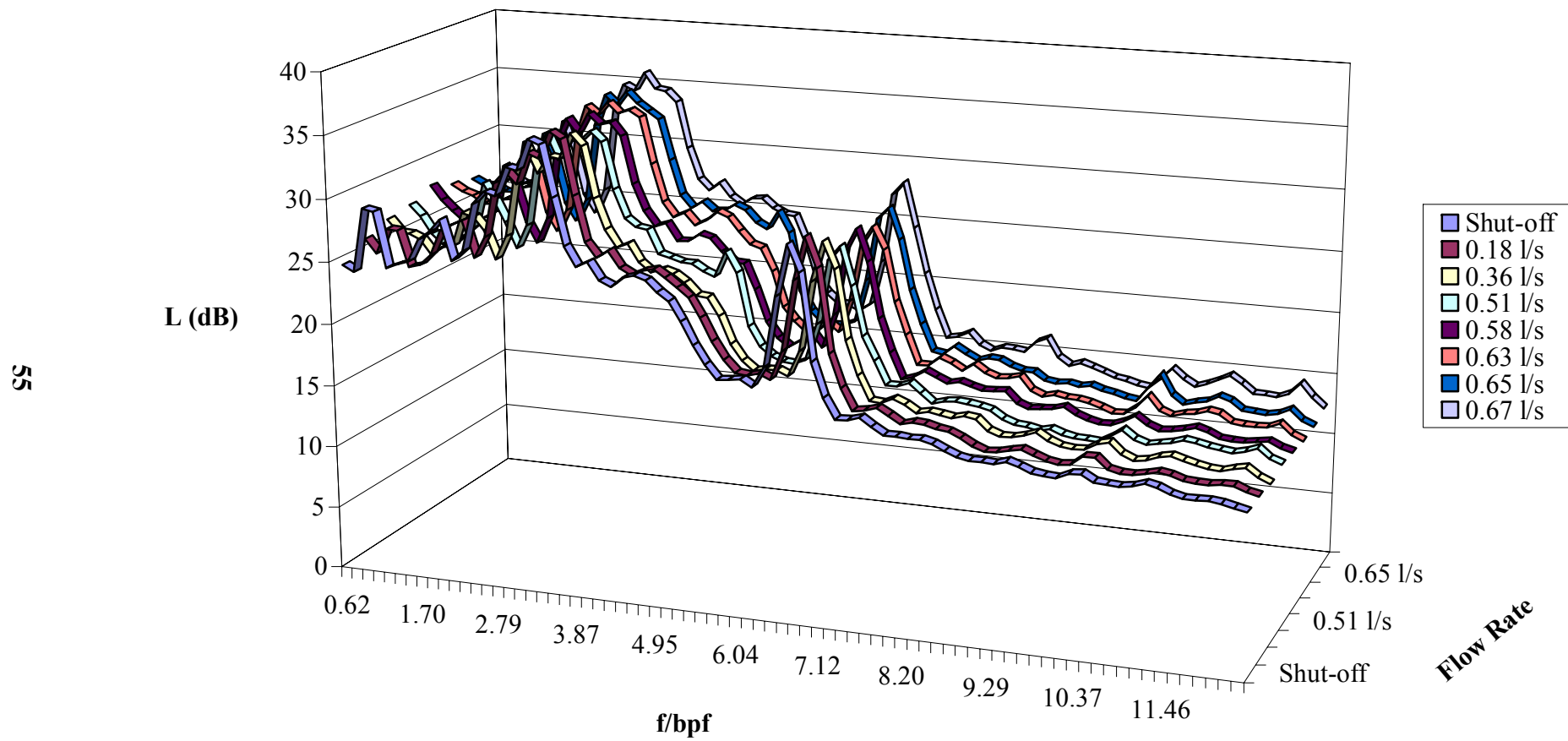
Figure 6.4. Small pump noise fft spectra for 2770 rpm.

Examined operating points for rotational speed of 2965 rpm were shut off, 0.12 l/s, 0.46 l/s, 0.58 l/s, 0.63 l/s, 0.67 l/s, 0.74 l/s. Sound spectra is shown in cascade form in Figure 6.5 for Pump speed 2965 rpm has a bpf of 346. However, peak at bpf disappears when the flow rate increased. Wide band frequency between 2.6 bpf (900 Hz) and 3.6 bpf (1250 Hz) has masked the peak at 3.5 bpf (1200 Hz).

Pump noise was measured at eight different operating points when the pump was operating at a rotational speed of 3160 rpm. Hence, shut off, 0.18 l/s, 0.53 l/s, 0.63 l/s, 0.71 l/s, 0.72 l/s, 0.75 l/s, 0.79 l/s are examined for 3160 rpm. Design point of the pump is 0.63 l/s. Sound spectra of 3160 rpm are plotted in cascade form in Figure 6.6. The real value of bpf is 369 Hz but it is located at 350 Hz on the spectra plot. The adjacent peaks occur with a frequency difference of 300 Hz. A dominant peak is observed at 2150 Hz and it is followed by a peak at 2450 Hz.

When the pump is operating at 3365 rpm, sound spectra for operating points of shut off, 0.16 l/s, 0.6 l/s, 0.73 l/s, 0.79 l/s, 0.83 l/s, 0.84 l/s, 0.85 l/s are given in cascade form in Figure 6.7. Design point of the pump is 0.84 l/s. Corresponding value of bpf is 393 Hz. When the pump is operated at low flow rates, 2.4 bpf (950 Hz) masks 1.78 bpf (700 Hz). When the flow rate is low 4 bpf (1600 Hz) masks 3.5 bpf (1375 Hz). As the flow rate increases, a wide band frequency between 3.3 bpf (1300 Hz) and 3.5 bpf (1375 Hz) appears.

There is peak at 2200 Hz for each spectrum. That is a dominating peak on Channel 2. It may be related with motor noise. One may claim that at 1100 Hz there is also a peak value on some spectra.

Figure 6.5. Small pump noise fft spectra for 2965 rpm.
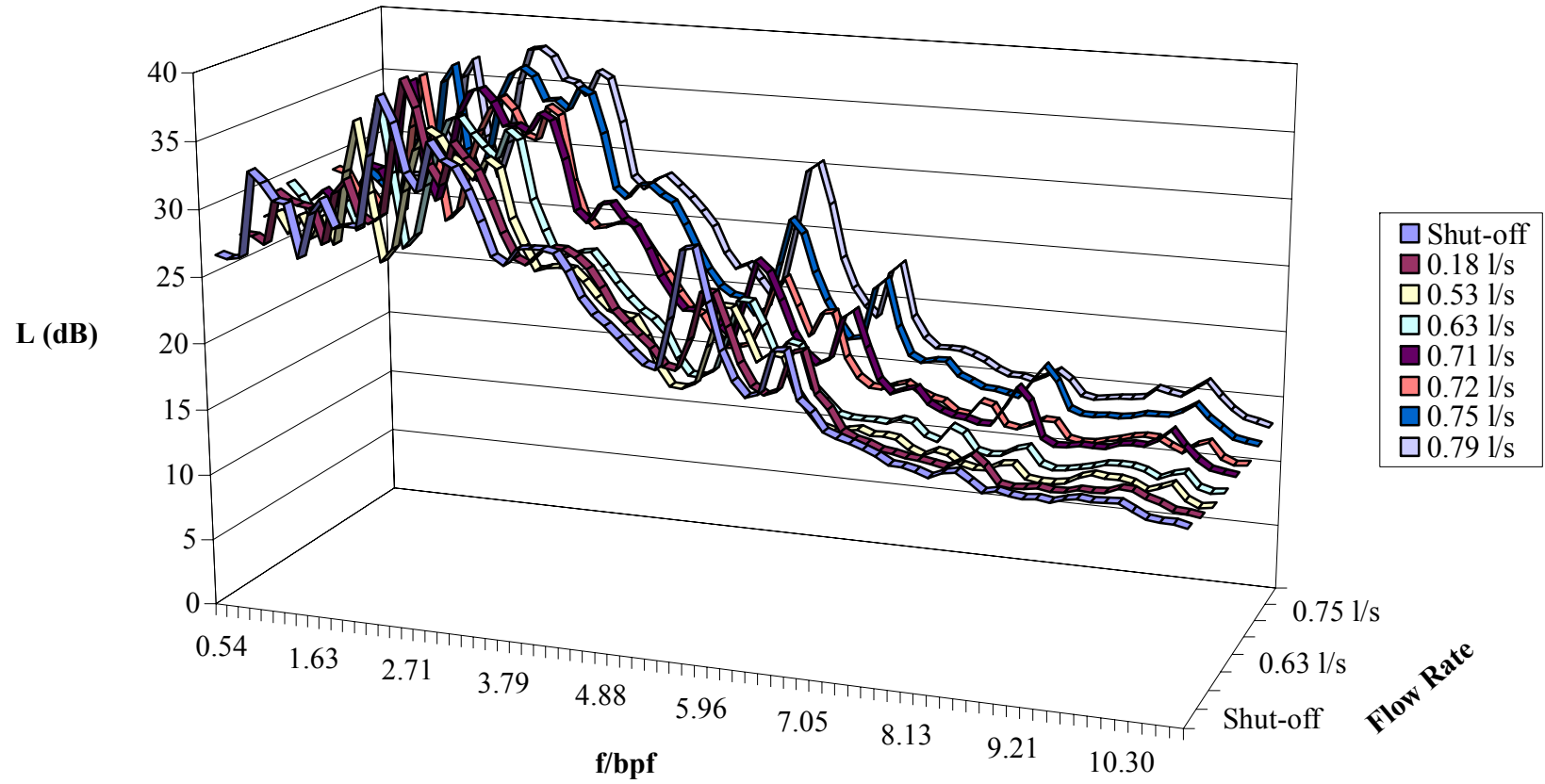
Figure 6.6. Small pump noise fft spectra for 3160 rpm.
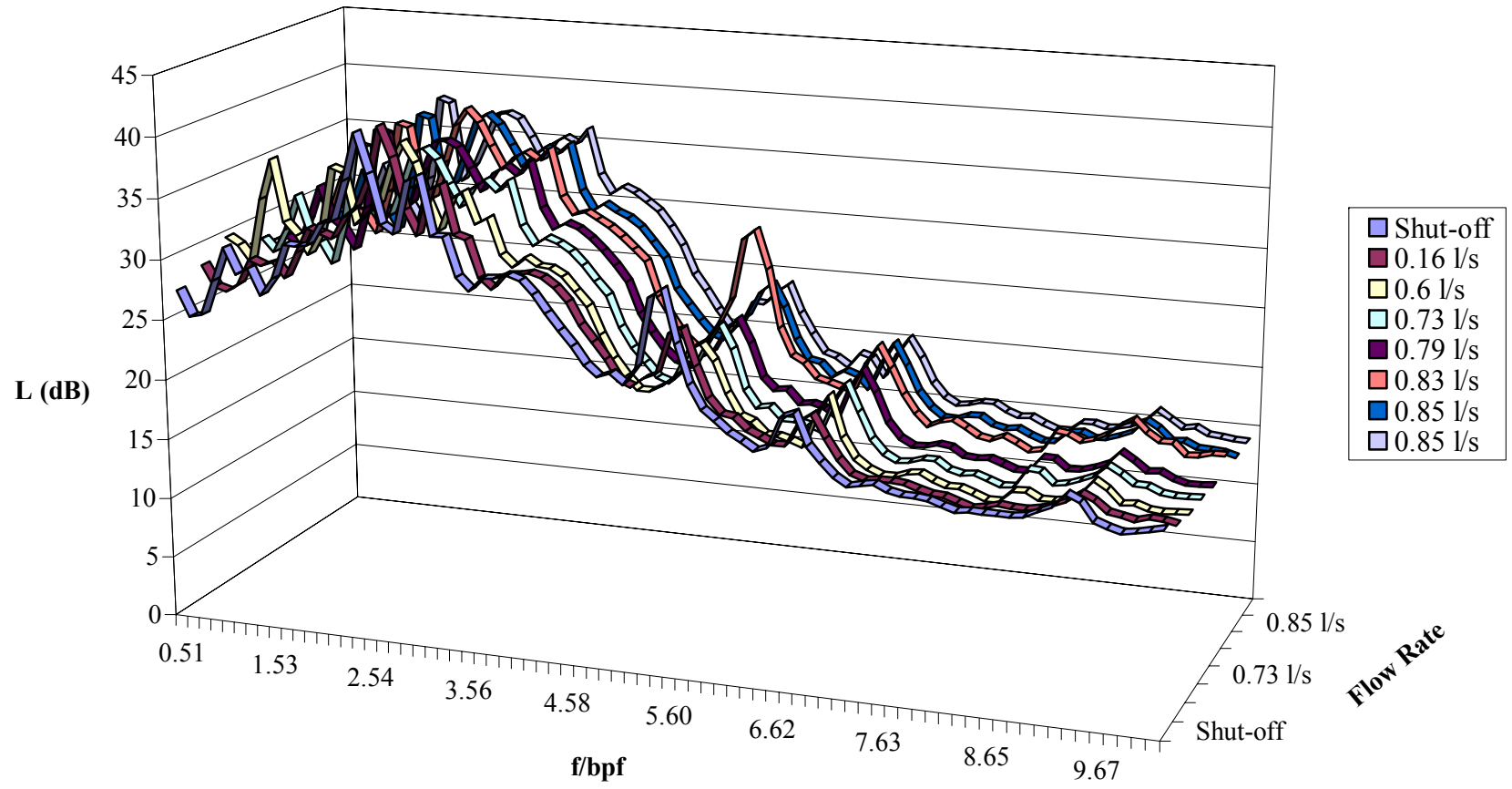
Figure 6.7. Small pump noise fft spectra for 3365 rpm

6.2. Sound and Pressure Variation of Small Pump

Noise of pump is correlated with hydraulic pressure variations. Set Up 2 was used for correlation experiments. Time dependent pressure at the pump inlet and outlet were measured synchronous to sound pressure measurement. The spectra measured in the second experimental set-up are plotted on a finer scale than those of the first set-up. Hence the former ones are plotted more accurately than the latter. This enables one to distinguish the peaks more precise. Correlation experiments were also conducted for various operating conditions at seven different rotational speeds. Sound spectra with pump inlet and outlet pressure variation fft spectra are given in Appendix D for all operating conditions.

6.2.1. Peaks on Sound Spectra

The fft spectra for sound of the pump at shut off condition is depicted in cascade form for different rotational speeds in Figure 6.8.

Harmonics of bpf distinguished on the sound spectra are given in Table 6.3 for seven different pump speeds.

Common peak frequencies are also marked on Figure 6.9. There is peak at blade passing frequency for each pump speed. Peak at 2 bpf is more distinguishable at low rotational speeds. On the other hand, peak at 1.7 bpf gets sharper as rotational speed increases. A peak has been observed for almost all of the sound spectra at the vicinity of 2150 Hz.

At rotational speed of 2175 rpm, pump is operated at shut off condition and flow rates of 0.41 l/s, 0.57 l/s, 0.66 l/s. The pump is over-loaded when the valve is fully opened. 3 bpf is observed only for low flow rates. Especially for high flow rates, peak at 4 bpf is masked.
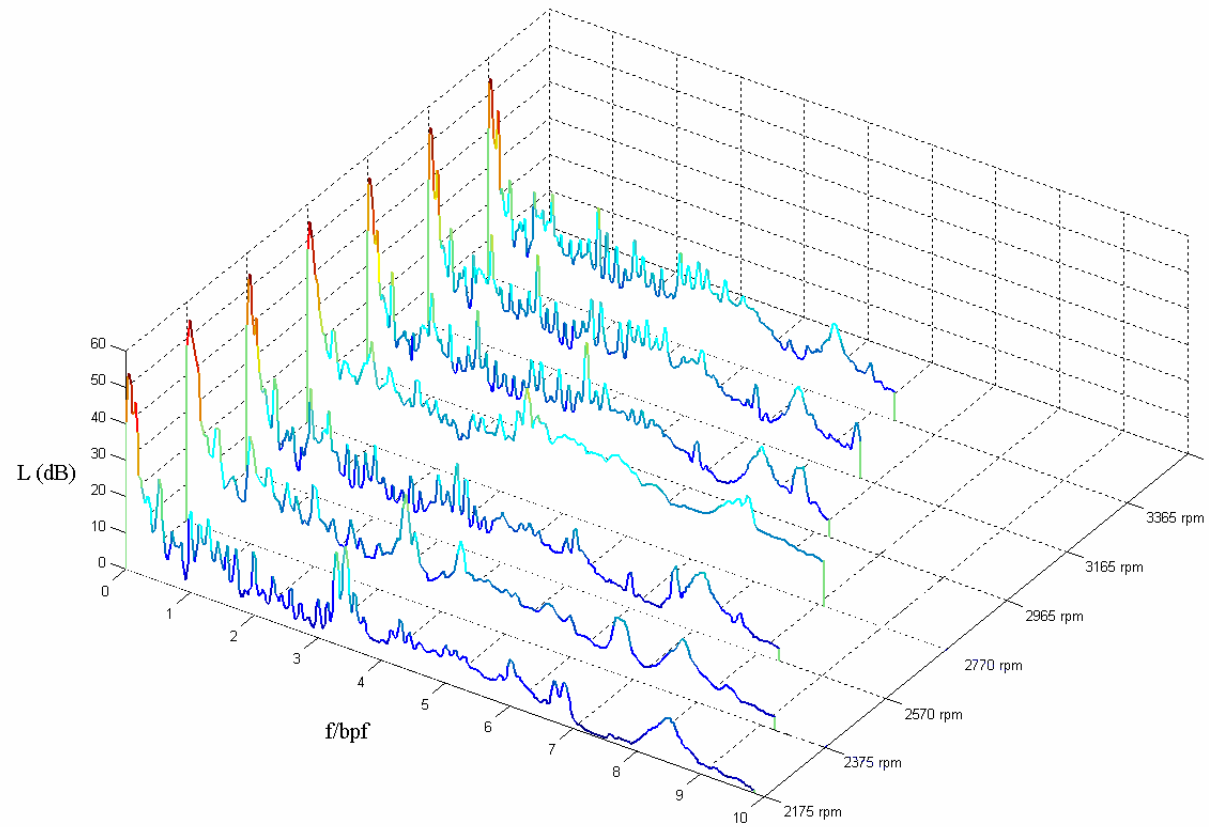
Figure 6.8. Small pump noise fft spectra at shut off.
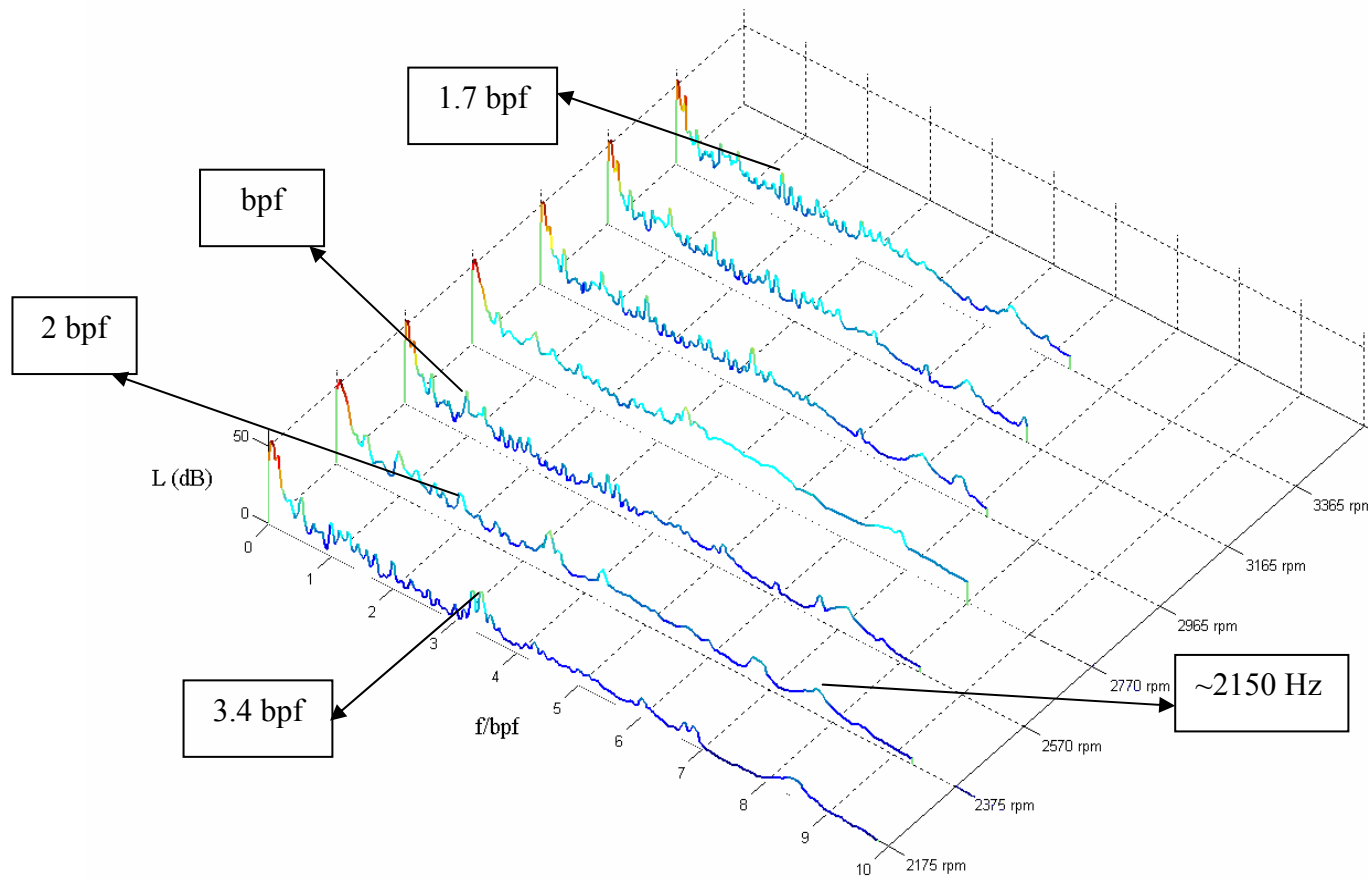
Figure 6.9. Most common peak frequencies on the sound pressure fft for seven pump speeds.

When the speed is 2375 rpm, pump is operated at shut off condition and flow rates of 0.486 l/s, 0.62 l/s, 0.69 l/s. Design point of the pump is 0.62 l/s. The first six harmonics of the bpf can be observed on the spectrum for shut off condition. However, peak at 4 bpf disappears when the valve is opened.

When the pump operates at 2570 rpm, noise and inlet outlet pressures of the pump are examined for shut off condition and for the flow rates of 0.4 l/s, 0.6 l/s, 0.73 l/s. Fully open valve condition coincides with the design point of the pump. Peak at 4 bpf is in a wide band frequency but it is distinguished by observing pressure spectra.

At 2770 rpm, pump is operated at shut of condition and at the flow rates of 0.38 l/s, 0.68 l/s, 0.76 l/s and 0.84 l/s. Design point of the pump is 0.68 l/s. Only first two harmonics have peaks on the spectrum for shut off condition. The 4 bpf and 5 bpf are masked. As the flow rate increases, higher harmonics become distinguishable.

At a pump operating speed of 2965 rpm, shut off condition and flow rates of 0.43 l/s, 0.67 l/s, 0.72 l/s, 0.77l/s are examined. Fully open valve condition is very close to the design point of the pump. If any peak is masked in the sound spectrum, pressure spectra will indicate the peak frequency. There are only two harmonics of bpf when the pump is operating with flow rate of 0.67 l/s. The 7 bpf is observed on the spectra for shut off condition and fully open valve condition.

At a speed of 3160 rpm, shut off condition and flow rates of 0.466 l/s, 0.59 l/s, 0.74 l/s, 0.82 l/s are evaluated. Design point of the pump is 0.74 l/s.

When the pump is operating at a speed of 3365 rpm, shut off condition and flow rates of 0.56 l/s, 0.63 l/s, 0.78 l/s, 0.875 l/s, 0.965 l/s, 0.97 l/s are examined. Design point of the pump is 0.78 l/s. 7 bpf is masked in the spectrum for shut off condition.

Table 6. 3. Harmonics of bpf observed on the sound spectra for seven pump speeds.

Rotational Speed (rpm)	bpf	2 bpf	3 bpf	4 bpf	5 bpf	6 bpf	7 bpf
2175	✓	✓	✓	✓	✓	✓	
2375	✓	✓	✓	✓	✓	✓	
2570	✓	✓	✓	✓	✓	✓	
2770	✓	✓		✓	✓		
2965	✓	✓	✓	✓	✓	✓	✓
3160	✓	✓	✓	✓	✓	✓	✓
3365	✓	✓	✓	✓	✓	✓	✓

6.2.2. Correlation of Sound and Pressure Spectra

Sound spectra and hydraulic pressure spectra are correlated for rotational speeds of 2375 rpm and 2965 rpm. Operating points which are very close to design point and a part loaded condition for each rotational speed are of interest for coherence. Sound spectrum from Channel 1 was the reference and hydraulic pressure spectra of pump inlet and outlet were the response for cross analysis. Coherence functions are plotted in Figures 6.10-6.17. Where peak frequencies exist correlations are listed in Table 6.4. Frequencies are normalized by bpf. Shaft speed is 1/7 bpf. On Table 6.4, 6/7 bpf and its harmonics are marked with asterisk.

Small pump delivers 0.62 l/s water when operating at design point of 2375 rpm. Coherence between Microphone Channel 1 and hydraulic pressures is given Figure 6.10. Part loaded operating point was chosen to be 0.5 l/s. Coherence for that condition is plotted in Figure 6.11.

Table 6.4. Coherent frequencies normalized by bpf at different operating points of 2375 rpm and 2965 rpm

	2375 rpm		2965 rpm		
	Design Point	Part Loaded Operation	Design Point	Part Loaded Operation	Comment
Inlet Pressure vs. Sound	0.14	0.14			Shaft speed (1/7 bpf)
		0.29		0.29	2/7 bpf
	0.86	0.86	0.87	0.87	6/7 bpf *
	1.71	1.71	1.72	1.72	12/7 bpf **
	2.57	2.57	2.58	2.57	18/7 bpf ***
	3.43	3.43	3.43	3.43	****
	4.29	4.29			*****
	5.14	5.14	5.15		******
	6	5.98	6	6	6 bpf (7*)
		6.83	6.87		8*
	7.71	7.69			9*
	8.57	8.57			10*
Outlet Pressure vs. Sound	0.14	0.14	0.14	0.14	Shaft speed (1/7 bpf)
			0.29	0.29	2/7 bpf
		0.43	0.43		3/7 bpf
				0.49	bpf/2
		0.63	0.63		bpf/7+bpf/2
	0.72	0.72	0.7	0.72	5/7 bpf
	0.86	0.86	0.87	0.87	6/7 bpf *

Table 6.4. Coherent frequencies normalized by bpf at different operating points of 2375 rpm and 2965 rpm (cont.)

	2375 rpm		2965 rpm		
	Design Point	Part Loaded Operation	Design Point	Part Loaded Operation	Comment
Outlet Pressure vs. Sound	0.99	0.99	0.99	0.99	bpf
	1.29	1.31	1.28	1.28	9/7 bpf
			1.43	1.43	10/7 pbf
	1.58		1.57	1.57	11/7 bpf
	1.71	1.71	1.72	1.72	**
	2.57	2.57	2.58	2.58	***
			2.73		19/7 bpf
			3.29		23/7 bpf
	3.43	3.43	3.43	3.43	****
	4.29	4.29		4.3	*****
	5.14	5.14	5.15	5.17	******
	5.98	5.98	6	6	6 bpf (7*)
	6.86		6.87		8*
	7.71	7.71			9*
	8.55	8.57			10*
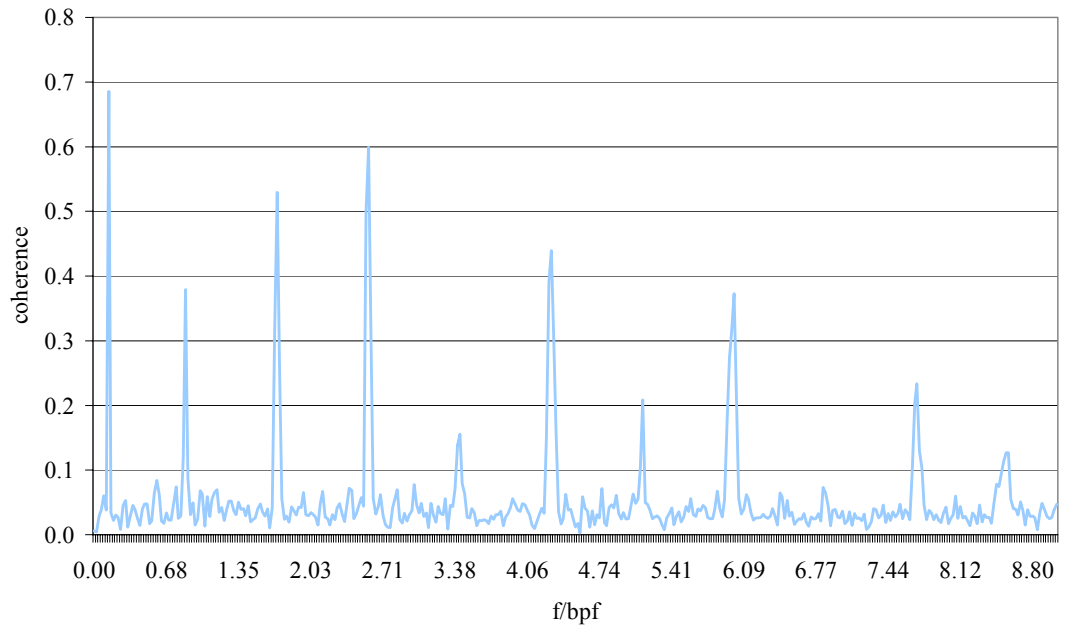
(a) Inlet Pressure vs. Sound
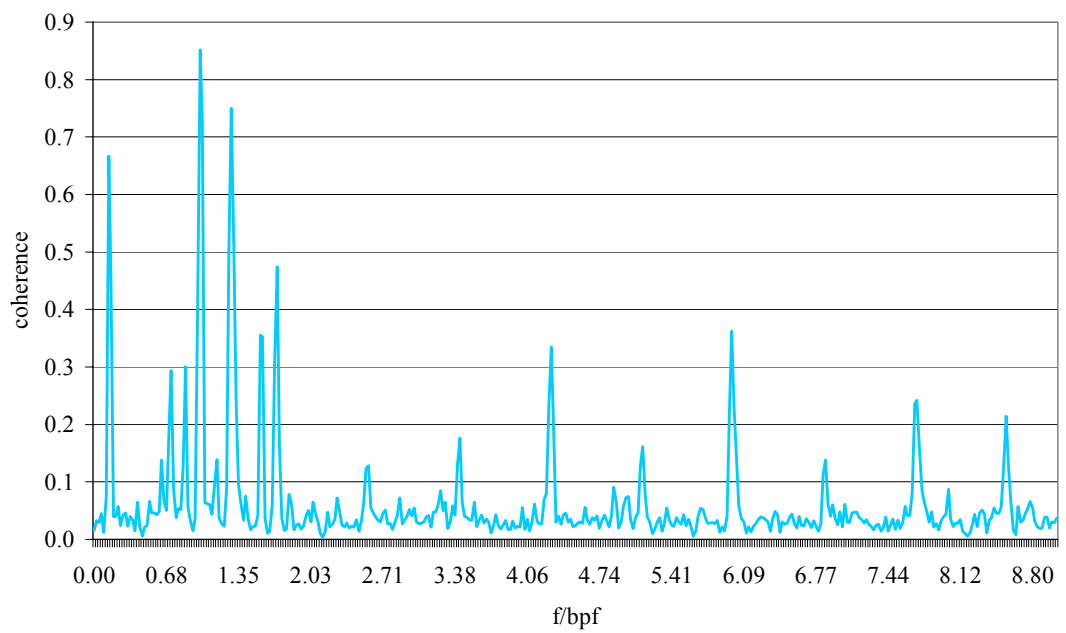
(b) Outlet Pressure vs. Sound

Figure 6.10. Coherence between sound and hydraulic pressures
at design point of 2375 rpm.
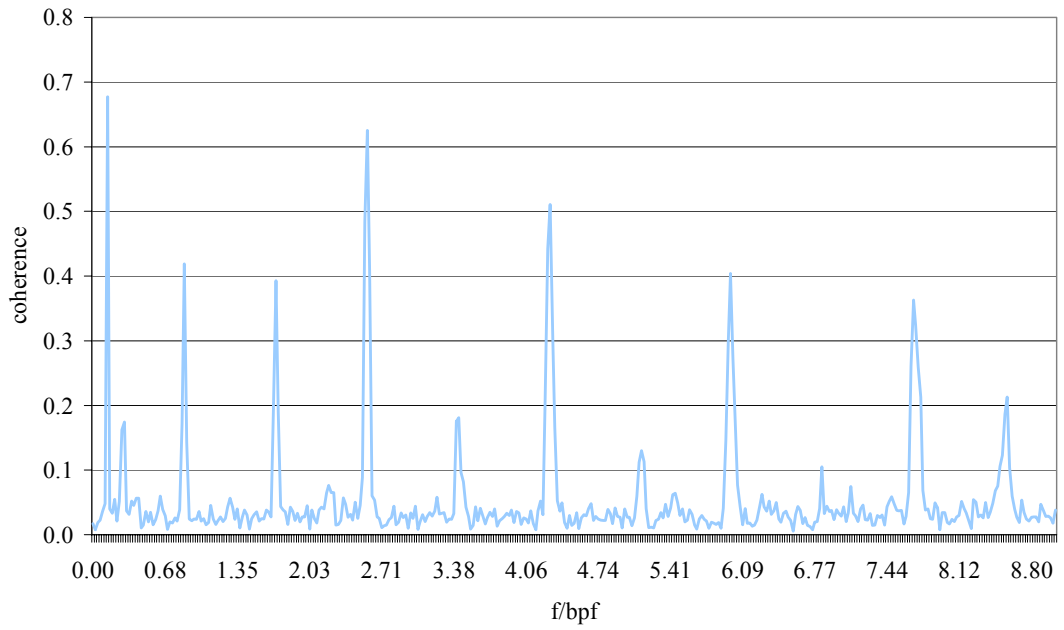
(a) Inlet Pressure vs. Sound
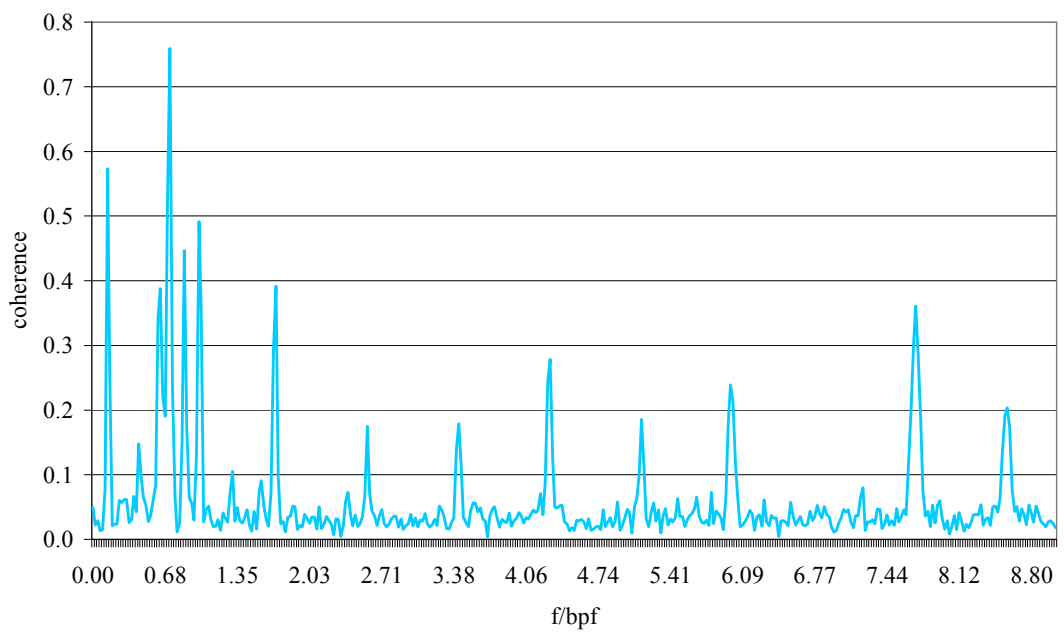
(b) Outlet Pressure vs. Sound

Figure 6.11. Coherence between sound and hydraulic pressures
at part loaded operation of 2375 rpm.

Design point of the pump at 2965 rpm is 0.8 l/s. Coherence between sound and hydraulic pressures for that condition are given in Figure 6.12. Pump is part loaded when it is delivering 0.73 l/s water at 2965 rpm. Coherence for that operating point is depicted in Figure 6.13.

The peaks on the coherence graph for inlet pressure versus sound also exist on the coherence graphs for outlet pressure vs. sound. However on the latter graphs, there are more peaks up to 2 bpf. Thus, outlet pressure is the source of noise for low frequencies.

Shaft rotation speed is 0.14 bpf (bpf/7) for seven blade impeller. On the coherence graphs for inlet pressure vs. sound, difference between adjacent peaks is 0.86 bpf. That is the difference between bpf and shaft speed. Sound and inlet pressure are incoherent at bpf. On the other hand, sound and outlet pressure are strongly coherent at bpf. At frequencies higher than 2 bpf, correlation between hydraulic pressures and sound is due to interaction of shaft rotation and blade passage because of the interval of 0.86 bpf.
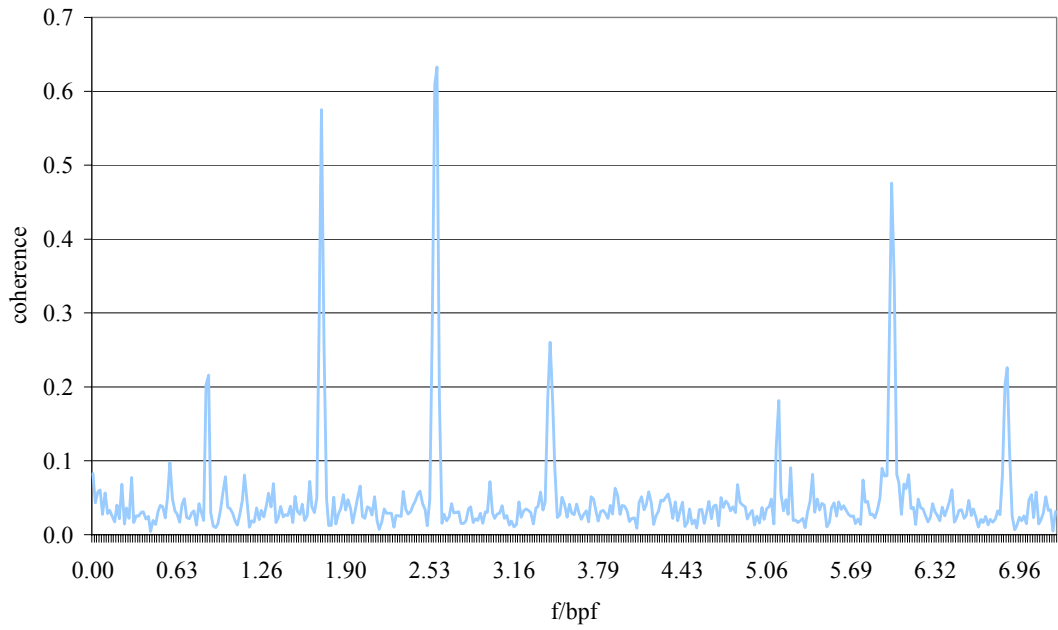
(a) Inlet Pressure vs. Sound
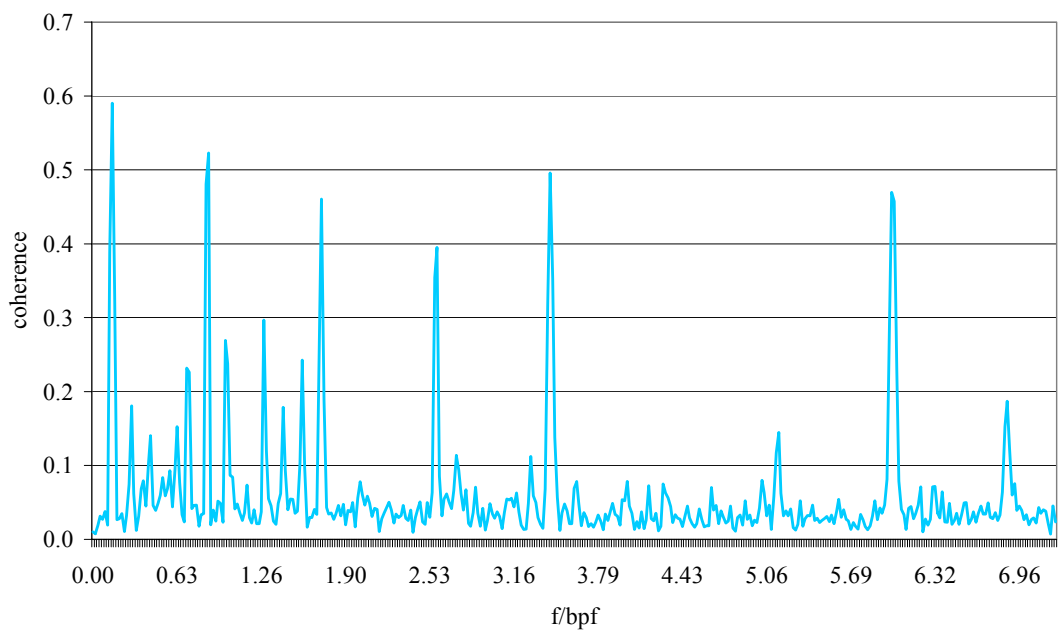
(b) Outlet Pressure vs. Sound

Figure 6.12. Coherence between sound and hydraulic pressures
at design point of 2965 rpm.
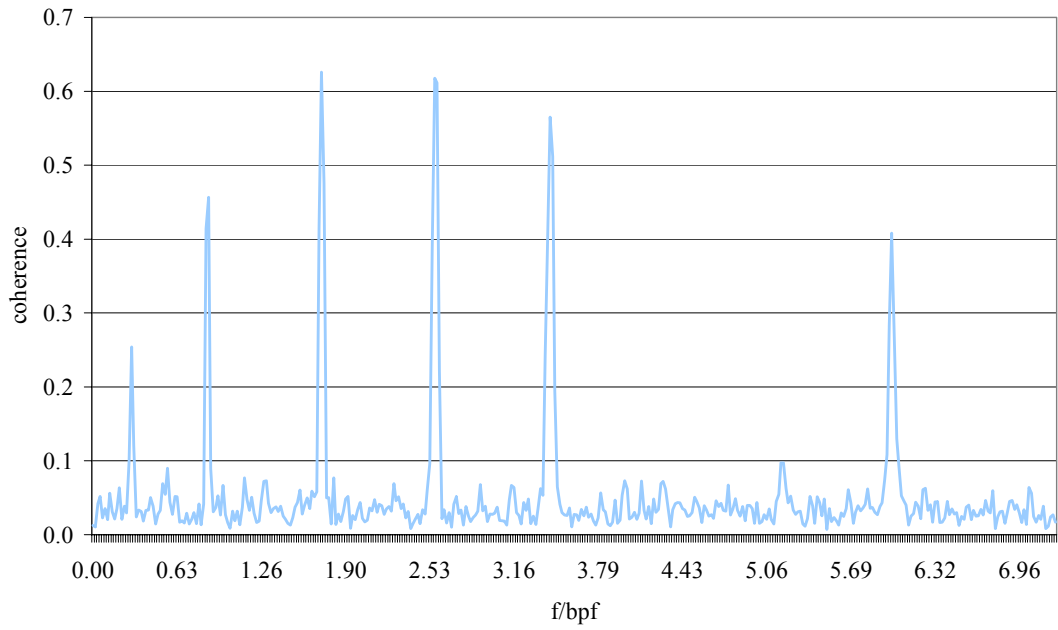
(a) Inlet Pressure vs. Sound
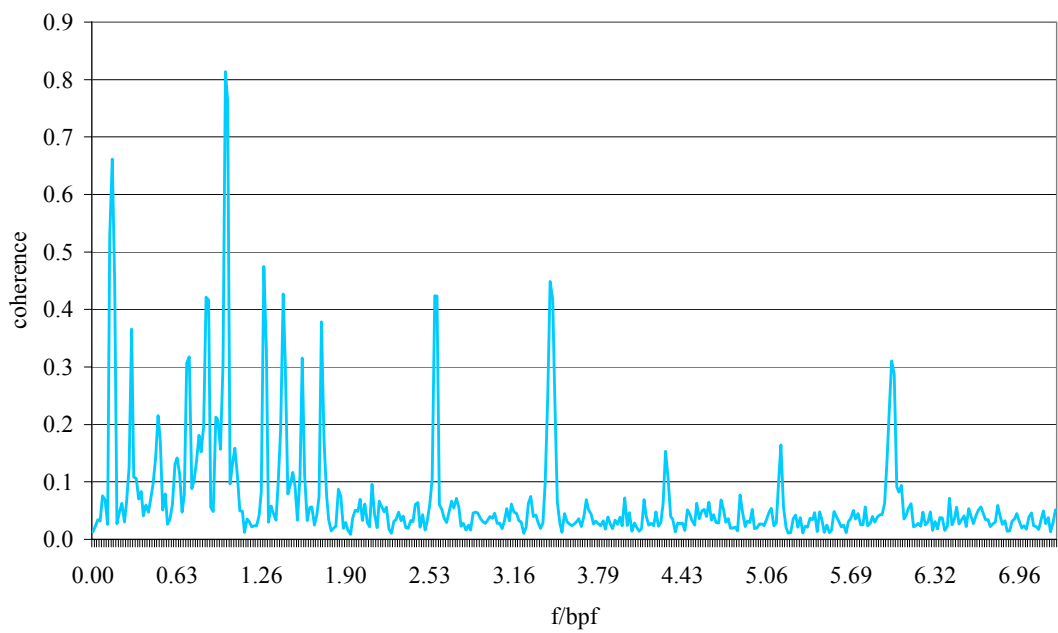
(b) Outlet Pressure vs. Sound

Figure 6.13. Coherence between sound and hydraulic pressures
at part loaded operation of 2965 rpm.

6.3. Sound and Pressure Variation of the Large Pump

Noise of the large pump was measured in the Set-up 2 as well as time dependent pressure variation at the inlet and outlet of pump. Operation of large pump was not completely steady state at high rotational speeds of pump. On the pump characteristic curves, unsteady operation region could not be avoided. Corresponding sound spectra, inlet and outlet pressure spectra are shown in Appendix D.

The sound levels and pressure fft are obtained at three different operating conditions for each pump rotation speed. Usually the peaks are located at the same frequencies with small pump spectra. However overall sound pressure level for large pump is higher than that of small pump for moderate frequencies. Sound levels get closer for high frequencies.

At a pump speed of 2175 rpm, shut-off, 0.39 l/s, 0.73 l/s operating points are examined. Pump operation was in steady state.

At a pump speed of 2375 rpm, shut off condition, flow rates of 0.70 l/sand 0.78 l/s are examined. Pump operation was steady. Third and forth harmonics of bpf are masked in the spectra of small pump but they are observable in the spectra of large pump.

Shut-off condition and flow rates of 0.69 l/s, 0.84 l/s are examined for a pump speed of 2570 rpm. Pump operation begins to deviate from the steady state, as compared to previous speeds. Especially pump outlet pressure rms started to fluctuate irregularly.

When the pump is operating at a speed of 2770 rpm, shut-off condition and 0.84 l/s, 0.88 l/s are examined. Pump operation was steady.

At a pump speed of 2965 rpm, shut off condition and 0.85 l/s, 0.94 l/s are examined. Pump operation became unsteady. There are peaks on the sound spectra at the

vicinity of 3.43 bpf separated from each other by an interval of shaft speed of 50 Hz. These adjacent sound peaks coincide with the peaks of the outlet pressure.

Shut-off condition and flow rates of 0.65 l/s, 0.95 l/s are examined when the pump speed is 3175 rpm. Outlet pressure rms fluctuates irregularly. As the flow rate increases, sound level difference between two pumps also increases.

At the highest pump speed of 3375 rpm, the examined operating points are shut-off, 0.77 l/s and 0.90 l/s. Neither the outlet pressure nor the inlet pressure is in steady state.

Peaks at the vicinity of 2150 Hz shifted to 2080 Hz for large pump sound spectra.

CHAPTER 7

DISCUSSION AND CONCLUSIONS

7.1. Comments on the Results

Two small size pumps are operated at different system conditions. Pumps have similar geometry but they differ in the size of impeller, volute and casing.

Noise of the pumps are recorded and correlated with fluctuations in hydraulic pressures at the pump inlet and outlet.

Two experimental set-ups are constructed. The first one, Experimental Set-Up 1, has a low geometric head. On the other hand, the second one, Experimental Set-Up 2 has a negative geometric head. Small pump is operated in both Set-Ups. Large pump is operated only in Set-Up 2.

Although the pumps are operated in systems with low or negative geometric head, frictional head losses caused the pumps to operate part loaded. Maximum flow rate in the Experimental Set-Up 2 is considerably higher than that in the Experimental Set-Up 1 for the small pump.

Maximum flow rate of the large pump is the highest obviously. However, the large pump operation is in unsteady region of the pump characteristic curves.

Despite the fact that the sound levels of the pumps are not high enough to obtain net spectra, background noise is low enough to conduct experiments.

Experimental Set Up 1 results are plotted at 50 Hz intervals. Peaks are not clearly distinguishable but when graphics are examined expected peaks are observed. These peaks are not affected from solo motor noise i.e. motor noise is not a considerable parameter for the noise of pump.

There are peaks at bpf for all pump speeds. The 3.5 bpf and 7 bpf had high amplitudes for all pump speeds. When the pump is operated at maximum shaft speed, sound level is expected to be the highest and 10.5 bpf is also distinguishable for this pump speed.

A peak at 2200 Hz is observed on almost all spectra. That frequency is independent of rotational speed.

On the sound spectra, amplitudes of some frequencies are increasing with the flow rate and some are decreasing. Also some frequencies are absolutely independent of flow rate. For some cases sound level is decreasing with the flow rate but there are sudden increases in the level when valve is fully closed. Hence, sound pressure level cannot be related with flow rate.

In order to investigate the cause of undefined peaks in the spectra, hydraulic pressure data are recorded as frequent as sound pressure data. Plots are obtained more precisely. Hence peaks are clearly distinguishable but number of peaks has increased.

Cross correlation analysis are conducted in order to find out consisting peak frequencies of sound and hydraulic pressure data. The coherent peaks are equally spaced. The difference between consecutive peaks is found out to be harmonic of shaft speed. Peak frequencies observed on inlet pressure and outlet pressure spectra usually coincided with each other especially at high frequencies. Up to 2 bpf, one may argue that pump outlet pressure is a source of noise.

Increase of the pump size increases the amplitudes i.e. the sound level of the pump, especially for moderate and high frequencies.

On the pressure spectra, adjacent peaks had an interval of twice shaft speed. For the large pump, six times the shaft speed is more distinguishable with higher amplitude. As the large pump speed increases, pressure data starts to form humps and shaft speed harmonics arise in the interval of twice shaft speed.

Part loaded pump noise is not affected by system characteristics. Shaft speed and pump size, i.e. pump characteristics affect the pump noise. Pump noise related to rotational speed has an interaction with pump outlet pressure.

7.2. Recommendation for Future Work

Because the test room was semi-anechoic, instead of sound pressure levels, sound power levels might be detected. Another improvement may be covering the floor of the room with sound absorbing materials and obtaining an anechoic test room. However, this will necessitate a series of modification in the room.

Dimensions of the test room are sufficient for near field measurements but for far field measurements, a larger test room may be used. Smaller sound sources may be detected for far field noise levels, in the present test room.

Two microphones are not enough for proper measurements, because one should change the microphone positions before each measurement. Four or more microphones will give more accurate results.

In the first series of experiments, only the sound of pump was measured. However, without pressure data, sound spectrum was insufficient to interpret. Hence, hydraulic pressure of pump should be measured. Inlet and outlet pressures of pump are collected as frequent as sound data in order to avoid aliasing when comparing these data.

Time dependent inlet and outlet pressure variations are observed but not recorded. fft spectra of these are recorded in terms of dB. Recording the inlet and outlet variations in terms of pressure might be useful for a thoroughly analysis.

It was hard to compare spectra for sound and pressure without applying any cross correlation analysis. The software used did not allow to process row time data and calculate a coherence function. It is possible to obtain time history of complex data with the "Cross Analysis Module" of SAMURAI. Coherence spectra between any two channels can be calculated using that module. However, correlation between two separate measurements is still not possible. In future studies, complex time histories can be processed with any common mathematical software in order to calculate coherency of two separate measurements.

REFERENCES

[1] Choi, J.S.; McLaughlin, D.K.; Thompson, D.E.; "Experiments on the Unsteady Flow Field and Noise Generation in a Centrifugal Pump Impeller"; *Journal of Sound and Vibration*, pp. 493-514, Vol. 263 (2003).

[2] Akın, R.; "An Experimental Investigation on the Part Load Performance of Centrifugal Pumps at Different Specific Speeds"; M. Sc. Thesis, Middle East Technical University, Mechanical Engineering Department (September 1994).

[3] Bies, D. A.; Hansen, C.H.; "Engineering Noise Control: Theory and Practice"; London: New York: E&FN Spon, 2nd Edition (1996).

[4] Mongeau, L.; Thompson, D.E.; McLaughlin, D.K.; "Sound Generated by Rotating Stall in Centrifugal Turbomachines"; *Journal of Sound and Vibration*, pp. 1-30, Vol. 163, no. 1 (1993).

[5] Maaloum, A.; Kouidri, S.; Bakir, F.; Rey, R.; "Effect of Inlet Duct Contour and Lack Thereof on the Noise Generated of an Axial Flow Fan"; *Applied Acoustics*, pp. 999-1010, Vol. 64 (2003).

[6] Breugelmans, F.A.E.; Şen, M.; "Prerotation and Fluid Recirculation in the Suction Pipe of Centrifugal Pumps"; Proceedings of the 11. Turbomachinery Symposium, pp. 165-180.

[7] Ali, N.W.; "An Experimental Investigation of Part Load Problems in Centrifugal Pumps"; M. Sc. Thesis, Middle East Technical University, Mechanical Engineering Department (September 1989).

[8] Neise, W.; Arnold, F.; "On Sound Power Determination in Flow Ducts"; *Journal of Sound and Vibration*, pp. 481-503, Vol. 244. no. 3 (2001).

[9] Kameier, F.; Neise, W.; "Rotating Blade Flow Instability as a Source of Noise in Axial Turbomachines"; *Journal of Sound and Vibration*, pp. 833-853, Vol. 203, no. 5 (1997).

[10] Holste, F.; Neise, W.; "Noise Source Identification in a Propfan Model by Means of Acoustical Near Field Measuremetns"; *Journal of Sound and Vibration*, pp. 641-665, Vol. 203, no. 4 (1997).

[11] Bayraktar, S.; "Theoretical and Experimental Investigation on Centrifugal Fans With Special Interest on Fan Noise"; PhD. Thesis, Middle East Technical University, Mechanical Engineering Department (December 2006).

[12] Neise, W.; "Sound Power Measurement Procedures for Fans"; *Acta Acustica*, pp. 473-485, Vol. 3 (1995).

[13] National Instruments; Tutorials: Anechoic Chamber (January 2007); <http://zone.ni.com/devzone/cda/tut/p/id/45>

[14] Üçer, A.Ş.; "Turbomachinery"; Ankara: Middle EastTechnical University (1982).

[15] Oruç, S.; "An Experimental Investigation on Off-Design Performance of Centrifugal Pumps by Spectral Analysis Techniques"; M. Sc. Thesis, Middle East Technical University, Mechanical Engineering Department (November 1991).

[16] Yedidiah, S.; "Unusual Problems with Centrifugal Pumps"; *Chemical Engineering*, pp. 143-145 (December 1986).

[17] Stepanoff, A.J.; "Centrifugal and Axial Flow Pumps: Theory, Design and Application"; New York: Wiley (1957).

[18] Yedidiah, S.; "Centrifugal Pump Problems: Causes and Cures"; Tulsa, Okla.: Petroleum Pub. Co. (1980).

[19] Cohen, H.; Rogers, G.F.C.; Sravanamuttoo, H.I.H.; "Gas Turbine Theory"; New York: Longman Scientific&Technical, 3rd Edition (1986).

[20] Word for the Day Archive "Anechoic" (January 2007); <http://www.sweetwater.com/insync/word.php?find=Anechoic>

[21] Çağlayan, İ.H.; "Değişik Tip Pompalarda Titreşim Ölçüm ve Analizi ile Arıza Tanımı"; 4th Congress and Exhibition on Pumps (November 2001).

[22] "Centrifugal Pump Diagram" Online image; Centrifugal Pumps (January 2007); <http://www.engineersedge.com/pumps/pump_menu.shtml>

[23] International Standard ISO 3745.

[24] Eralp, O.C.; Çalışkan, M.; Kayhan, C.; Şahin, F.C.; "Ufak Boyda Santrifüj Pompa ve Fanların Gürültü Seviyelerinin Uygun Ortamda Ölçülmesi ve Gürültüye Yönelik Tasarım Parametrelerinin Belirlenmesi"; Research Project 104M405, Scientific and Technical Research Council of Turkey (2006-2007).

APPENDIX A

A.1. TEST ROOM CALIBRATION

Sample Calculation for Test Room Calibration

For 315 Hz, on path 1;

Equation (4.2)

$$\delta = L_{p1} - L_{p2} - 10 \cdot \log\frac{S_2}{S_1} = 93.49 - 88.2 - 10 \cdot \log(1.6^2) = 1.21 > 0.5$$

From equation (3.2)

$$L_W - L_{p1}(315) = 10 \cdot \log(\frac{4 \cdot \pi \cdot r^2}{Q_\theta(315)}) = 95 - 93.49 = 1.51$$

$$L_W - L_{p2}(315) = 10 \cdot \log(\frac{4 \cdot \pi \cdot r^2}{Q_\theta(315)}) = 95 - 88.2 = 6.8$$

$$S_1 = 4 \cdot \pi \cdot r_1^2 = Q_\theta(315) \cdot 10^{\frac{1.51}{10}} = 1.42 \cdot Q_\theta(315)$$

$$S_2 = 4 \cdot \pi \cdot r_2^2 = Q_\theta(315) \cdot 10^{\frac{6.8}{10}} = 4.79 \cdot Q_\theta(315)$$

$$\frac{S_2}{S_1} = \frac{4.79}{1.42} = 3.38$$

Table A.1. Raw data for Test Room calibration

		Rope 1		Rope 2	
fc[Hz]	BG[dB]	Lp(r₁=1m)	Lp(r₂=1.6m)	Lp(r₁=1m)	Lp(r₂=1.6m)
40	55,96	58,36	60,2	56,45	58,54
50	50,97	65,58	56,99	67,71	58,22
63	54,1	78,82	68,86	79,04	72,61
80	61,51	83,99	76,87	84,98	74,85
100	51,91	94	83	89,3	81,76
125	54,23	99,04	89,98	97	89,62
160	58,31	98,13	90,76	97,65	89,87
200	50,83	91,99	85,83	93,67	85,95
250	54,37	91,69	90,9	92	92,99
315	60,15	93,49	88,2	95,11	89
400	51,58	95,47	90,64	95,2	91,4
500	54,5	98,92	93,65	97,11	91,2
630	59,07	99,97	94,77	99,22	95,64
800	52,37	96,97	92,27	97,87	92,64
1000	54,63	90,11	86,68	90,78	86,75
1250	60	91,62	85,16	90	83,63
1600	53,49	87,66	83,78	84,67	83,64
2000	54,33	93,79	87,78	94,13	87,26
2500	60,32	91,42	85,57	92,76	87,43
3150	55,1	83,21	78,26	82,98	77,69
4000	54,86	83,39	77,85	82,5	79,01

A.2. ABSORPTION COEFFICIENTS OF COATING MATERIALS

Table A.2. Amplitudes for frequencies 250 Hz, 1000 Hz and 2000 Hz.

	Foam			Rock Wool		
Frequency (Hz)	250	1000	2000	250	1000	2000
Max. Amplitude, V_1 (mV)	130	525	95	325	125	45
Min. Amplitude, V_2 (mV)	5	30	15	13.75	30	32.5
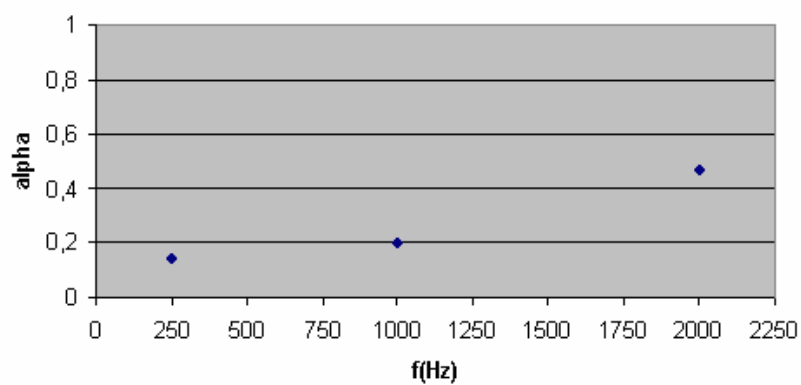
Figure A.1. Absorption coefficient of foam.
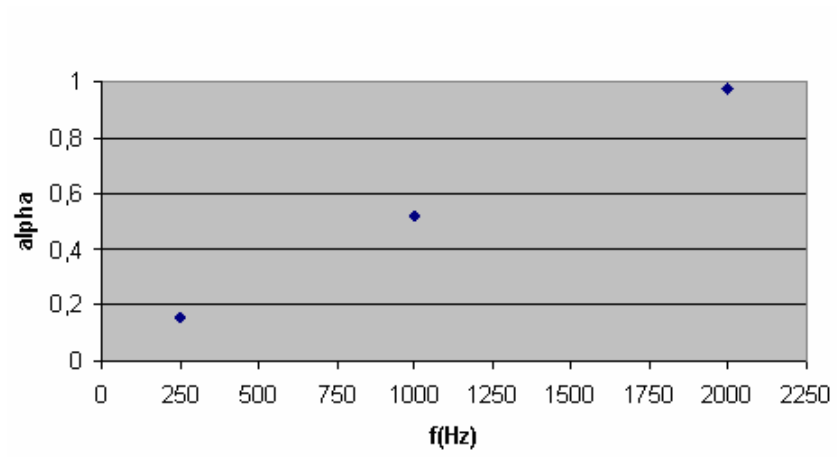
Figure A.2. Absorption coefficient of rock wool.
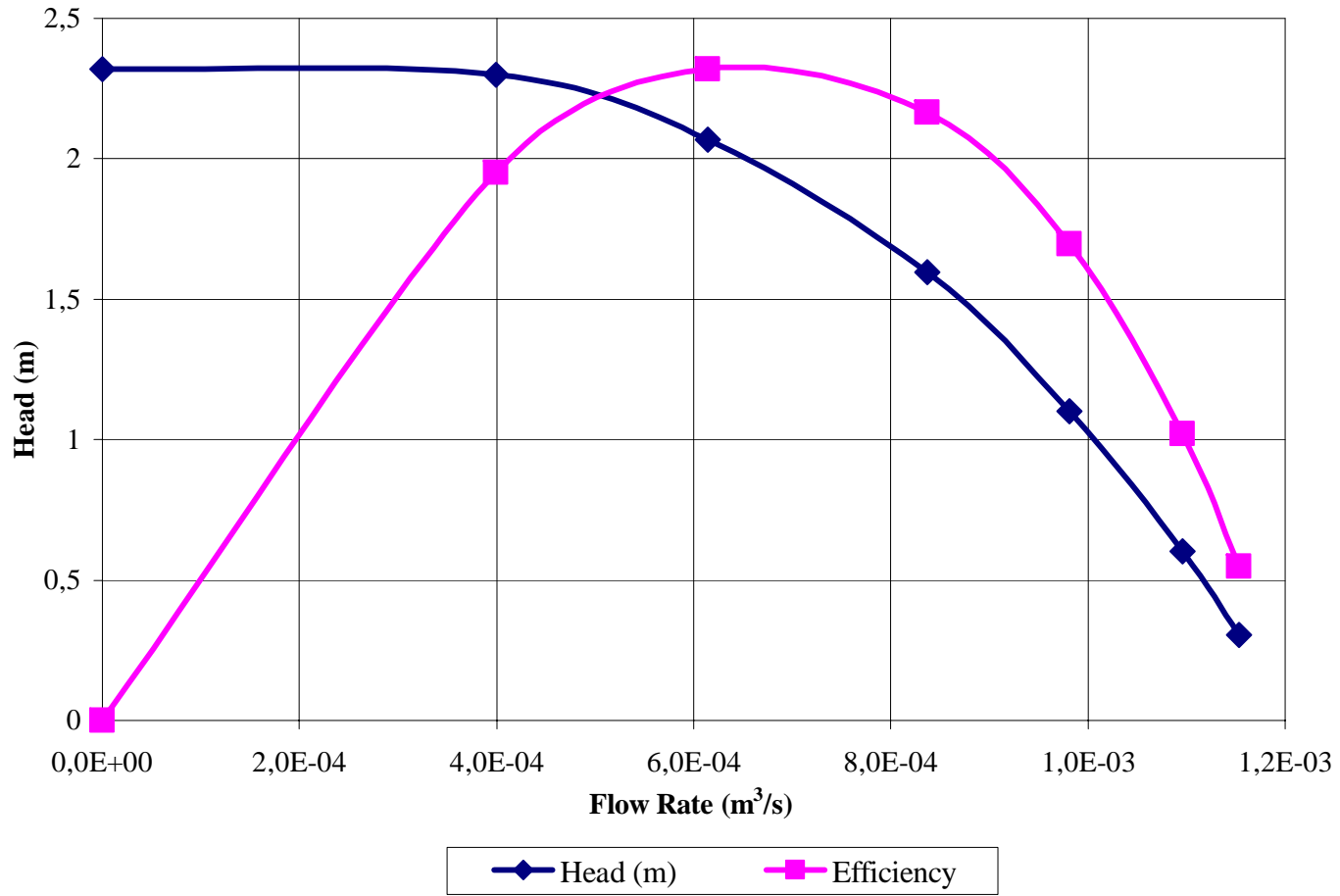
Figure B.1. Small pump characteristic at 2175 rpm.
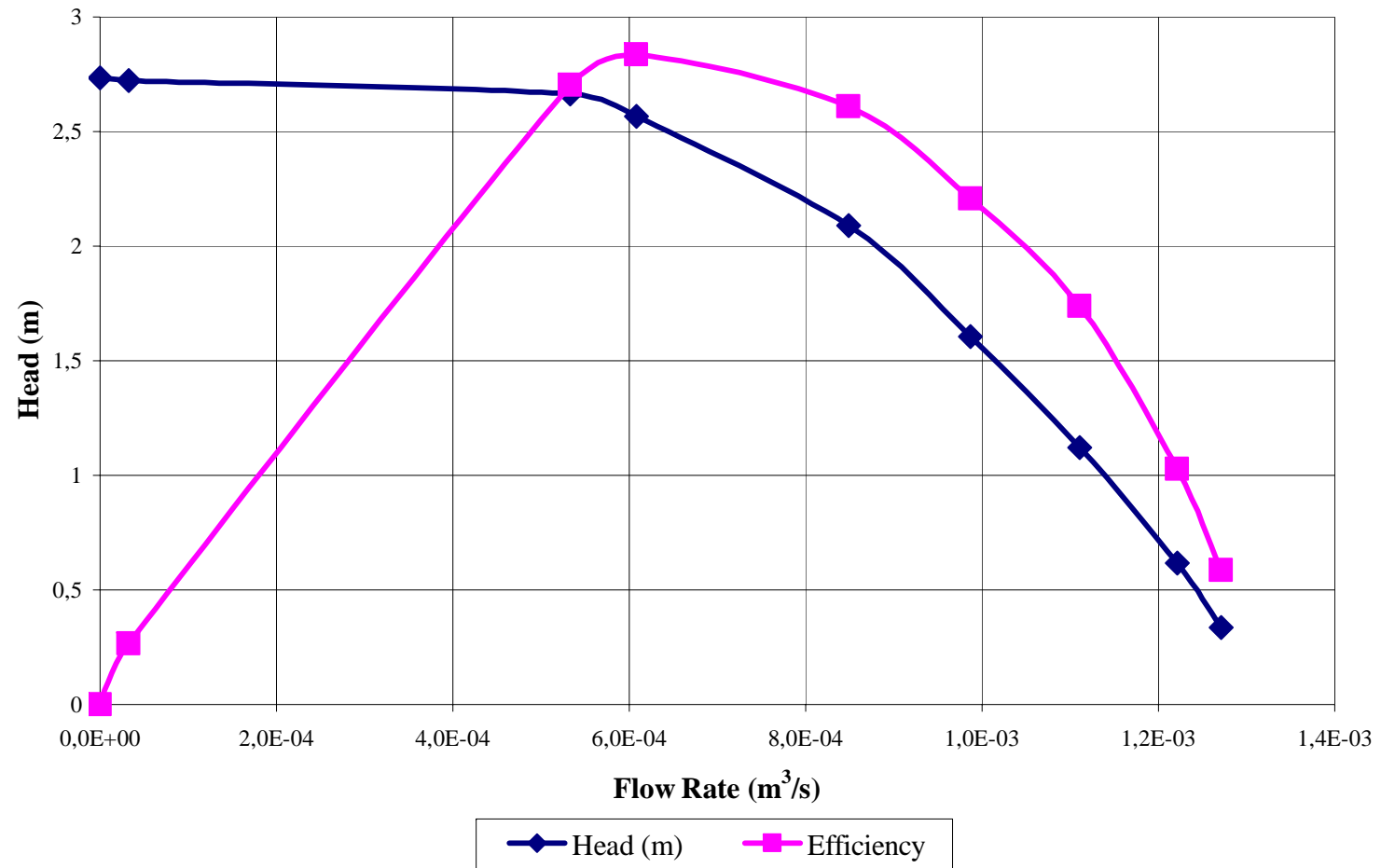
Figure B.2. Small pump characteristic at 2375 rpm.
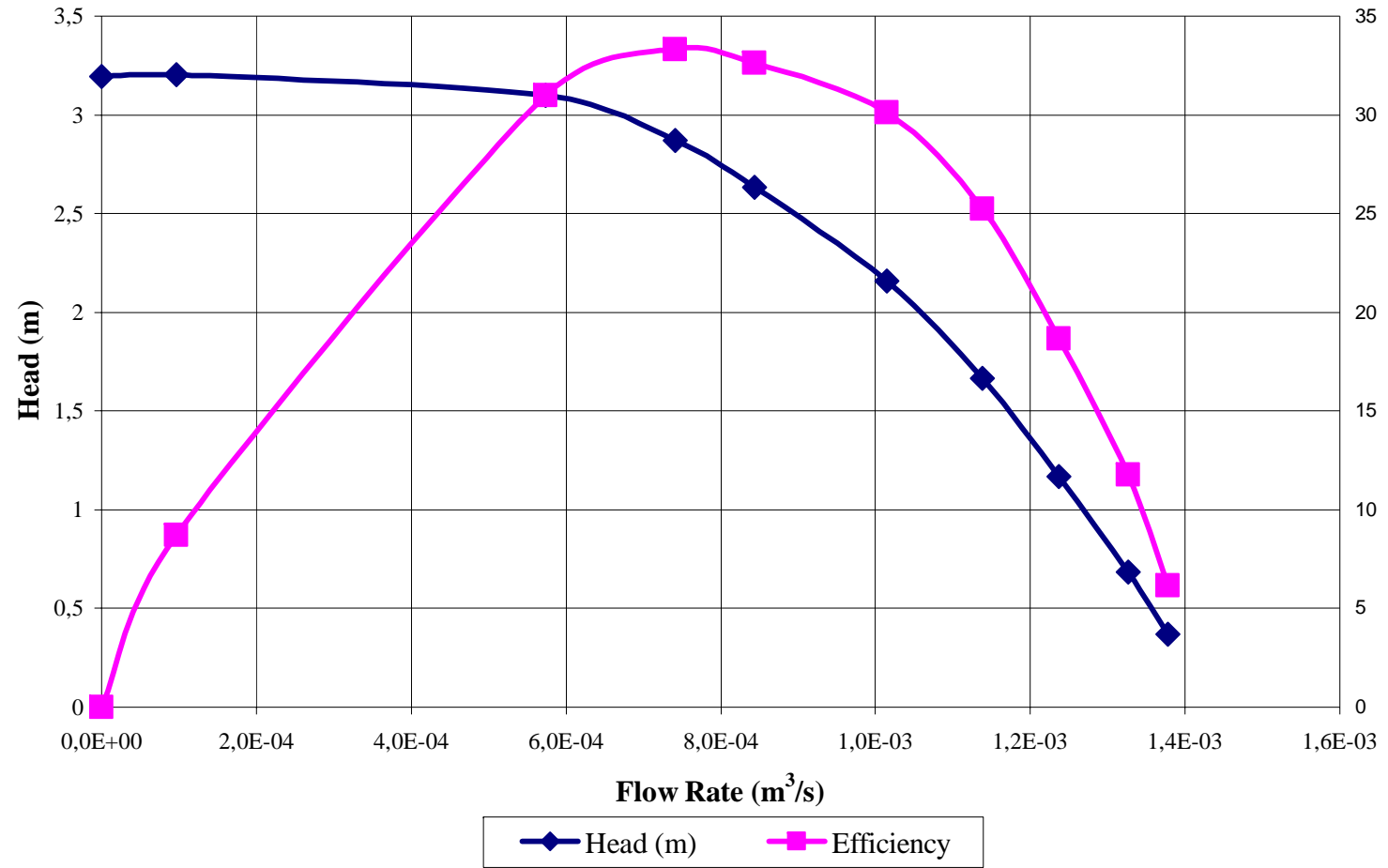
Figure B.3. Small pump characteristic at 2570 rpm.
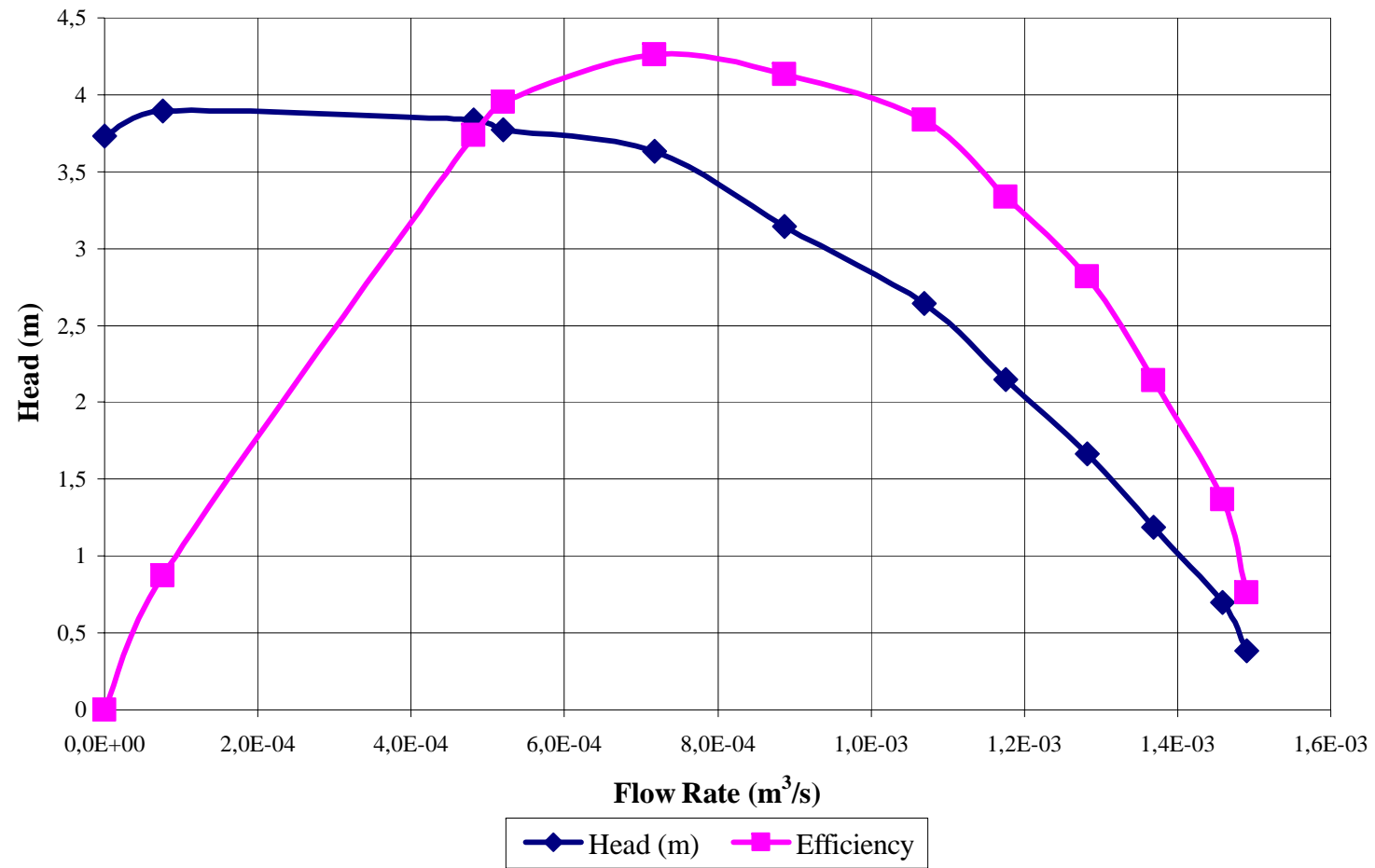
Figure B.4. Small pump characteristic at 2770 rpm.
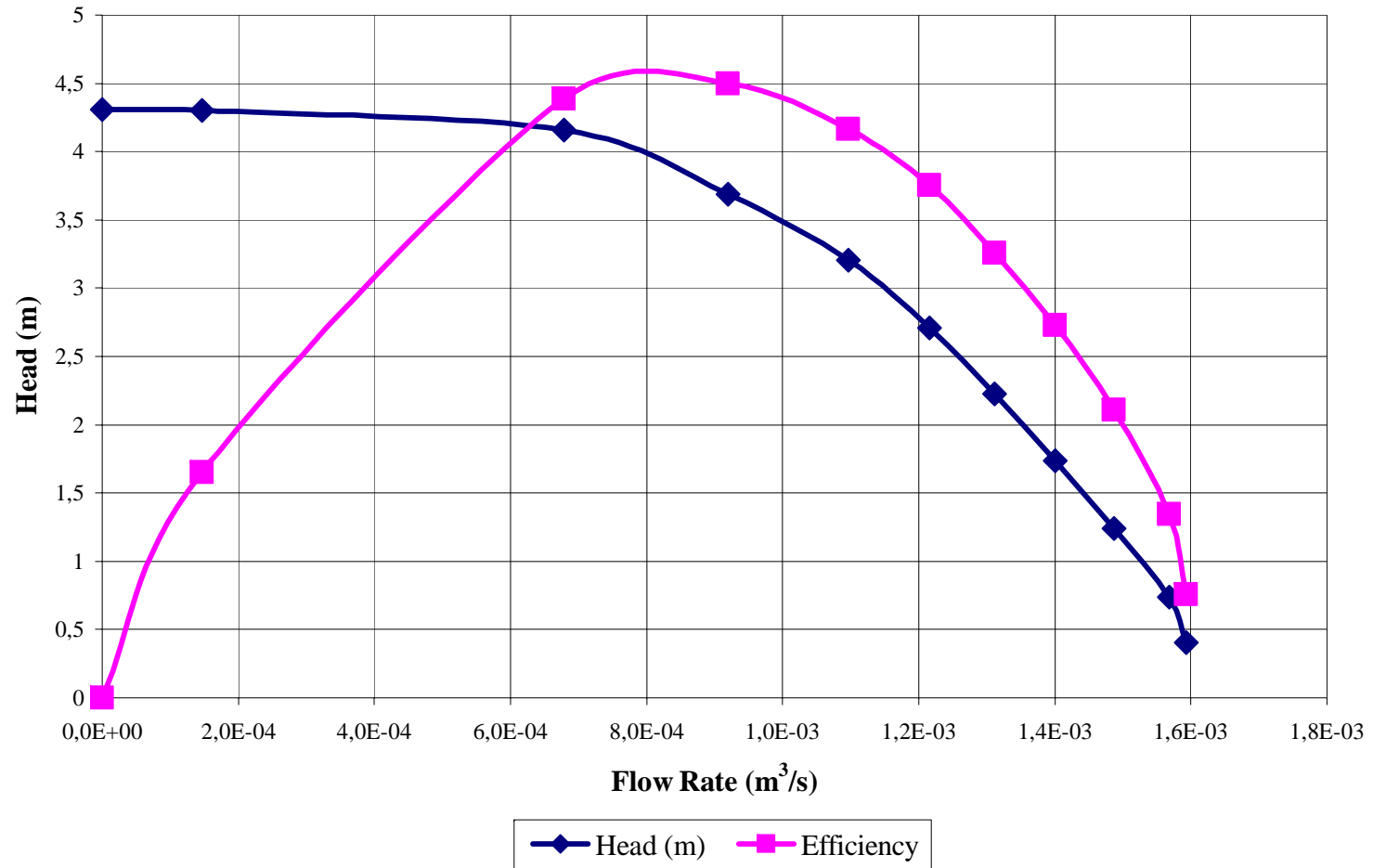
Figure B.5. Small pump characteristic at 2965 rpm.
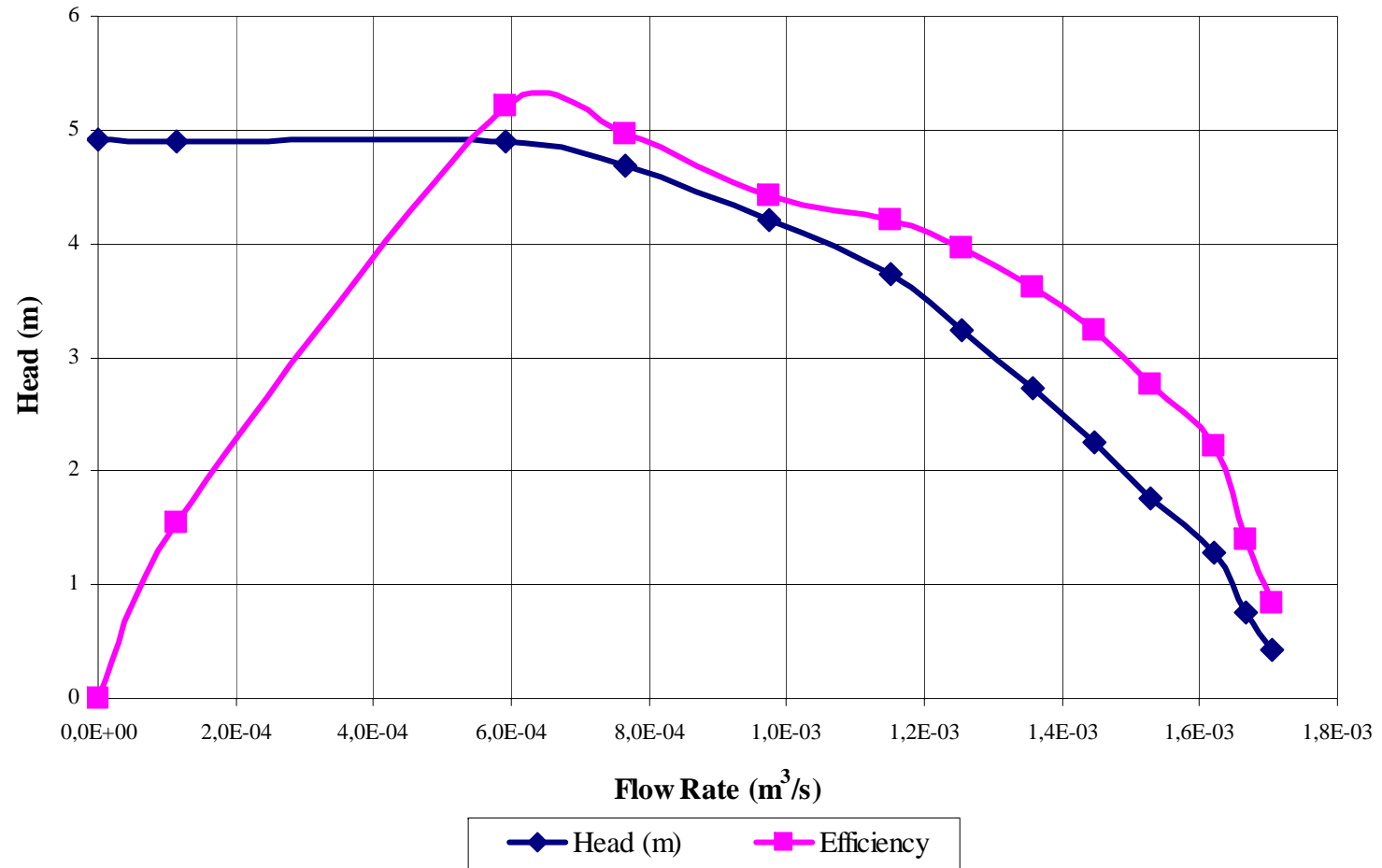
Figure B.6. Small pump characteristic at 3160 rpm.
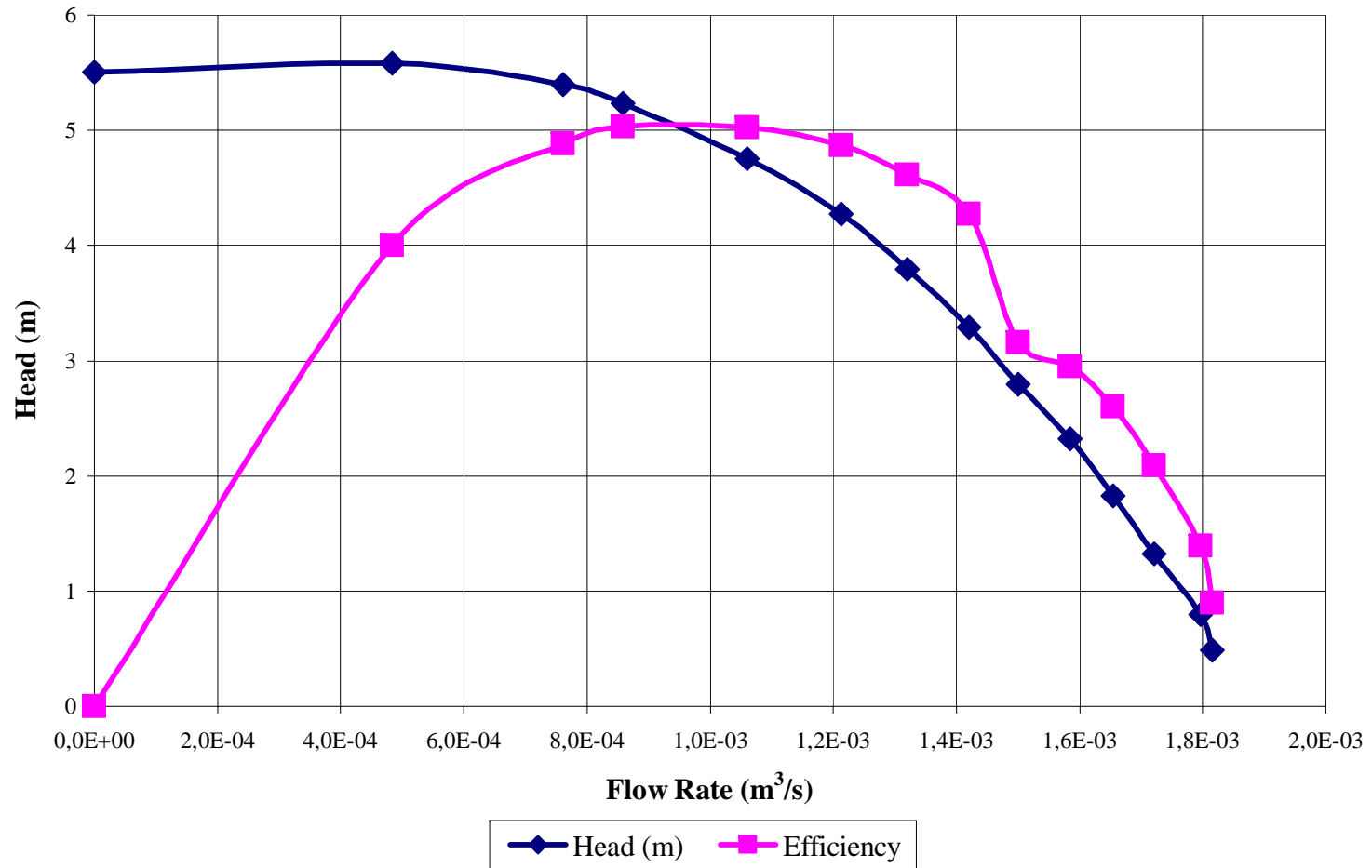
Figure B.7. Small pump characteristic at 3365 rpm.
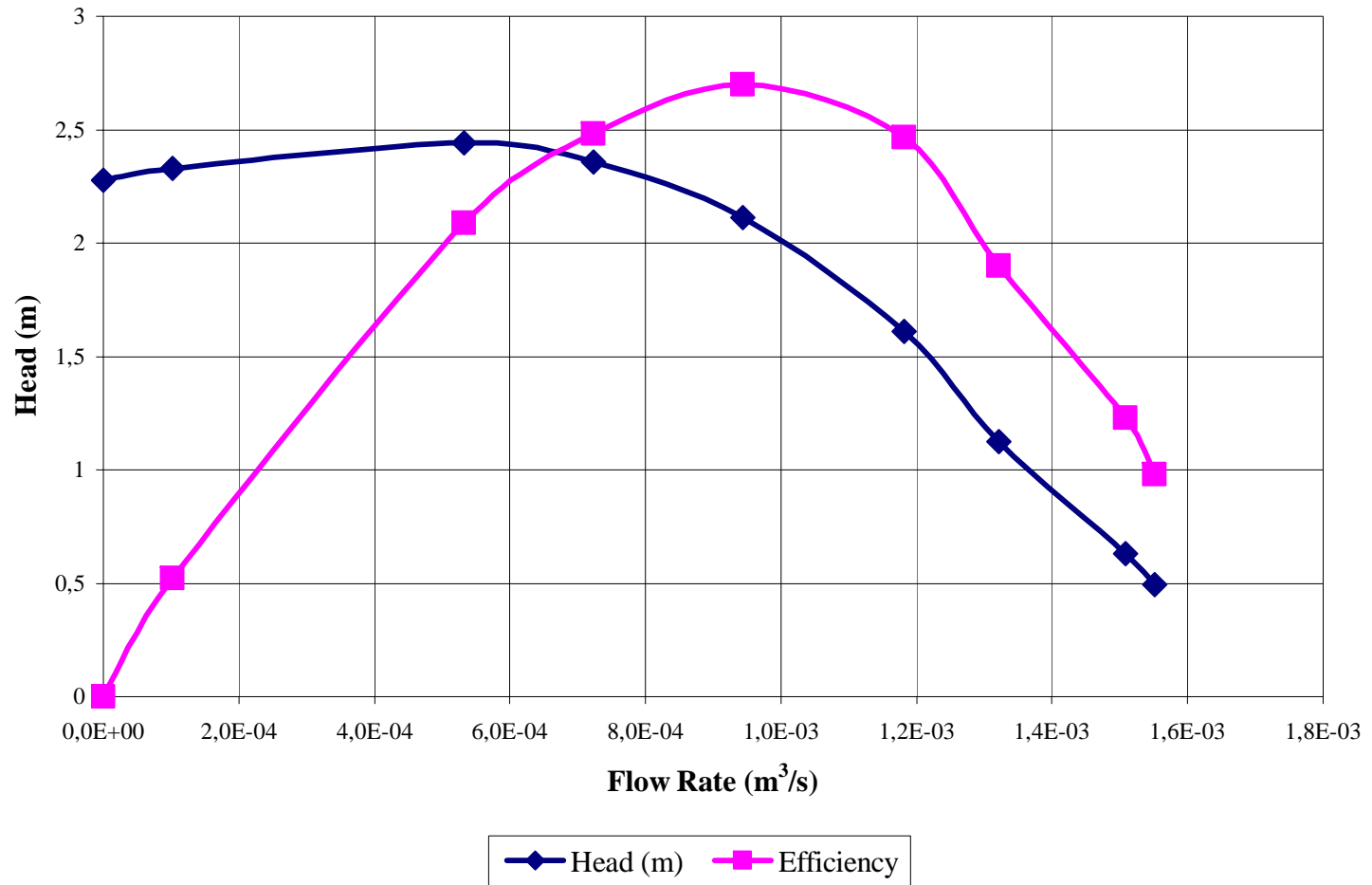
Figure B.8. Large pump characteristic at 2175 rpm.
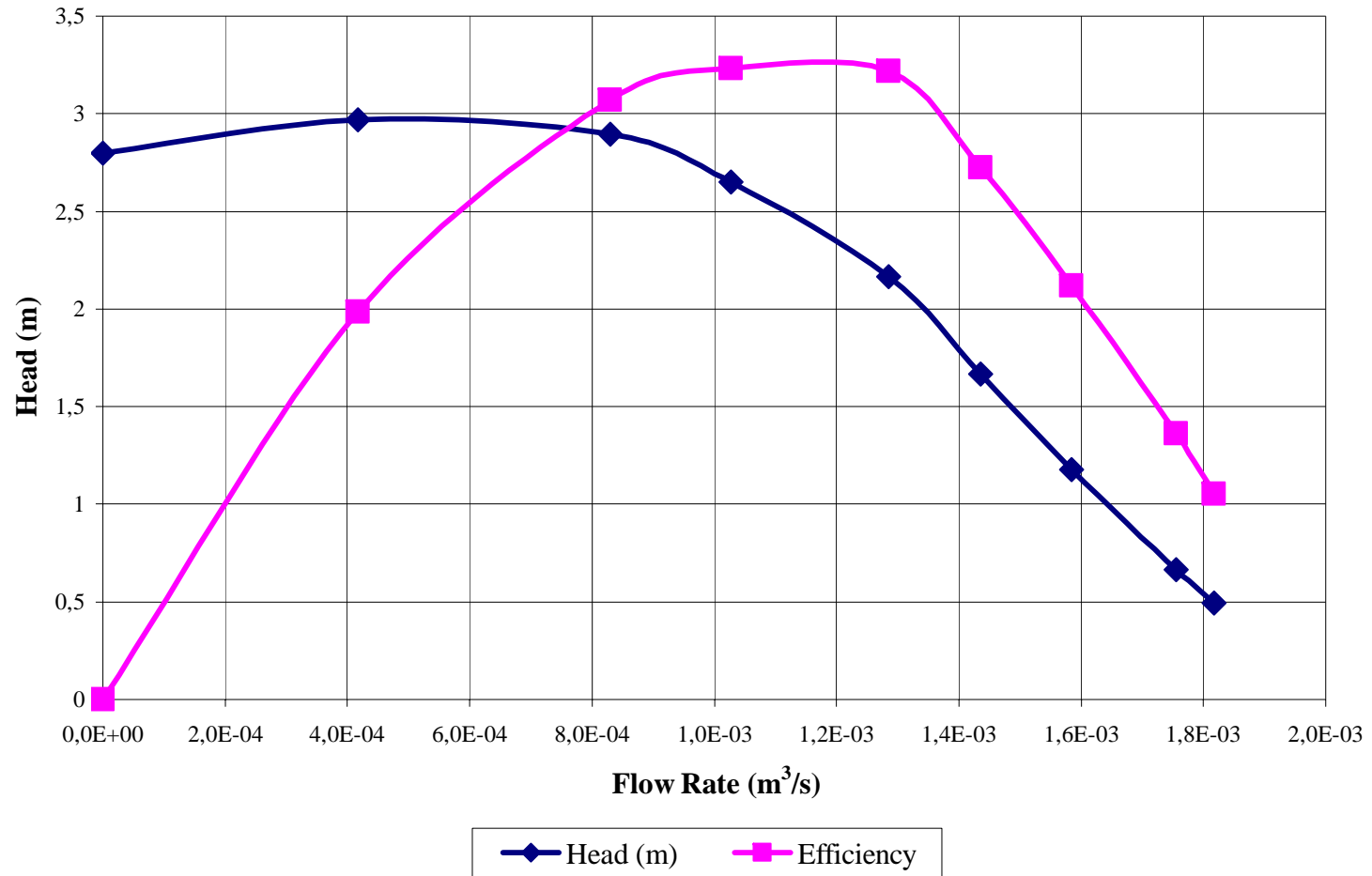
Figure B.9. Large pump characteristic at 2375 rpm.
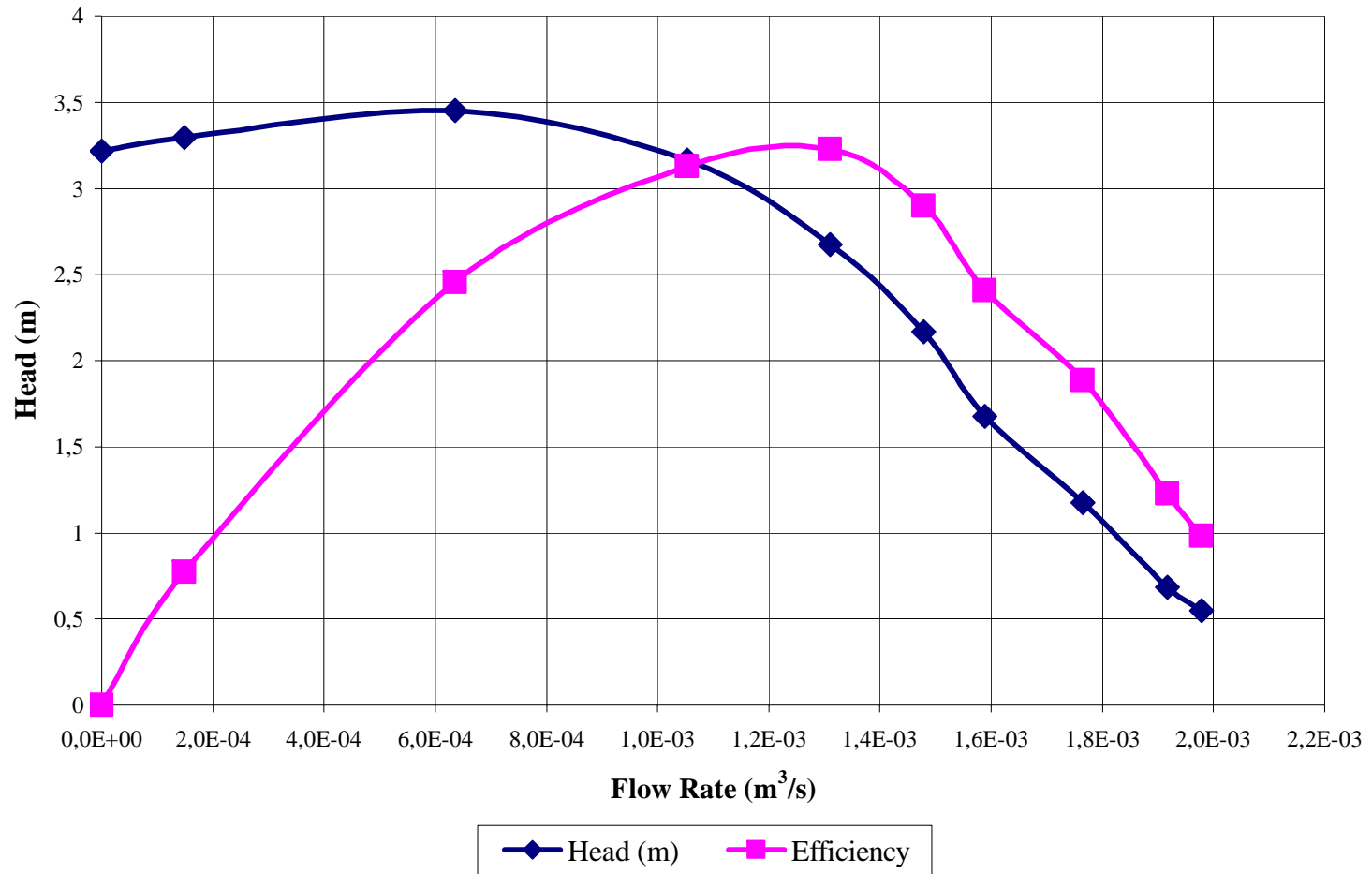
Figure B.10. Large pump characteristic at 2570 rpm.
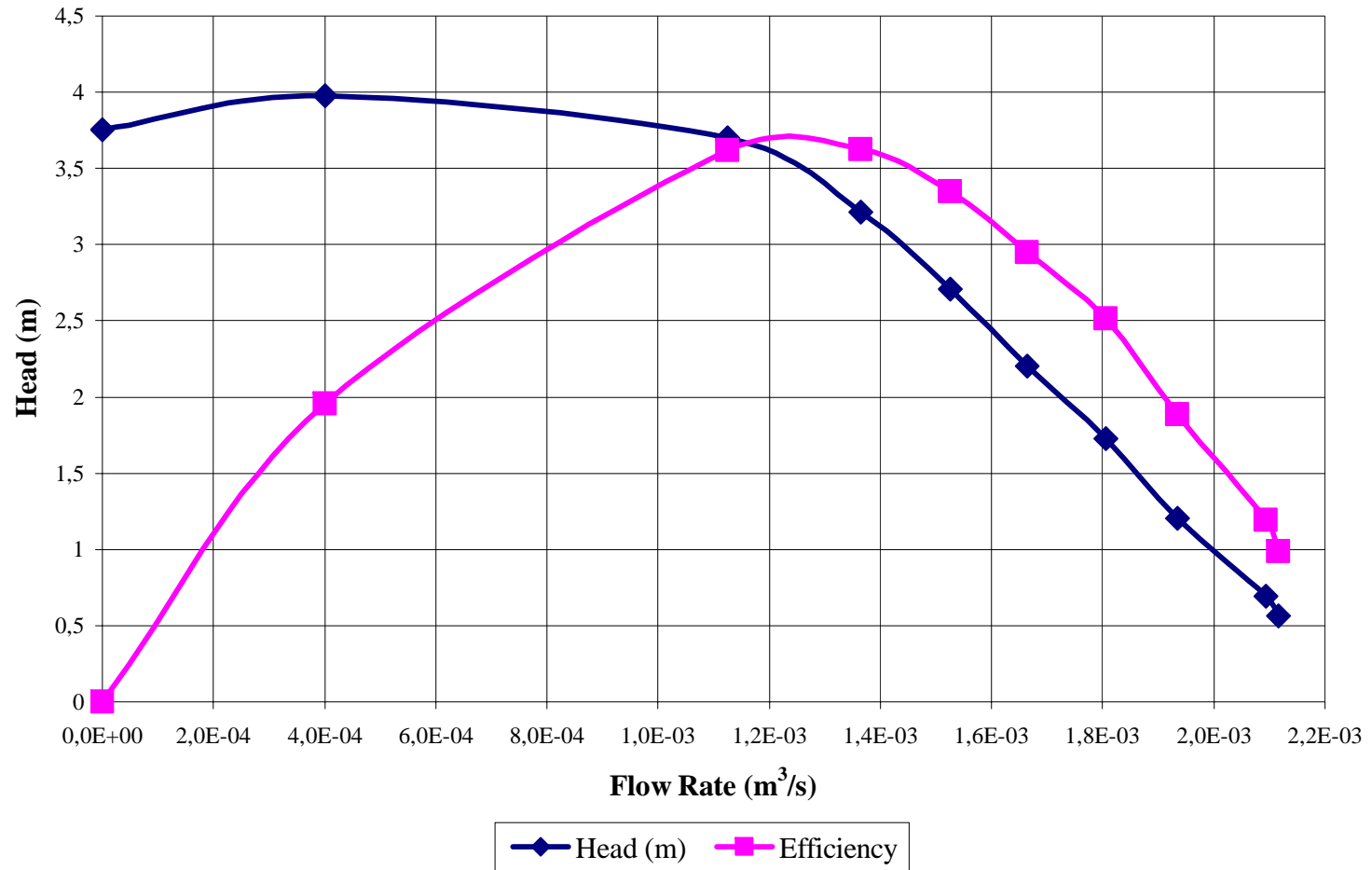
Figure B.11. Large pump characteristic at 2770 rpm.
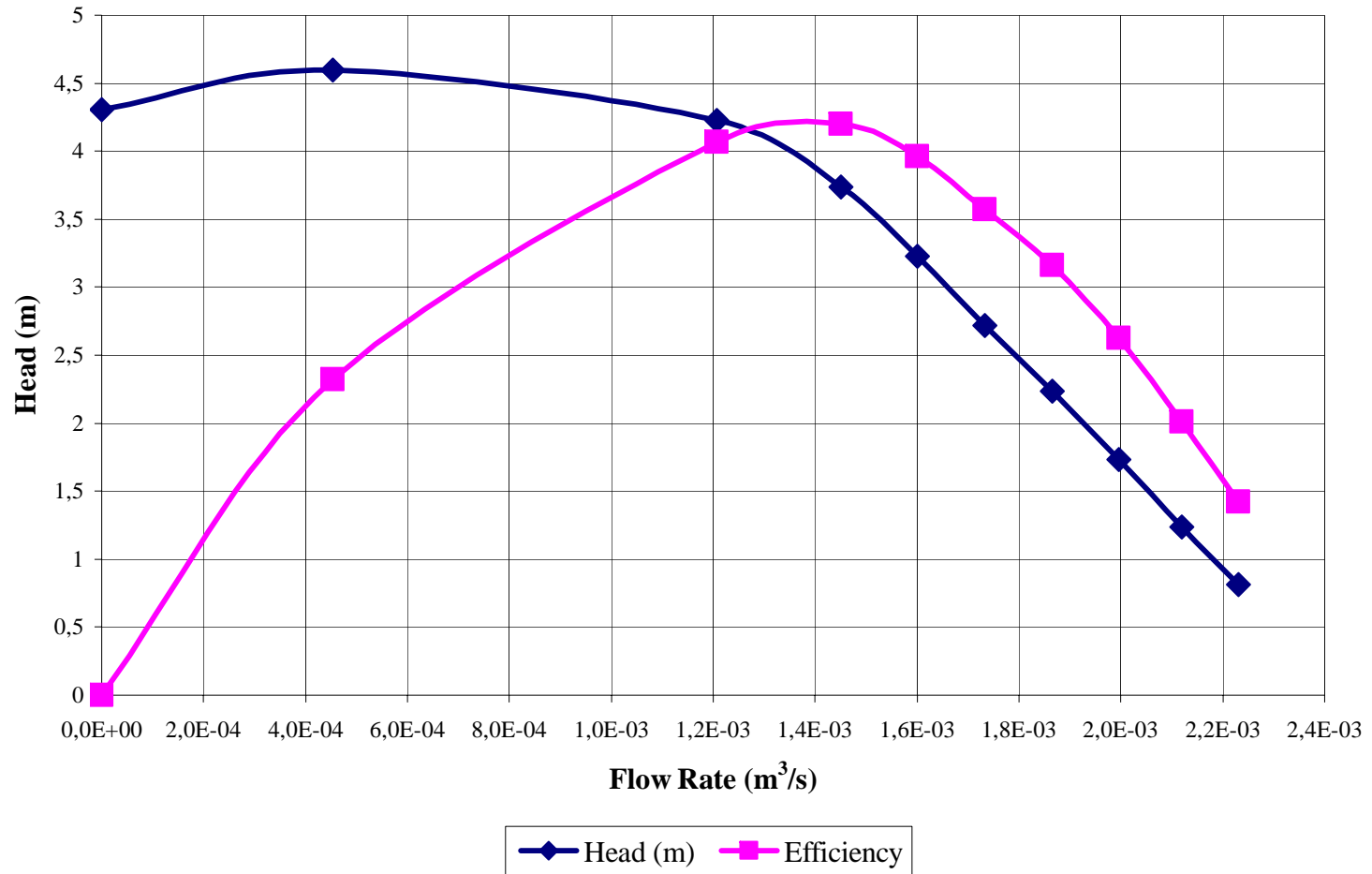
Figure B.12. Large pump characteristic at 2965 rpm.
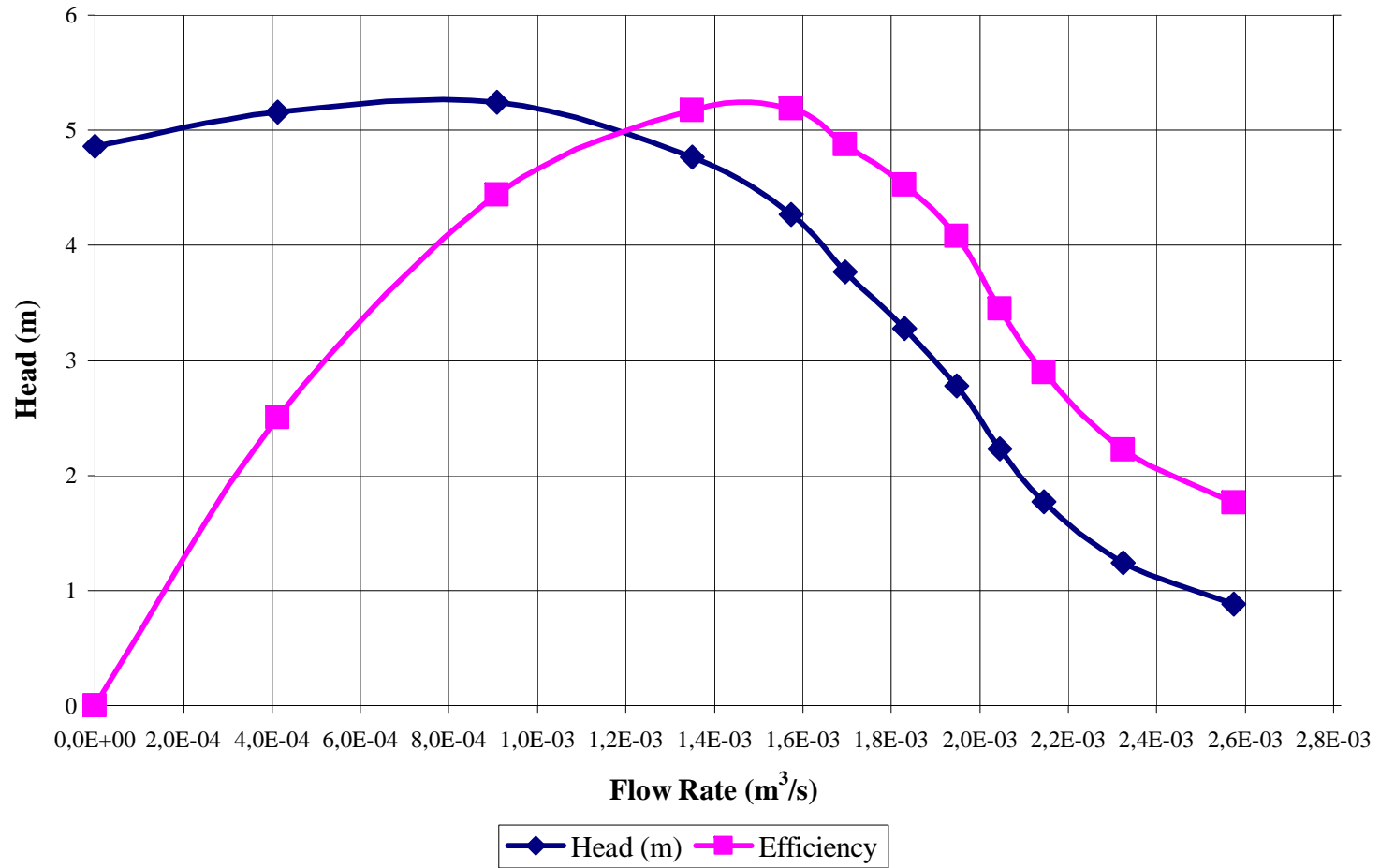
Figure B.13. Large pump characteristic at 3160 rpm.
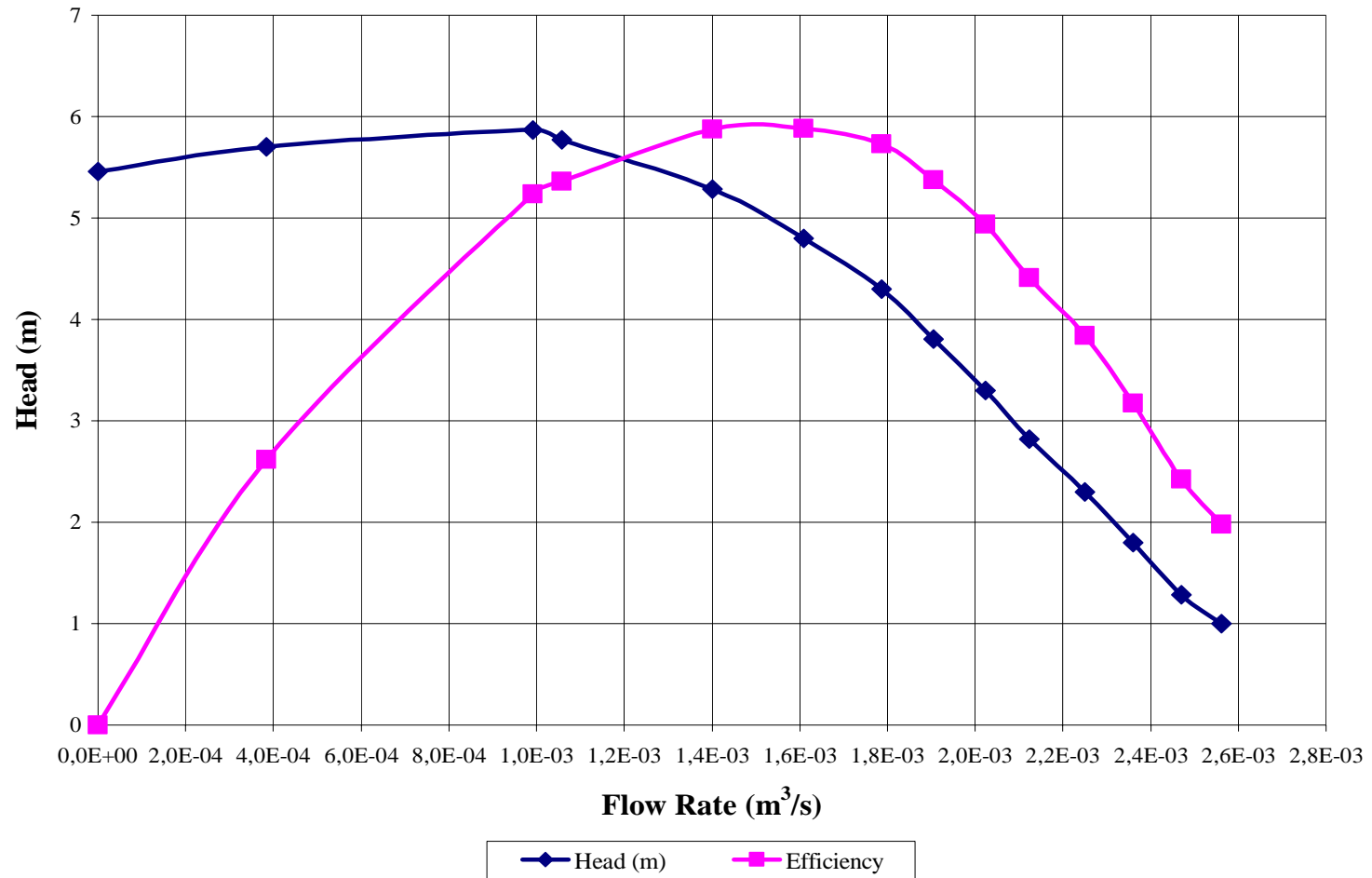
Figure B.14. Large pump characteristic at 3365 rpm.

APPENDIX C

C.1. PICTURES FOR EXPERIMENTAL SET-UP AND EQUIPMENT
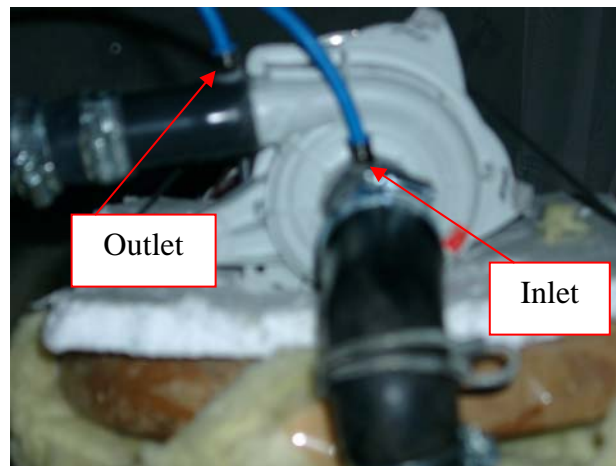
Figure C.1. Small pump.
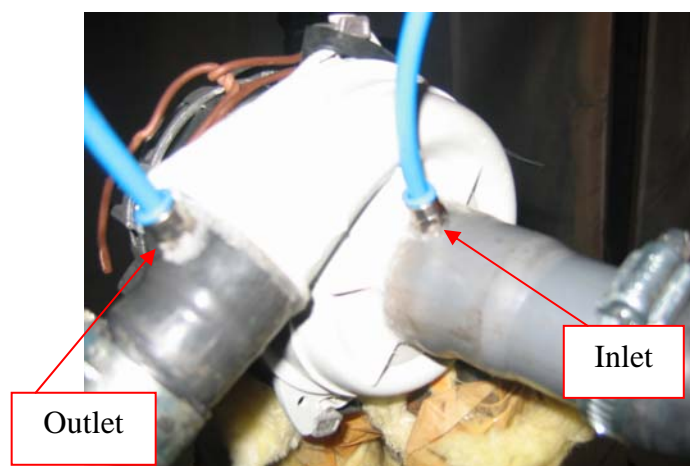
Figure C.2. Large pump.
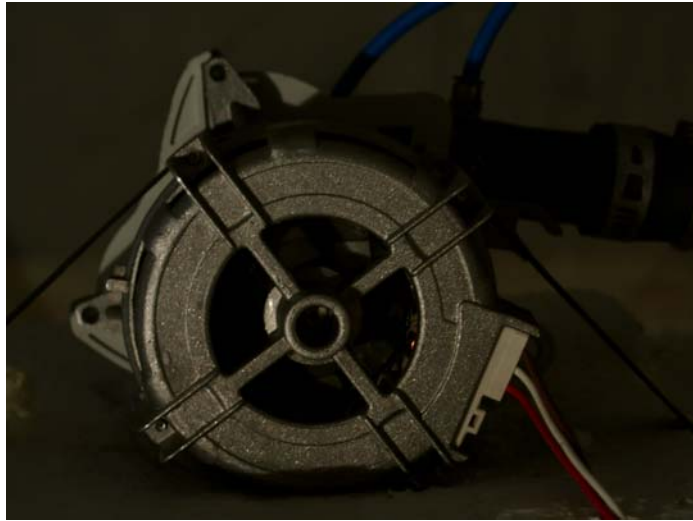
Figure C.3. Motor.
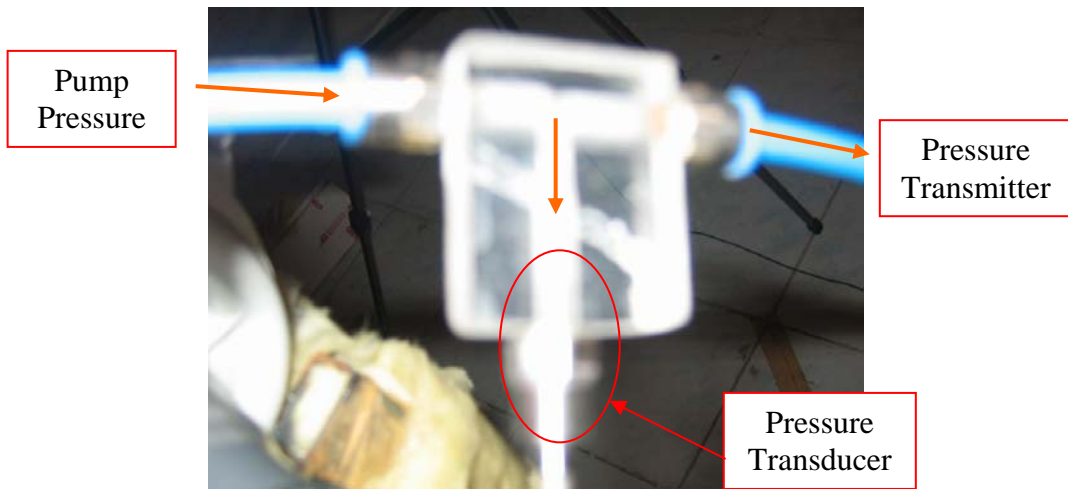
Figure C.4. T-connection for pressure measurement.

**Figure C.5.** Scale for volumetric flow rate measurement.
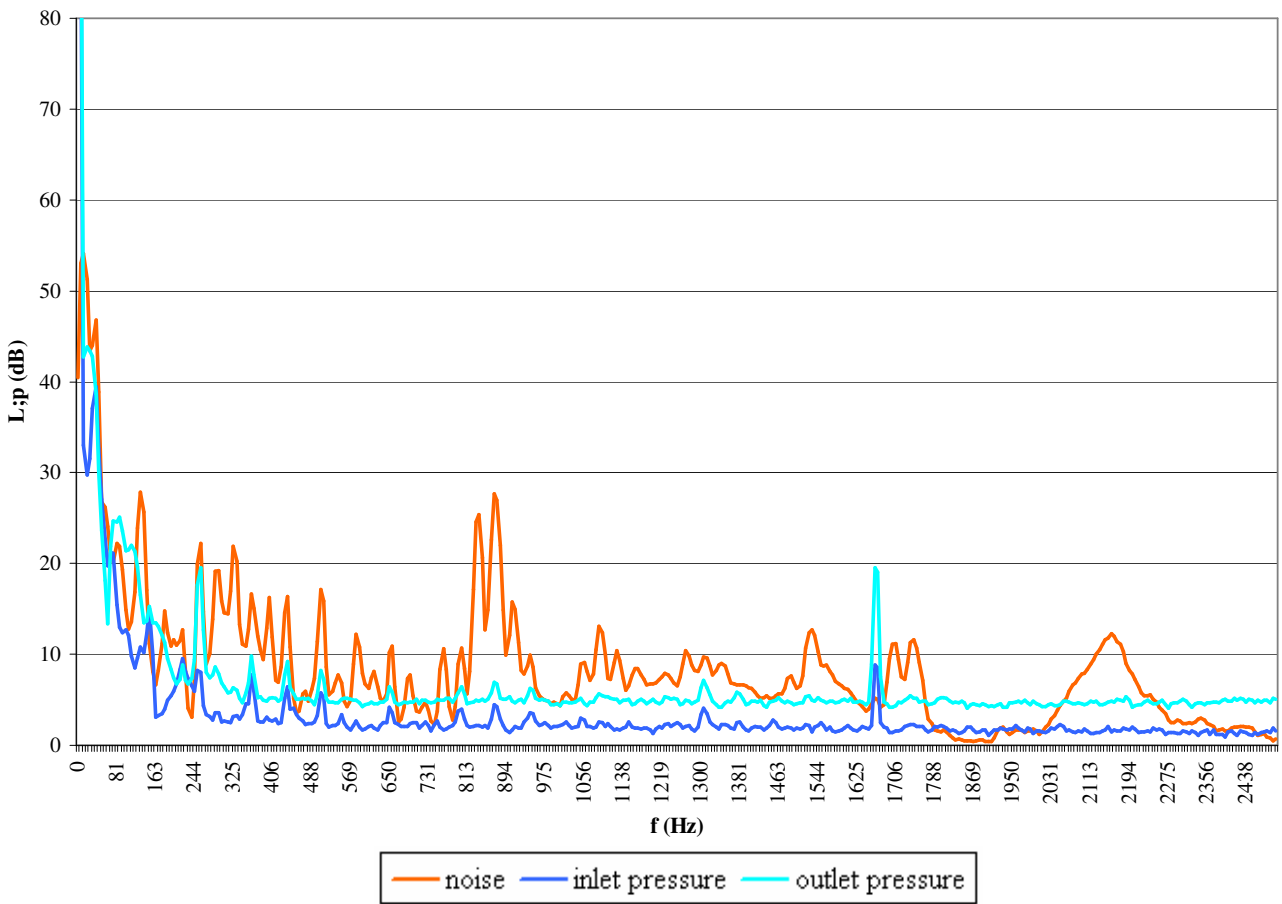
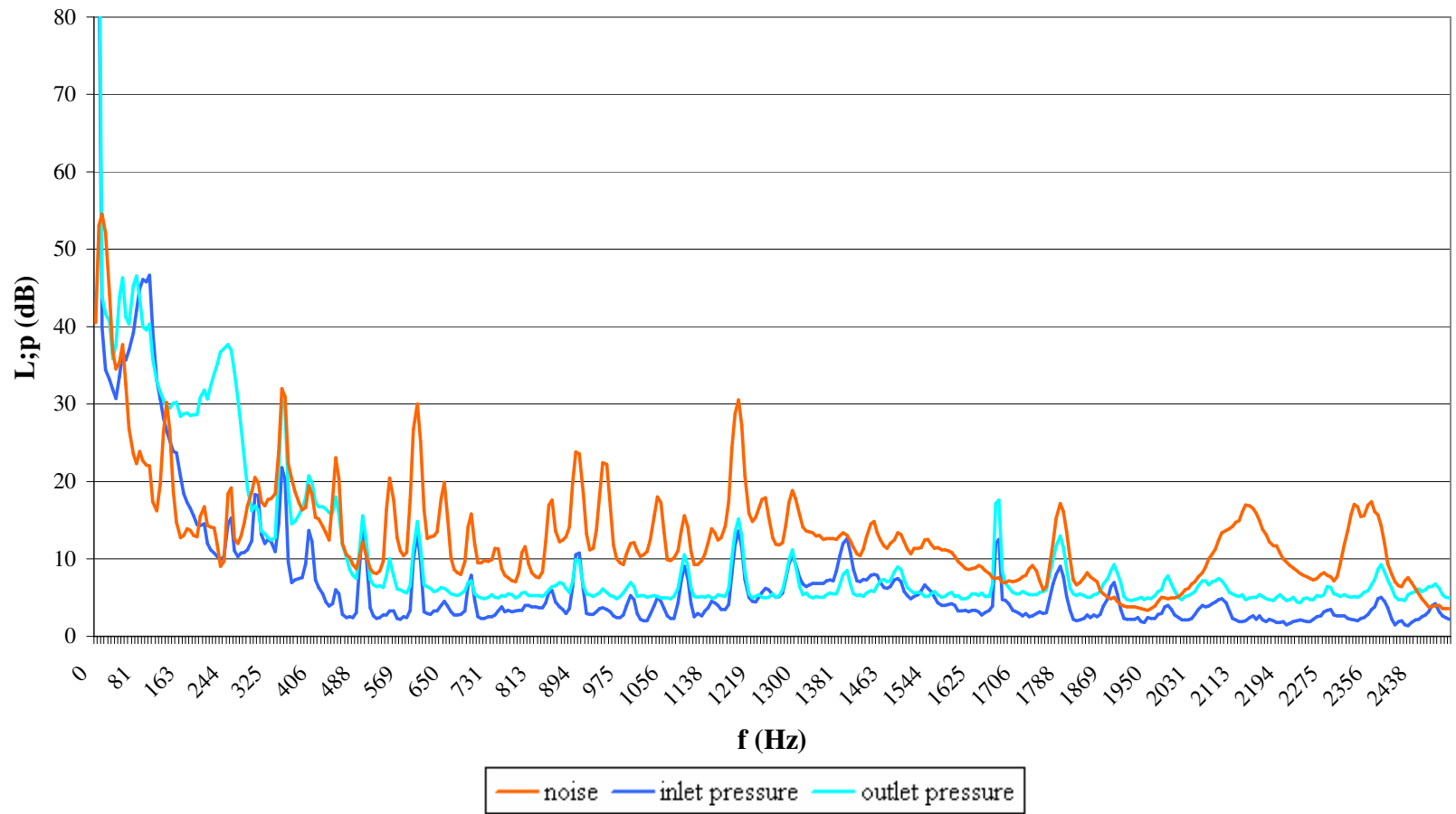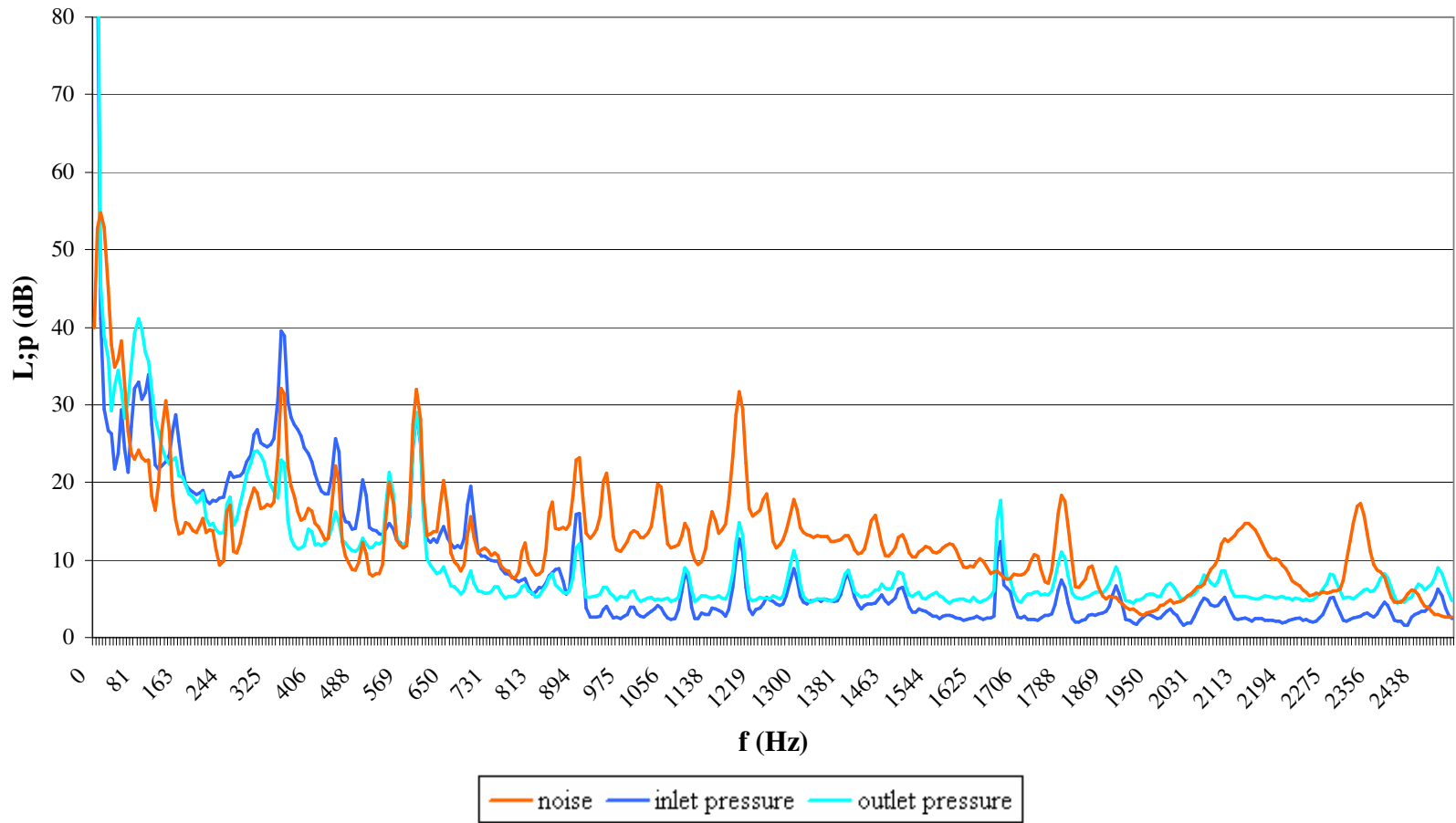**Figure D.1.** Small pump noise fft spectra for 2175 rpm, shut off.
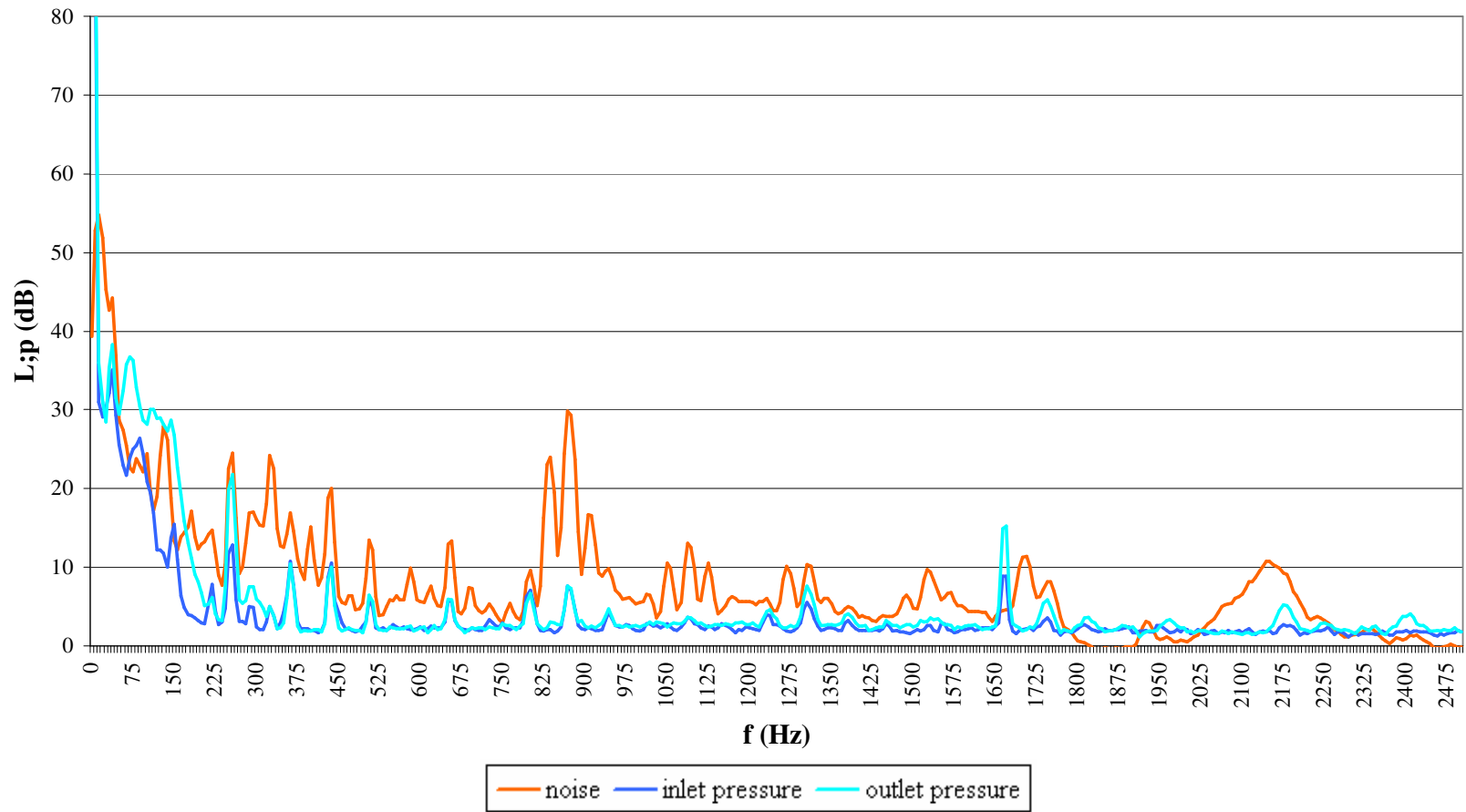
Figure D.2. Small pump noise fft spectrum for 2175 rpm, 0.41 l/s.
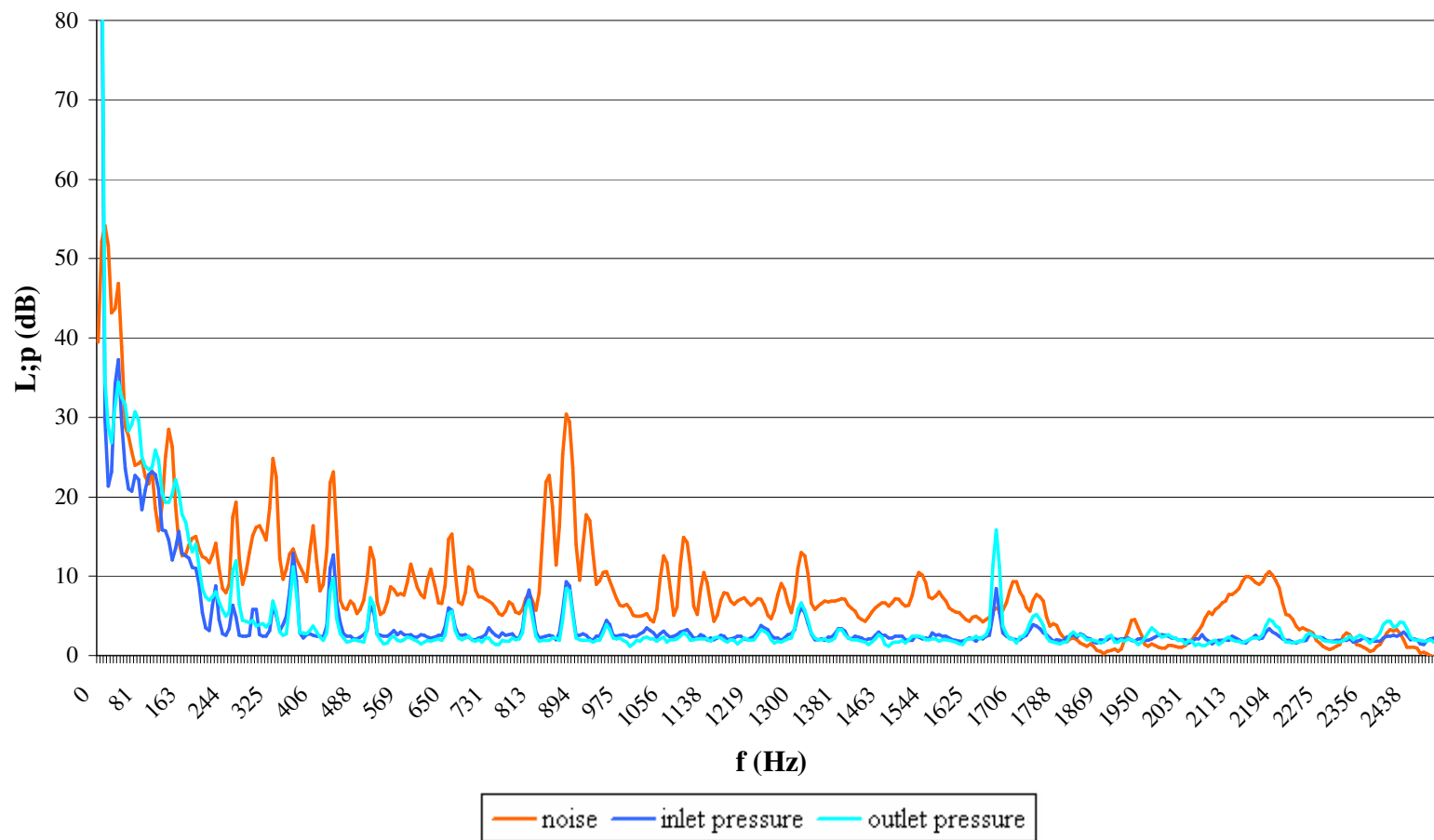
Figure D.3. Small pump noise fft spectrum for 2175 rpm, 0.57 l/s.
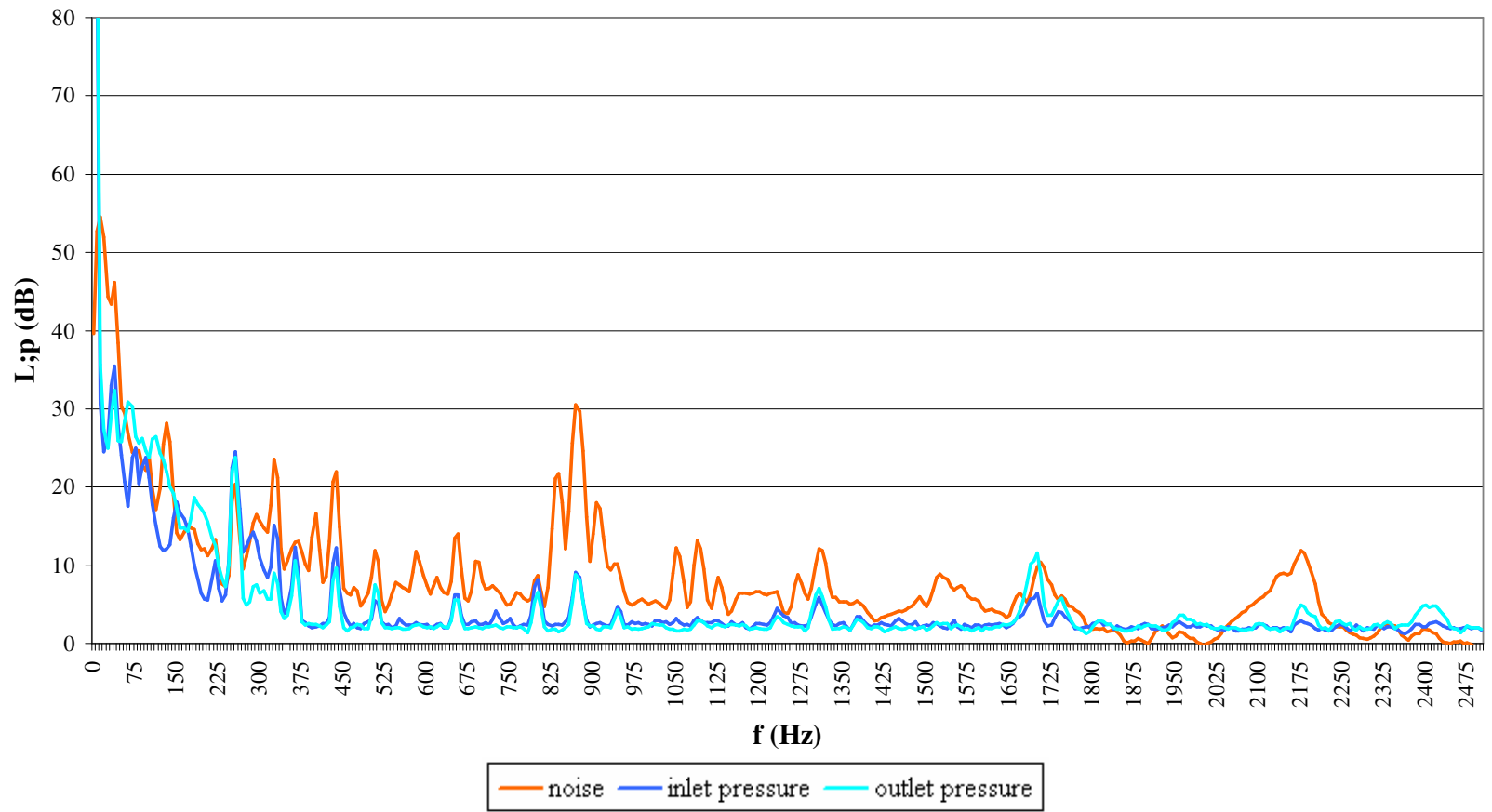
Figure D.4. Small pump noise fft spectrum for 2175 rpm, 0.66 l/s.
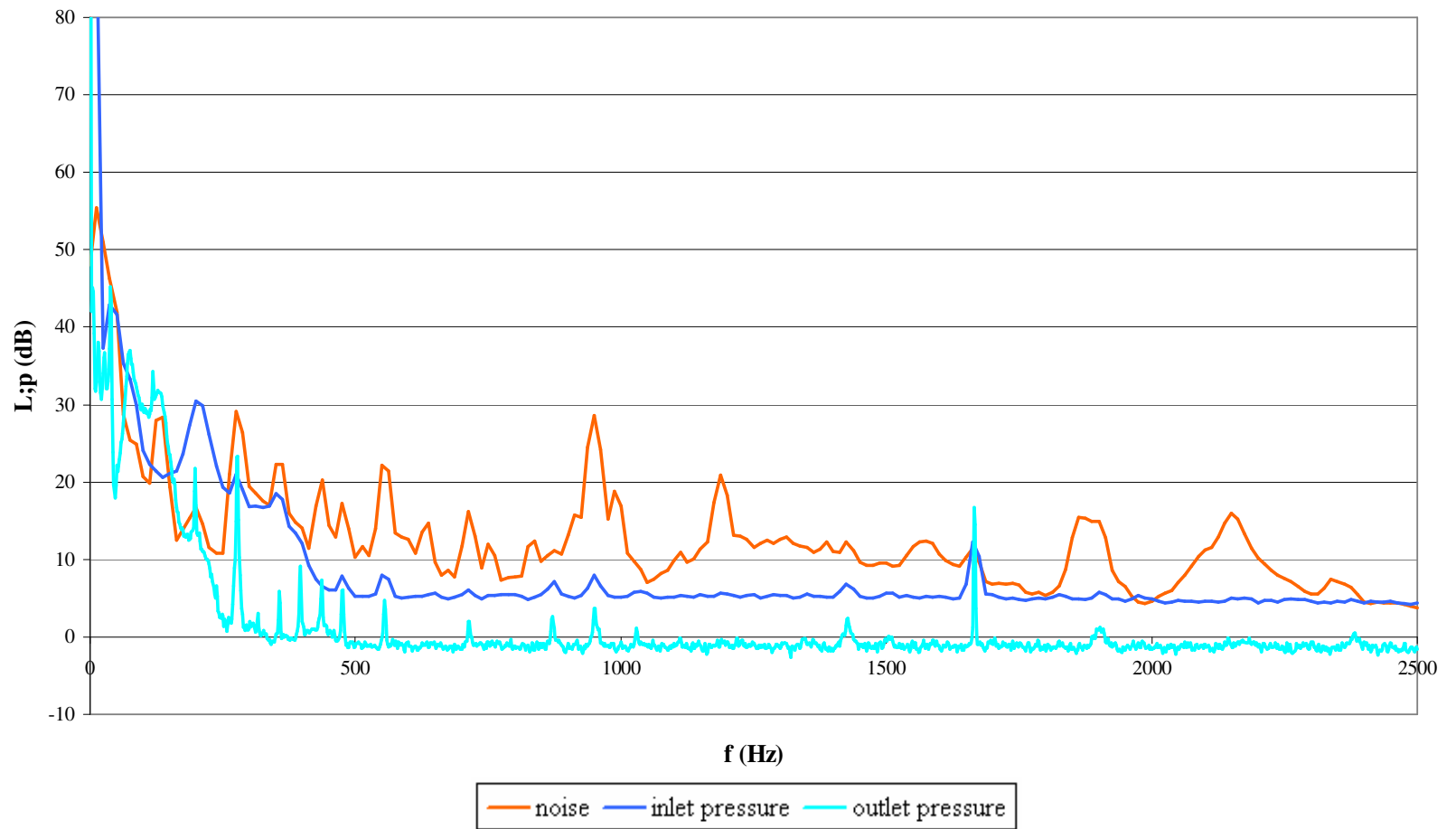
Figure D.5. Small pump noise fft spectrum for 2375 rpm, shut off.
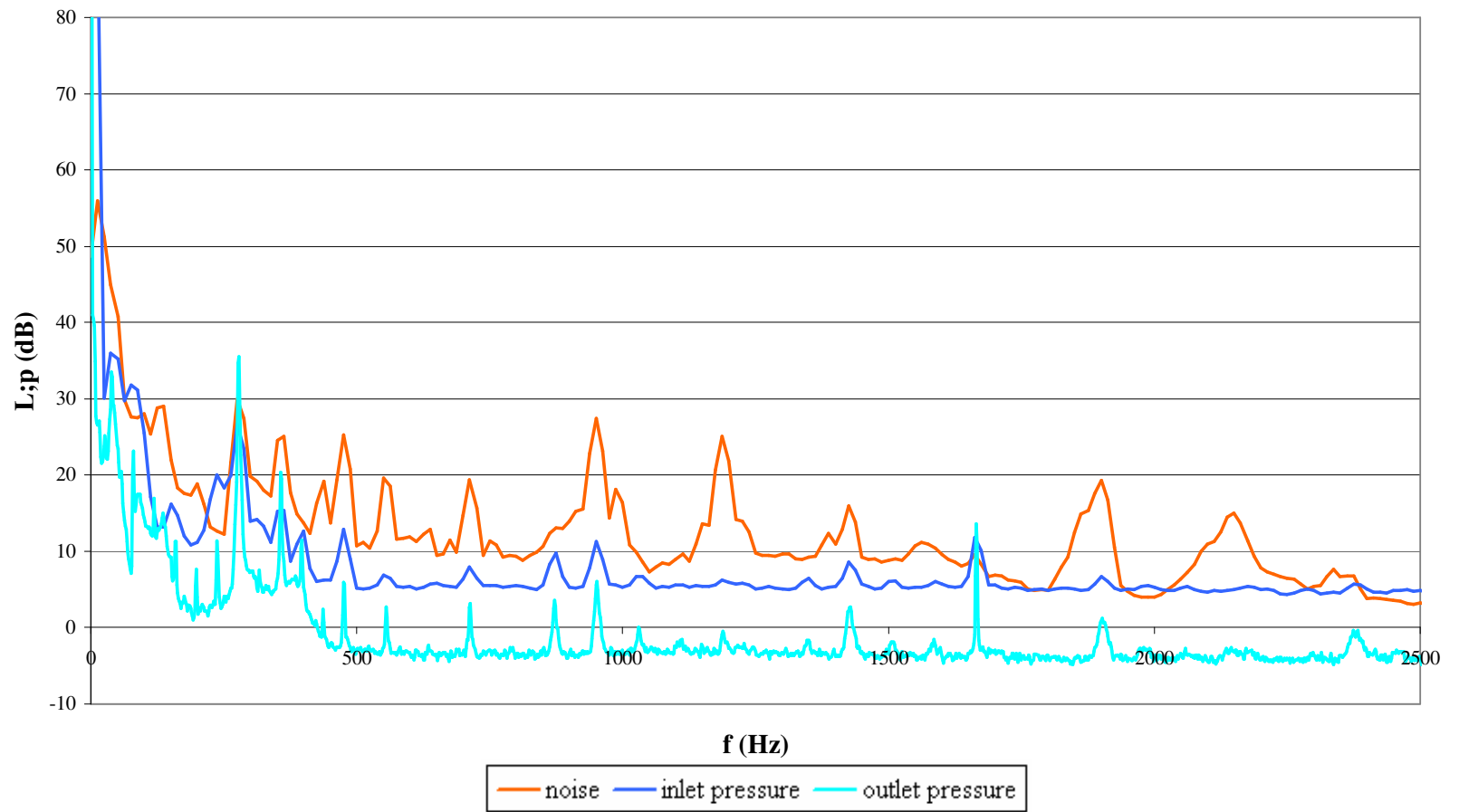
Figure D.6. Small pump noise fft spectrum for 2375 rpm, 0.486 l/s.
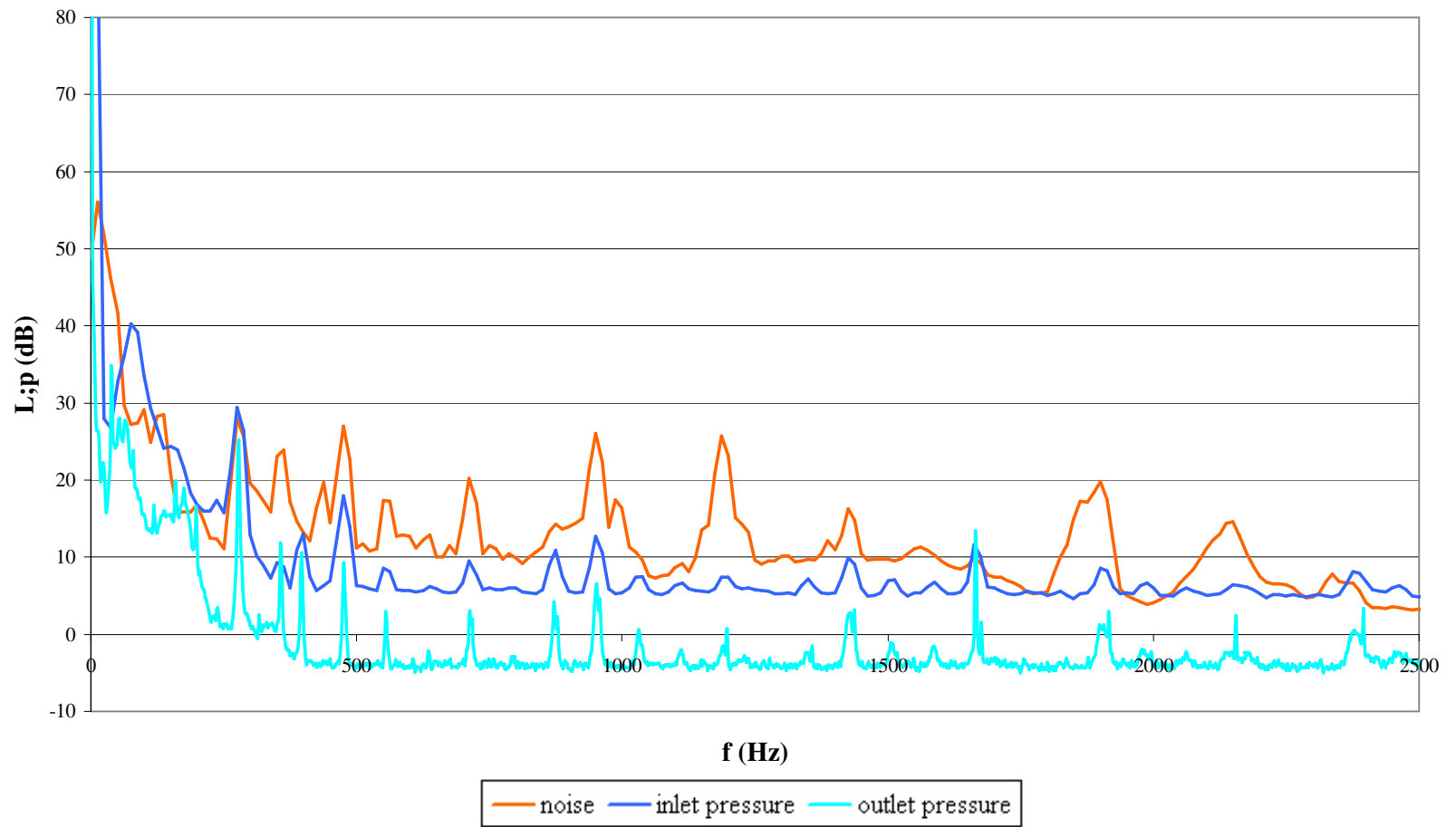
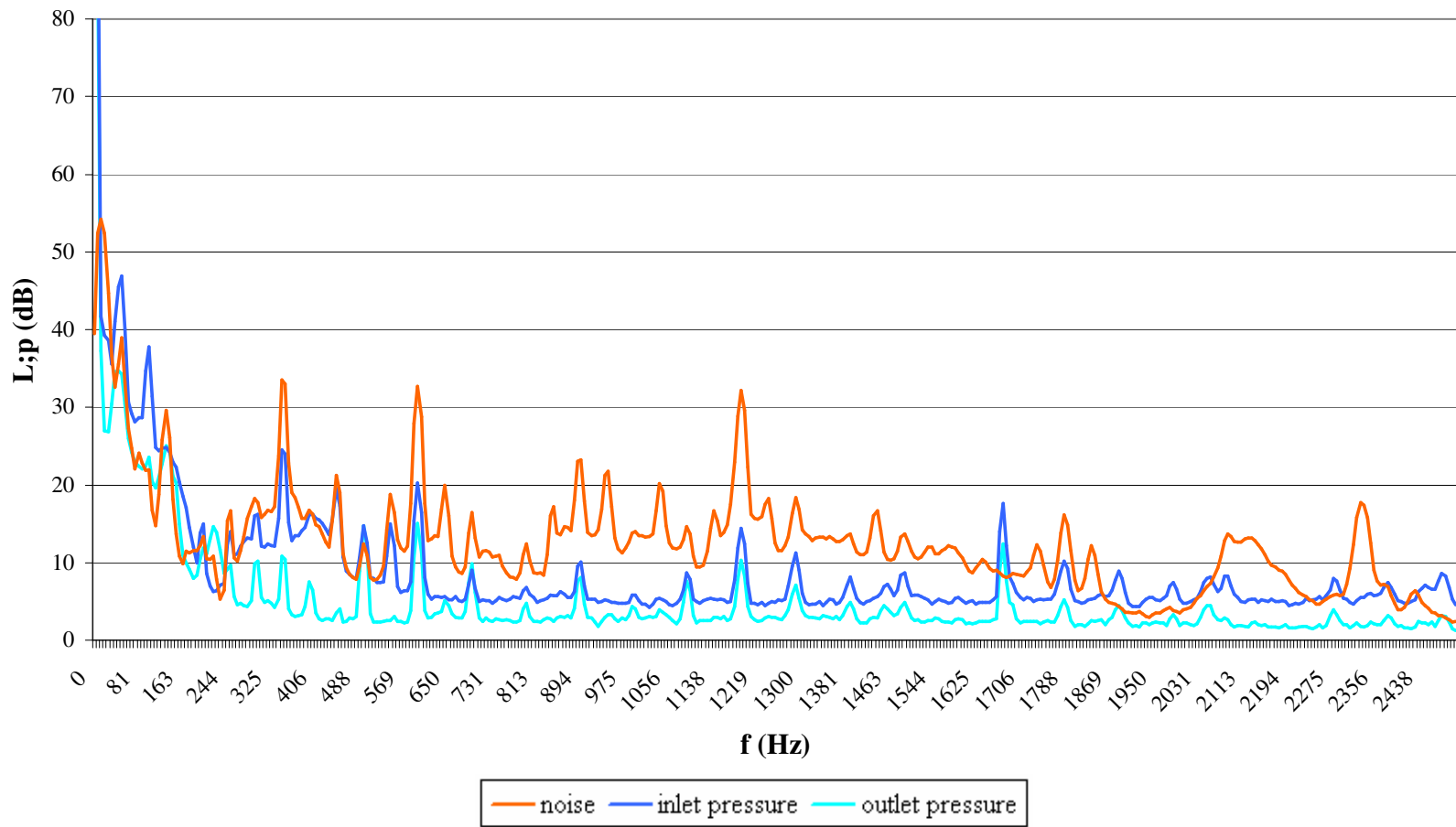**Figure D.7.** Small pump noise fft spectrum for 2375 rpm, 0.62 l/s.
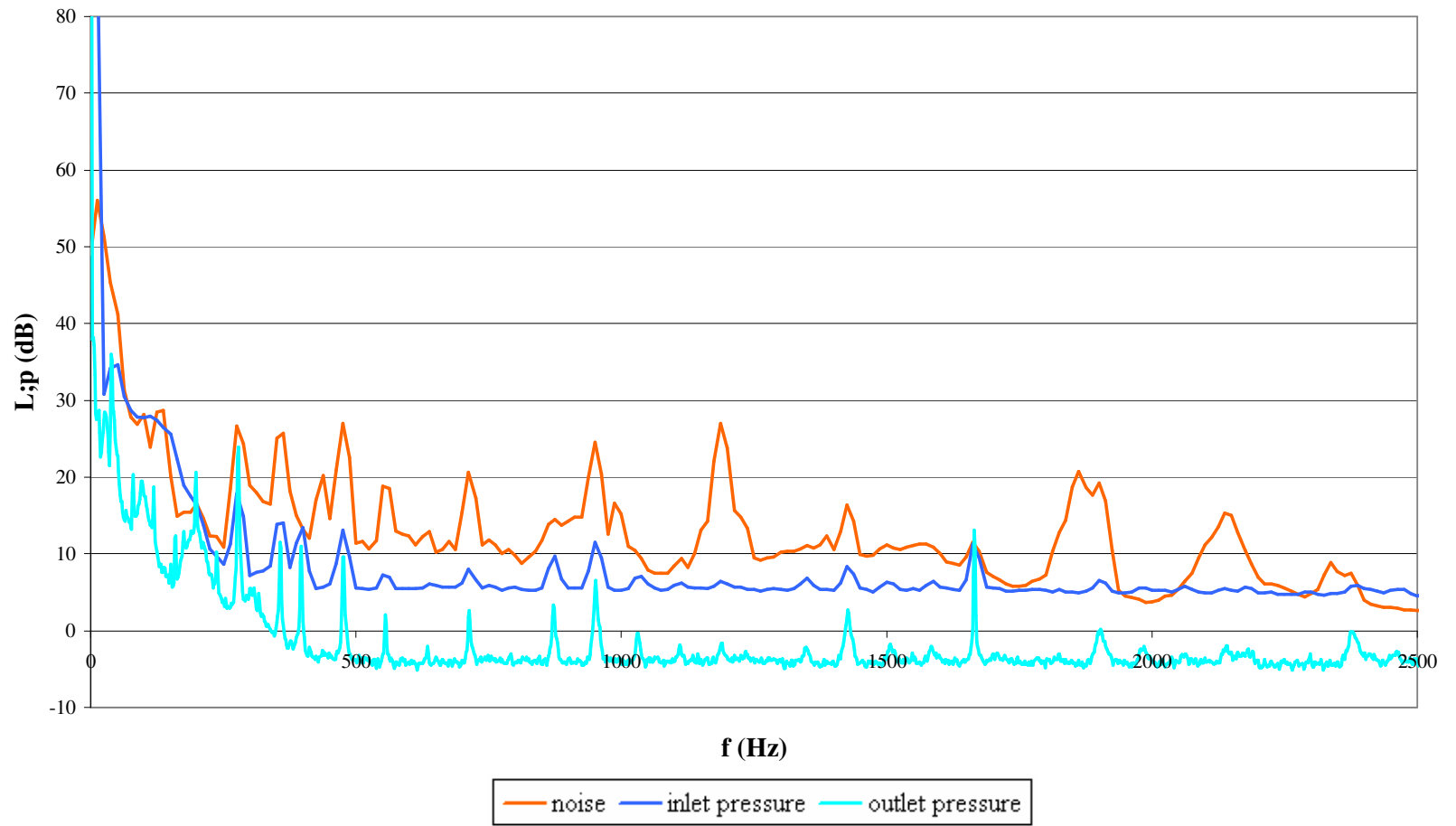
Figure D.8. Small pump noise fft spectrum for 2375 rpm, 0.69 l/s.
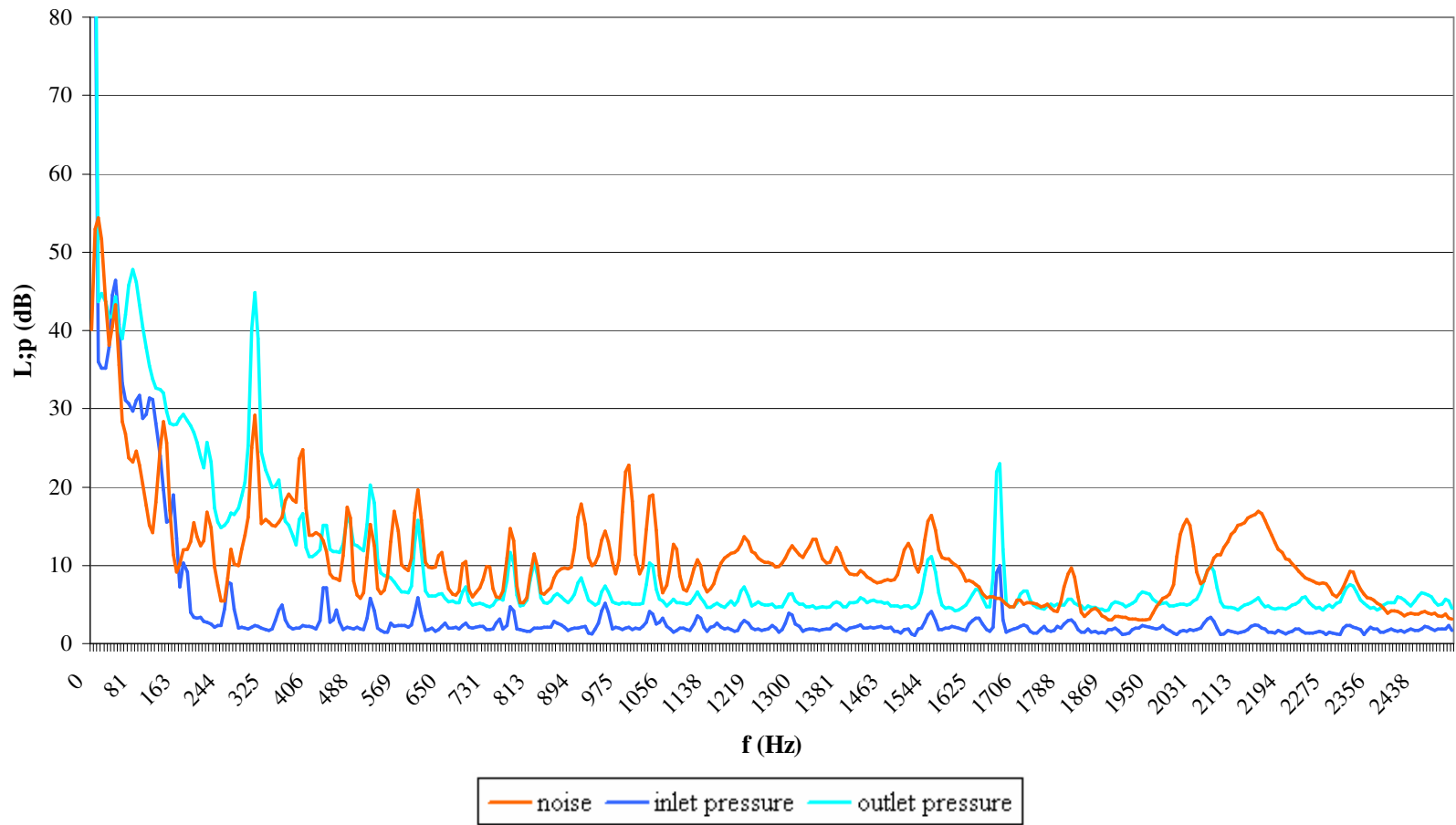
Figure D.9. Small pump noise fft spectrum for 2570 rpm, shut off.
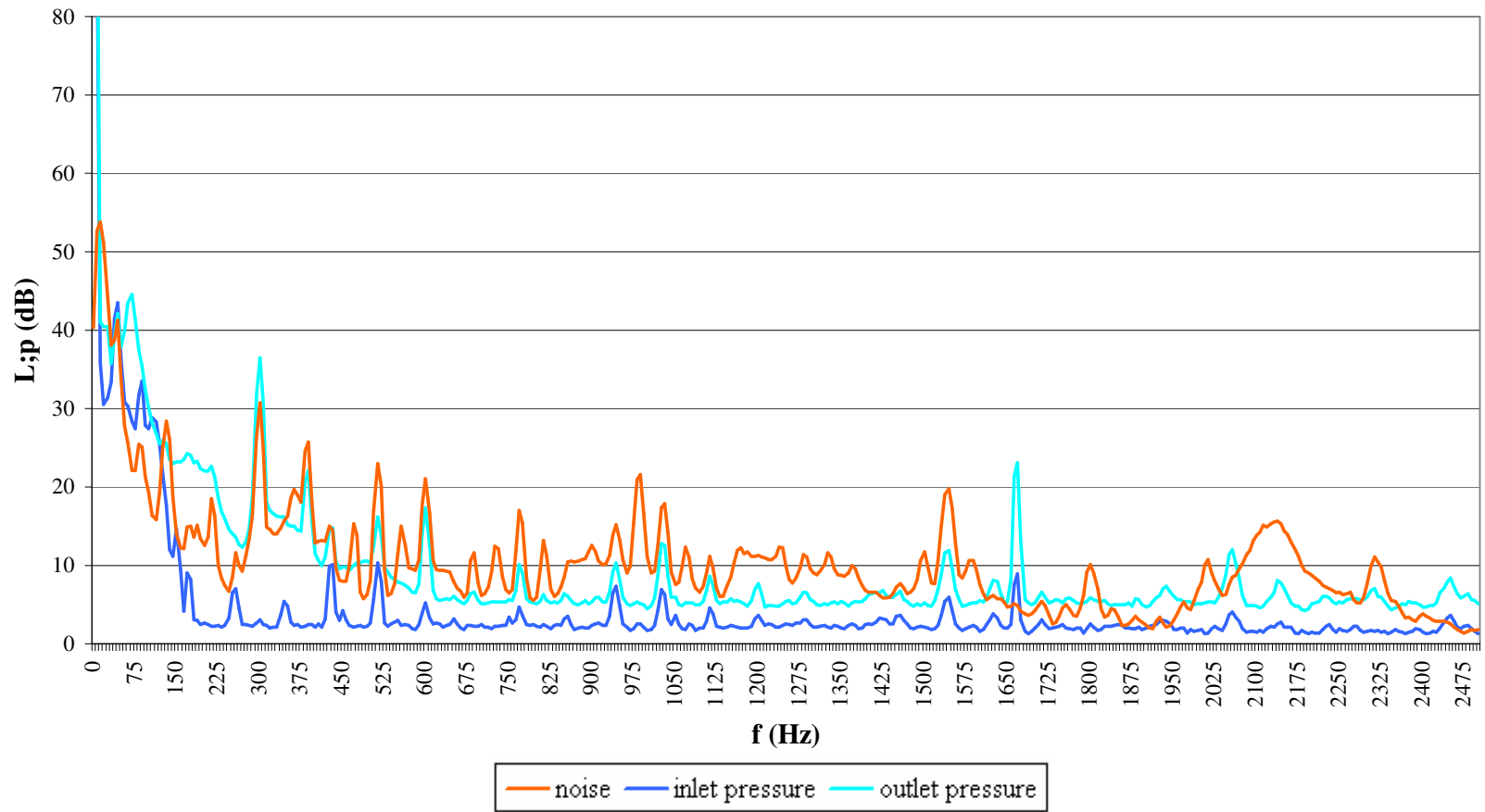
Figure D.10. Small pump noise fft spectrum for 2570 rpm, 0.40 l/s.
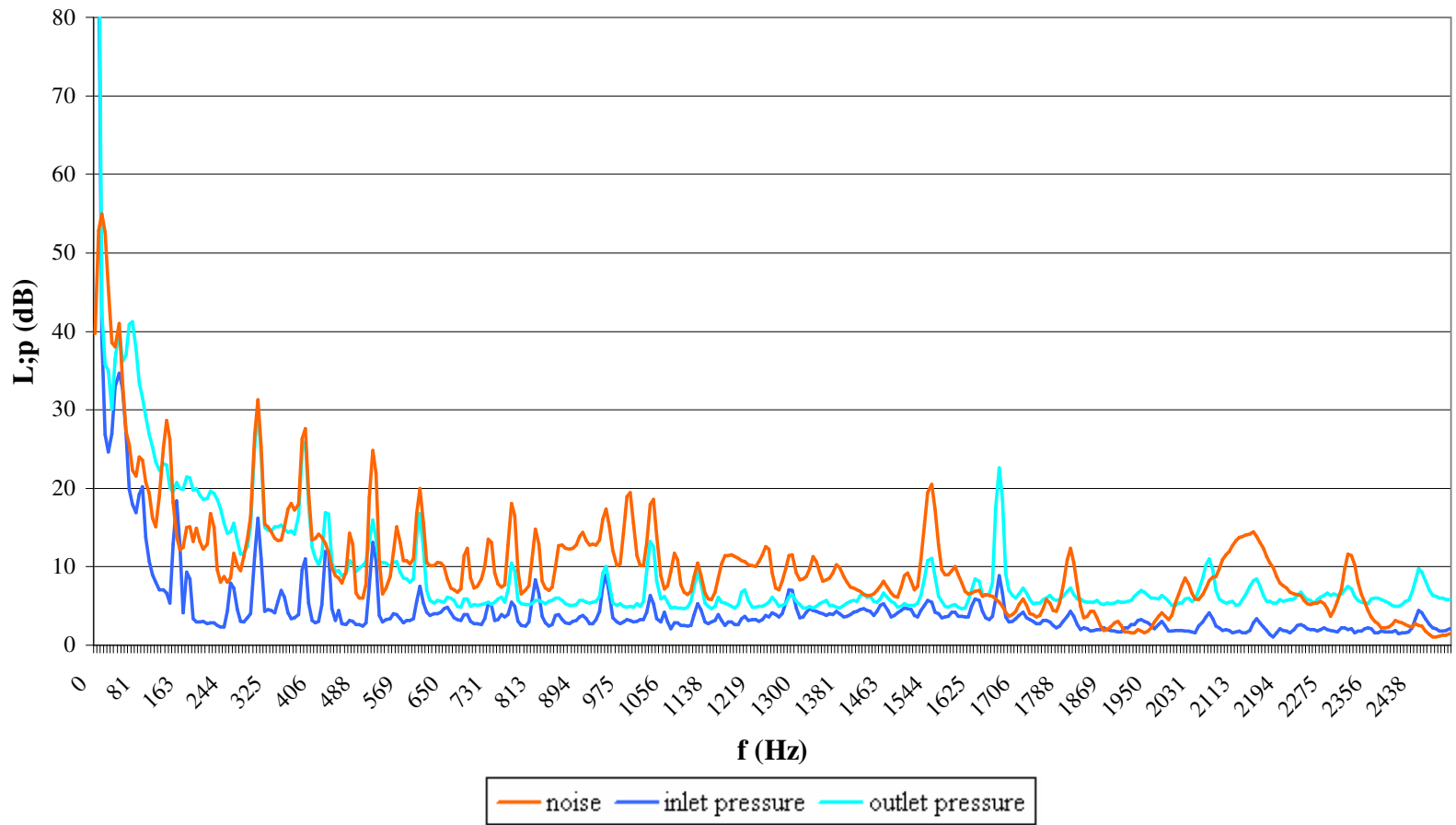
Figure D.11. Small pump noise fft spectrum for 2570 rpm, 0.60 l/s.
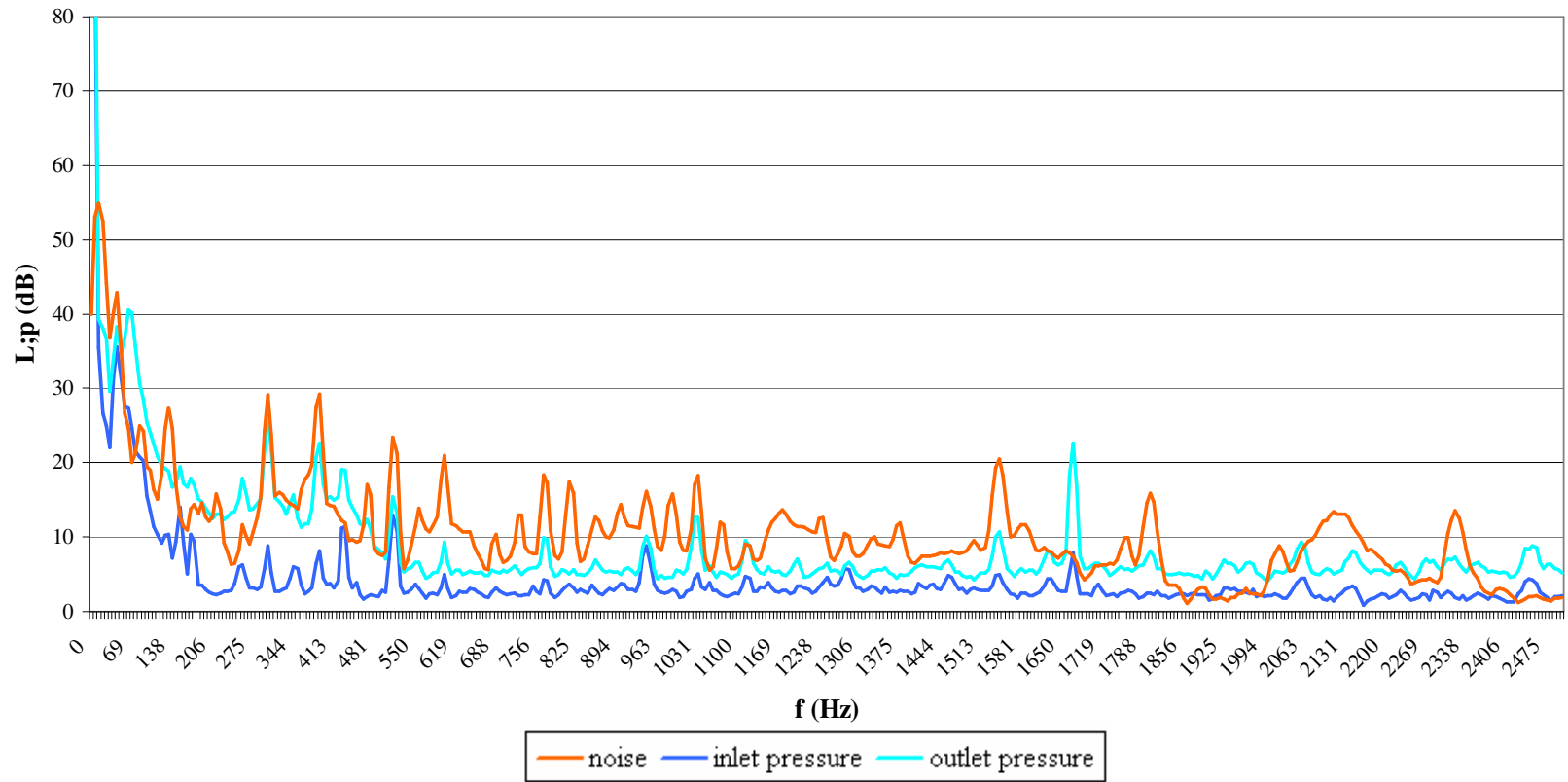
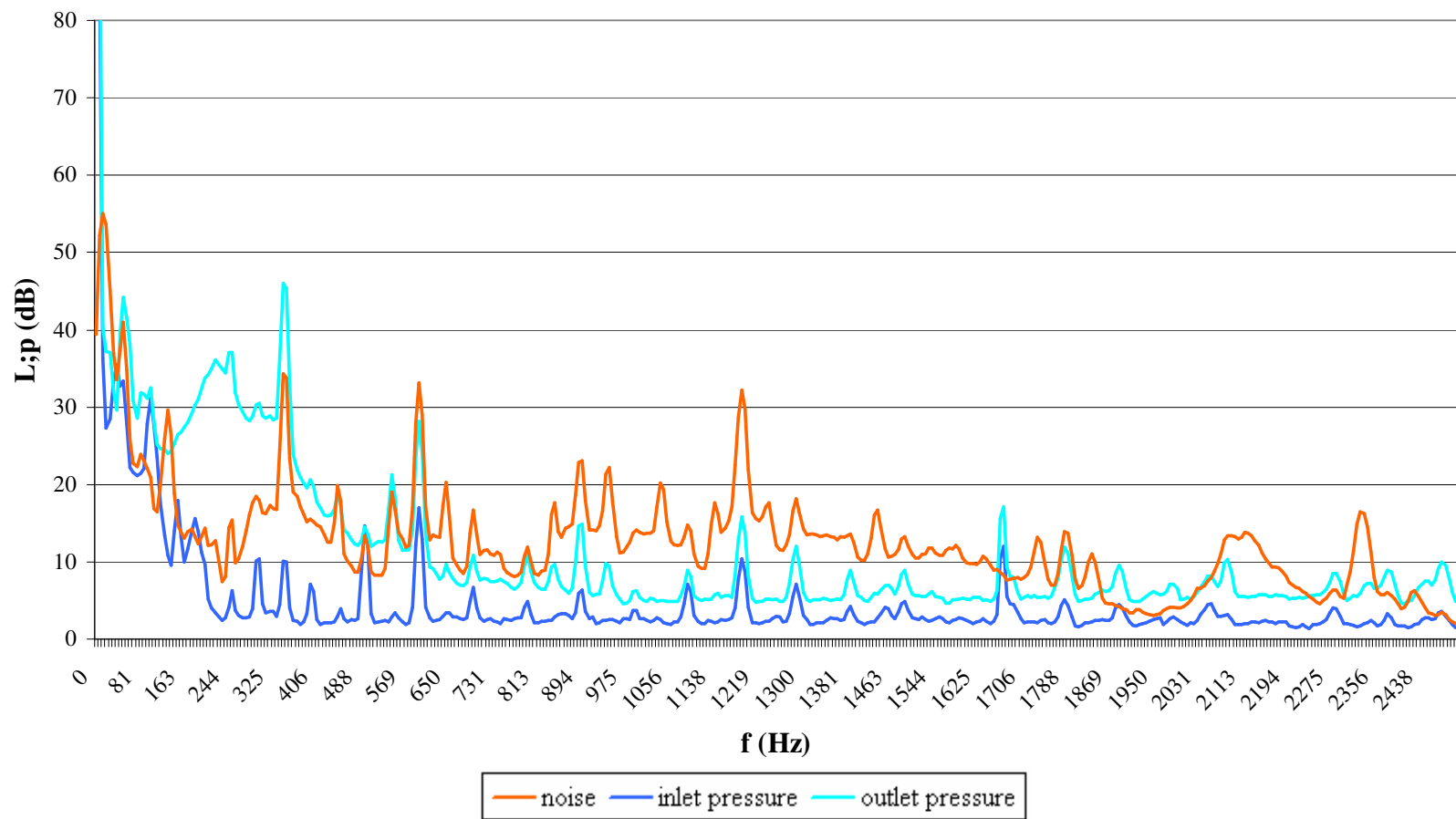**Figure D.12.** Small pump noise fft spectrum for 2570 rpm, 0.73 l/s.
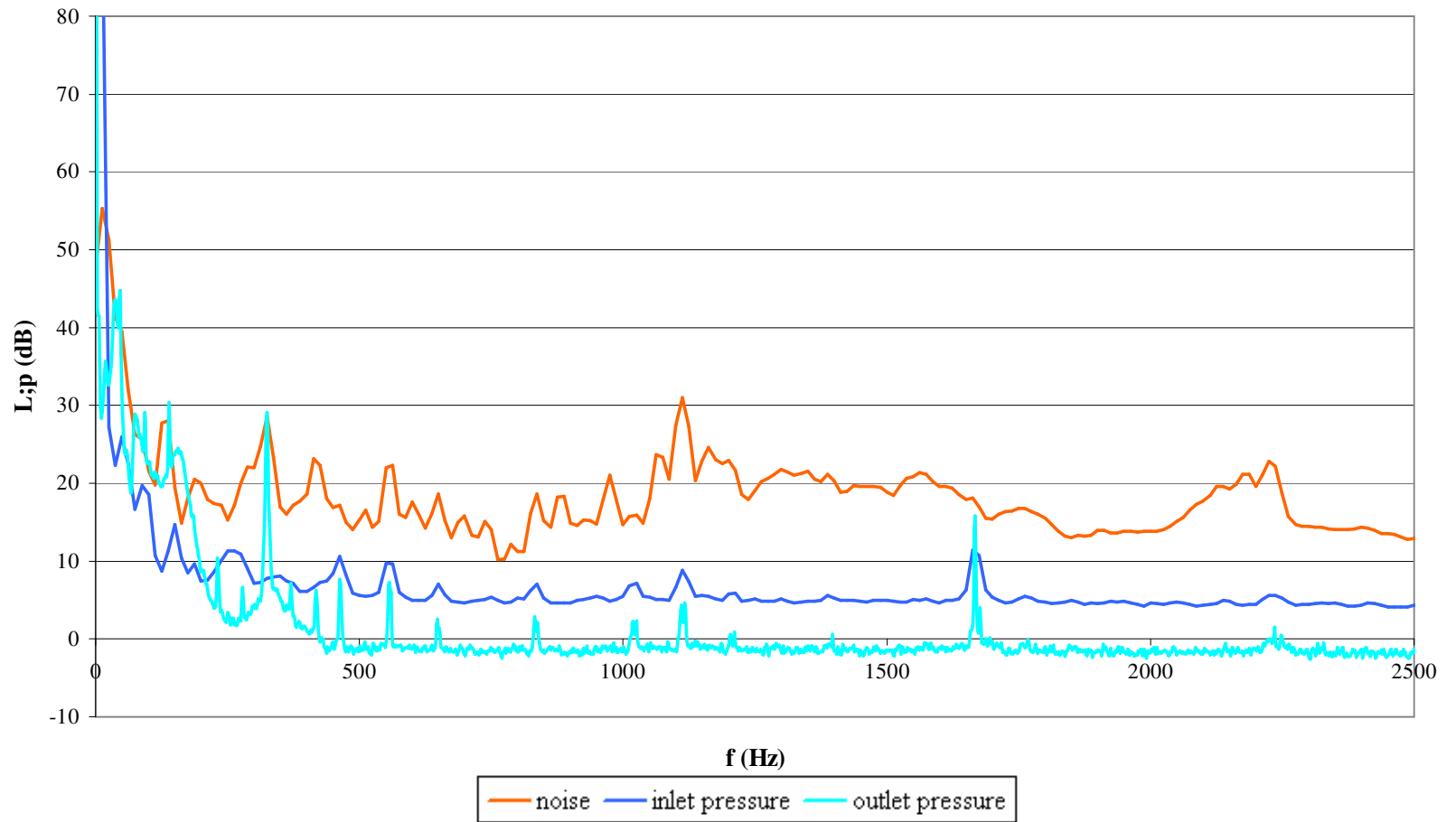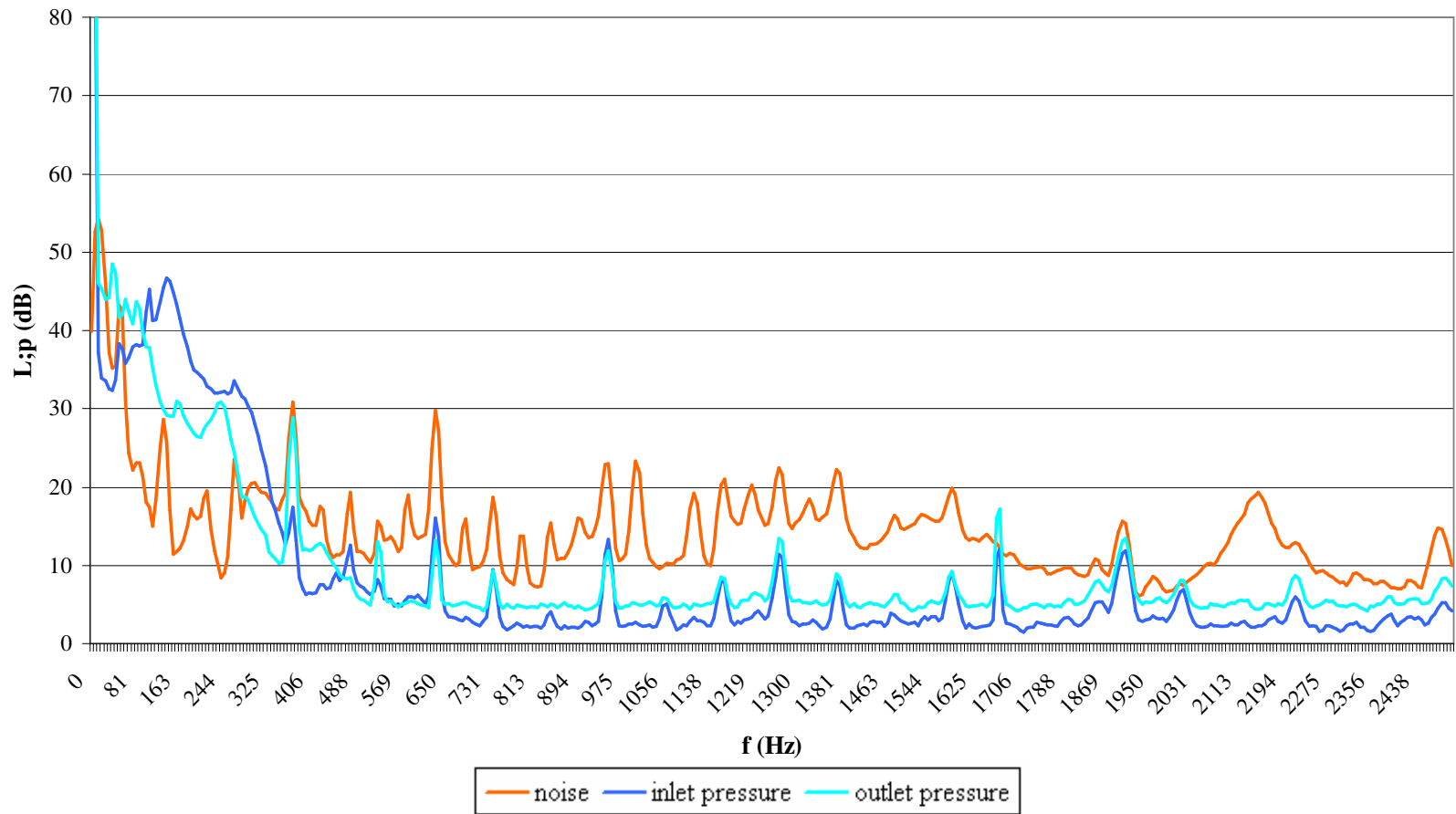
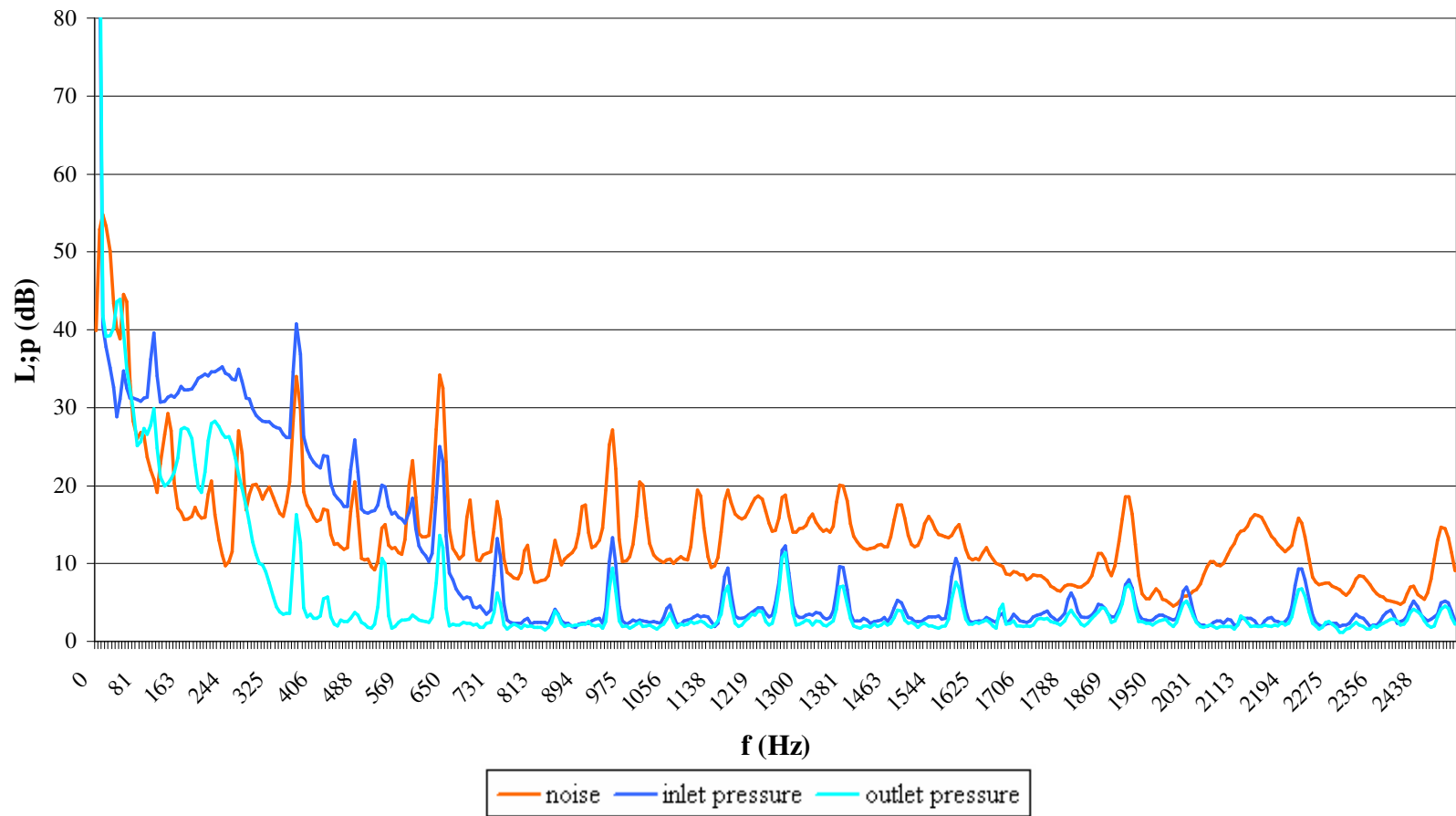**Figure D.13.** Small pump noise fft spectrum for 2770 rpm, shut off.
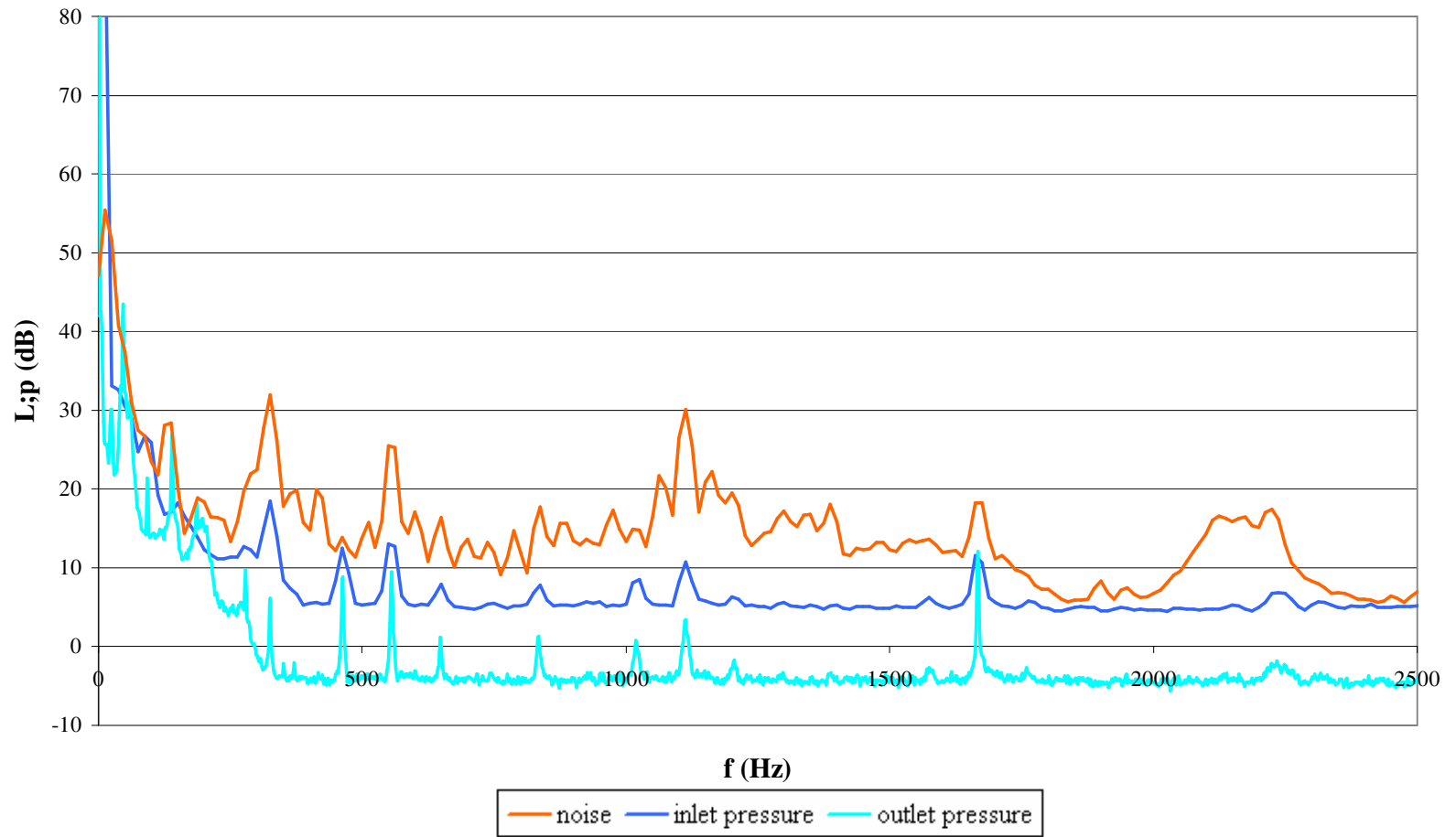
Figure D.14. Small pump noise fft spectrum for 2770 rpm, 0.38 l/s.
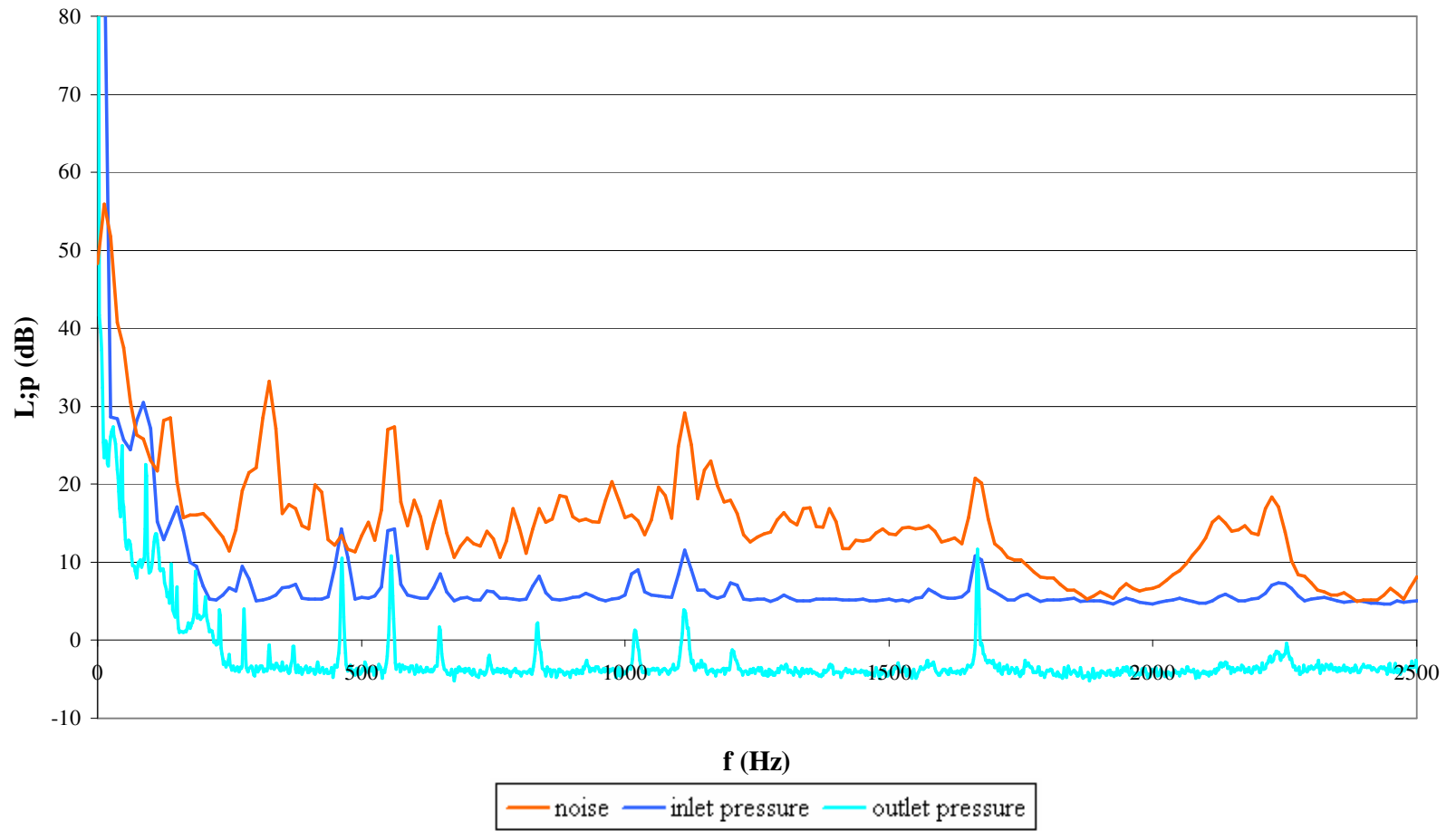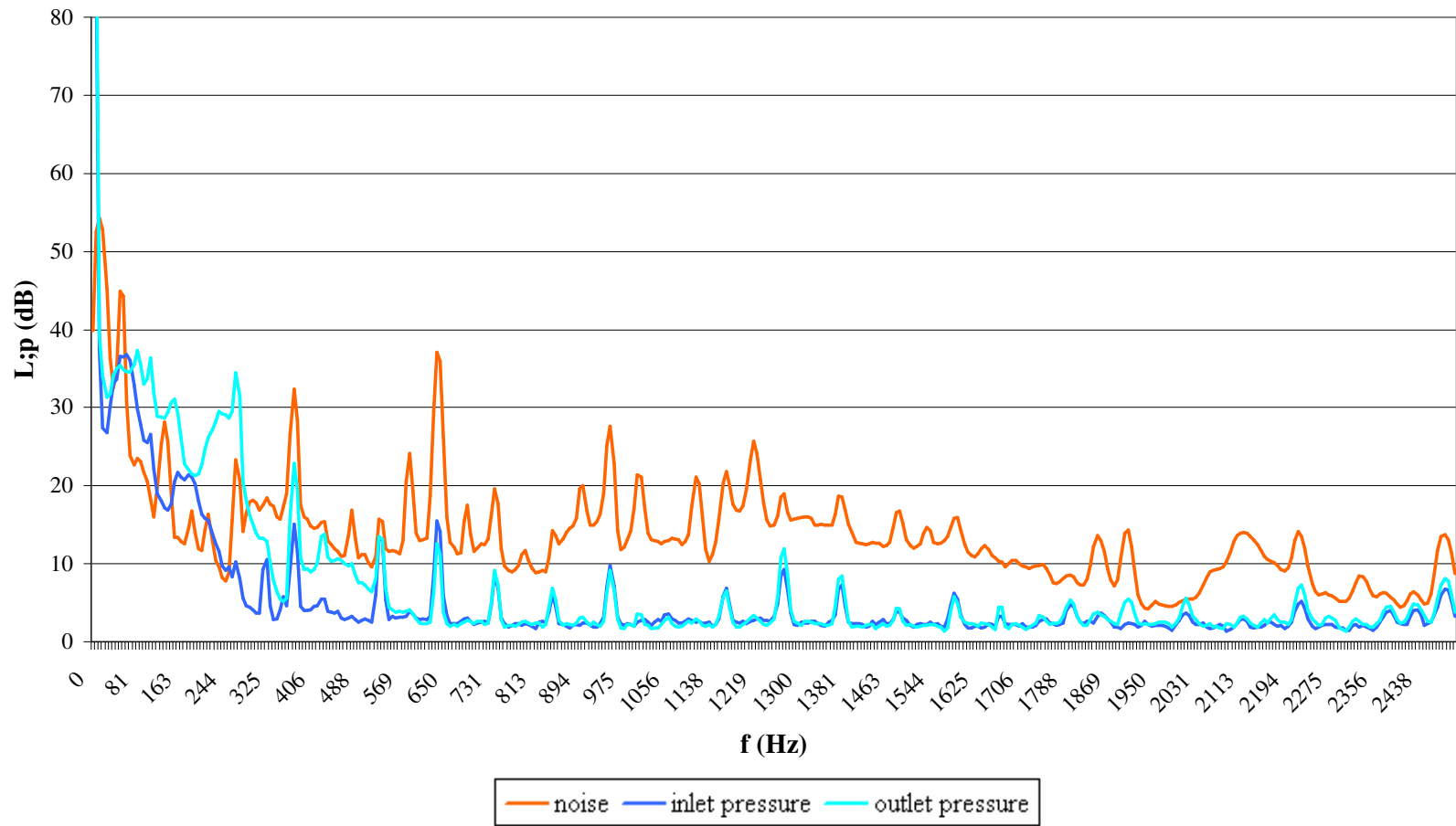
Figure D.15. Small pump noise fft spectrum for 2770 rpm, 0.68 l/s.
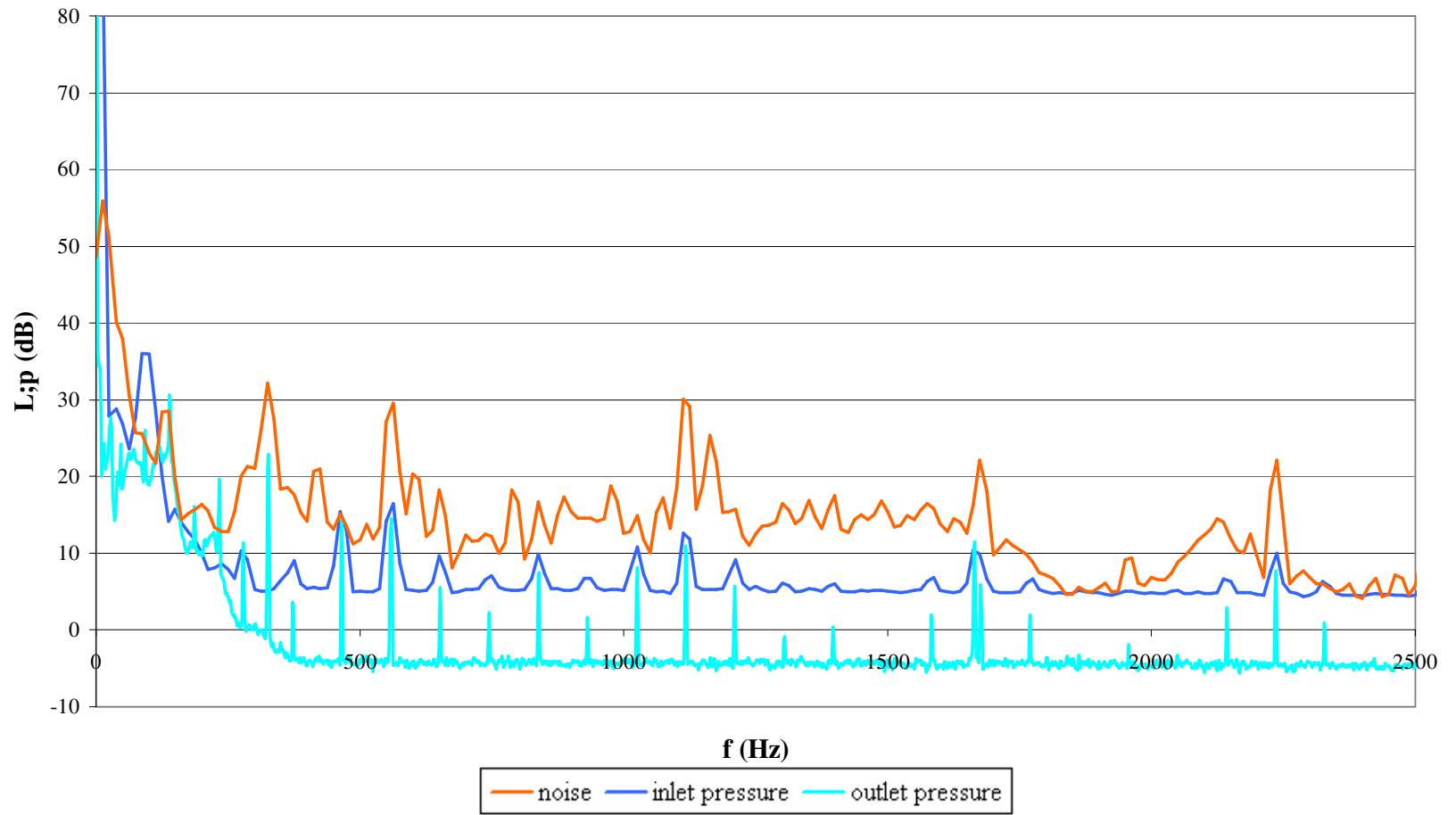
Figure D.16. Small pump noise fft spectrum for 2770 rpm, 0.76 l/s.
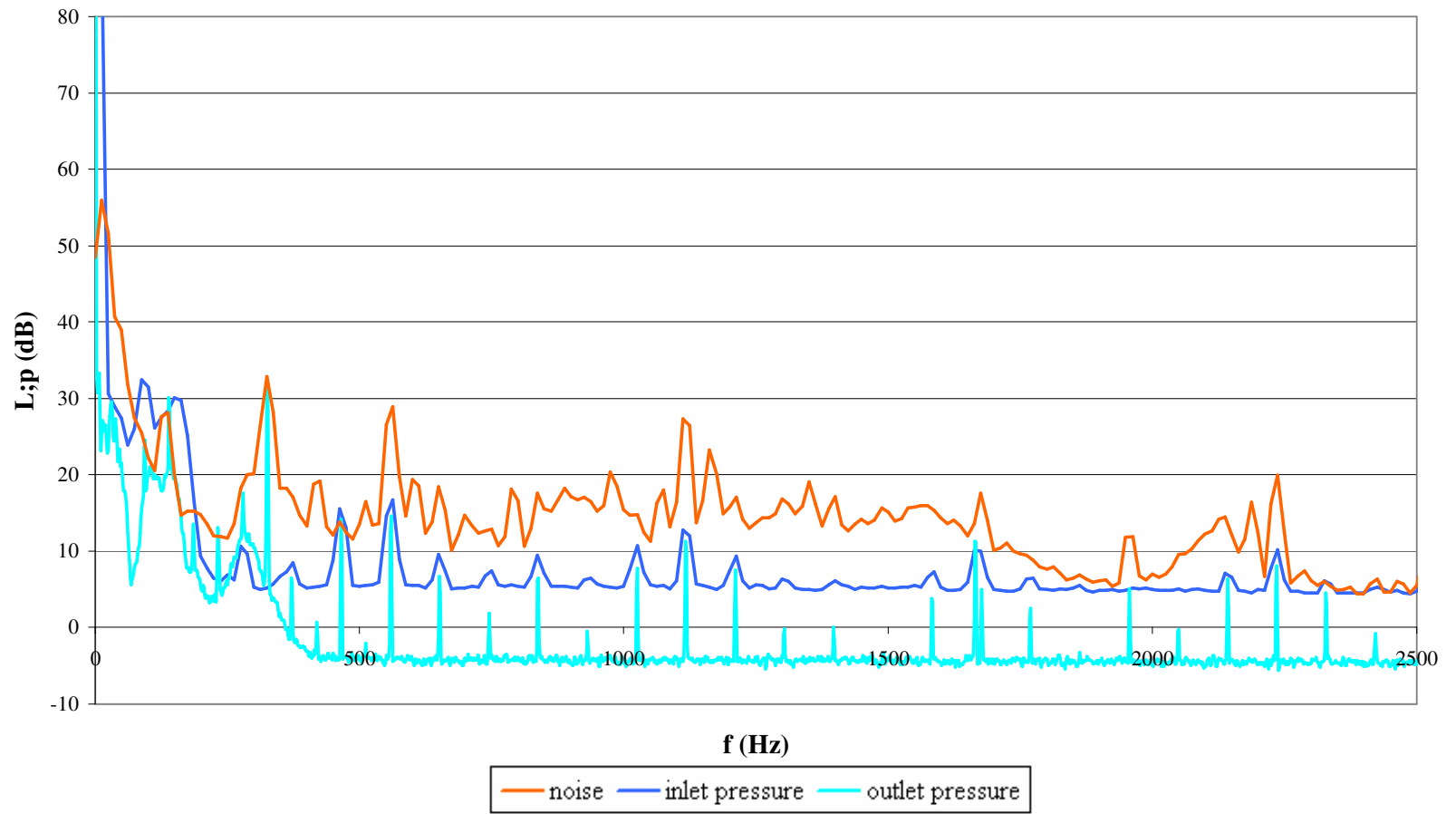
Figure D.17. Small pump noise fft spectrum for 2770 rpm, 0.84 l/s.
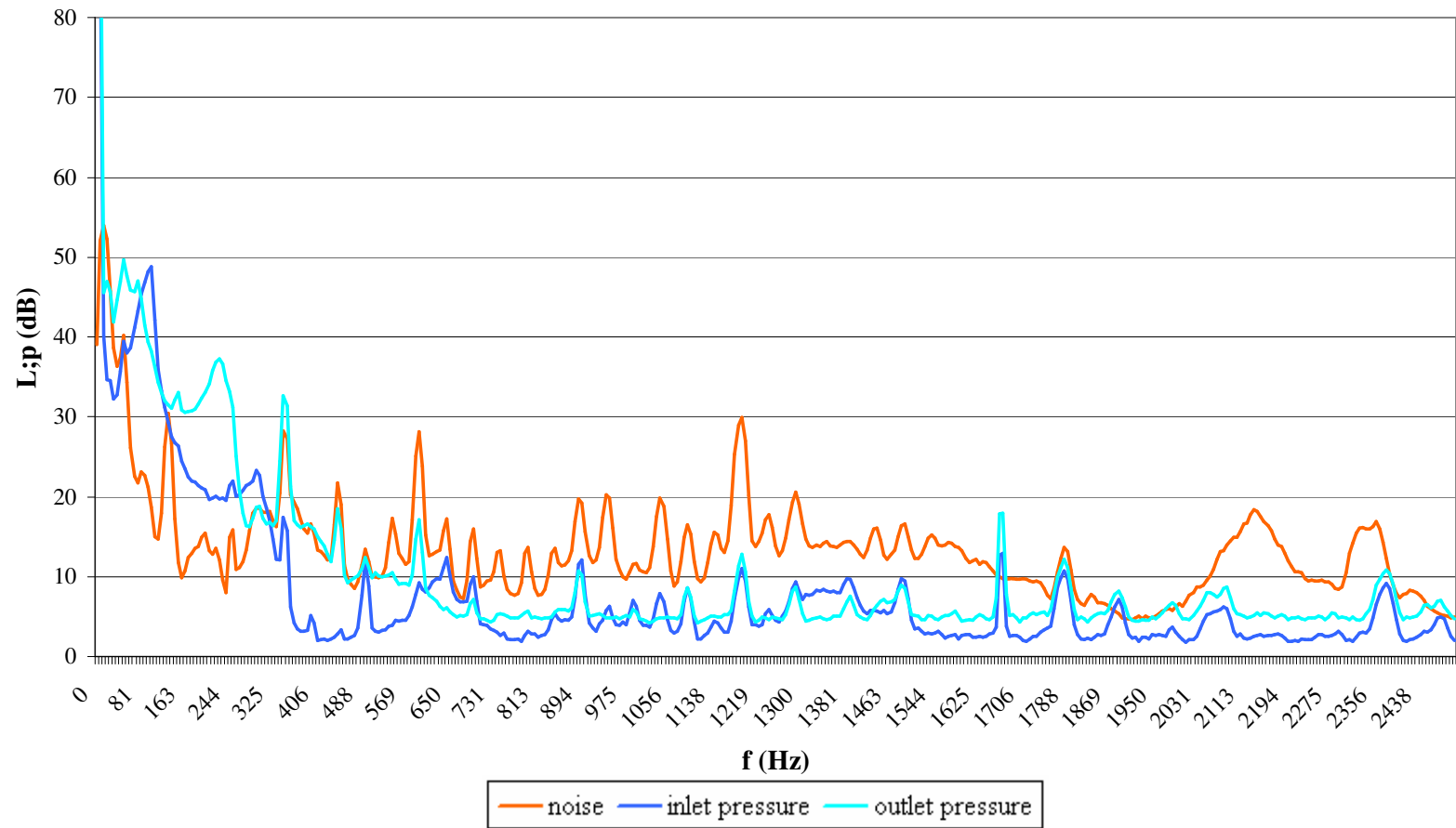
Figure D.18. Small pump noise fft spectrum for 2965 rpm, shut off.

Figure D.19. Small pump noise fft spectrum for 2965 rpm, 0.43 l/s.

Figure D.20. Small pump noise fft spectrum for 2965 rpm, 0.67 l/s.

Figure D.21. Small pump noise fft spectrum for 2965 rpm, 0.72 l/s.

Figure D.22. Small pump noise fft spectrum for 2965 rpm, 0.77 l/s.

Figure D.23. Small pump noise fft spectrum for 3160 rpm, shut off.

Figure D.24. Small pump noise fft spectrum for 3160 rpm, 0.466 l/s.

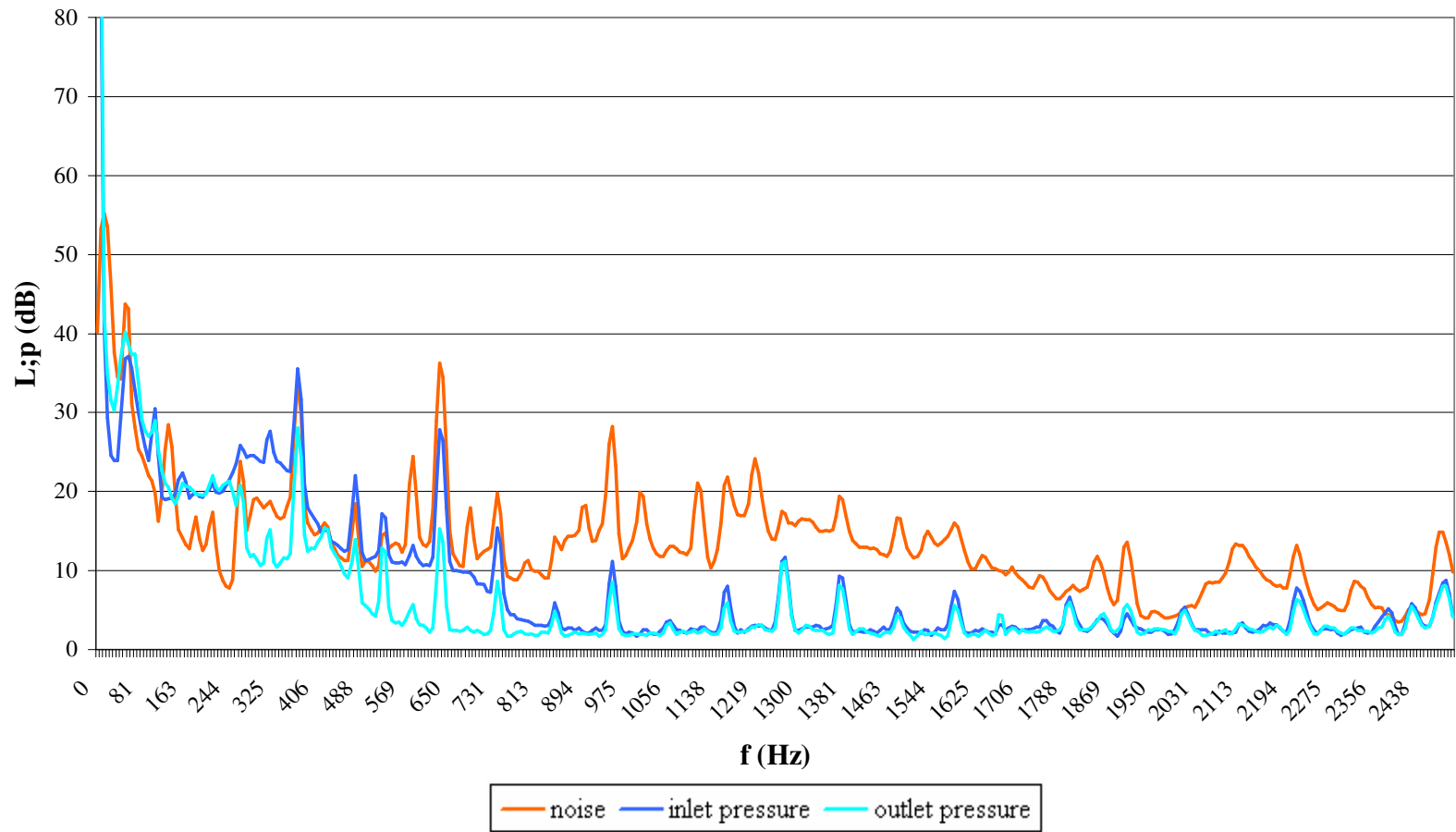**Figure D.25.** Small pump noise fft spectrum for 3160 rpm, 0.59 l/s.

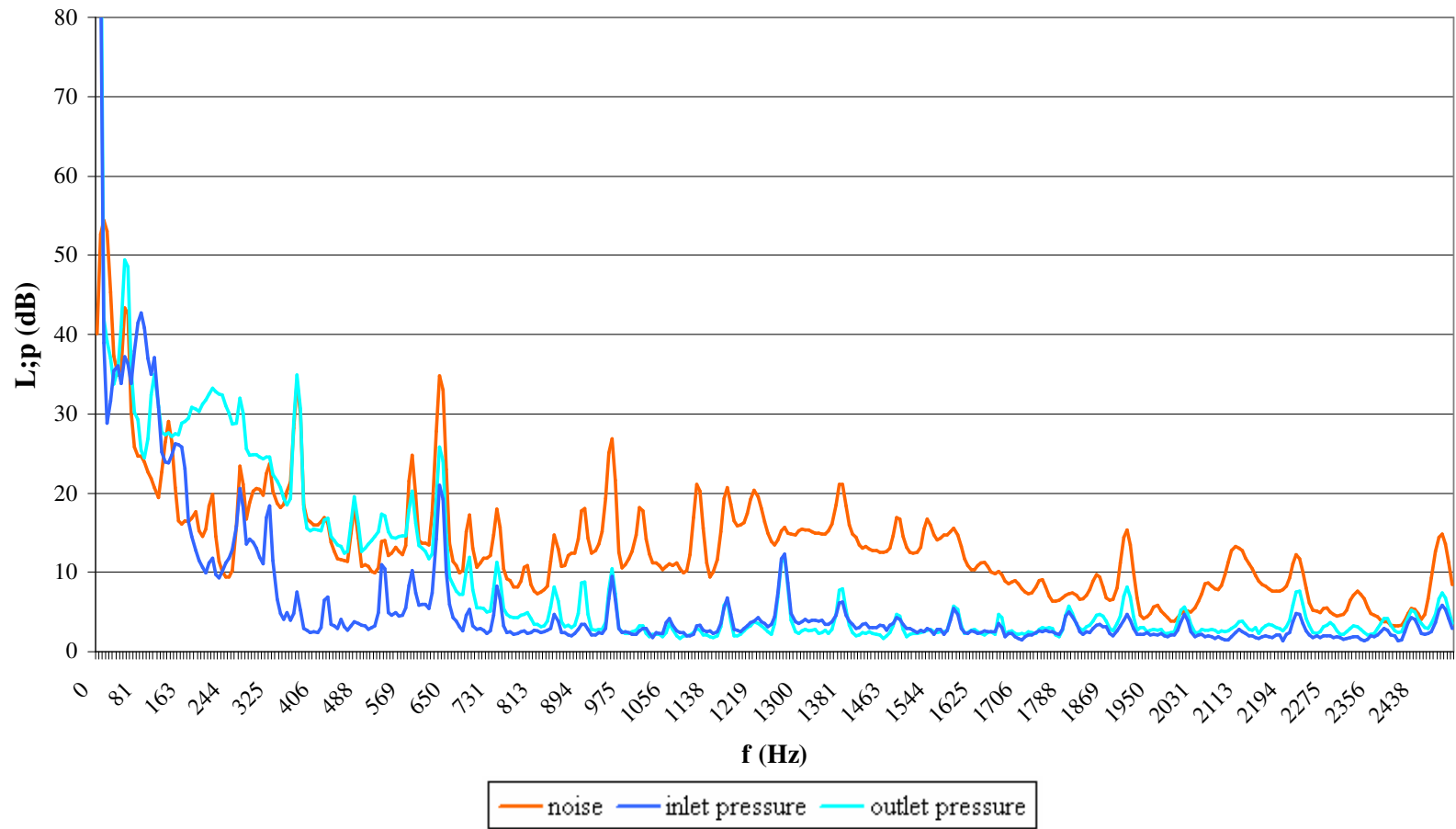**Figure D.26.** Small pump noise fft spectrum for 3160 rpm, 0.74 l/s.

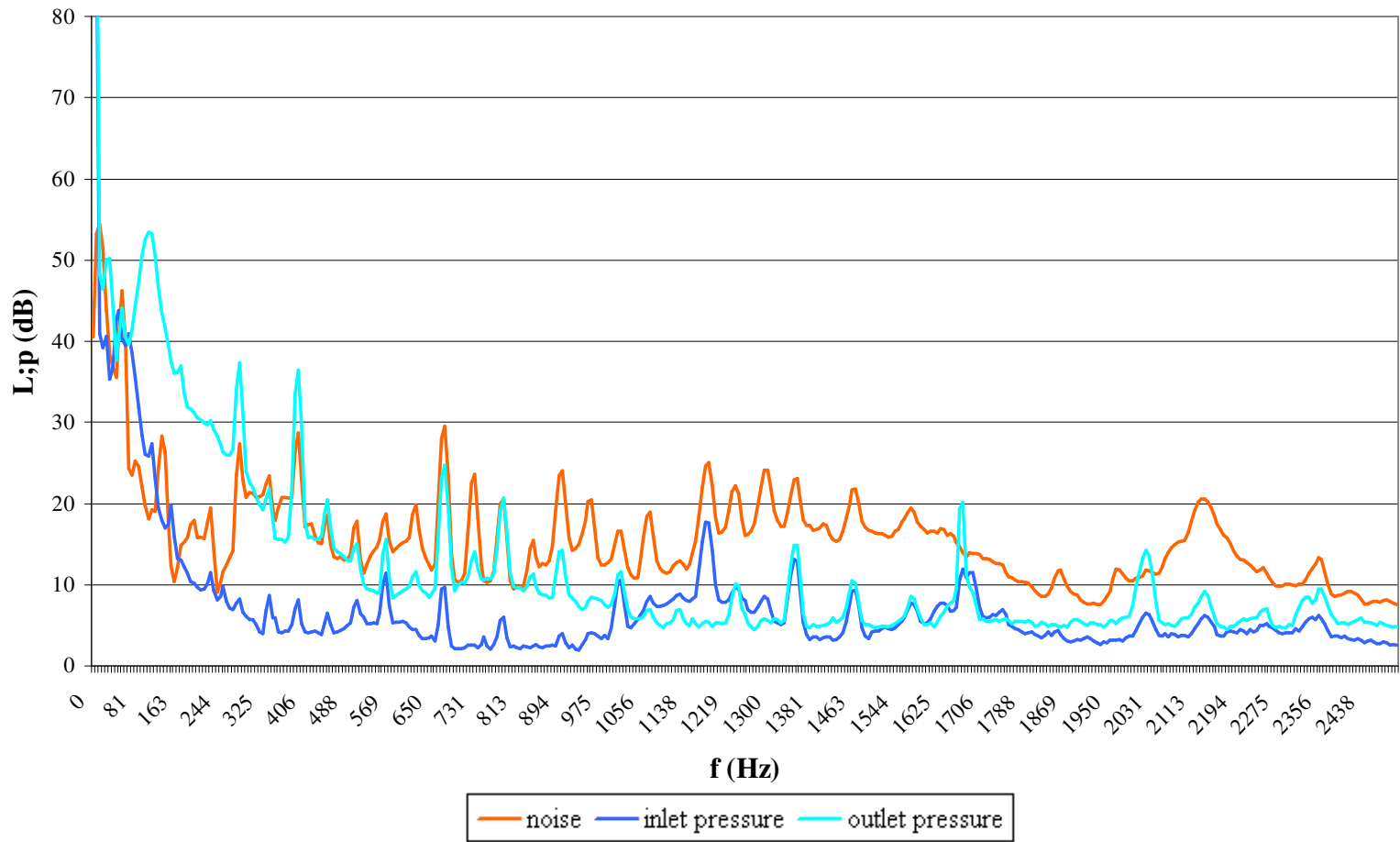**Figure D.27.** Small pump noise fft spectrum for 3160 rpm, 0.82 l/s.

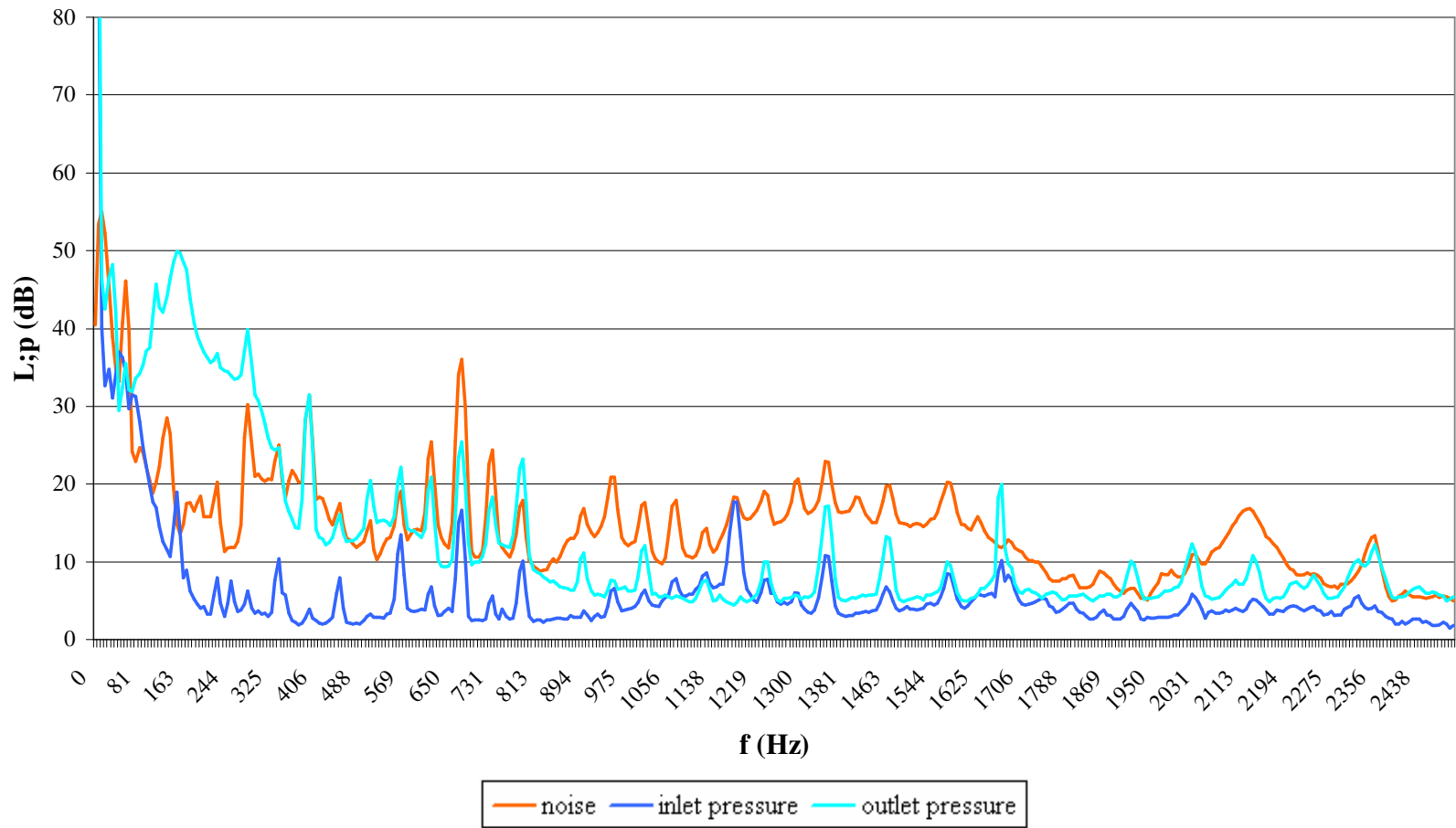**Figure D.28.** Small pump noise fft spectrum for 3365 rpm, shut off.

Figure D.29. Small pump noise fft spectrum for 3365 rpm, 0.56 l/s.
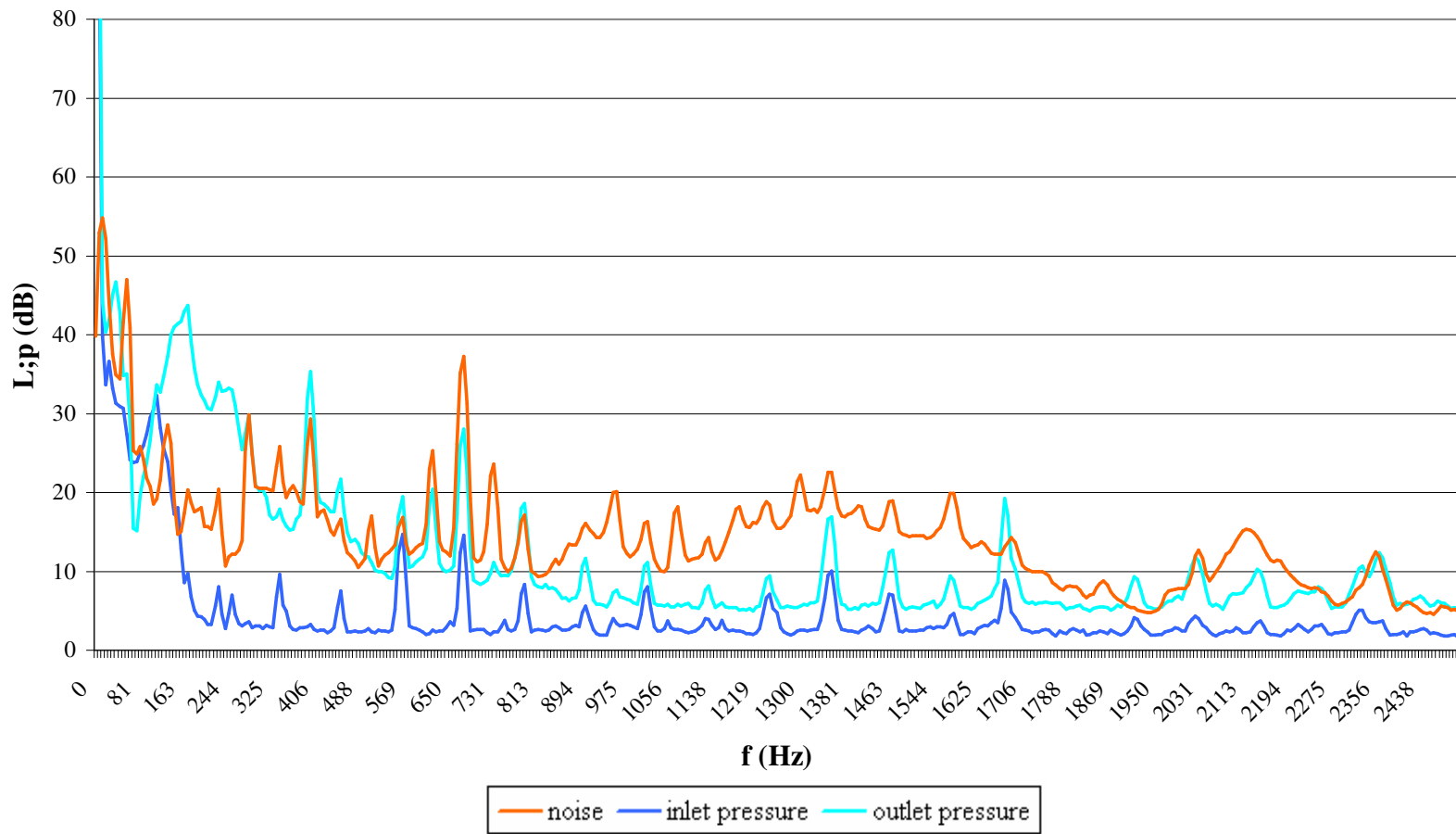
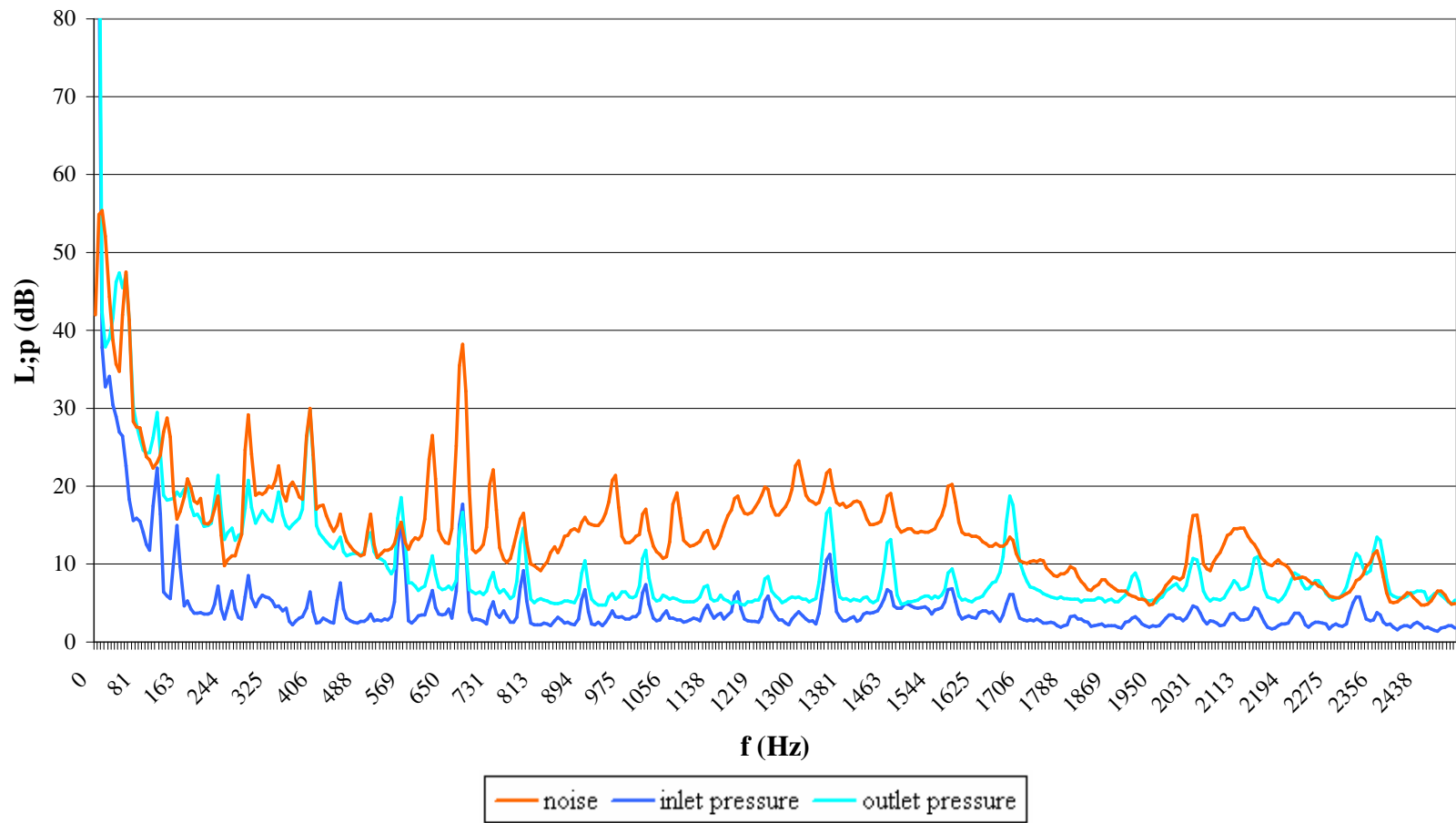**Figure D.30.** Small pump noise fft spectrum for 3365 rpm, 0.63 l/s.

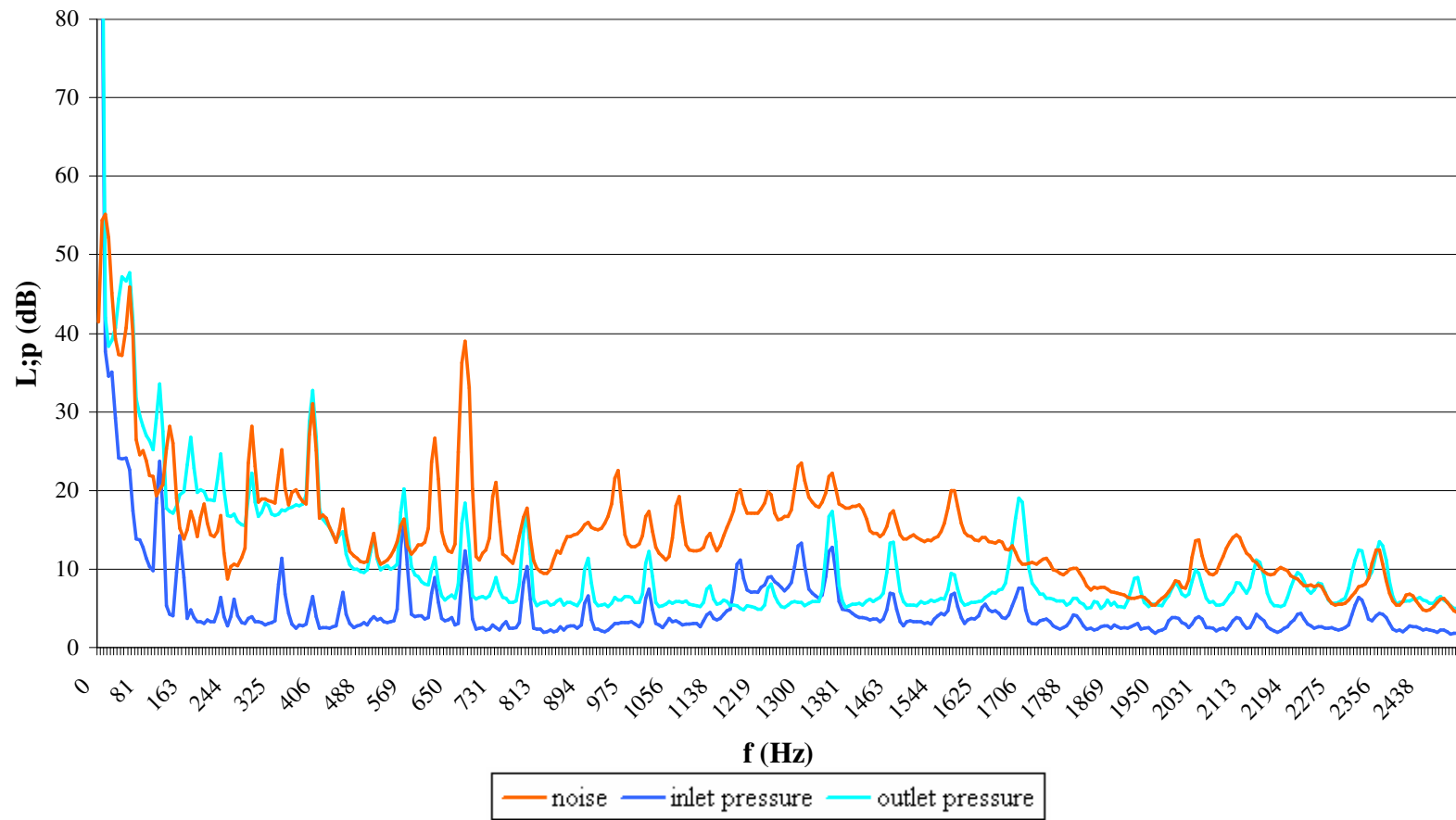**Figure D.31.** Small pump noise fft spectrum for 3365 rpm, 0.78 l/s.

Figure D.32. Small pump noise fft spectrum for 3365 rpm, 0.875 l/s.

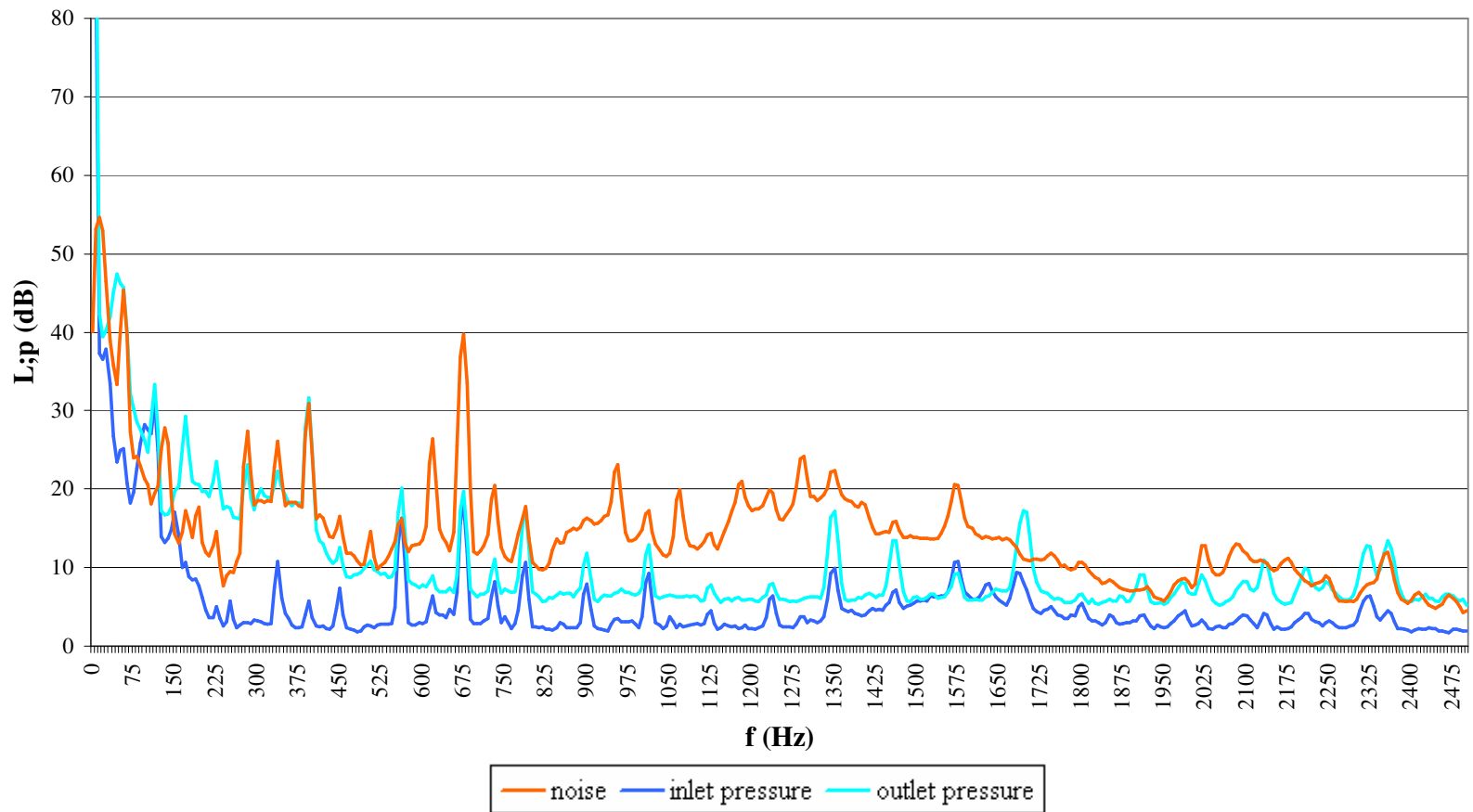**Figure D.33.** Small pump noise fft spectrum for 3365 rpm, 0.965 l/s.
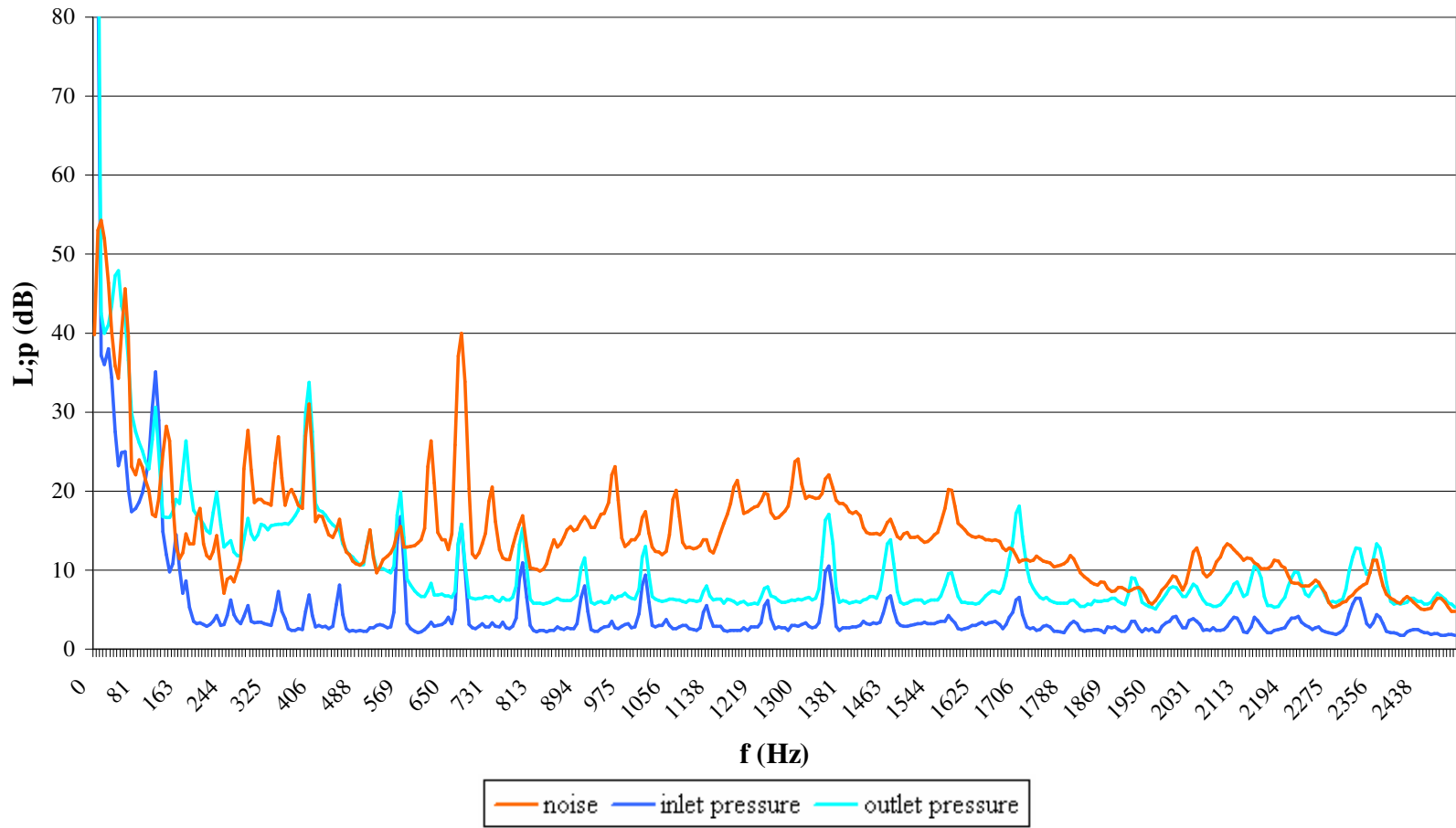
Figure D.34. Small pump noise fft spectrum for 3365 rpm, 0.97 l/s.

Figure D.35. Large pump noise fft spectrum for 2175 rpm, shut off

Figure D.36. Large pump noise fft spectrum for 2175 rpm, 0.39 l/s

Figure D.37. Large pump noise fft spectrum for 2175 rpm, 0.73 l/s

Figure D.38. Large pump noise fft spectrum for 2375 rpm, shut off

Figure D.39. Large pump noise fft spectrum for 2375 rpm, 0.70 l/s
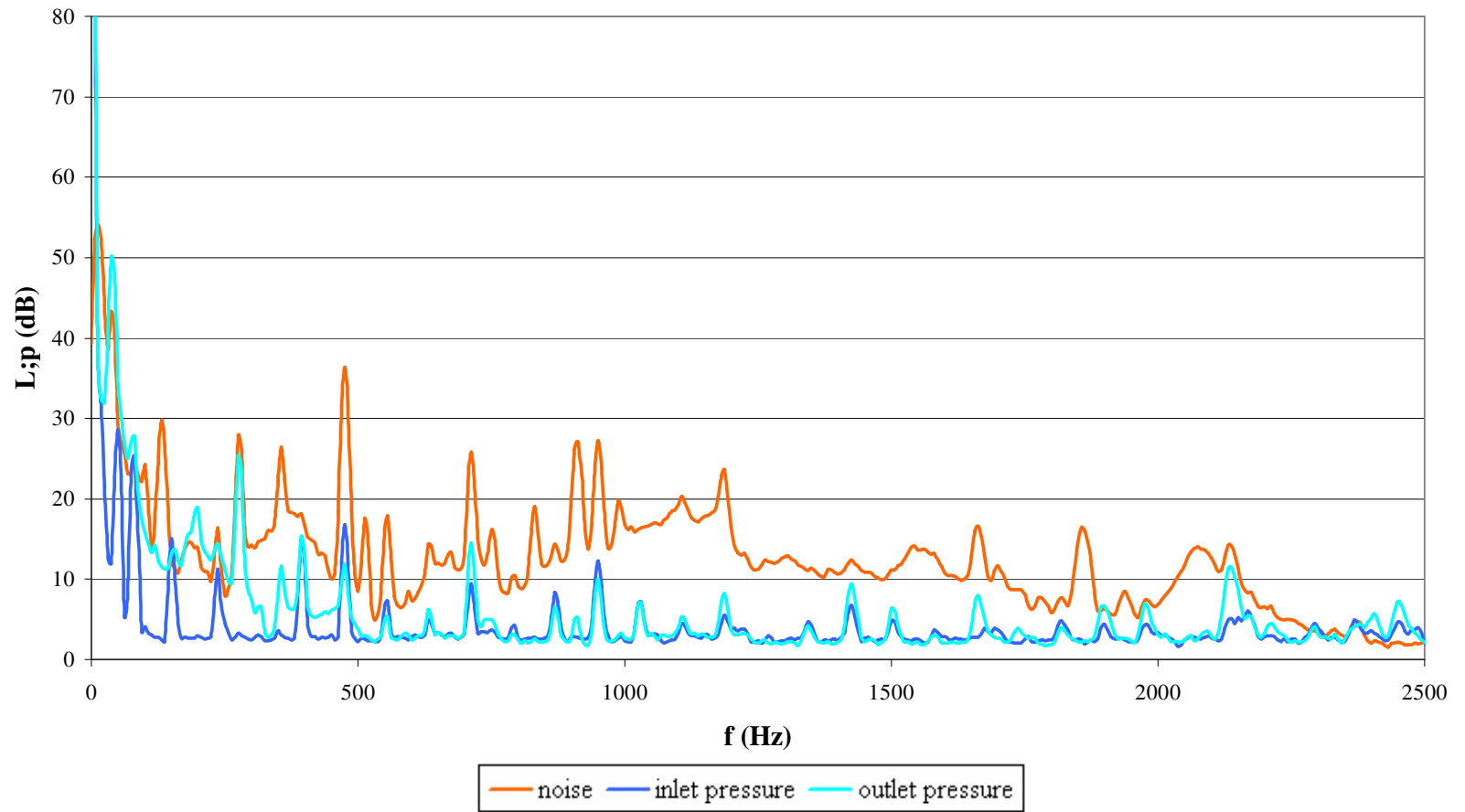
Figure D.40. Large pump noise fft spectrum for 2375 rpm, 0.78 l/s
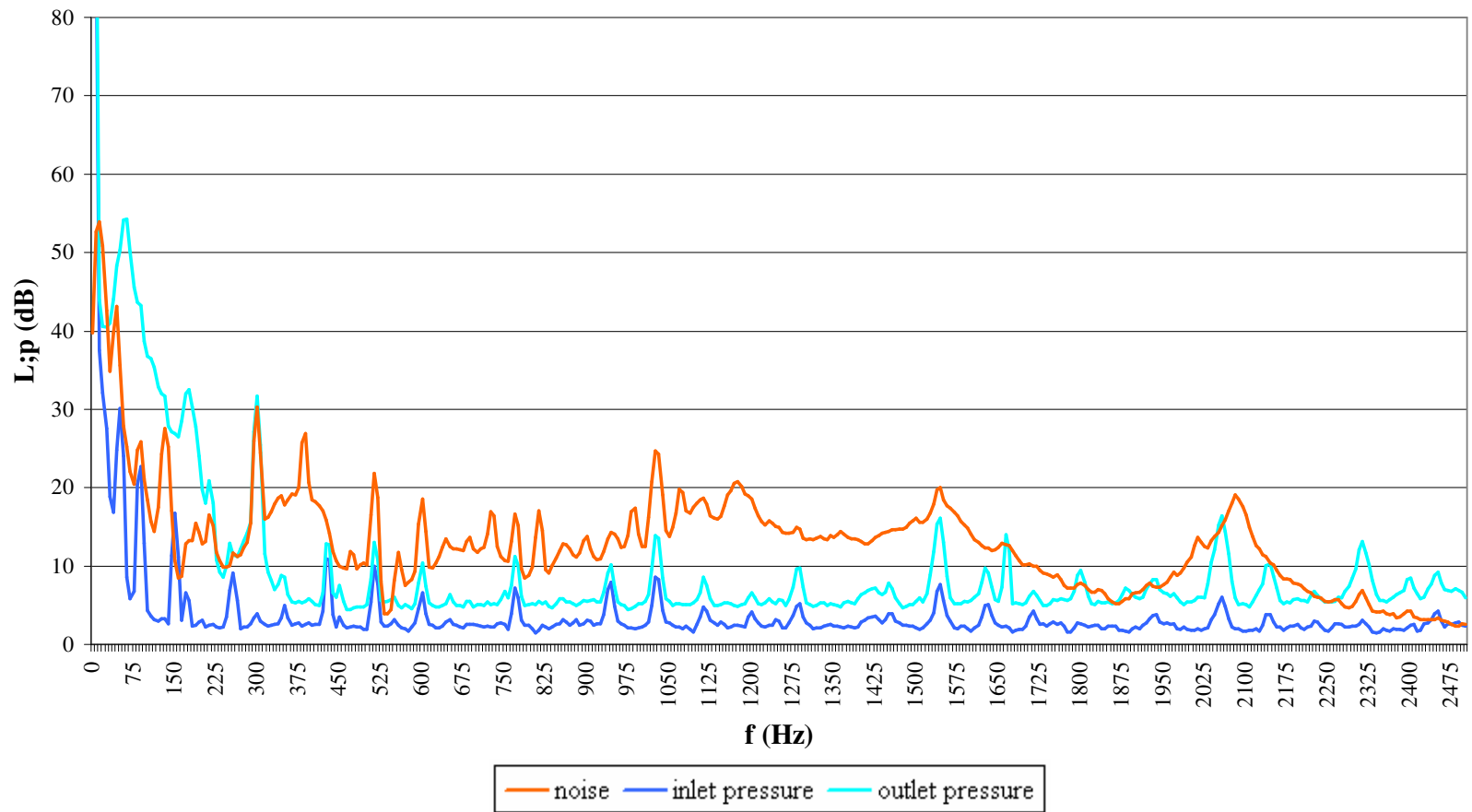
Figure D.41. Large pump noise fft spectrum for 2570 rpm, shut off
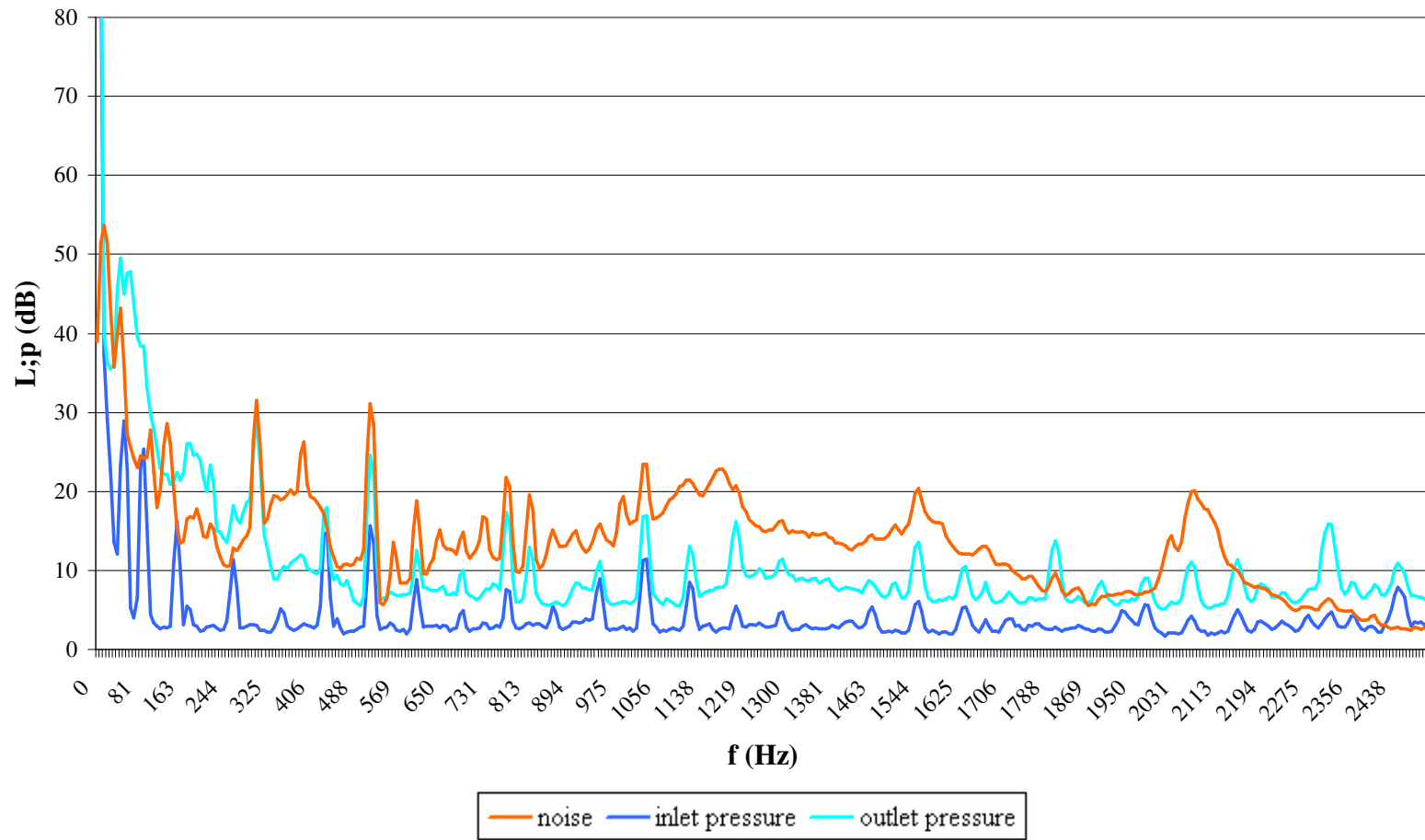
Figure D.42. Large pump noise fft spectrum for 2570 rpm, 0.69 l/s
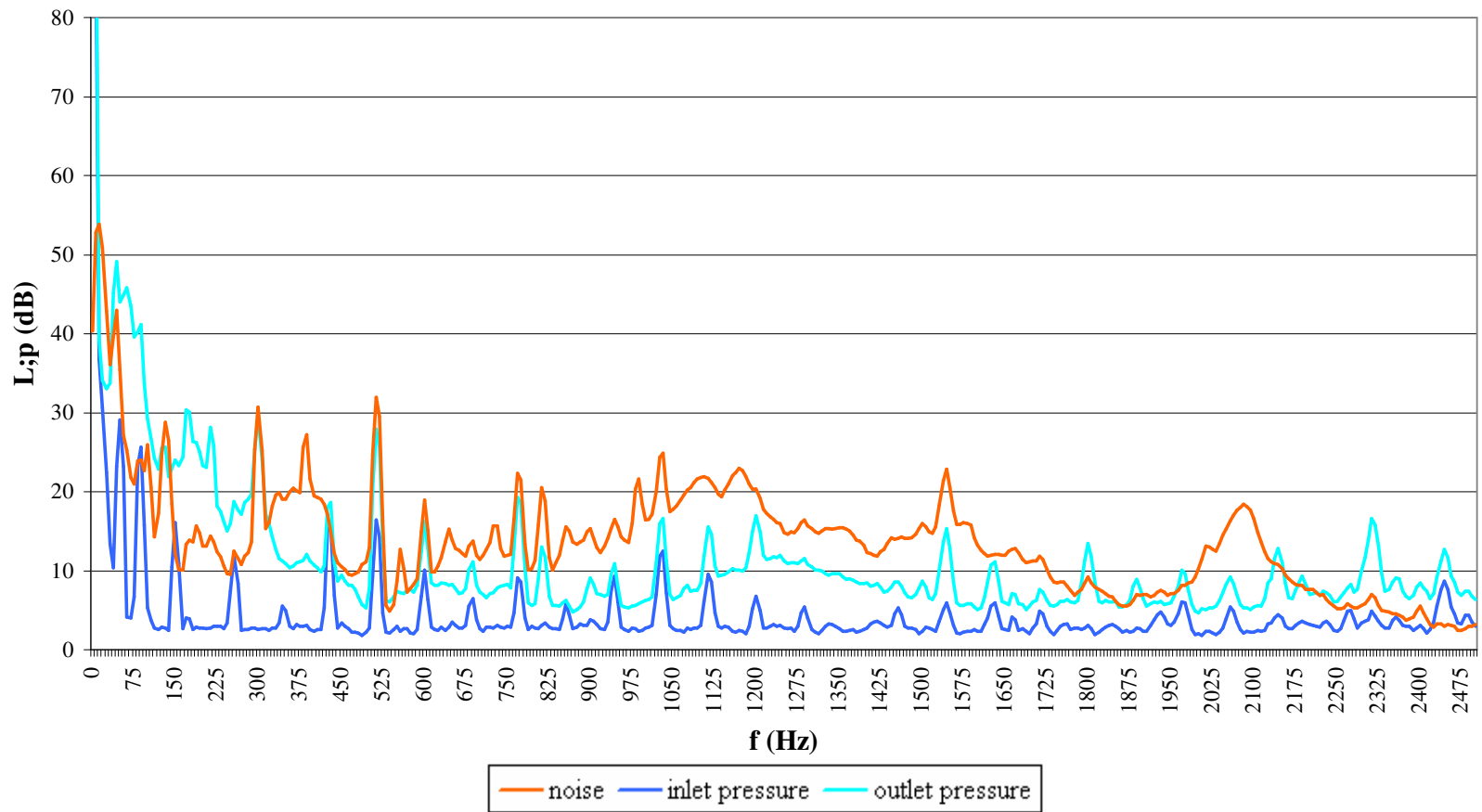
Figure D.43. Large pump noise fft spectrum for 2570 rpm, 0.84 l/s
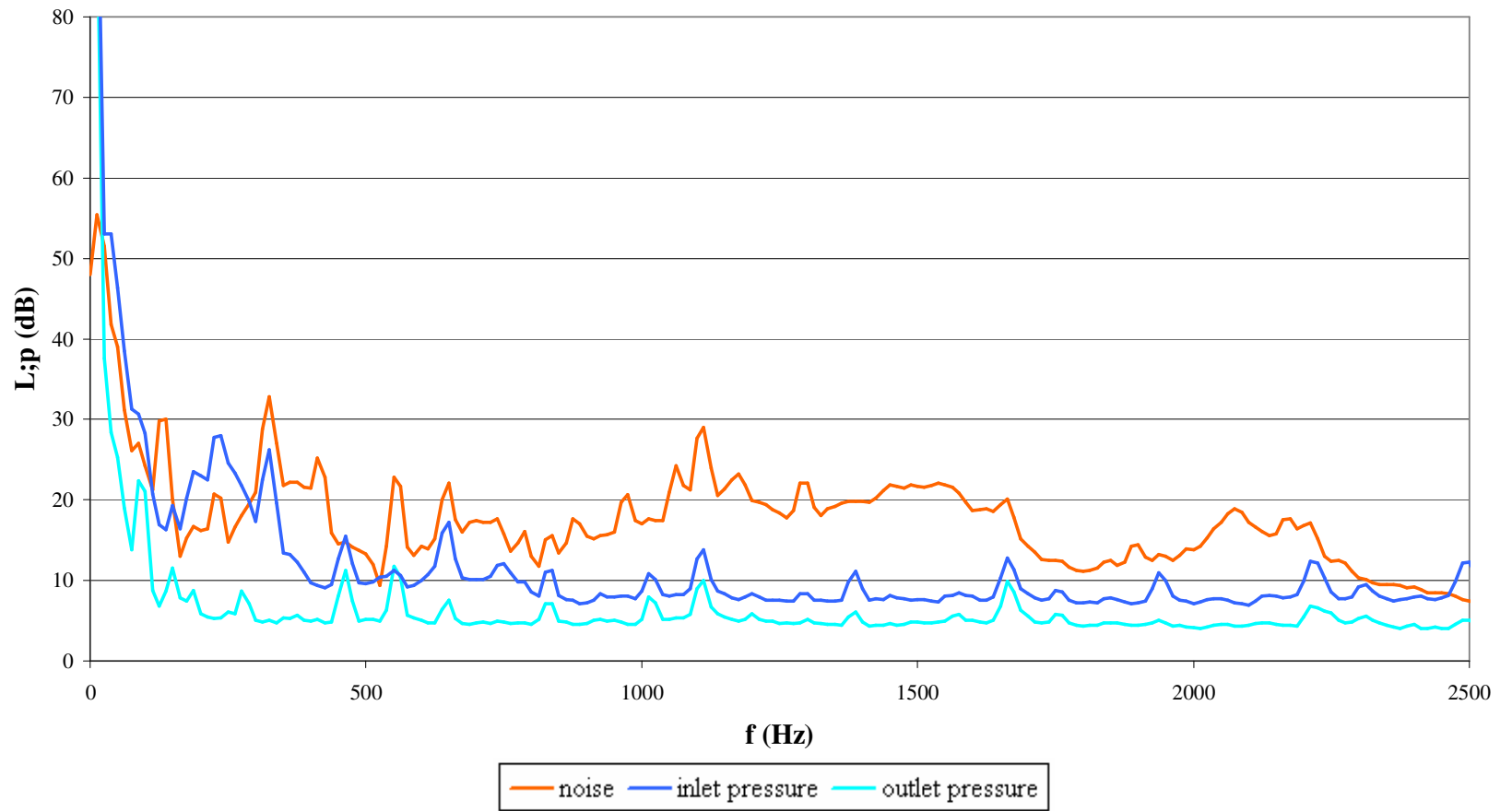
Figure D.44. Large pump noise fft spectrum for 2770 rpm, shut off
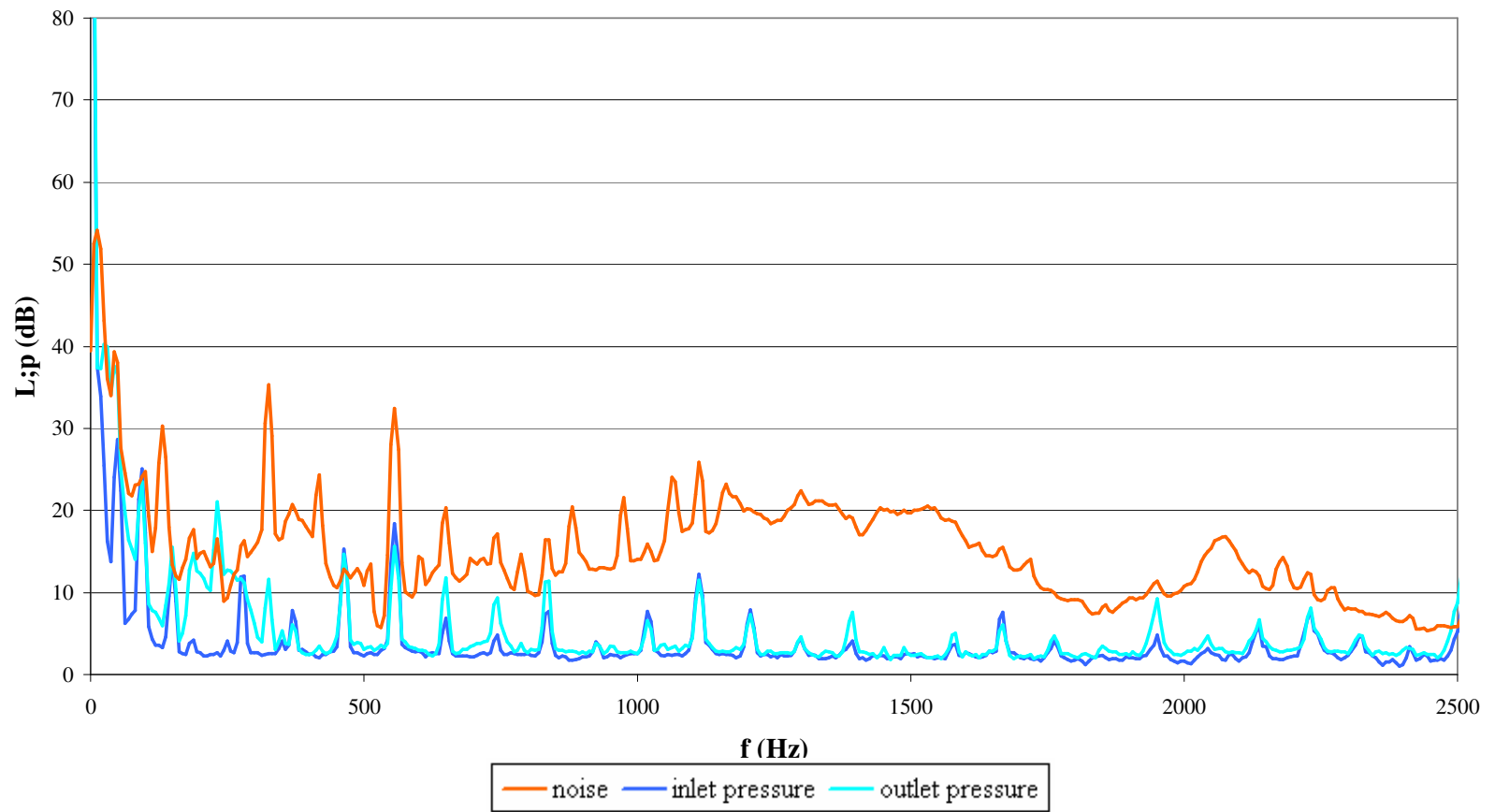
Figure D.45. Large pump noise fft spectrum for 2770 rpm, 0.84 l/s
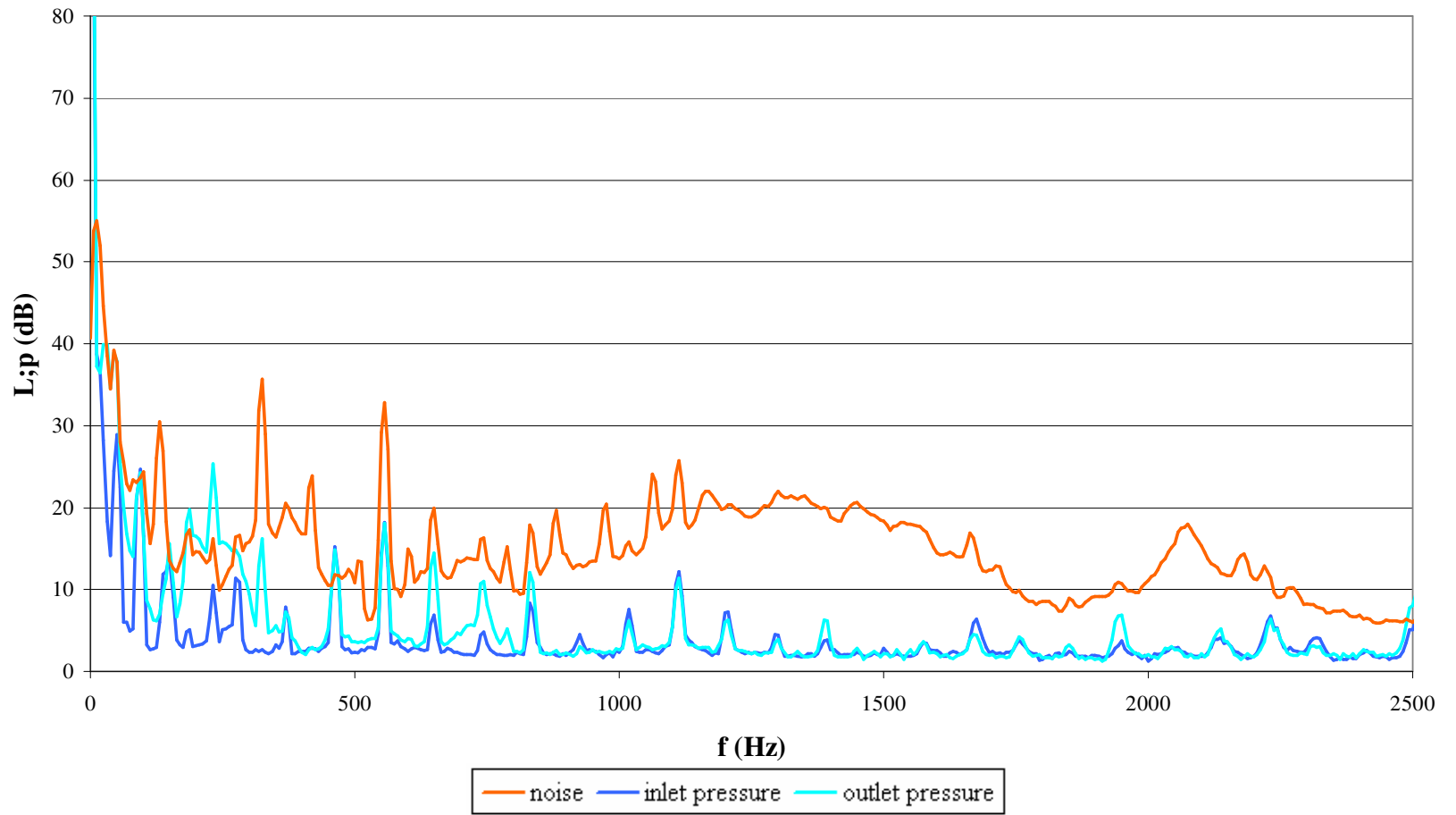
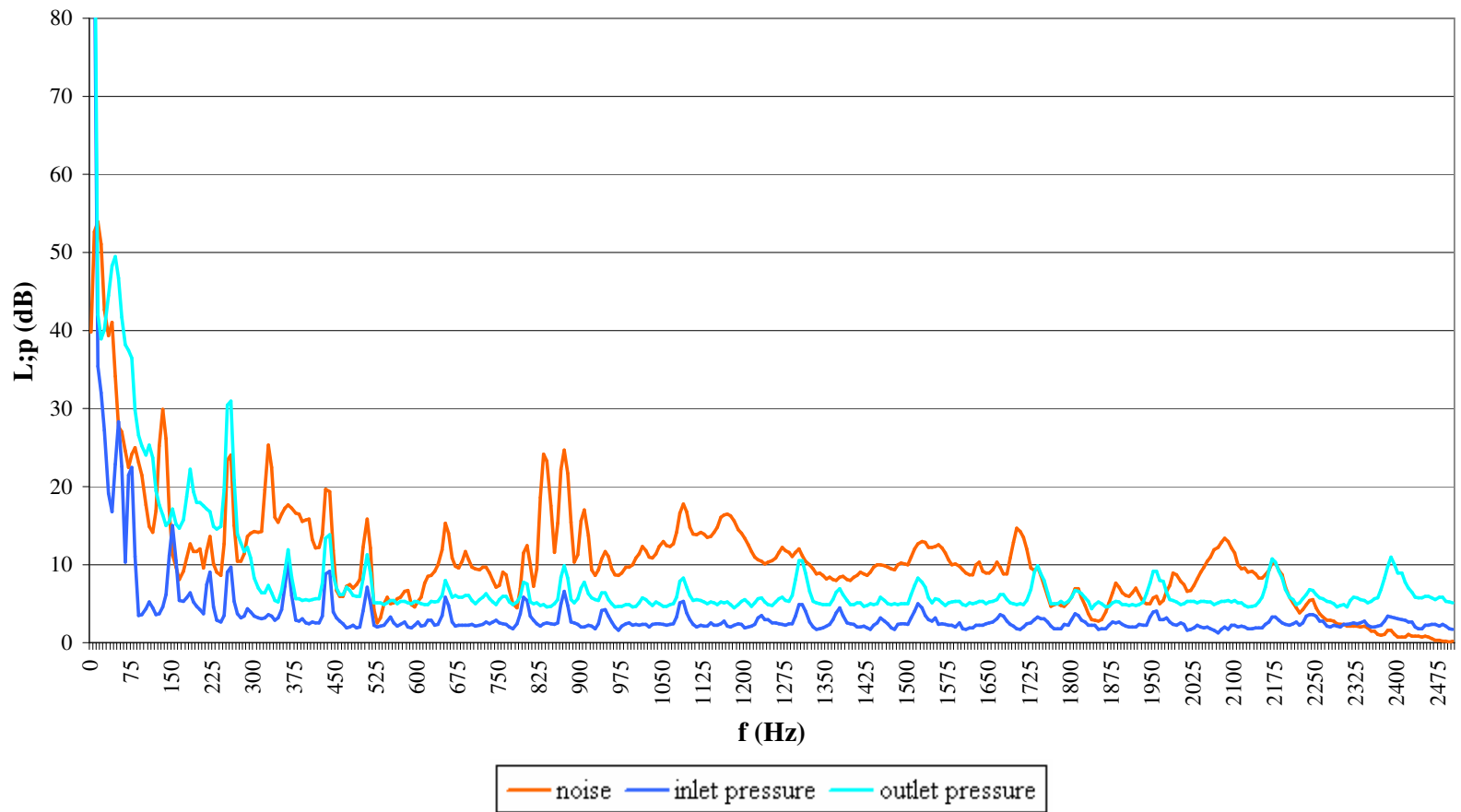**Figure D.46.** Large pump noise fft spectrum for 2770 rpm, 0.88 l/s
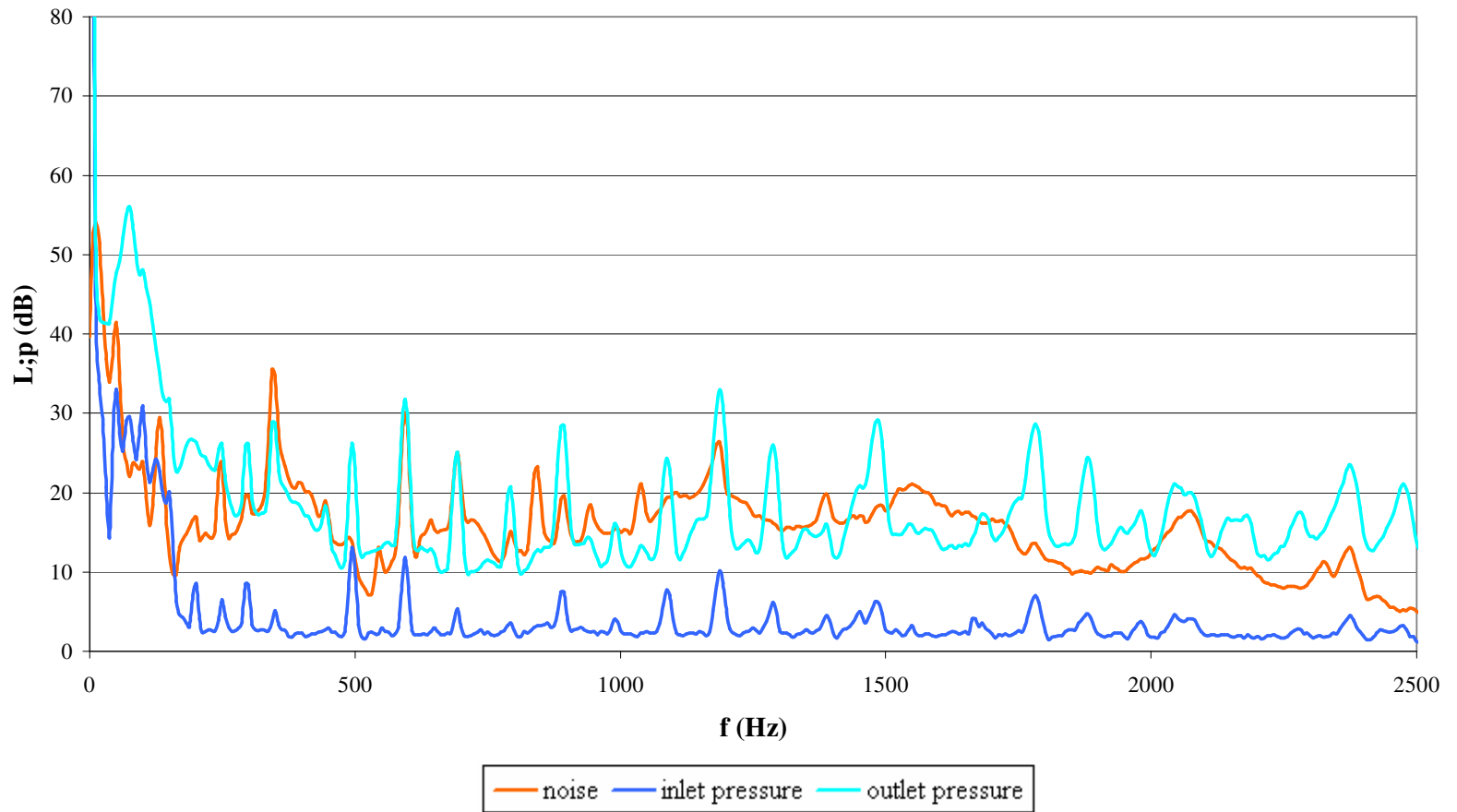
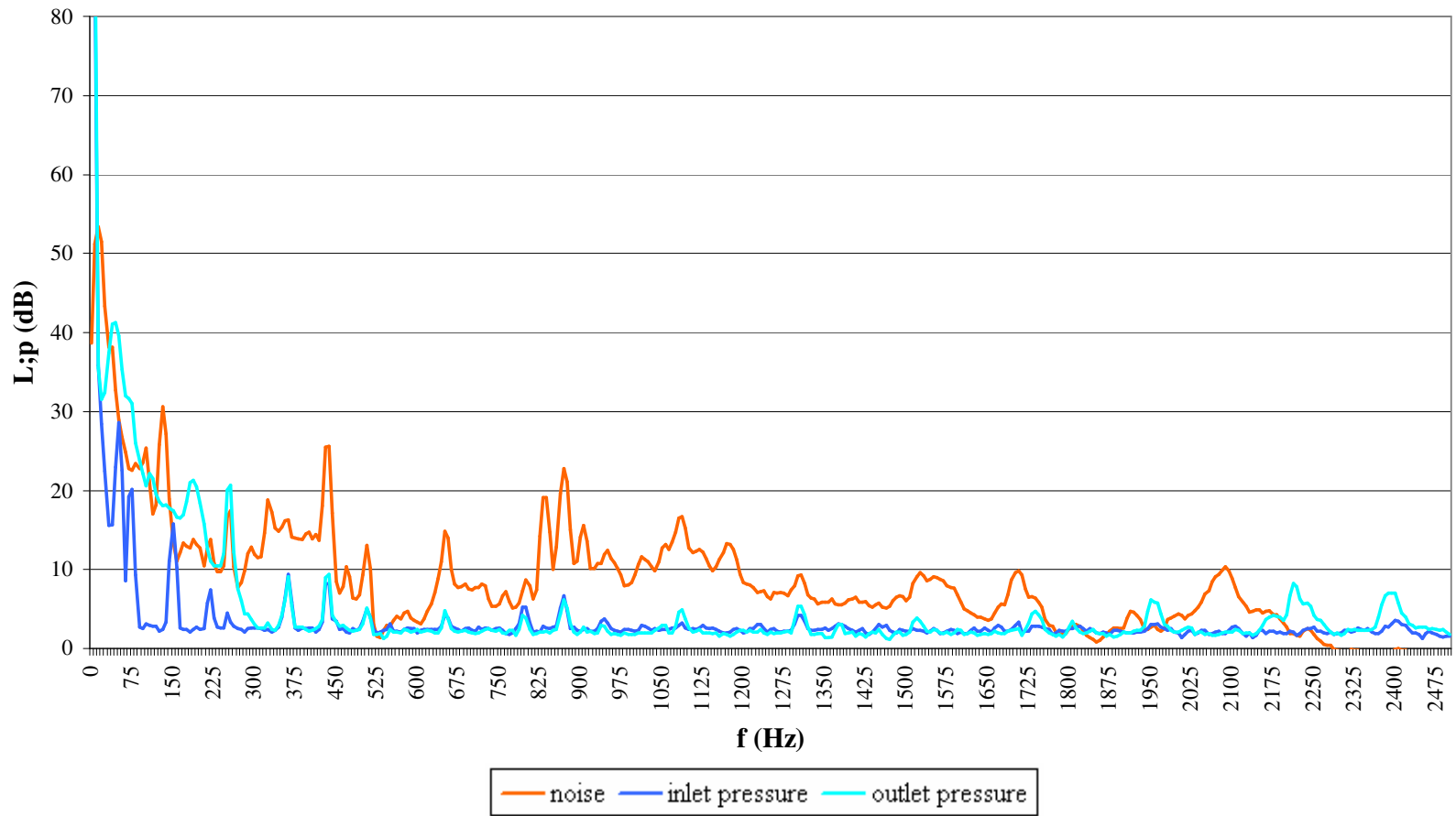**Figure D.47.** Large pump noise fft spectrum for 2975 rpm, shut off
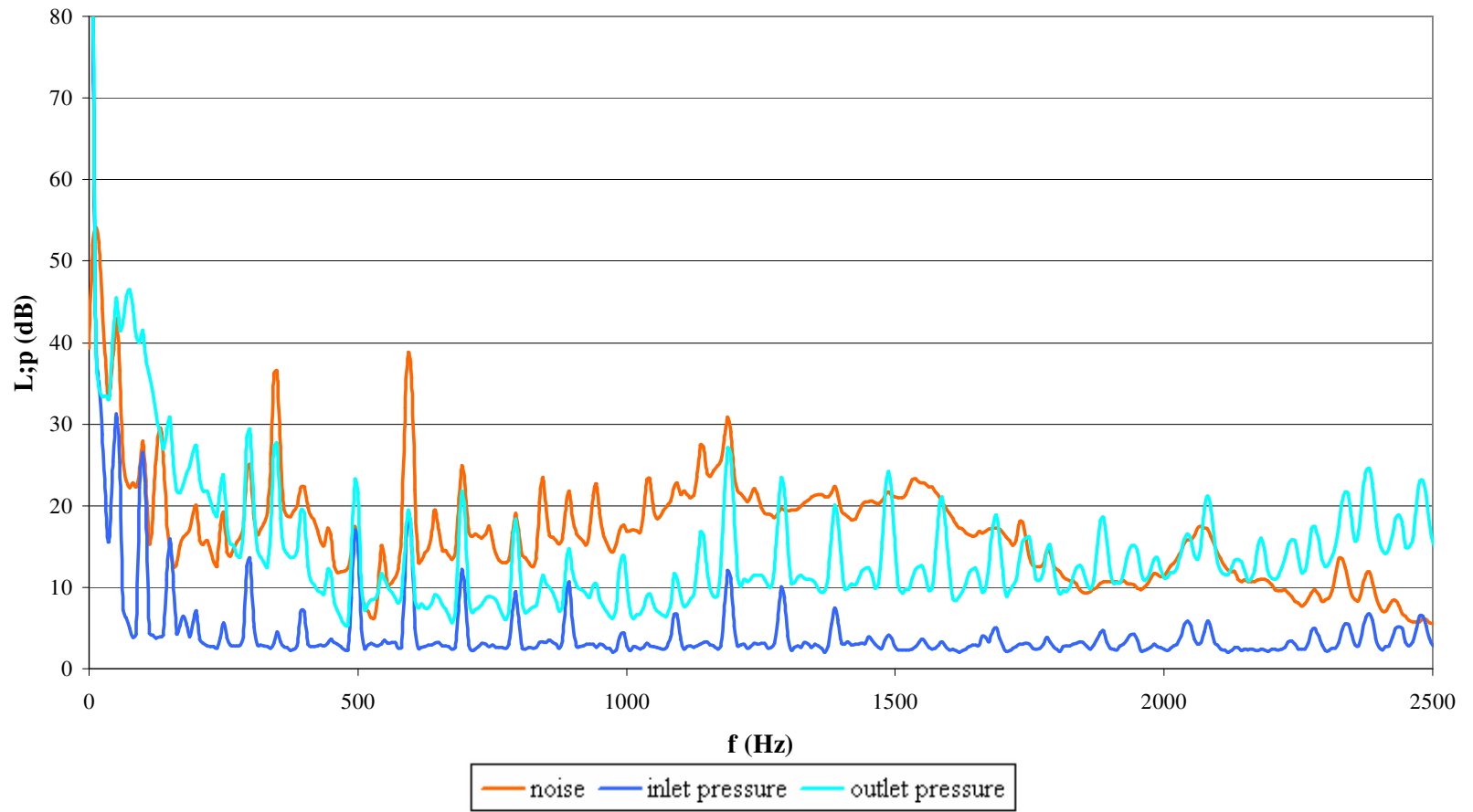
Figure D.48. Large pump noise fft spectrum for 2975 rpm, 0.85 l/s
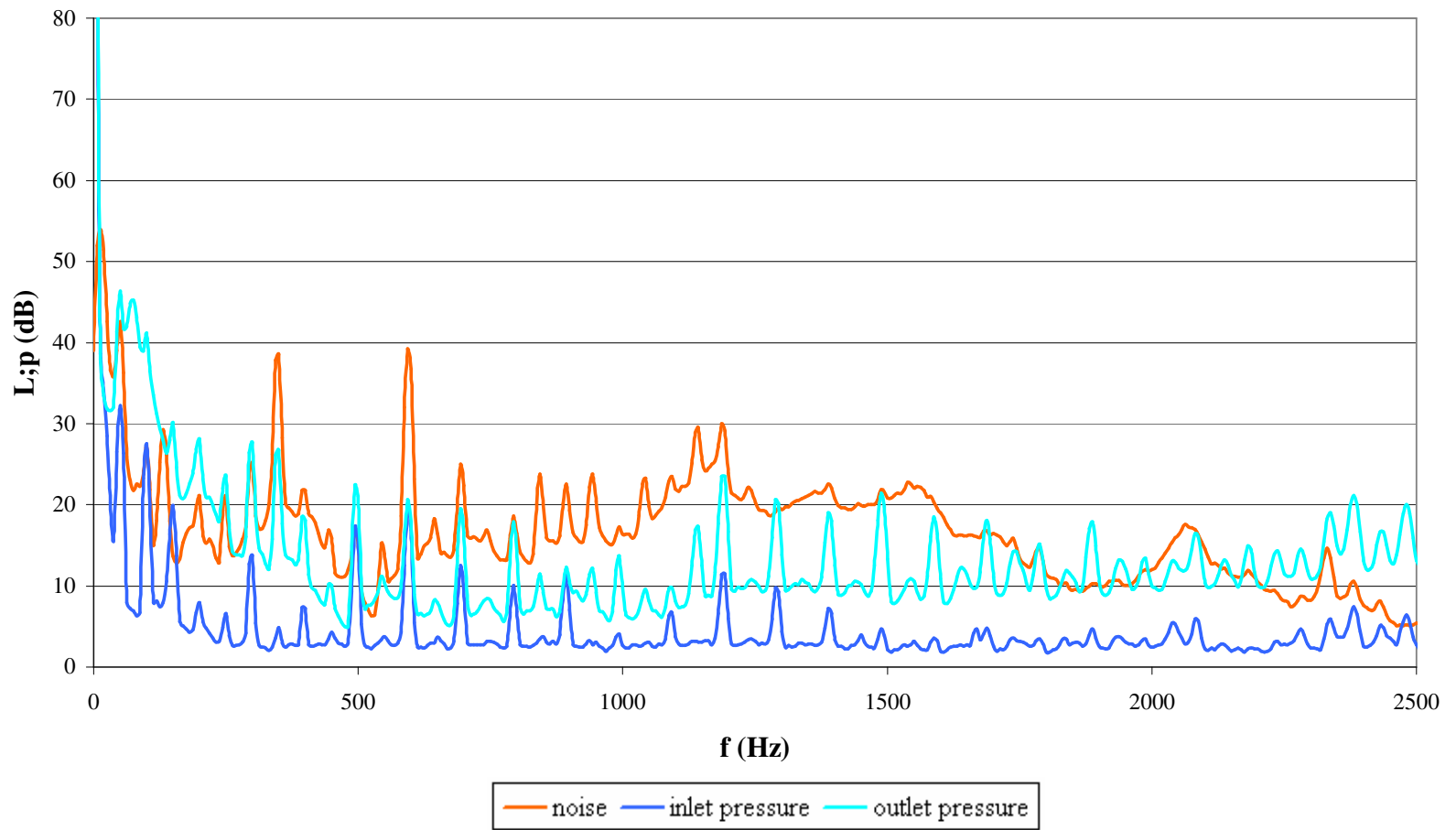
Figure D.49. Large pump noise fft spectrum for 2975 rpm, 0.94 l/s
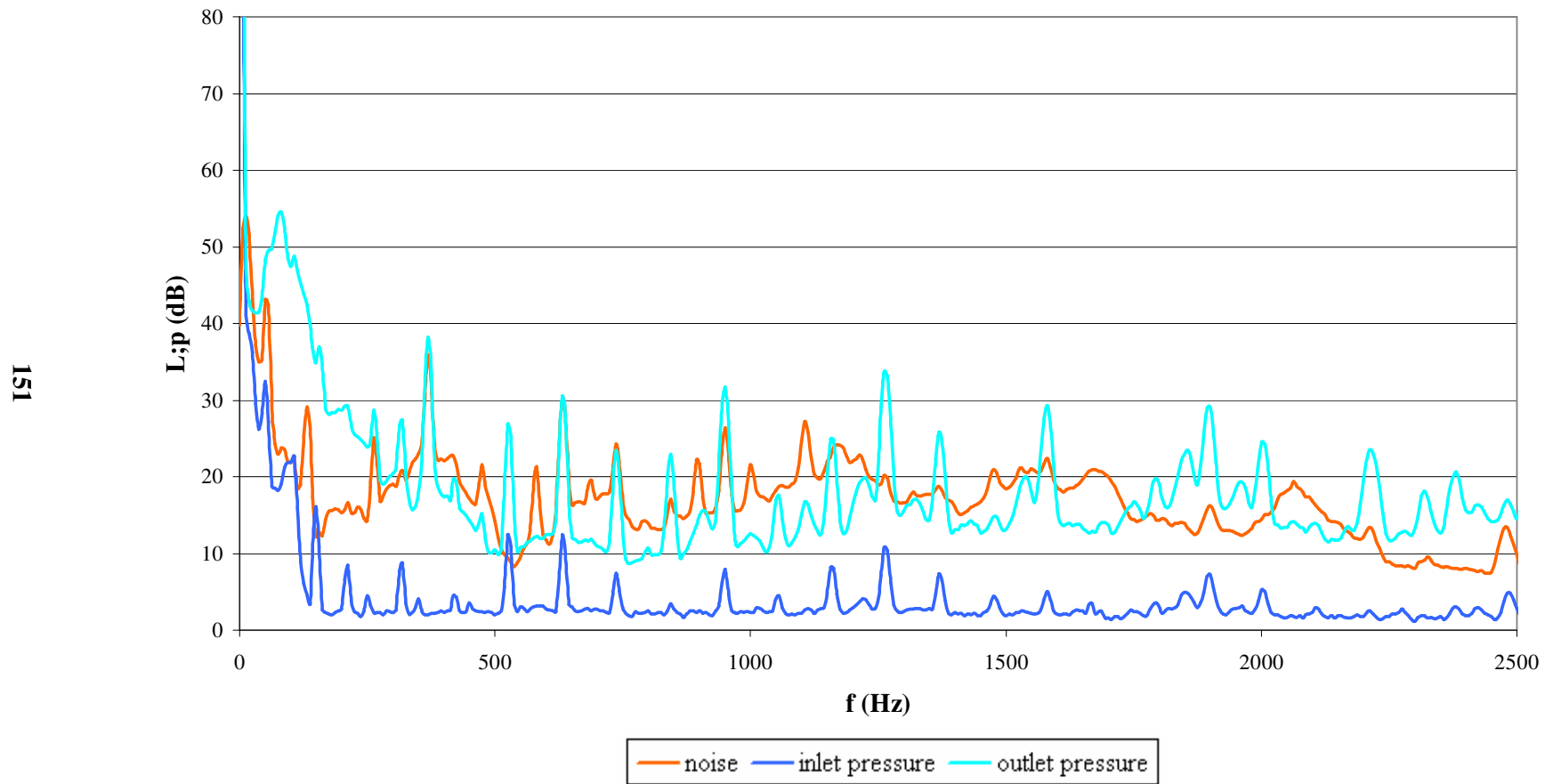
Figure D.50. Large pump noise fft spectrum for 3175 rpm, shut off

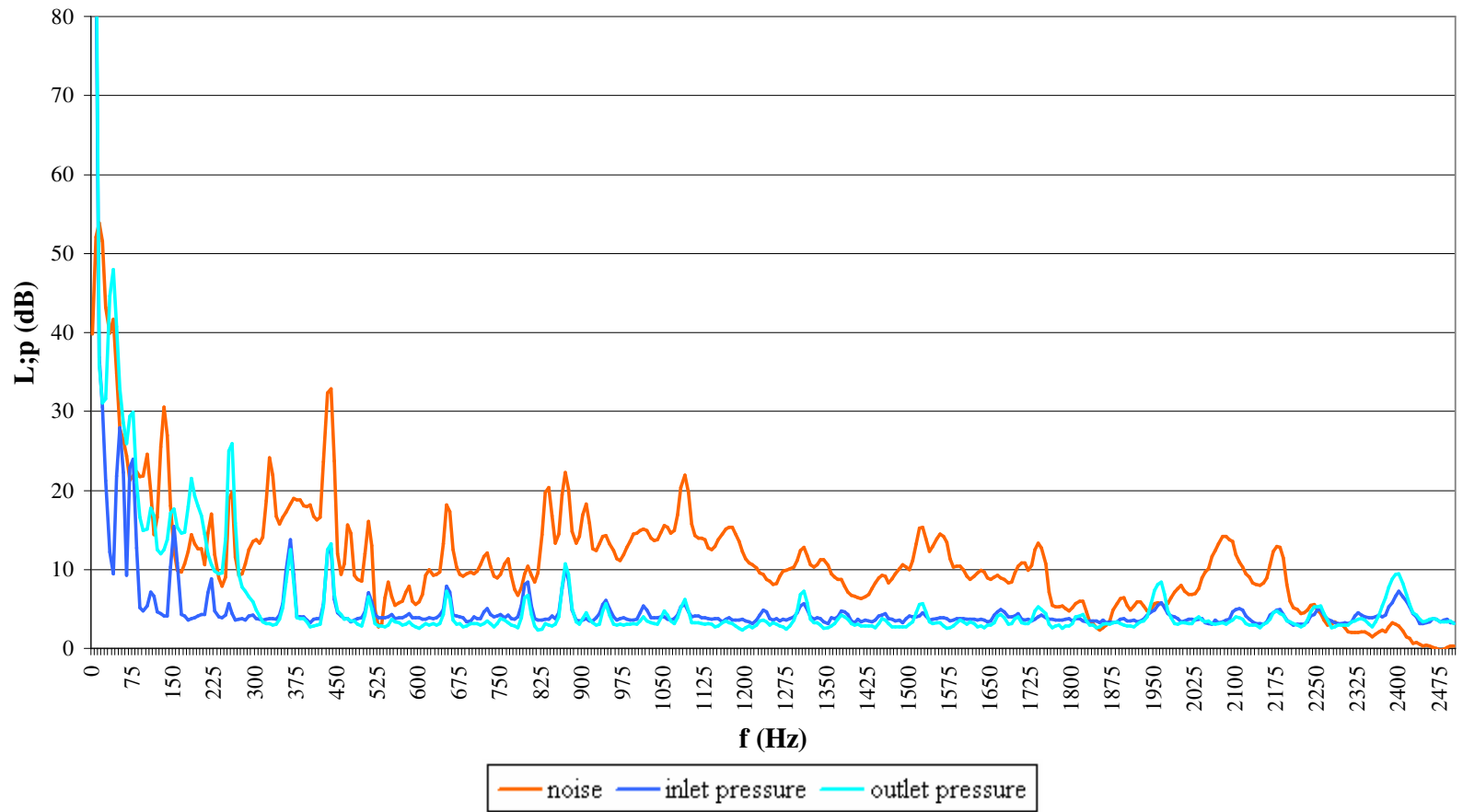**Figure D.51.** Large pump noise fft spectrum for 3175 rpm, 0.65 l/s
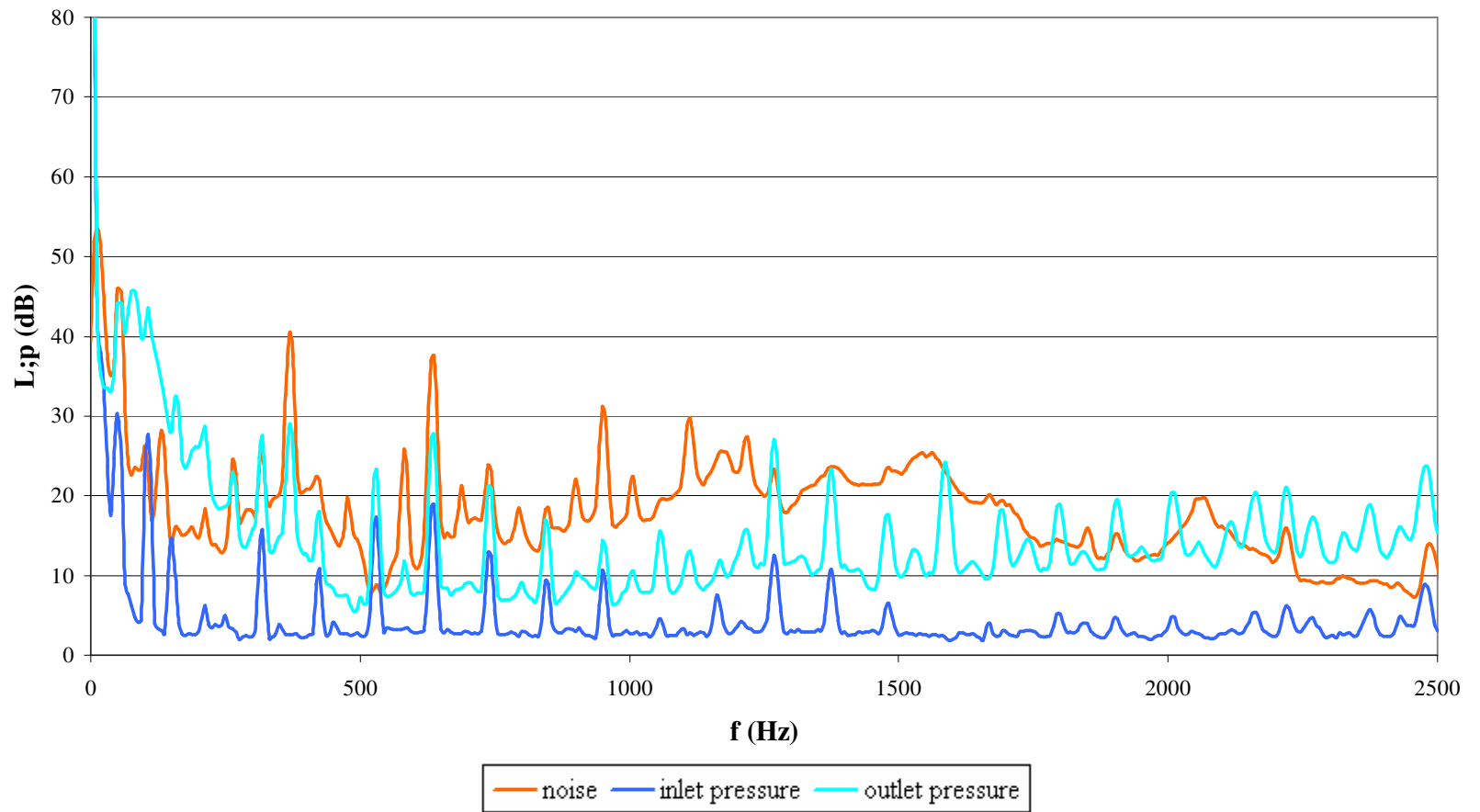
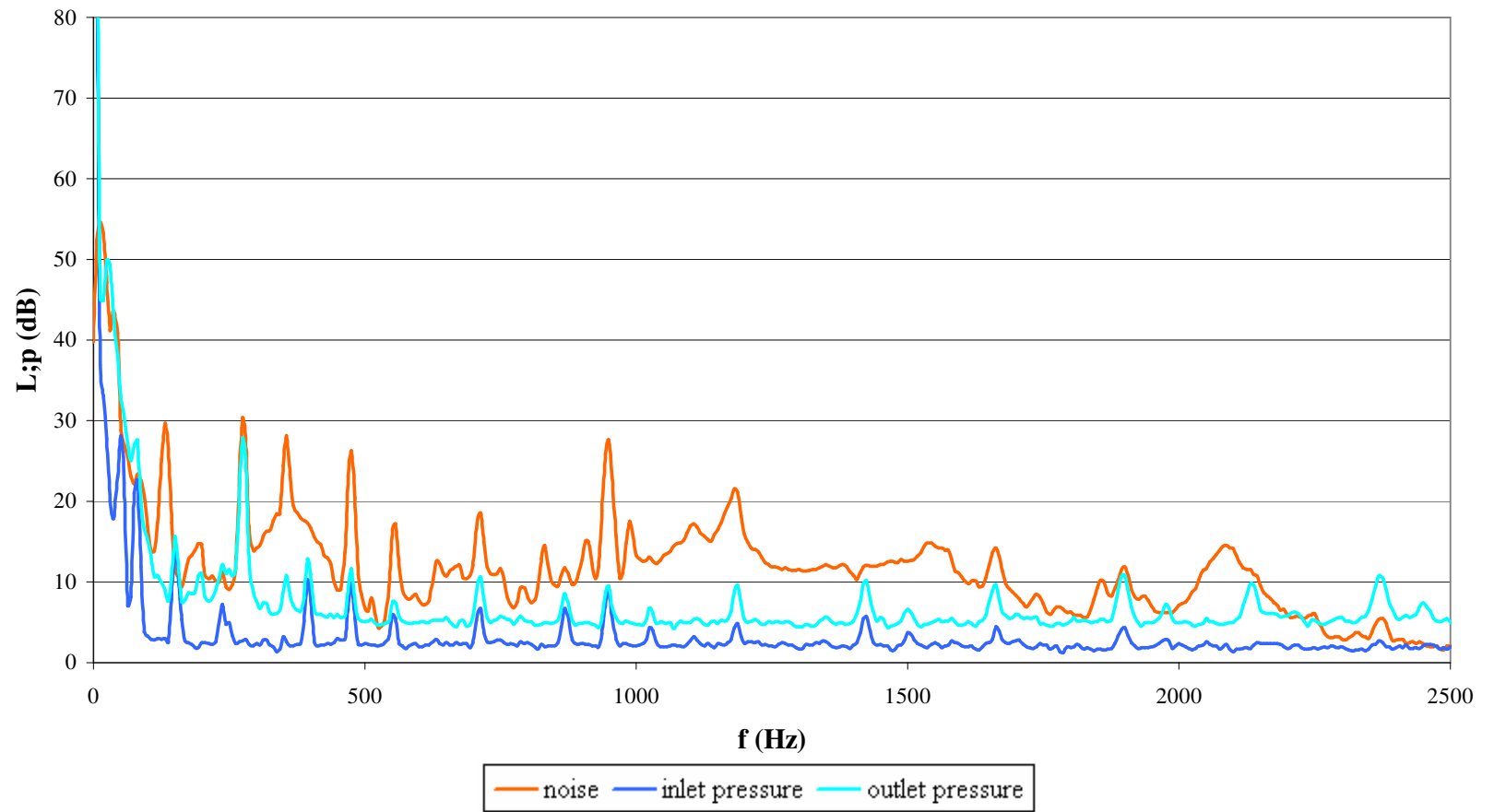**Figure D.52.** Large pump noise fft spectrum for 3175 rpm, 0.95 l/s
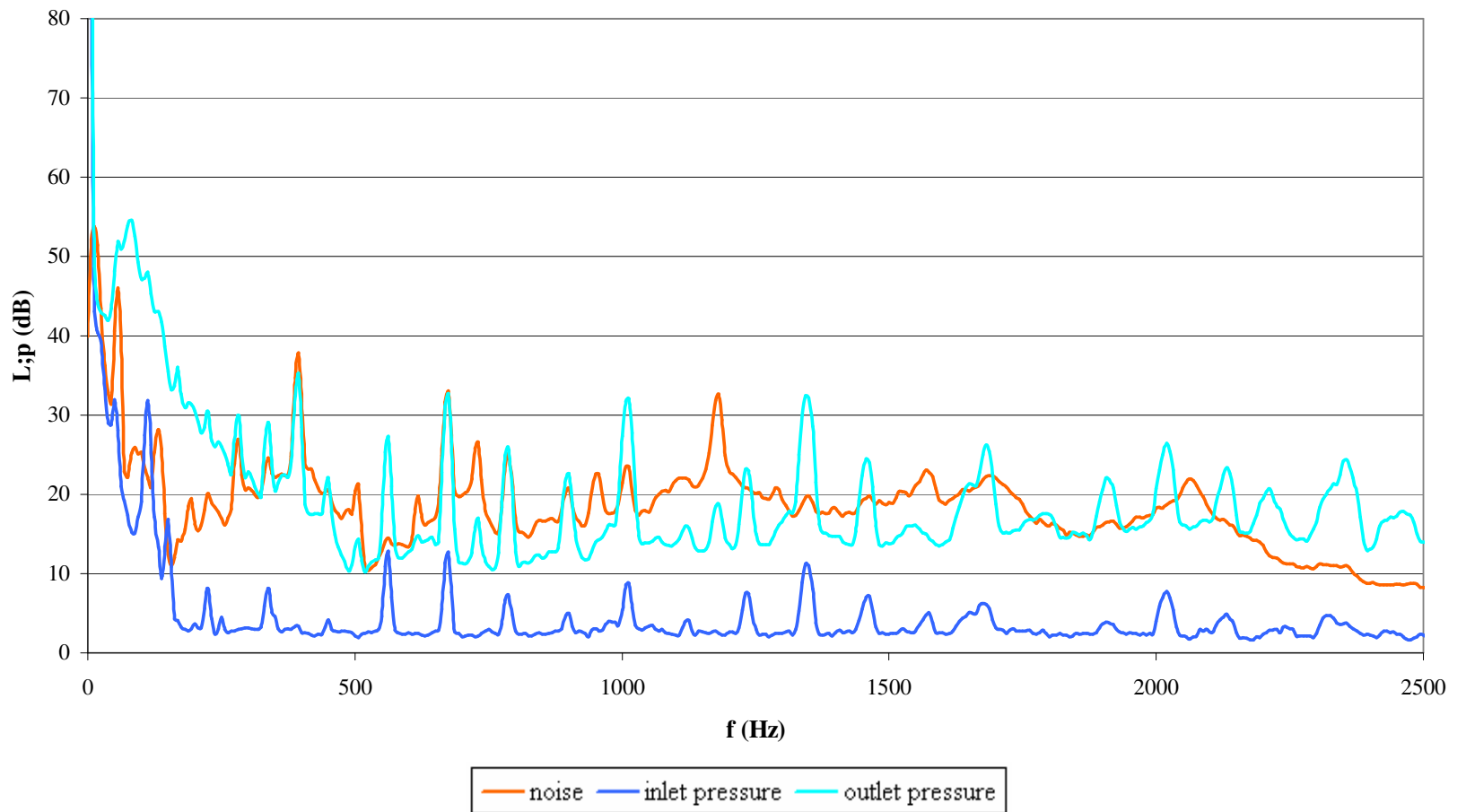
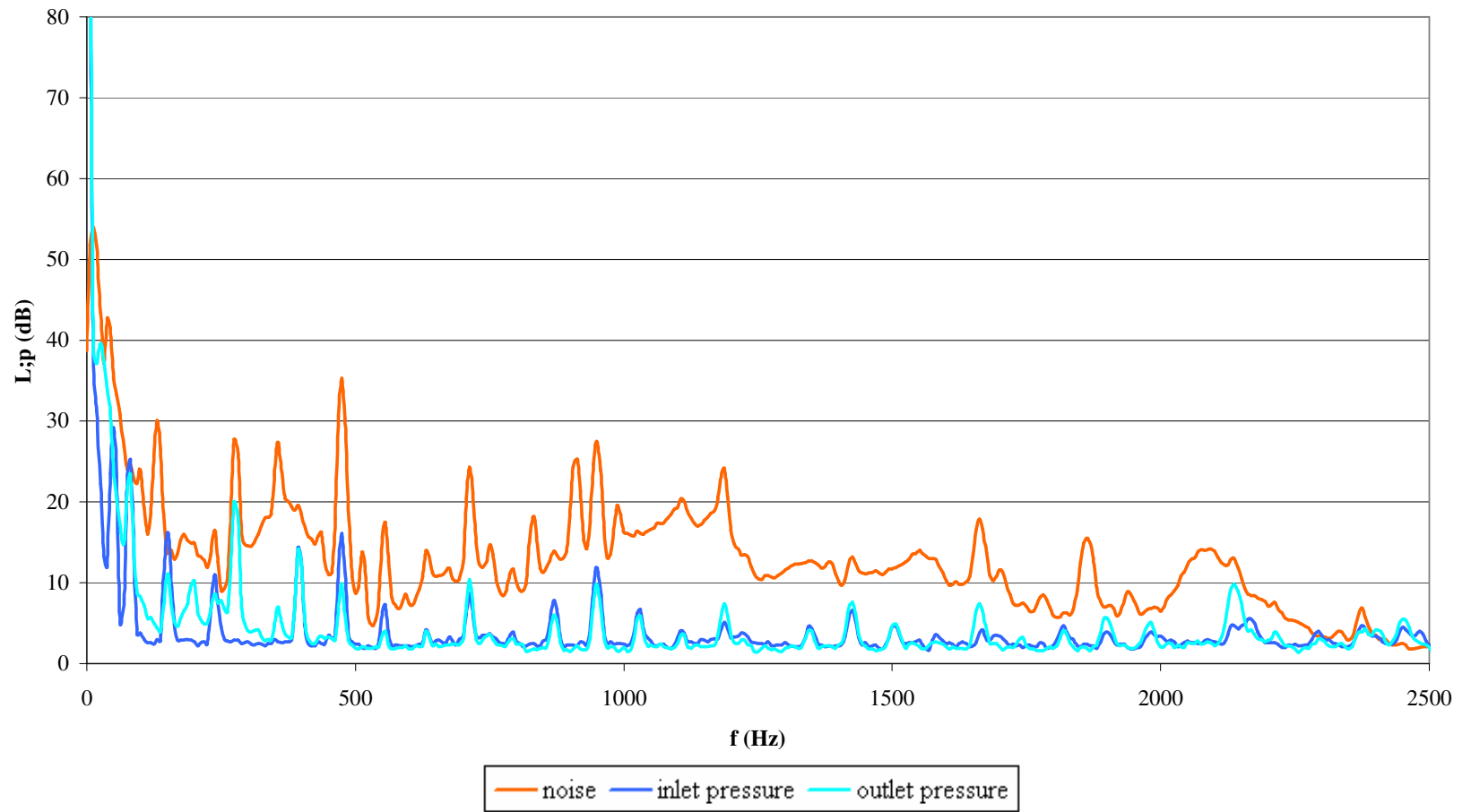**Figure D.53.** Large pump noise fft spectrum for 3375 rpm, shut off
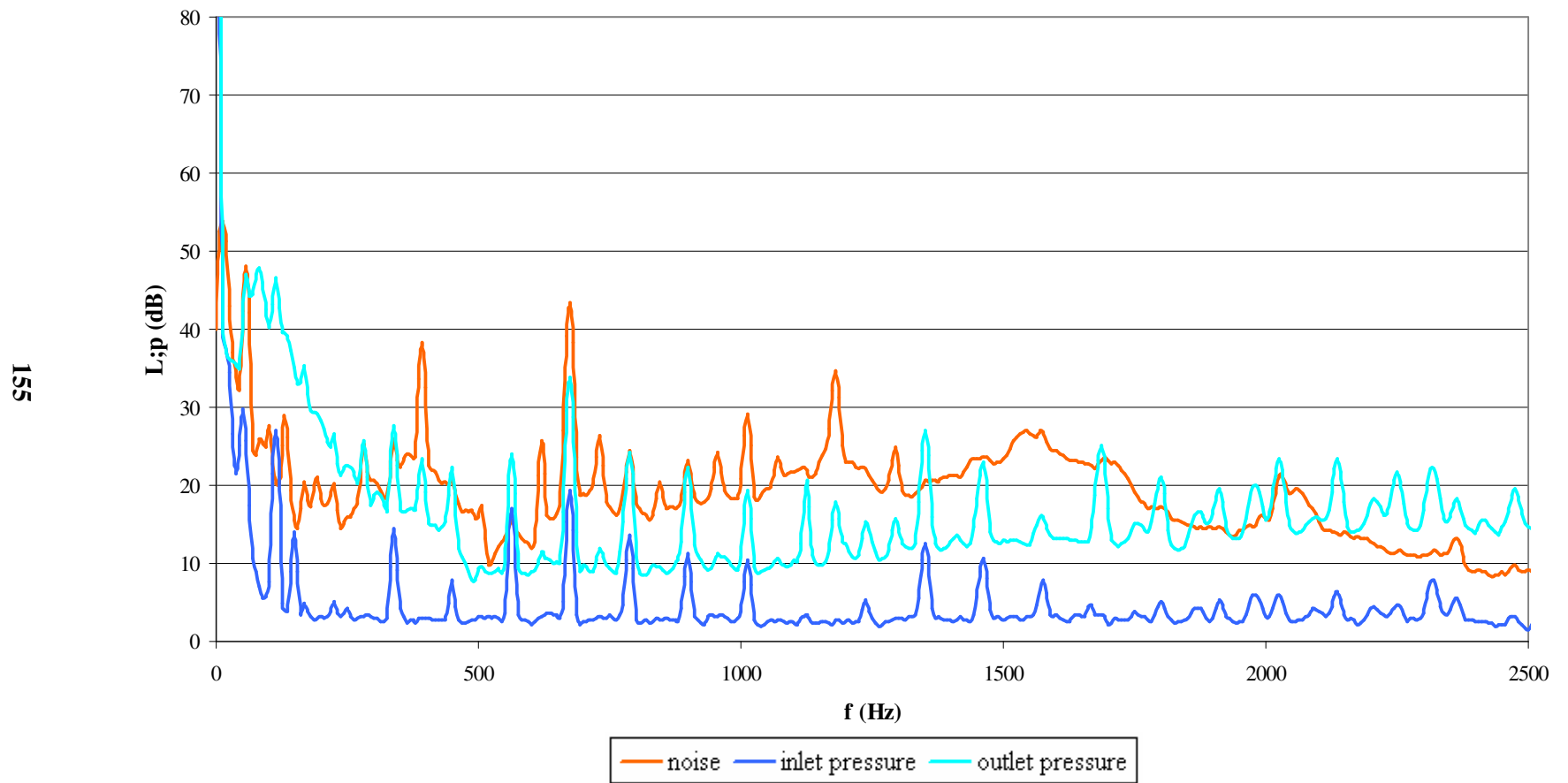
Figure D.54. Large pump noise fft spectrum for 3375 rpm, 0.77 l/s
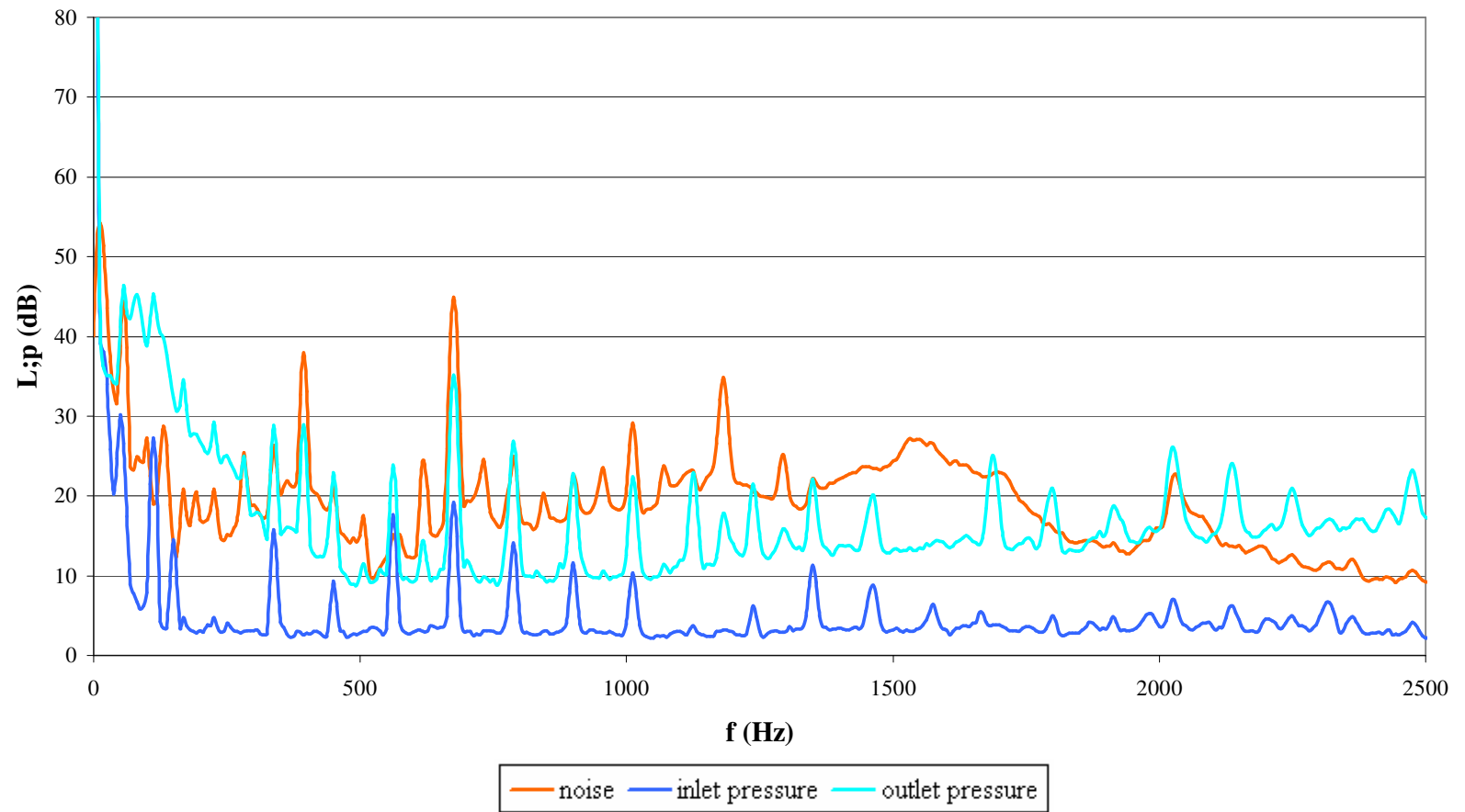
Figure D.55. Large pump noise fft spectrum for 3375 rpm, 0.90 l/s

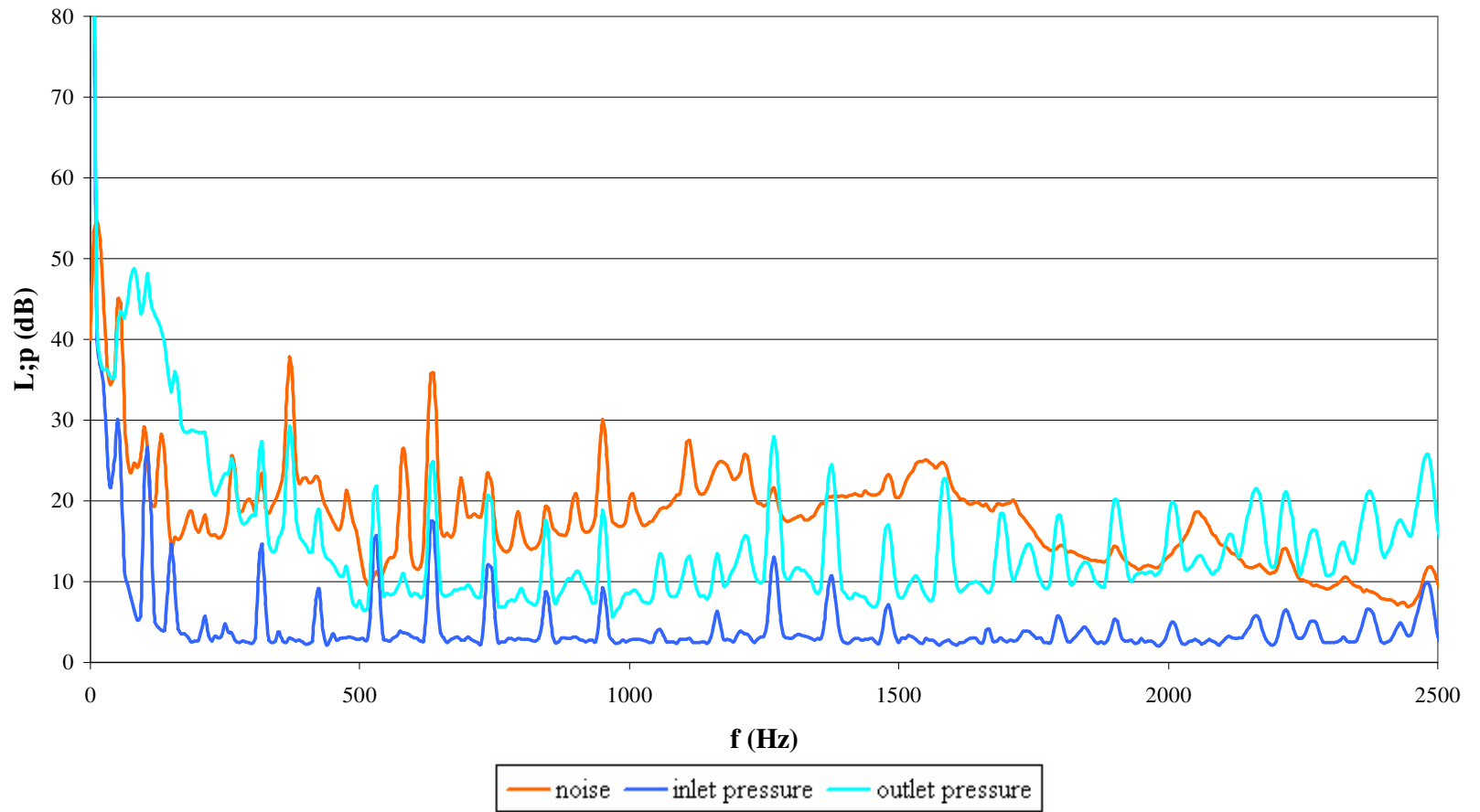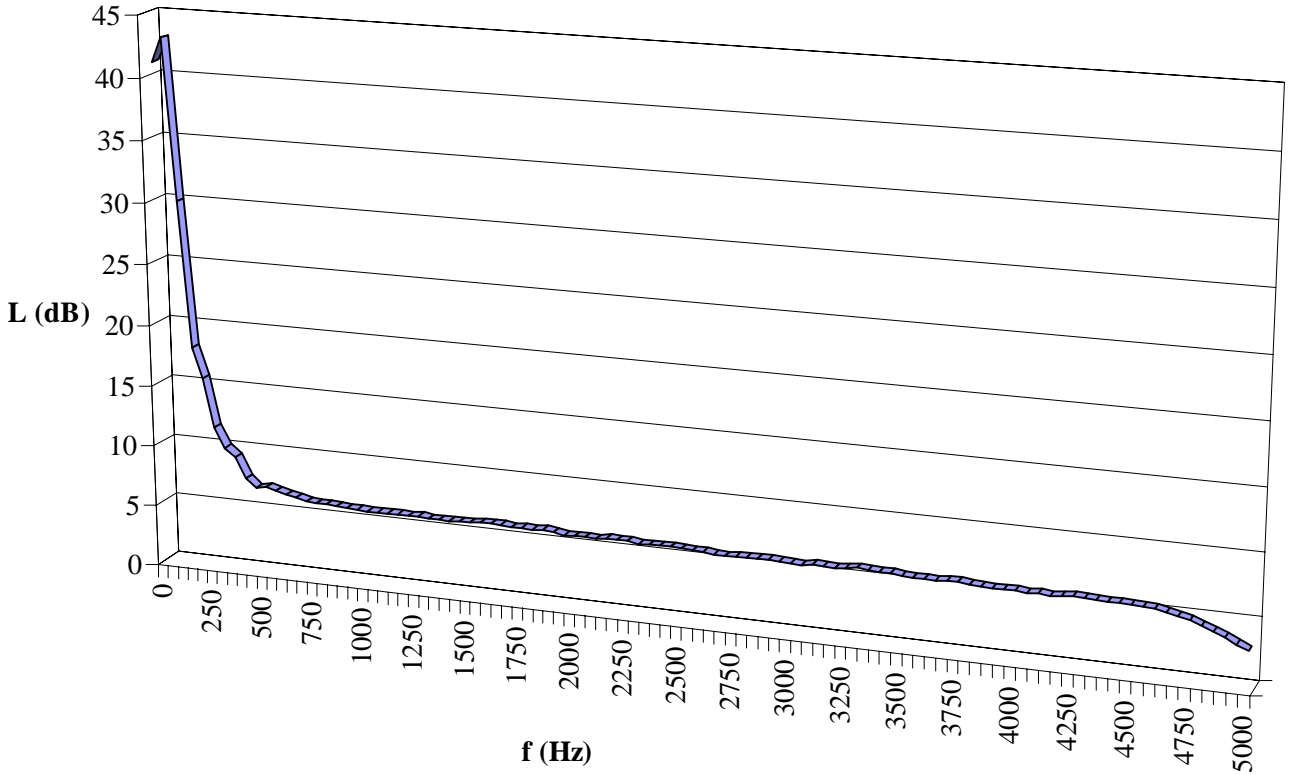**Figure E.1.** Background noise fft spectrum for the first system
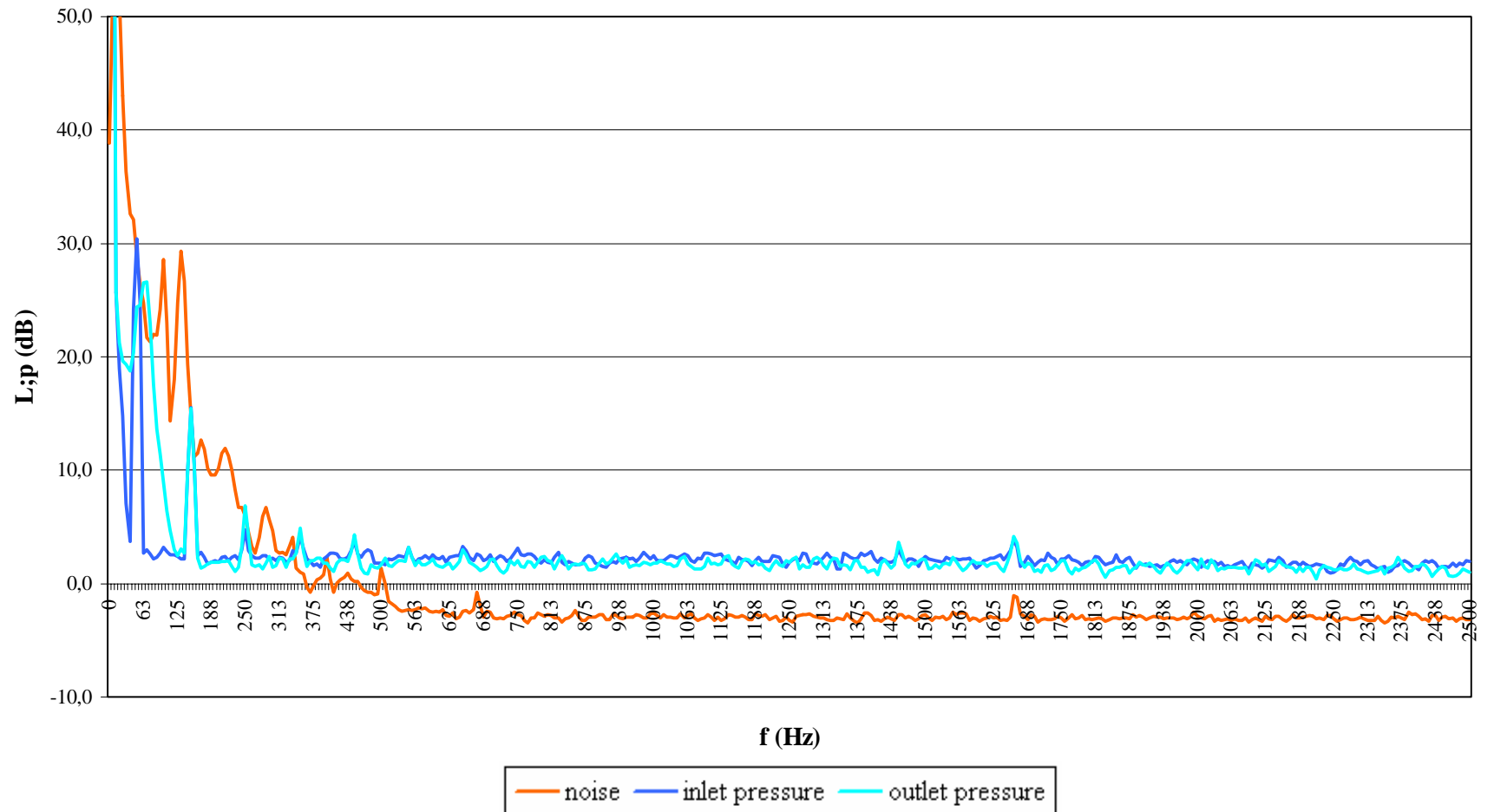
Figure E.2. Background noise and pressure fft spectrum for the second system
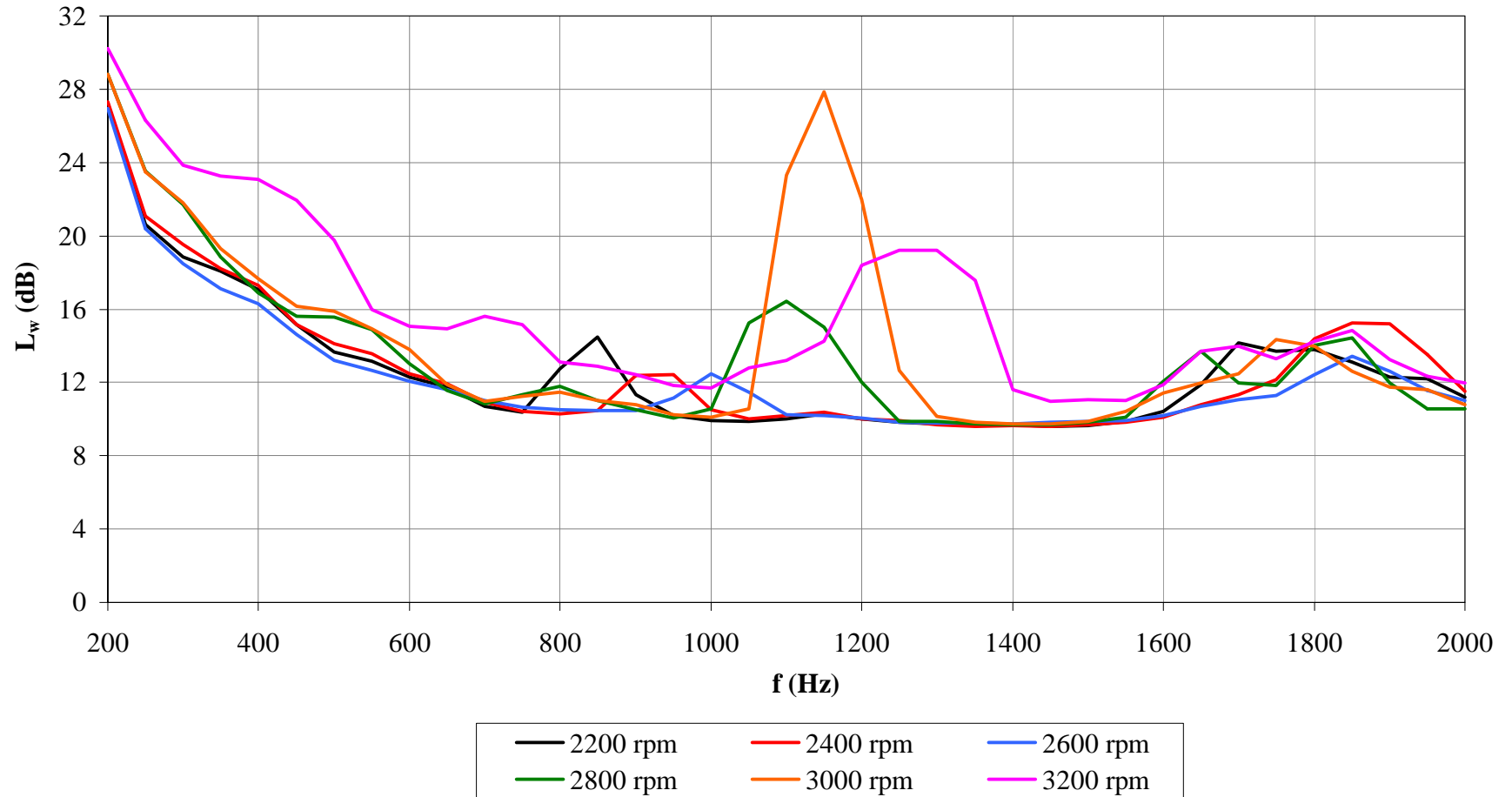
Figure E.3. Sound level spectra for solo motor
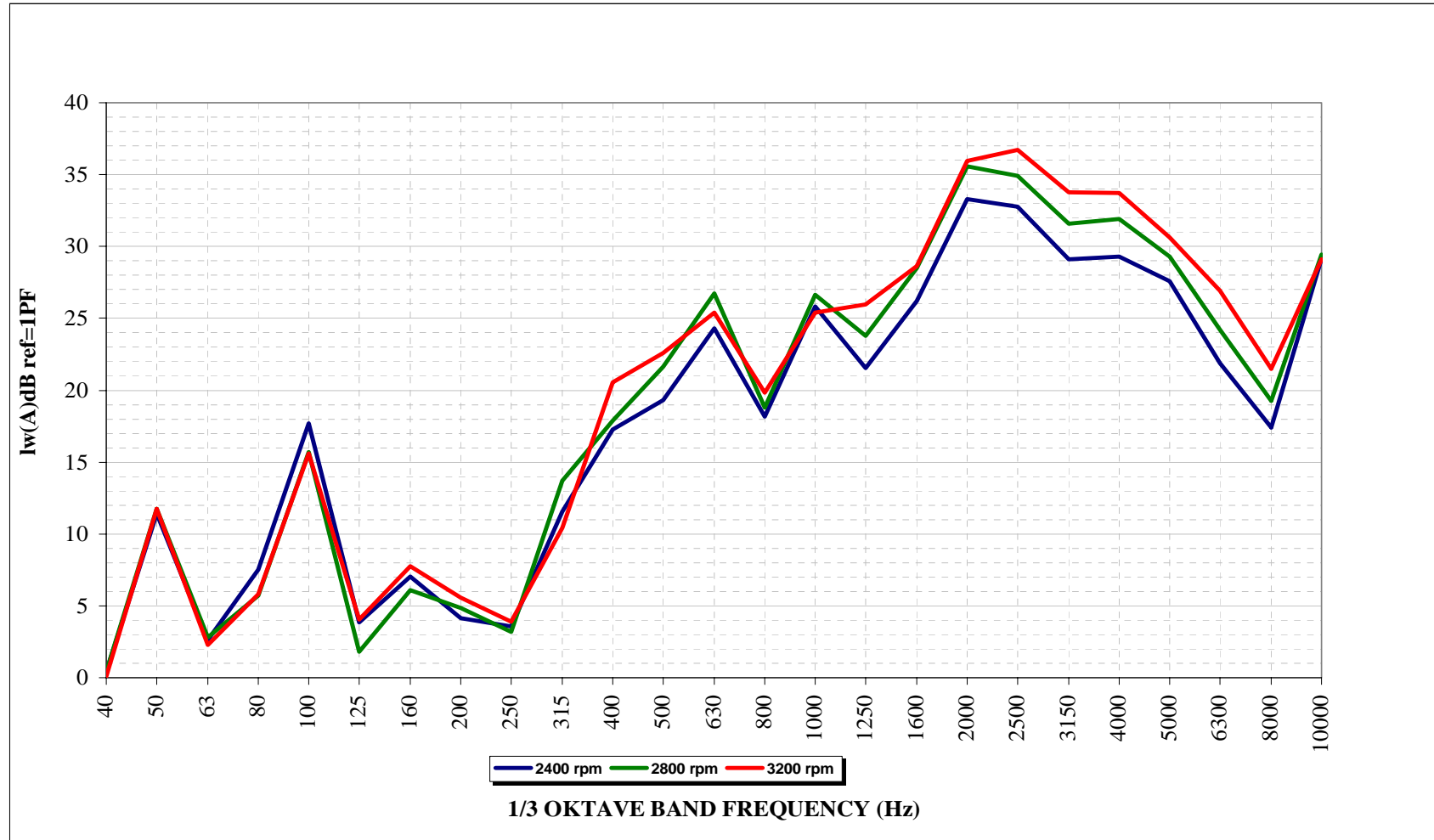
Figure E.4. Sound level spectra for solo motor, 1/3 Octave Band

F.1. TECHNICAL SPECIFICATIONS FOR PREAMPLIFIER AND PRESSURE TRANSDUCERS

Product Data and Specifications

Typical applications

■ **CCP inputs**

■ **Prepolarized microphones**

■ **½-inch precision microphones**

■ **High levels and high frequencies**

The G.R.A.S. ½-inch Preamplifier Type 26CA is a general purpose preamplifier optimized for use with prepolarized condenser microphones. It is a small, robust unit and uses a G.R.A.S. CCP[1] supply, e.g. Type 12AL. It has a very low inherent noise level, a large dynamic range and a frequency response from below 2 Hz to above 200 kHz.

Its small ceramic thick-film substrate has a very high input impedance, and is shielded by a guard ring to minimise the influence of stray capacitance and microphonic interference.

The Type 26CA is delivered with a built-in TEDS[2] chip, and can be programmed as a single unit with a microphone fitted.

½-inch Preamplifier Type 26CA

It can be used with all G.R.A.S. prepolarized microphones, namely:

½-inch microphones:
Types 40AE, 40AD and 40AQ

¼-inch microphones:
Types 40BE and 40BD, using the optional ½-inch to ¼-inch adaptor RA0019

It has an integrated BNC output connector.

The casing is made of stainless steel for maximum strength and durability.

[1] Constant Current Power
[2] Transducer Electronic Data Sheet - as proposed by IEEE-P1451.4

Specifications

Frequency response (cable load 4.7 nF):	**Maximum signal-output voltage (peak):**
2 Hz - 200 kHz . . . . ±0.2 dB	±8.0 V
Input impedance:	**Temperature:**
20 G Ω, 0.4 p F	Operation:. . . . . -30 ºC to +70 ºC
Output impedance (Cs = 20 p F, f=1000Hz):	Storage: . . . . - 40 ºC to +85 ºC
<50 Ω	**Relative humidity:**
Noise (measured with 20 pF ½-inch dummy mic.):	Operation:. . . . . 0 to 95 %
A-weighted:. ≤2.2 µV rms	Storage: . . . . 0 to 95 %
(typically 1.8 µV rms)	**Connector type:**
Linear (20 Hz - 20 kHz): ≤6 µV rms	BNC
(typically 3.5 µV rms)	**Dimensions and weight:**
Gain:	Diameter:. . . . . 12.7 mm (½-inch)
Typically:. . . . . -0.25 dB	Length: . . . . 73 mm (2.9 inches)
Power-supply:	Weight: . . . . 26 g (0.9 oz)
2 m A to 20 m A (typically 4 m A)	

Figure F.1. Technical specifications for ½-inch preamplifier type 26CA

Range (F. S.)			

0-2, 0-5, 0-10, 0-20, 0-35, 0-50, 0-100, 0-200 and 0-350 bar, gauge, sealed gauge or absolute

Over-range

Without Damage : 2 x F.S.
Without Destruction : 5 x F.S.

Accuracy

Linearity : ±0.25% F.S. (±0.35% for ≤10 bar model)
Hysteresis : ±0.25% F.S.
Repeatability : ±0.2% F.S.

Temperature Range

Operating Temperature Range (OTR) : -40 to 120 °C
Compensated Temperature Range (CTR) : 0 to 60 °C
Zero Shift in CTR : <2.5% F.S. / 60 °C (<3.5% for 2 bar model)
Sensitivity Shift in CTR : <2% of reading / 60 °C

Electrical Characteristics

Model	XPM5	XPM5-A1	XPM5-A2
Supply Voltage	10 Vdc	10 to 30 Vdc	±15 Vdc (±12 to ±18 Vdc)
F.S. Output 2 bar model	50 mV	4 V ±5% F.S.	5 V ±5% F.S.
F.S. Output >2 bar model	100 mV	4 V ±5% F.S.	5 V ±5% F.S.
Zero Offset	<±10 mV	0.5 V ±5% F.S.	0 V ±5% F.S.
Input Impedance/Consumption	1500 Ω	<25 mA	<25 mA
Output Impedance	500 to 800 Ω	<10 Ω	<10 Ω
Insulation under 50 Vdc	≥100 MΩ	≥100 MΩ	≥100 MΩ

Electrical Termination

Shielded cable with 4 Teflon wires (AWG28), standard length 2 m with strain relief spring

Tightening Torque

Nominal : 5 N.m (zero and sensitivity shift <1%)
Maximal : 10 N.m

Mechanical Characteristics

Material : Body and flush diaphragm in titanium, laser welded
Resonance Frequency : 100 kHz to 800 kHz
Self centered sealing ring
Protection Index : IP 50

XPM5-SC

Product References

Low Level Output Transducer
    Model
        Full Scale Range (F.S.)
        In bar G (gauge), S (sealed gauge), A (absolute)
            Option(s)
            HA : Accuracy (CNL&H) ≤±0.25% F.S. (≤±0.35% for ≤10 bar model)
            SI : Sensitivity shift ≤1% of reading / 60 °C (except 2 and 5 bar model)
            ZI : Zero shift ≤1.5% F.S. / 60 °C (except 2 and 5 bar model)
            ET1 : CTR -20 to 100 °C
            ET3 : CTR -40 to 150 °C OTR=CTR
            SC : Connector output, prewired, cable length 2 m
            P5 : IP65 protection
            P7 : IP67 protection
            LC"X" : Additional cable length in m

XPM5	20G	ET1

High Level Output Transducer
    Model
        Power Supply Reference
        A1 : Unipolar-tension
        A2 : Bipolar-tension
            Full Scale Range (F.S.)
            In bar G (gauge), S (sealed gauge), A (absolute)
                Option(s)
                HA : Accuracy (CNL&H) ≤±0.25% F.S. (≤±0.35% for ≤10 bar)
                SI : Sensitivity shift ≤1% of reading / 60 °C (except 2 and 5 bar model)
                ZI : Zero shift ≤1.5% F.S. / 60 °C (except 2 and 5 bar model)
                ET1 : CTR -20 to 100 °C
                ET2 : CTR -40 to 120 °C
                P5 : IP65 protection
                P7 : IP67 protection
                LC"X" : Additional cable length in m
                TS : Tolerance on F.S. output ≤±2% F.S.

XPM5	A1	20G	ET1

"X" = Custom value

Wiring Schematic
XPM5

+Excit. (Red)
+Signal (Green or Yellow)
-Excit. (Black or Blue)
-Signal (White)
Shield

XPM5-A1

+Excit. (Red)
+Signal (Green or Yellow)
-Excit./-Signal (Black or Blue/White)
Shield

XPM5-A2

+Excit. (Red)
+Signal (Green or Yellow)
-Excit. (Black or Blue)
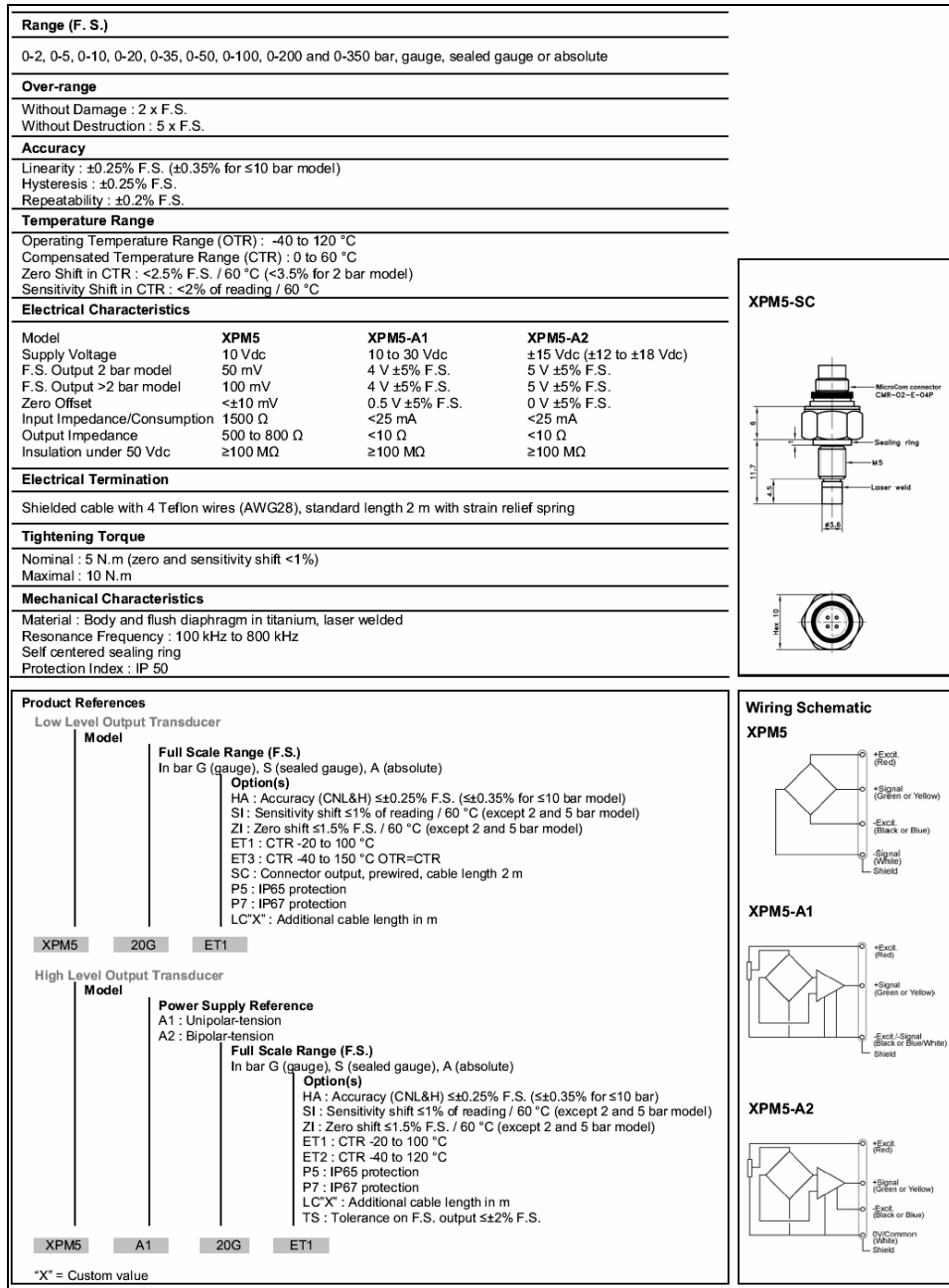0V/Common (White)
Shield

Figure F.2. Technical specifications for XPM5 series miniature pressure transducer